The "Strange Case" of Phenylacetylene:
Competition between H-π and n-σ* Contacts, Studied using
Matrix Isolation Infrared Spectroscopy and *Ab Initio* Computations

A thesis submitted in partial fulfillment of requirements for the
Degree of Doctor of Philosophy

By

Ginny Karir

(PH12152)

Research Advisor
Prof. K. S. Viswanathan

Department of Chemical Sciences

Indian Institute of Science Education & Research, Mohali

Sector 81, Knowledge City, Manauli P.O.

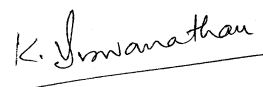**SAS Nagar, Punjab-140306, India**

August 2017

Dedicated to my Parents....

CERTIFICATE

I hereby certify that the thesis titled 'The "Strange Case" of Phenylacetylene : Competition between H-π and n-σ* Contacts, Studied using Matrix Isolation Infrared Spectroscopy and *Ab Initio* Computations' submitted for the degree of Doctor of Philosophy by Ms. Ginny Karir is the record of research work carried out by her during the period January 2013 to August 2017 under my guidance and supervision and further state that this work has not formed the basis for the award of any degree, diploma or a fellowship to any other University or Institute. I further state that this work in this thesis was carried out independently by Ms. Ginny Karir.

In my capacity as the supervisor of the candidate's PhD thesis work, I certify that the above statements are true to the best of my knowledge.

Prof. K.S. Viswanathan

(Research Supervisor)

Place: Mohali

Date: 16 January 2018

DECLARATION

The work presented in this thesis has been carried out by me under the guidance of Prof. K. S. Viswanathan at the Indian Institute of Science Education and Research Mohali.This work has not been submitted in part or in full for a degree, a diploma, or a fellowship to any other university or institute. Whenever contributions of others are involved, every effort has been made to indicate this clearly, with due acknowledgement of collaborative research and discussions. This thesis is a bonafide record of original work done by me and all sources listed within have been detailed in the bibliography.

Ginny Karir

Acknowledgements

I would like to express my sincere gratitude to my supervisor **Prof. K.S Viswanathan**, who gave me the opportunity to work under his guidance. It has been a privilege knowing him all these years. His academic lessons and research endeavour have enriched me immensely, and provided me with new insights into the scientific world. His constant encouragement and guidance to excel professionally as well as personally has been invaluable to me. I am thankful to him for trusting in my capabilities. He has always been an inspirational figure for me to be a good human being and an enthusiastic researcher. Truly he made my experience at IISER Mohali a memorable one.

I owe my sincere thanks to Doctoral committee members **Dr. Sugumar Venkataramani** and **Dr.P. Balanarayan** for the regular assessment of my thesis and for their valuable suggestions which helped me enormously in the writing of my thesis.

I would like to thank **Prof. D.P. Sarkar**, Director, and **Prof. N. Sathyamurthy**, former Director, IISER Mohali, for supporting me with all the facilities, to pursue my doctoral work.

I would like to thank the **Dr. S. Arulananda Babu**, Head, Department of Chemical Sciences, for his encouragement and for providing all the necessary support for my research.

I am grateful to my colleagues **Dr. Anamika, Pankaj, Kanupriya, Jyoti, Priyanka, Divita, Amala** and all the previous lab members; **Kapil, Gaurav, Vivek, Deepak, Mariyam, Srijit, Sruthy, Ravi, Sumit, Piyush, Gargi**, who provided me with a positive and a learning lab environment. I would also like to thank **Dr. Bishnu Prasad Kar** for his invaluable help and discussions in the lab during the time the facility was being set up. I would like to specifically thank my colleagues, **Gaurav and Mariyam**, who collaborated on some of the experiments. I am grateful to **Prithwish** for helping me in the preparation of DCl.

I am grateful for the financial support provided by the MHRD during my stay at IISER Mohali.

I wish to thank my friends **Aastha, Gaganpreet, Summit, Gagandeep, Kapil Dave, D.J. Pradeep, Mehreen Khaleel, Swagatam Nayak, Dr. Rishu**, **Mrs. Yogeet** for their joyful company and for being my social support system. I would specially like to thank **Mrs. Chitra Viswanathan, Dr. Deepika, Dr. Janakiraman and Medhini** for their love and support.

This thesis would not have been possible without the unconditional love and affection from my parents, **Mrs. Suman Karir** and **Mr. Sanjeev Karir**. They were always there to support me during my tough times. Their trust in me has been a constant source of motivation for me. I would like to extend my heartfelt gratitude to my grandmother Late **Smt. Prem Lata Karir** for her blessings. Last but not the least, I would especially like to thank my brother **Ankush Karir** for his unfailing faith in my capabilities.

Ginny Karir

CONTENTS

LIST OF FIGURES

iii

LIST OF TABLES

LIST OF ABBREVIATIONS

PhAc	Phenylacetylene
FA	Formic acid
$PhAc_D$	Phenylacetylene-D
MeOH	Methanol
DEE	Diethyl Ether
FT	Fourier Transform
Ac	Acetylene
UV	Ultra Violet
Elec	Electrostatic
Ind	Inductive
Dis	Dispersive
Rep	Repulsive
Pol	Polarization
GM	Gifford-McMahon
KBr	Potassium Bromide
HF	Hartree-Fock
MP	Møller–Plesset perturbation theory
DFT	Density Functional Theorem
CC	Coupled cluster
SCF	Self- Consistent Field
M06	Minnesota functional
FWHM	full width at half maximum
ZPE	Zero point vibrational energy
BSSE	Basis Set Superposition Error
AIM	Atoms –in-molecules
CP	Critical point
NBO	Natural Bond Orbital
LMOEDA	Localized Molecular Orbital Energy Decomposition Analysis

List of Publications

Journal publications based on work from this thesis

1. Phenylacetylene-water complex: Is it n···σ or H···π in the matrix? **G. Karir**; K.S. Viswanathan ; J. Mol. Struct.; 1107 ; **2016** ; 145-156.

2. The elusive ≡C-H··O complex in the hydrogen bonded systems of Phenylacetylene: A Matrix Isolation Infrared and *Ab Initio* Study. **G. Karir**; M.Fatima; K.S. Viswanathan; J. Chem. Sci; 128(10) ;**2016**; 1557-1569.

3. H-π landscape of the Phenylacetylene-HCl System: Does this provide the gateway to the Markovnikov addition? **G. Karir*** and K.S. Viswanathan*; J. Phys. Chem. A.;121(31); 2017; 5797-5808.

4. Multiple Hydrogen Bond Tethers for the Grazing Formic Acid in its Complexes with Phenylacetylene. **G. Karir***, G. Kumar, B.P. Kar and K.S. Viswanathan*. J. Phys. Chem. A. (Under Revision)

Manuscript under preparation

5. C-H…O Secondary Interactions: Lead or Supporting Actors? G. Karir* and K.S. Viswanathan*

Journal publication based on work not included in this thesis

1. Matrix Isolation Infrared and Ab Initio Study of the Interaction of N-Heterocyclic Carbene with Water and Methanol:A Case Study of a Strong Hydrogen. A. Raut ; G. Karir; K.S. Viswanathan; J. Phys. Chem. A.;120(47); 2016; 9390-9400.

Book Chapter

"Matrix Isolation Spectroscopy – A Window to Molecular Processes" in Molecular Spectroscopy and Lasers"; Pankaj Dubey; Jyoti Saini; Kanupriya Verma; **Ginny Karir**; Anamika Mukhopadhyay; K. S. Viswanathan (Elsevier).

Synopsis

S.1 Introduction

The correlation between structure, function and dynamics, plays a pivotal role in chemical, physical and biological processes. The key to decipher the link between them is to study the structural characteristics of the chemical entities involved at the molecular level and explore their intermolecular interactions. Of the intermolecular interactions, non-covalent interactions, such as the hydrogen bonding contacts, hold a special position. Molecular recognition, enzyme catalysis, supramolecular chemistry and materials chemistry to name a few, have benefited from our increased understanding of hydrogen bonding interactions. Hydrogen bond is a directional interaction associated with energies far less than covalent interactions. The strength of the hydrogen bond ranges from ~1 kcal/mol to ~40 kcal/mol. It is this uniqueness of the energy range which lies between very weak van der Waal and strong covalent interactions that provides hydrogen bonds the flexibility to associate and dissociate quickly at ambient temperatures, in short time spans; a property which forms the basis of molecular recognition. The directional control and the ability of weak hydrogen bonds to produce strong yet extremely flexible supramolecular assemblies has given rise to the most delicate but robust architectures. Thus the need for an accurate and in depth knowledge of these non-covalent interactions has driven numerous experimental and theoretical chemists to probe them rigorously.

The hydrogen bonding interactions come in a variety of hues and shades. The very strong category of hydrogen bonds fall in energy range of 15-40 kcal/mol, such as those found in [F-H⋯F]⁻ which has stabilization energy of ~39 kcal/mol. Strong hydrogen bonds, such as those observed in O-H⋯O , N-H⋯O or O-H⋯N systems have stabilization energies in the range of 4-15 kcal/mol. Hydrogen bonds with stabilization energies in the range of 1-4 kcal/mol are termed as weak hydrogen bonds, and involve proton donors, such as C-H or S-H and acceptors such as π systems. While strong hydrogen bonds have been known to play a significant role in the determination of the properties of many substances, the weak hydrogen bonds are no less important in chemistry and biology. These weak interactions have been shown to play, through co-operativity effects, a significant role in the determination of conformations and supramolecular architecture.

Investigation of weak interactions is challenging both experimentally and theoretically. Many experimental techniques, such as X-ray, NMR, calorimetry and optical

spectroscopy have been employed for studies on hydrogen bonding interactions. Of the optical spectroscopic techniques, infrared spectroscopy has been a popular method, employed for the study of hydrogen bonds. Shifts in the vibrational frequencies of donor and acceptor groups in hydrogen bonded complexes, indicate the presence, nature and strength of hydrogen bonds. In particular, matrix isolation technique and supersonic jet expansion methods have become the techniques of choice, because of the highly resolved spectra that they offer, which consequently makes it possible to make unambiguous assignments of hydrogen bonded structures. In addition, the two techniques very often prove to be complementary; while the supersonic jet technique prepares species in their lowest energy structure, the global minimum, matrix isolation spectroscopy can often trap structures in both global and local minima. The two studies therefore allow for a better understanding of the potential surface of the weak complexes.

S.2 Motivation

Phenylacetylene has always been an enigmatic molecule, due to its multiple hydrogen bonding sites. It has the ability to exchange roles; from being a proton donor to a proton acceptor, akin to the transformation from "Jekyll to Hyde" in the R. L. Stevenson novel "The strange case of Dr. Jekyll and Mr. Hyde"; (the title of this thesis mildly refers to the title of the novel). For the same reason, phenylacetylene has also been termed as a chameleon. A study of this dual behaviour is therefore interesting. With an acidic acetylenic hydrogen and two π systems, phenylacetylene, in principle, can show a wide spectrum of structures, ranging from n-σ* to H-π contacts. Given that matrix isolation spectroscopy can locate local minima, we set out to examine the possibility of observing H- π and n-σ* structures of hydrogen bonded complexes of phenylacetylene with various precursors and study the role reversal referred to earlier. The factors affecting the stabilities of the various structures and the competition between them, were the main objectives of studying hydrogen bonding interactions of phenylacetylene. Furthermore, comparing the hydrogen bonding interactions in benzene and acetylene, the constituent moieties of phenylacetylene, with those observed in phenylacetylene, could provide useful insights.

S.3 Experimental and Computational details

Experiments were performed using matrix isolation infrared spectroscopy. The spectra of the matrix isolated species, were recorded in the region 4000-400 cm^{-1} using a Bruker Tensor 27 FTIR spectrometer, at a resolution of 0.5 cm^{-1}. The matrix was then annealed at 27 K (N$_2$) or 32 K (Ar), and the spectrum again recorded after recooling the matrix to 12 K, to observe the product bands. Experiments were performed in both Ar and

N_2 matrices. The experimental results were corroborated with *ab intio* computations performed at various levels of theory. The computational study was carried out using Gaussian-09 suite of programs. All computations were performed at M06-2X and MP2 levels, using 6-311++G(d,p) and aug-cc-pVDZ basis sets. Interaction energies of various complexes were also calculated at MP2/CBS and CCSD(T)/CBS limits. AIM, EDA and NBO analysis were performed to explore the nature, physical origin and the strength of the non-covalent interactions.

S.4 Phenylacetylene-Water Complex: Is it n···σ* or H···π in the Matrix?

In this chapter, we have revisited the hydrogen bonded system of phenylacetylene (PhAc) and water, both experimentally and computationally. PhAc has two types of π electron systems – the acetylene π and the phenyl π system, both of which can act as proton acceptor sites. In addition, the acidic acetylenic hydrogen of PhAc can also serve as a proton donor. Similarly H_2O can also serve as a proton donor or a proton acceptor. In effect, therefore, this system can be expected to show at least three types of hydrogen bonded complexes. Patwari and co-workers studied the hydrogen bonded interactions in PhAc and H_2O, using IR-UV double resonance spectrosocopy. Arunan *et al.* studied the same system using gas phase microwave spectroscopy. Both groups concluded that the global minimum corresponded to a cyclic quasi planar structure having dual interactions involving the O-H···π and C-H···O interactions. Computations indicated two other structures (Fig. S.1) which were local minima. One of these local minima, corresponded to a structure where the acetylenic hydrogen of PhAc was the proton donor; a structure not observed in the gas phase experiments. Such a structure, is referred to as the n···σ* complex, which involves a ≡C-H···O interaction. The n···σ* complex, a local minimum in the PhAc-H_2O system, actually turns out to be the global minimum in the C_2H_2-H_2O heterodimer and which has been experimentally observed. The question that we asked is whether the hydrogen bonded structures corresponding to local minima in PhAc-H_2O can at all be observed in matrix isolation experiments; a technique which is known to trap local minima.

Our experiments in N_2 and Ar matrix, have provided unambiguous evidence, through red shift of ~60 cm^{-1} in the ≡C-H stretch and the blue shift of ~ 108 cm^{-1} in the phenyl –CH out-of-plane bending modes, for the formation of the n···σ* complex, which has been observed for the first time. This conclusion was further confirmed through experiments using PhAc$_D$ and D_2O. We have not been, however, able to obtain evidence for the H···π structure,

the global minimum, in our experiments. It is likely that features due to the H⋯π structure were masked by spectral interferences of the monomer bands. Fig. S.1 shows the structures of hydrogen bonded complexes of PhAc-H_2O complexes and the spectra obtained in N_2 matrix , together with their interaction energies.

It can be inferred from the above discussion, that the structure of the global minimum of the PhAc-H_2O complex is therefore different from that in C_2H_2-H_2O complex. Interestingly the PhAc-H_2O system is also different from the C_6H_6-H_2O complex. These studies clearly indicate that changes in the interacting partners can result in significant changes in the structure of the complex.
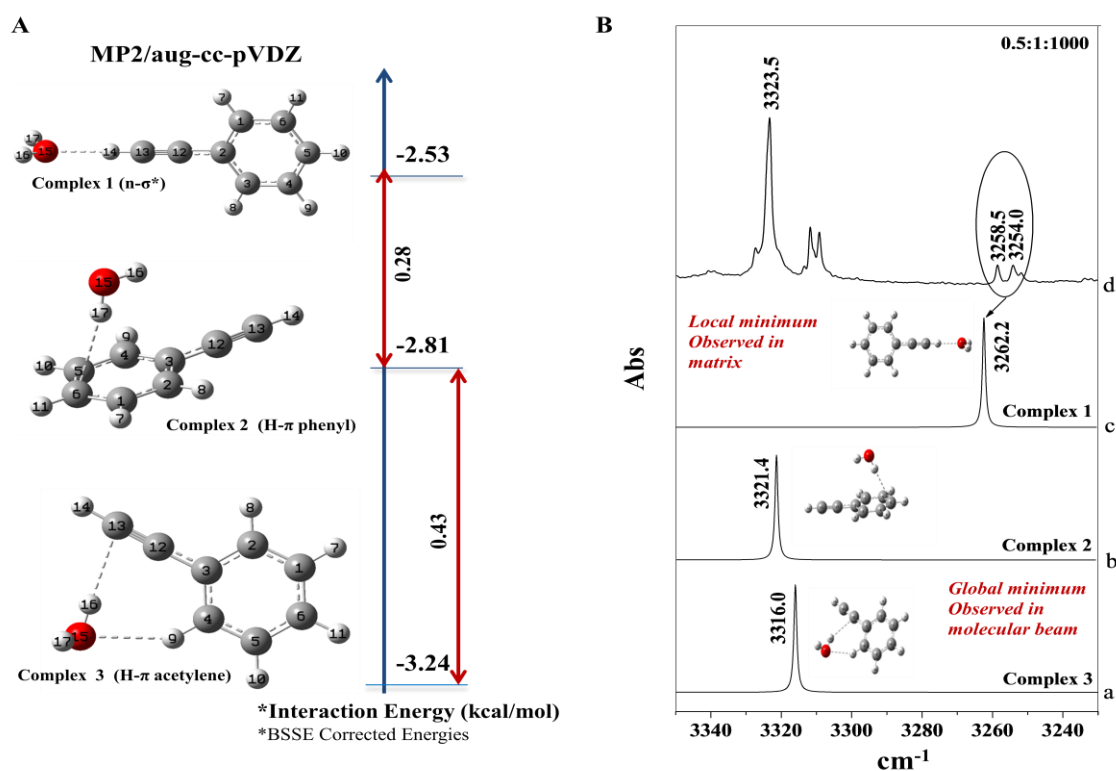
Fig. S.1 (A) Hydrogen bonded structures of PhAc-H_2O computed at MP2/aug-cc-pVDZ level of theory (B) Experimental and computed infrared spectrum of PhAc-H_2O complexes over the spectral regions 3350-3230 cm^{-1} corresponding to the ≡CH stretch of PhAc.
(a)-(c) Computed spectra of complex 3, 2, 1 respectively (d) Experimental spectrum of PhAc-H_2O (0.5 : 1: 1000) recorded after annealing N_2 matrix at 30 K.

S.5 Confirmation of the Presence of the Elusive n···σ* Complex in the Hydrogen Bonded Systems of Phenylacetylene: A Study of the PhAc-DEE and PhAc-MeOH Complexes.

With an aim of confirming the presence of the n-σ* ($\equiv$C-H··O) complex in the matrix unequivocally, we performed experiments with diethylether (DEE) and phenylacetylene. This system can perforce be expected to manifest only the n-σ* hydrogen bonded complex. A comparison of the shifts in the $\equiv$C-H vibrational frequency in PhAc-DEE with that observed for PhAc-H$_2$O would unambiguously confirm the presence of this type of interaction in these complexes. The $\equiv$C-H shift observed in the PhAc-DEE was ~90 cm^{-1} to the red, which was of the same order of magnitude as observed for PhAc-H$_2$O.

The PhAc-methanol (MeOH) system presents a dichotomy, similar to PhAc-H$_2$O system. Computations on PhAc-MeOH indicated two types of nearly degenerate O-H··π complexes, where MeOH donates a proton to the π system of either the phenyl ring or the acetylenic system of PhAc. Gas phase studies, using UV-IR double resonance as the probe, clearly identified the O-H··π complex where MeOH donated its hydroxyl proton to the phenyl ring of PhAc. Furthermore, the n-σ* complex, where PhAc donates a proton to the oxygen of MeOH was not observed in their experiments, though computations indicated this complex to be a local minima, which was only marginally less stable than the O-H··π global minimum. It was therefore thought interesting to examine if this local minimum could be observed in the matrix, much like in the PhAc-H$_2$O system.

In the case of PhAc-MeOH both n-σ* and O-H··π complex were observed in the N$_2$ matrix. The n-σ* complex was identified through the large shifts in the $\equiv$C-H vibrational wavenumbers, which corroborated with our computations. Reassuringly, the shift in the same mode in both the H$_2$O and MeOH complexes was comparable thus providing unequivocal evidence for the observation of the n-σ* complex. It might not be out of place to mention that in the case of C$_2$H$_2$, complexes with H$_2$O and MeOH yield the n-σ* complex as the global minimum. The dual interactions observed in the case of the H-π complex in PhAc, probably causes a reversal in the energy ordering in the O-H··π and n-σ* complex compared with C$_2$H$_2$. Until the work described in this thesis was reported, experiments had only identified H-π structures in phenylacetylene-H$_2$O and MeOH, and not any n-σ* isomers.

S.6 H-π Landscape of the Phenylacetylene-HCl System: Does This Provide the Gateway to the Markovnikov Addition?

In the systems described earlier with H_2O and MeOH, PhAc displayed two structures, involving n-σ* as well as H-π contacts. In the case of PhAc-DEE complexes the system was forced to display only n-σ* contact. We next addressed the question if we could choose a system that would perforce produce only the H-π contact. We chose HCl as the hydrogen bonding precursor with PhAc, since the strong acidity of HCl could be expected to produce a dominant H-π complex. Earlier experimental studies on HCl-acetylene in low temperature matrices by Barnes *et al.* and Mcdonald *et al.* observed hydrogen bonded H-π complex. Later Legon, Aldrich and Flygare studied HCl-acetylene heterodimer using Fourier Transform Microwave Spectroscopy in the gas phase and observed a T-shaped complex with HCl lying along the C_2 axis of C_2H_2. Kelsell *et al.* also performed matrix isolation experiments in Ar and observed the C_2H_2-HCl complex, where the HCl stretch was red shifted by approximately 125 cm^{-1}, from that of the uncomplexed HCl. Computations were also performed by Pople *et al.* to corroborate experimental findings on the H-π complexes.

Studies have also been reported on the π-bonded complexes, involving aromatic π systems, such as benzene. Experiments and theoretical studies undertaken by various groups, to understand the H-π interaction between benzene and HCl concluded that HCl interacts with benzene lying on the C_6 axis of benzene with the hydrogen pointing towards centre of the ring.

The combination of aromatic and acetylenic π moieties a single molecule such as PhAc poses an interesting question as to which of the two π electron systems will preferentially interact with HCl, to form the most stable isomer. Furthermore, HCl, in addition to manifesting hydrogen bonding interactions, may also exhibit halogen bonding contacts, an interaction that has been increasingly explored in recent times. PhAc-HCl system, therefore promised to be an interesting puzzle.

In this system, experimentally, we observed H-π complexes involving the acetylenic (H-π_{Ac}) and phenyl (H-π_{Ph}) contacts, which were unambiguously discerned by shifts in the infrared frequencies of the HCl vibration. Our computations also indicated the presence of both (H-π_{Ac}) and (H-π_{Ph}) interactions. Furthermore, computations also indicate the H-π_{Ac} complex to have two conformers, complex 1a and 1b, with complex 1a being the global minimum. Interestingly both conformers of the H-π_{Ac} complex and the H-π_{Ph} complex were nearly isoergic at the CCSD(T)/CBS limits, with interaction energies of ~ -4.1 and 3.6 kcal/mol respectively. The experimentally observed complexes 1a and 1b, had multiple

minima on the potential surface delineated by very small barriers, which allows for the possibility of the HCl molecule conducting a free rotation around the acetylenic triple bond. Furthermore, these H-π_{Ac} complexes also appeared to be prereaction complexes for Markovnikov addition, with complex 1b possibly serving as a gateway complex.

It was also interesting to note that while the H-π_{Ac} and H-π_{Ph} complexes had nearly equal interaction energies, they manifested different vibrational wavenumbers of the HCl submolecule. This observation was explained based on the occupancies of the σ^* orbital of HCl in the complex, calculated using the NBO methodology.

In addition, computations also predicted interactions involving the chlorine of HCl. One of these was an n-σ^*complex where the PhAc was the proton donor to the Cl of HCl, through its acetylenic hydrogen. Two other complexes were also optimized, which were likely Cl-π contacts, with bond distances between 3-3.5 Å. However, none of the complexes, n-σ^* or chlorine bonded, were observed experimentally.

S.7 The Many Facets of Phenylacetylene-Formic Acid hydrogen Bonded Complexes

In this chapter, we looked at the H-π complexes of Phenylacetylene with an organic acid which was weaker than HCl. We studied the complexes of PhAc with Formic acid (FA). FA has proton donor and acceptor sites. So is the case with PhAc, as has been explained earlier. In addition, FA exists in two conformers-trans and cis, the hydroxyl hydrogen being located on the same or opposite side of the hydrogen attached to carbonyl carbon. Consequently a number of isomers are possible for the hydrogen bonded PhAc-FA complexes, and the heterodimer potential surface therefore offers a rich landscape. While this situation is a theorists delight, it is an experimentalists' nightmare.

Interaction energies of the different isomers of PhAc-FA complexes ranged from -1 to -5 kcal/mol. Computations indicated more than 10 hydrogen bonded isomeric structures for the PhAc-FA system, involving one or more C-H···π, C-H···O and O-H···π contacts. For comparison with experiments, only those complexes involving the trans-formic acid have been considered, as the trans geometry is more stable than the cis by almost 4 kcal/mol.

Amongst all the complexes, an isomer with an O-H···π interaction, in which FA acts as proton donor through O-H group, to the acetylenic π cloud of PhAc, was indicated to be the global minimum. Experimentally, product features, which were red shifted by ~180 cm^{-1} from the features of the FA submolecule, were assigned to structures involving a O-H···π_{Ac} interaction. In addition a product feature, with a red shift of 110 cm^{-1} was also observed, which could be assigned to O-H···π_{Ph} complex.

Experiments with phenylacetylene deuterated at the acetylenic hydrogen (PhAc$_D$) were also performed, to confirm the above observation, through the isotopic effect. Clearly, the PhAc-FA system presents a challenging and interesting study, with one of the richest landscapes for hydrogen bonding complexes.

S.8 Phenylacetylene-H$_2$S and Phenylacetylene-CO Complexes

We also investigated weakly bonded complexes of PhAc-H$_2$S and PhAc-CO, both experimentally and computationally. The motivation to study these complexes was to understand the differences between PhAc-H$_2$O system and PhAc-H$_2$S in terms of structure, energy and vibrational frequencies. In our matrix isolation experiments, we could not observe any evidence for the formation of PhAc-H$_2$S complex. Computationally PhAc-H$_2$S complexes had smaller interaction energies compared with the oxygen analogue (PhAc-H$_2$O complexes). We also performed computations on the PhAc-CO system, where again no experimental evidence was obtained for the formation of this complex, in the matrix isolation experiments. In the PhAc-CO system, our computations predicted two types of n-σ* complexes; one in which the acetylenic hydrogen was bonded to C, while in the other the hydrogen was bonded to O, with interaction energies of approximately -1 kcal/mol . In this chapter, we will discuss the computational results on PhAc-H$_2$S and PhAc-CO systems.

S.9 Conclusions

We have presented an in depth study of the hydrogen bonded interactions of phenylacetylene with various precursor molecules. The interaction energy and the structure of the various complexes changes as the nature of interacting partner changes. Phenylacetylene has been shown, both experimentally and computationally, to present a variety of hydrogen bonded interactions, having stabilization energies in the range of 1 to 5 kcal/mol. All the interactions were either of H-π or n-σ* contacts. We also found that in a number of cases, secondary interactions working cooperatively with the H-π interactions, played a significant role in determining the preference of the H-π interaction over the n-σ* interaction. This aspect will be discussed with examples in the thesis.

It was also observed that some isomers of H-π complexes in PhAc-HCl and PhAc-FA systems, while being almost isoenergetic in terms of the interaction energies, displayed very different red shifts in vibrational modes of the proton donors (HCl or FA). This difference was rationalized through the analysis of electron occupancies in σ* orbitals, studied through NBO analysis.

In summary, this thesis provides direct evidence of both global and local minima of the hydrogen bonded complexes of phenylacetylene, which involves n-σ* and H-π contacts. This study therefore amply demonstrates the ability of role reversibility of the title molecule.

<h1 align="center">Chapter 1</h1>

<h2 align="center">Introduction</h2>

1.1 Introduction

The study of non-covalent interactions is one of the most widely researched topic, both experimentally and theoretically, as these interactions have been known to play a pivotal role in the structure and dynamics of many chemical and biological phenomena[1-6]. To a materials chemist, a knowledge of non-covalent interactions, allows him to tune these interactions to advantage in the design of materials for specific functions. To an organic chemist, a knowledge of non-covalent interactions, such as hydrogen bonding, leads to an understanding of many reaction pathways and conformational stability. A biologist is mainly interested in understanding the details of non-covalent interactions, as these interactions are responsible for structural stabilization of biomolecules and their specific action. For example, DNA, the carrier of genetic material has a double helical structure, the two strands being held together by hydrogen bonding interactions between the base pairs. Supramolecular chemistry uses the directionality of hydrogen bonding interactions to control the assembly of molecules at a large scale. These are but some of the examples which highlight the importance of these weak interactions and the study of which, therefore, needs no apology or defence.

Amongst the non-covalent interactions, hydrogen bonding contacts have attracted special attention. The unique characteristics of hydrogen bonding interactions originate rather ironically from the weakness of these bonds. Hydrogen bond is a type of directional interaction associated with energies far less than covalent interactions. The strength of the hydrogen bond ranges from ~1 kcal/mol to ~40 kcal/mol.[7] It is this energy range, that provides hydrogen bonds the flexibility to associate and dissociate quickly at ambient temperatures and in short time scales; a property which forms the vital basis of molecular recognition. The directional control and the ability of weak hydrogen bonds to produce strong yet extremely flexible supramolecular assemblies has given rise to the most delicate but robust architectures. Thus the need for an accurate and in depth knowledge of these non-covalent interactions has driven numerous studies in experimental and theoretical chemistry to probe them. Over last two decades a number of books and reviews have been written on hydrogen bonding interactions, which exemplifies the need to understand these non-covalent interactions[8-12].

The earliest definition of a hydrogen bond considered hydrogen to be attached to an

electronegative atom, such as oxygen, nitrogen or halogens, which then forms a bond with another electronegative atom. The concept of weak attractive interaction between two highly electronegative atoms bridged by hydrogen was first given by Latimer and Rodebush[13] in 1920. In 1935, Linus Pauling used the term 'hydrogen bond' for the first time to account for the residual entropy of ice.7 Pauling was clear and unambiguous in the use of the word *bond* when he stated that under certain conditions an atom of hydrogen is attracted by rather strong forces to two atoms, instead of only one, so that the hydrogen may be considered to be acting as a bond between the two atoms. In recent times, a number of examples of the hydrogen bond has been observed, which did not fit exactly into the earlier definition of hydrogen bond, which therefore necessitated a redefinition of this bond. One such example is the C-H$\cdots$O contact, which was first proposed by June Sutor in 1962. [14] Her original proposal met with stiff opposition, but today the C-H$\cdots$O contact is well recognized in many supramolecular architectures. Similarly, hydrogen bonds involving π systems as proton acceptors, have also been reported, such as the O-H$\cdots\pi$, N-H$\cdots\pi$ and C-H$\cdots\pi$ contacts. All these contacts manifest interaction energies ranging from a few kcal/mol to many tens of kcal/mol. Thus a large variety of hydrogen bonds have been observed now, which were earlier not considered under the realm of hydrogen bonding interactions. An IUPAC task force[15] has recently proposed a revised definition which incorporates the unconventional hydrogen bonds : *"The hydrogen bond is an attractive interaction between a hydrogen atom from a molecule or a molecular fragment X–H in which X is more electronegative than H, and an atom or a group of atoms in the same or a different molecule, in which there is evidence of bond formation."*

Electronic structure calculations have also been extensively used to study these interactions. Advances in computational methodologies and computer hardware have led to growing use of computational methods, to accurately describe these interactions. Computations together with experiments, has remarkably improved our understanding of these weak but important interactions. These interactions have also been modelled and rationalized using Pearson's hard-soft acid-base (HSAB) principle.[16] Nishio and Hirota[17] classified the hydrogen bonding interactions into four categories, based on the HSAB principle, which are; (1) conventional hydrogen bond, (2) XH/π hydrogen bonds, (3) CH/n hydrogen bonds, where 'n' is an electron lone pair and (4) CH/π hydrogen bonds, where the carbon is usually in an 'sp' or 'sp^2' hybridization. Contribution from the electrostatic forces was found to be dominant in the first three interactions, while dispersion was considered to be

important in the CH/π contact. Gilli *et al.* proposed the pK_a 'slide rule' concept, to predict hydrogen bonding strength. The binding energies and contact distances in hydrogen bonding interactions do not simply depend on the properties of donor and acceptor molecules but is also a function of difference between acidities or pK_a values (ΔpK_a) of hydrogen bond donor and acceptor.[18] It was concluded that strong hydrogen bonds contain a mixture of electrostatic and covalent components whereas the weaker ones are largely electrostatic in nature. This rule predicts that as the ΔpK_a approaches zero, it results in the formation of a very strong and symmetrical hydrogen bond interaction, having more covalent character than electrostatic character.

The hydrogen bonding interactions come in a variety of hues and shades. The *very strong* hydrogen bonds have interaction energies ranging from -15 to -40 kcal/mol, such as those found in $[F\text{-}H\cdots F]^-$. *Strong* hydrogen bonds, such as those observed in $O\text{-}H\cdots O$, $N\text{-}H\cdots O$ or $O\text{-}H\cdots N$ contacts, are classified as hard acid-hard base interactions and have interaction energies in the range of -4 to -15 kcal/mol. The weak hydrogen bonds, have interaction energies in the range of -1 to -4 kcal/mol, and usually involve proton donors, such as $–C\text{-}H$ or $-S\text{-}H$, and π systems as proton acceptors. These interactions correspond to the soft acid-soft base and hard acid-soft base interactions, like those observed in $O\text{-}H\cdots\pi$, $N\text{-}H\cdots\pi$ interactions, involving π electrons of acetylenic or phenyl systems. The $C\text{-}H\cdots O$ or $C\text{-}H\cdots N$ contacts can be categorized as soft acid-hard base interactions. These weak interactions have been shown to play, through co-operativity, a significant role in the determination of conformations and supramolecular architecture. While strong hydrogen bonds play a significant role in the determination of the properties of many substances, the weak hydrogen bonds are no less important in chemistry and biology.[19]

Investigation of weak interactions is challenging both experimentally and theoretically.9 Many experimental techniques, such as X-ray, NMR, calorimetry and optical spectroscopy have been employed to study hydrogen bonding interactions. In recent times, dynamics of formation and breaking of these weak bonds have caught the attention of experimentalists and theorists. These studies, using 2-D infrared spectroscopy[20] and molecular dynamics simulation,[21] have addressed the role of water in many of the transport processes in biology, involving the hydrogen bonds. Of the optical spectroscopic techniques, infrared spectroscopy has been a popular method employed for the study of hydrogen bonds.[22] Shifts in the vibrational frequencies of donor and acceptor groups in hydrogen bonded complexes, indicate the presence, nature and strength of hydrogen bonds. In

particular, matrix isolation technique in combination with infrared spectroscopy, and supersonic jet expansion methods have become the techniques of choice, because of the highly resolved spectra that they offer, which consequently makes it possible to make unambiguous assignments of the infrared features of hydrogen bonded structures.[23-25] In addition, the two techniques, matrix isolation and molecular beams very often prove to be complementary; while the molecular beam technique prepares species in their lowest energy structure, the global minimum, matrix isolation spectroscopy can often trap structures in both global and local minima[26], which is one of the points that this thesis will highlight. The two studies therefore allow for a better understanding of the potential surface of the weak complexes.[27-29] Experiments have also been performed where a supersonic jet source was coupled to matrix isolation experiments, to get the best of both worlds.[30]

1.2 Weak Hydrogen Bonds

The hydrogen bonding interaction is represented as 3-centre 4-electron interaction (X-H...A) between a hydrogen bond donating group X-H and hydrogen bond acceptor A.[31] In conventional hydrogen bonded systems, atoms of high electronegativity, such as oxygen, nitrogen or fluorine can act as proton acceptors, while groups such as O-H, N-H and F-H serve as proton donors. On the other hand, in weak hydrogen bonds, both donors and acceptors are of moderate electronegativity, such as π systems (proton acceptors) and –C-H, -S-H,-Se-H, -As-H, -Si-H (proton donors). In purely electrostatic terms, hydrogen bonding interaction with π systems can be regarded as the interaction of a proton donor group with a negative π electron density or the interaction of dipole with a quadrupole, such as in benzene or acetylene.

The origin of the concept that electron donors for hydrogen bonding could be π electrons and not necessarily lone pairs, was proposed by Dewar.[32] Although before Dewar could formally announce π acceptors as hydrogen bonding partners, Wolf et al.[33] studied the infrared spectra of ortho-substituted phenols in dilute CCl_4 solution and found that O-H stretch was red shifted by ~40 cm^{-1}. Consequently many gas phase and solution phase experiments confirmed that H···π interactions can indeed be termed as hydrogen bonded interactions[34-37]. It was observed in general that H-π interactions yielded spectral shifts in donor groups (X-H), smaller than in conventional hydrogen bond. A huge variety of H-π interactions exist due to variations in proton donors and proton accepting π systems. The most commonly studied π systems are benzene, acetylene and ethylene moieties.[38-41] which have many applications in biology , supramolecular chemistry and material sciences. The π

electron cloud of benene as a proton acceptor has been studied with a range of proton donors such as H_2O, HCl, NH_3 and C_2H_2. The potential energy surface of hydrogen bonded complexes of benzene show a flat potential giving rise to dynamic effects. Gas phase studies of benzene-water complex, by Zwier *et al.*,[42] shows that water molecule sits perpendicularly to the aromatic π cloud with one of the hydrogens pointing towards benzene ring and the second hydrogen pointing away. It was shown that water molecule exhibits a motion where the roles of the two hydrogen atoms are reversed. *Ab-initio* calculations predicted the interaction energy of this complex to be as low as -1.8 kcal/mol. Benzene-ammonia heterodimer was also studied in which ammonia forms a monodentate hydrogen bond with π electron density of benzene ring, with ammonia sitting on the top of plane of benzene molecule. Ammonia molecule also undergoes free internal rotation.[43] Viswanathan *et al.* studied the H-π complexes between benzene and acetylene in an Ar matrix, using matrix isolation infrared spectroscopy and *ab initio* computations.[41] They observed that while both acetylene and benzene could serve as proton acceptors through their π electron cloud, the global minimum was a structure where acetylene acts as proton donor to π cloud of benzene ring. The presence of the complex in the matrix was signalled by vibrational shifts in both acetylene and benzene submolecules. The ≡C-H stretch of acetylene which acts a proton donor in the complex showed a red shift of ~15 cm^{-1} whereas the degenerate bending mode was blue shifted by ~3 cm^{-1}. The –C-H bending mode of benzene showed a blue shift of 4.4 cm^{-1}. Acetylene can act as an amphiprotic molecule manifesting a dual role of proton donor as well as an acceptor. In case of acetylene-water[44], acetylene-ethylene[39], acetylene-benzene[41], acetylene-phenylacetylene[45], it acts as a proton donor whereas in acetylene-chloroform, acetylene-HCl it acts as a proton acceptor.[46] It should be noted that the magnitude of vibrational shifts can help in distinguishing whether molecule serves as a proton donor or proton acceptor. Generally a proton donor shows large red shifts in stretching vibrational modes, whereas proton acceptor is evidenced by smaller red shifts.[39] For example in acetylene-ethylene heterodimer, the complex in which acetylene acts as proton donor is the global minimum and shows a red shift of ~20 cm^{-1} in the ≡C-H stretch, whereas in the local minimum, acetylene serves as a proton acceptor and shows a shift of ~3 cm^{-1}.

Another class of H-π interactions which is being increasingly investigated is the S-H···π contact. Wategaonkar et al. studied hydrogen bonded complexes of H_2S with indole and 3-methyl-indole.[47] H_2S shows a preference for the formation of π type complex (S-H···π) as

1.3 Motivation of the thesis

Study of hydrogen bonding interactions in multifunctional molecules is an important area of study as real life situations often involve precursors with multiple hydrogen bonding sites. The molecule chosen in this study is one such: phenylacetylene (PhAc) (Fig. 1.1). PhAc has always been an enigmatic molecule, due to its multiple hydrogen bonding sites. It has the ability to exchange roles; from being a proton donor to being a proton acceptor, akin to the transformation from "Jekyll to Hyde" in the R. L. Stevenson novel "The strange case of Dr. Jekyl and Mr. Hyde"; (the title of this thesis mildly referring to the title of the novel). PhAc has for the same reasons also been termed as a chameleon.[58] A study of this dual behaviour is therefore interesting. With an acidic acetylenic hydrogen and two π systems, PhAc in principle, can show a wide spectrum of structures, ranging from n-σ* to H-π contacts. Given that matrix isolation spectroscopy can locate local minima, we set out to examine the possibility of observing H-π and n-σ* structures of hydrogen bonded complexes of PhAc with various precursors and study the role reversal referred to earlier. The main objective was to study the factors governing the stabilities of the various H-π and n-σ* structures, involving PhAc. The experiments were carried out using matrix isolation infrared spectroscopy and the experimental results were corroborated by high level *ab intio* computations.

We used various molecules which could act as partners with PhAc to study the hydrogen bonding interactions. The following molecules were used: H_2O, methanol (MeOH), diethyl ether (DEE), HCl and formic acid (FA), which provided for us (as will be shown by the end of the thesis) a complete panorama of structures – from a purely n-σ* interaction in

Phenylacetylene (PhAc)

→ Proton Donor Site
→ Proton Acceptor Site
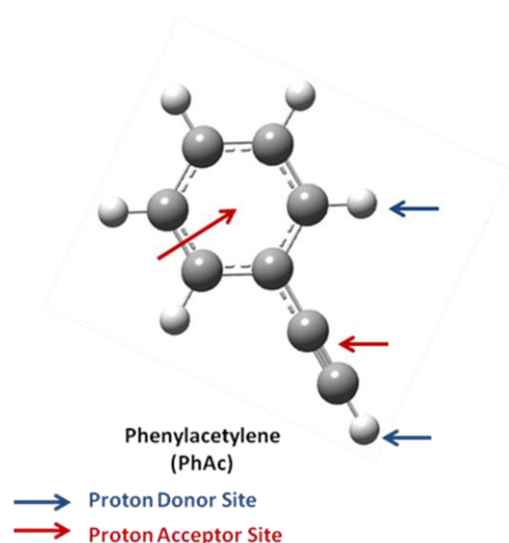
Fig. 1.1 Phenylacetylene : A molecule having multiple hydrogen bonding sites.

the case of PhAc-DEE to a dominantly H-π complex in the PhAc-HCl, with other precursors showing both possibilities. The interesting and intriguing differences between the various hydrogen bonded structures originate from subtle differences in the relative proton donating and accepting abilities of the various precursors. Conversely, these interactions can be discussed in terms of electron donation and acceptance. The ability to donate electrons in hydrogen bonded systems, is a function of energy difference between donor-acceptor orbitals, the extent of overlap between the donor acceptor orbitals and the electron occupancy in the donor orbital.

This thesis focuses on studying the effect of different precursors in fine tuning the hydrogen bonding interactions of PhAc. We have also compared the hydrogen bonding interactions in corresponding systems involving benzene and acetylene, the constituent moieties of PhAc. This comparison helped us to obtain an insight into how the structural changes in π systems can alter the geometry and hence the nature of the hydrogen bonded structure.

1.4 Phenylacetylene-WaterComplex: Is it n-σ* or H-π in the Matrix?

In this chapter, we have revisited the hydrogen bonded system of PhAc and H_2O, both experimentally and computationally. In the PhAc-H_2O complex, the global minimum was the H-π structure, which was independently observed in the gas phase, by the groups of Patwari and Arunan.[28,29] The question that we asked is whether the hydrogen bonded structure corresponding to the n-σ* complex, involving a ≡C-H···O interaction in PhAc-H_2O, which was a local minimum, can at all be observed in matrix isolation experiments; a technique which is known to trap local minima. We also further addressed the question as to what transforms the n-σ* complex from being a global minimum in C_2H_2-H_2O to a local minimum in PhAc-H_2O.

1.5 Another Look at the Elusive ≡C-H···O Complex in the Hydrogen Bonded Systems of PhAc: A Study of PhAc-DEE and PhAc-MeOH Complexes

With an aim of unequivocally confirming the presence of the n-σ* complex of PhAc-H_2O in the matrix, we performed experiments with diethylether (DEE) and PhAc. The PhAc-DEE system can perforce be expected to manifest only the n-σ* hydrogen bonded complex. A comparison of the shifts in the ≡C-H stretching frequency in PhAc-DEE, with that observed for PhAc-H_2O, would unambiguously confirm the presence of this type of interaction in both these complexes. The PhAc-DEE was shown to demonstrate one end of spectrum of hydrogen bonded complexes of PhAc, showing only n-σ* structure.

The PhAc-methanol (MeOH) system presents a dichotomy similar to PhAc-H_2O system. Computations on PhAc-MeOH indicated two types of nearly degenerate O-H···π complexes, where MeOH donates a proton to the π system of either the phenyl ring or the acetylenic system of PhAc. Gas Phase experiments inferred that the observed complex was the one where MeOH donated its hydroxyl proton to the phenyl ring of PhAc.[59] Furthermore, the n-σ* complex, where PhAc donates a proton to the oxygen of MeOH was not observed in the gas phase experiments, though computations indicated this complex to be a local minima, which was only marginally less stable than the O-H···π global minimum. It was therefore thought interesting to examine if this local minimum could also be observed in the matrix, much like in the PhAc-H_2O system.

1.6 H-π Landscape of the PhAc-HCl System: Does This Provide the Gateway to the Markovnikov Addition?

In the systems described earlier with H_2O and MeOH, PhAc displayed two structures, involving n-σ* as well as H-π contacts. In the case of PhAc-DEE complex, the system was forced to display only the n-σ* contact. We next addressed the question if we could choose a system that would dominantly manifest the H-π contact. We chose HCl as the hydrogen bonding precursor with PhAc, since the strong acidity of HCl could be expected to show a dominant H-π complex. The question that arises in PhAc-HCl system, is that which of the two π systems; the acetylenic or the phenyl in PhAc, would serve as the proton acceptor in the global minimum structure. Furthermore, HCl, in addition to manifesting hydrogen bonding interactions, may also exhibit halogen bonded contacts, an interaction that has been increasingly explored in recent times.[60,61] PhAc-HCl system, therefore promised to be an interesting puzzle.

1.7 The Many Facets of PhAc-FA Hydrogen Bonded Complexes

In the this chapter, we discuss our results on the H-π complexes of PhAc with an organic acid, FA, which was weaker than HCl and was therefore expected to show a complete panorama of structures. In acidity, it comes between water on the one hand and HCl on the other. In addition, it has strong proton acceptor sites. Furthermore, FA exists in two conformers-cis and trans, the hydroxyl hydrogen being located on the same or opposite side of the hydrogen attached to carbonyl carbon. Consequently a number of isomers are possible for the hydrogen bonded PhAc-FA complexes, and the heterodimer potential surface therefore offers a rich landscape.

1.8 Complexes of Phenylacetylene-H$_2$S and Phenylacetylene-CO

We have studied weakly bonded complexes of phenylacetylene-H$_2$S in an attempt to understand the structure and vibrational features of the S analogue of H$_2$O. It was interesting to study changes in hydrogen bonding pattern on going from H$_2$O to H$_2$S. Matrix isolation FTIR experiments were performed in N$_2$ matrix along with computational investigation using *ab initio* calculations. In gas phase experiments performed by Arunan and co-workers, an H-π complex was observed in the PhAc-H$_2$S system, where H$_2$S acts as proton donor to the phenyl π electron cloud of PhAc.[62] We, therefore studied this system to explore the vibrational features of the PhAc-H$_2$S heterodimer.

PhAc-CO system was also studied to understand the weak interaction involving CO as a base with PhAc. CO can form two kinds of n-σ* complexes with PhAc, with the acetylenic H of PhAc interacting with either the C or O end of CO. It was interesting to study which of the two isomers would be observed in matrix experiments.

In summary, this thesis, using both experimental (matrix isolation infrared spectroscopy) and computational methods to corroborate the experiments, aims at studying an assortment of hydrogen bonded complexes, ranging from n-σ* to H-π systems. The study also aims at trapping not just the global minimum but also local minima, where possible; thus offering to open a large window in the study of weak hydrogen bonded systems. This study attempts to demonstrate and rationalize the role reversibility of the title molecule; from being a proton donor in some cases to a proton acceptor in the others.

Chapter 2
Experimental and Computational Methods

2.1 Introduction

Matrix isolation is an experimental technique which involves trapping molecules of interest in an inert solid, which serves as the matrix. This procedure attempts to isolate the analyte molecules by diluting them with a large excess of an inert gas, such as Ar, N_2, Kr etc, and depositing the mixture as a solid film, on to a cold substrate, maintained at a very low temperature of ~10 K. It is a technique generally used to study highly reactive species, reaction intermediates, exotic molecules, non-covalently bonded complexes and molecular conformations. The cartoon shown in Fig.2.1 below, depicts a character, frozen in ice, much like the analyte molecules in a cryogenic inert matrix.[63] In essence, this technique oftentimes can preserve reactive species by freezing them in the matrix, to be studied at leisure. This sample preparation technique is coupled with spectroscopic tools to study the chemical structure, bonding and reactivity of the trapped species.

The technique was initially developed independently by Pimental and Broida to study reactive species, which otherwise was difficult to study due to their fleeting lifetimes.[64-68] For want of a reaction partner, these reactive intermediates are prohibited to undergo reactive collisions, which consequently leads to an increased lifetime, and thus enabling one to study these species. Even if the molecule had the possibility of undergoing unimolecular reactions, the relatively large barrier at the low temperatures, due to the pooling of the molecules into their lowest rovibrational levels, prohibits their reaction.

In this experiment, the vapours of sample molecule are mixed with a large excess of an inert gas, in ratios of 1000:1 (matrix:sample). This gas mixture is then effused through a nozzle, into a vacuum system, housing a cryostat, onto which a substrate is mounted. The sample together with the matrix gas, deposits on the substrate, forming a thin film. After sufficient amount of material is deposited on the substrate, a spectrum of the deposited sample is recorded. The temperature of the cryotip is usually maintained at ~10 K, though ~4 K has also been used. Since the molecules are immobilized in inert matrix at cryogenic temperatures, broadenings due to collision and Doppler effects are absent. The low temperature in the matrix also ensures that only lowest rovibronic and electronic levels of the analyte are populated, which results in significant reduction of spectral congestion. Furthermore, the high dilutions employed in the experiments, causes the analyte molecules to

be isolated from each other and surrounded only by the inert gas atoms; in other words the analyte molecule resides in a cage of inert matrix atoms. The inert environment, small linewidths and uncongested spectral features makes this technique a powerful tool for the study of weak non-covalent interactions, conformations and reactive species. The line widths obtained in matrix isolated spectra range from 2-4 cm^{-1} as compared with the 40-60 cm^{-1} linewidths, typical of condensed phase spectra. At such large dilutions, intermolecular interactions between the sample molecules are almost negligible. Fig.2.2 highlights the technique of matrix isolation depicted as a cartoon.

The basic technique of matrix isolation uses a combination of several distinct technologies, which are interdependent on each other and work cooperatively to produce the desired low temperature rigid matrix film. The need for rigid matrix requires a low temperature, which is provided by cryogenic technology, which in turn work efficiently only under high vacuum conditions. The thin films produced and maintained under high vacuum, can only be probed by spectroscopic methods. In summary this technique effectively utilizes the high vacuum technology for maintenance of low temperature and purity required for the experiment, cryogenic methods for production of very low temperatures and a spectroscopic probe to analyse the rigid film produced.

Various spectroscopic probes can be employed to study and characterise the matrix isolated species. UV/visible,[69] infrared, fluorescence[70] and ESR Spectroscopy[71] have been used to study the matrix isolated species. In addition to these techniques, other spectroscopic tools such as Raman spectroscopy, is also becoming popular.[72] The choice of cold window, which acts as a substrate for deposition of matrix, depends on the technique used for analysis. KBr or NaCl windows can be used for infrared spectroscopy for the range of 4000-400 cm^{-1}, whereas for analysis below 400 cm^{-1}, CsBr or CsI windows are used. For UV/visible spectroscopy, quartz is often used, while for ESR, copper or sapphire tipped copper rods are used as matrix substrates.

The success of matrix isolation experiment greatly depends upon the choice of matrix material used. The most important characteristic is chemical inertness of the material, to avoid any reaction between the matrix and the trapped species. It should be free from impurities and be transparent in the range, where the analyte absorbs, to prevent any spectral interference. Rigidity of matrix material at low temperature is also essential to prevent diffusion of sample molecules. Rare gases, such as Ar, Kr, Ne, Xe and other chemically inert gases like N_2 are generally used as matrix gases.

Fig. 2.1 Cartoon depicting the process of matrix isolation: a character trapped (isolated) in ice matrix.
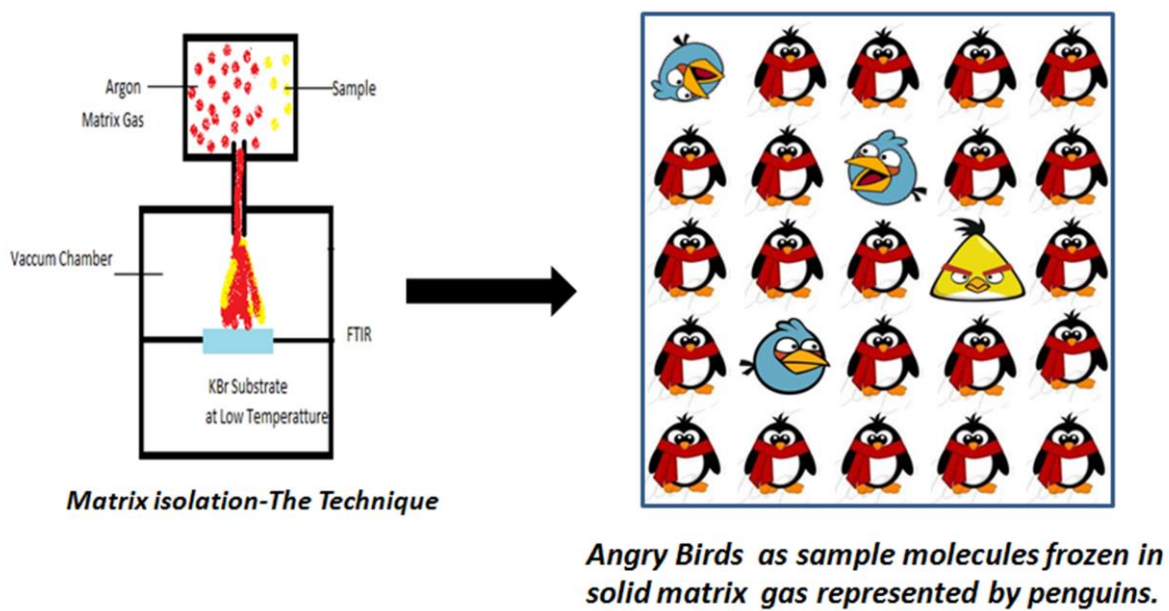
A

B

Fig.2.2 Matrix Isolation-(A) procedure (B) result

These materials fulfil the necessary condition of chemical inertness and transparency in the working window employed; hence are most commonly used. As a rule of thumb, the temperature of the cold window should be kept at 30% below the melting point of the matrix material used, to ensure rigidity of the matrix material. Below this temperature, essentially no diffusion of isolated species is expected to occur. Experiments using fluorescence spectroscopy as a technique to detect matrix isolated species use alkanes as a matrix material, often referred to as Shpolskii matrices. Materials other than the above mentioned matrices, which can be employed as matrix materials are-hydrocarbons such as CH_4, O_2, CO_2, SF_6, CO etc. But all these materials suffer from other disadvantages, such as reactivity to the host material and spectral absorptions in the window of interest.

The inert matrix material is supposed to have minimal interactions with the sample molecules ideally, but in actual practice the matrix-isolated species are not completely free of intermolecular interactions, since there exists no chemical that is perfectly inert. The magnitude of these effects are however negligible in solid rare gases. While the inert gases are minimally perturbing, it must be recognized that the trapped species are perturbed by the matrix material and thus the role of matrix cannot be ignored. The various effects of the matrix are described in following sections.

2.2 Advantages of Matrix Isolation Technique

The most important advantage of matrix isolation technique is that it provides spectra with very sharp line widths (2-4 cm^{-1}) as compared to the spectra obtained in condensed phase spectroscopy, as already mentioned in the earlier section. The small line widths of the trapped species result from isolation of the analyte molecules in the cage of solidified inert matrix which minimizes the intermolecular interactions. The sharp linewidths obtained in matrix isolation spectra are used to advantage for studying non-covalent interactions. The non-covalent interactions result in vibrational frequency shifts which range from ~2 cm^{-1} for very weak interactions to 800 cm^{-1} for the very strong hydrogen bonded complexes. Sharp line widths are therefore useful, or even imperative, for detecting very weak hydrogen bonded complexes showing a frequency shift of a few to a few tens of wavenumbers, which otherwise are not easy to identify in condensed phase spectra. Matrix Isolation FTIR is particularly advantageous to detect unambiguously such weak hydrogen bonded complexes.

2.3 Challenges in Matrix Isolation Technique

The technique of matrix isolation technique requires that the sample to be studied have sufficient vapour pressure, at easily attainable temperatures, which can be deposited on the cold substrate, so as to obtain a detectable signal. However, the use of high temperatures is associated with the danger of decomposing the sample molecule itself. Therefore non-volatile substances having negligible vapour pressure are difficult to be studied through matrix isolation technique.

2.4 Solvation Effects of Matrix

a. Matrix Shifts

As mentioned above, the so called chemically inert matrix (rare gas/N_2) does interact with the sample molecules, which is evident from the shifts in frequencies of molecules trapped in the matrix, compared with their gas phase spectra. These frequency shifts represent the magnitude of perturbation of vibrational levels of the sample molecules by the matrix molecules. The strength of this interaction can be elucidated from the difference in frequency ($\Delta\nu$), of the sample molecule in matrix relative to the gas phase values

$$\Delta\nu = \nu_{matrix} - \nu_{gas}$$

The interaction of matrix material with the sample molecules arise mainly due to following interactions - electrostatic ($\Delta\nu_{elec}$), dispersion ($\Delta\nu_{disp}$), inductive ($\Delta\nu_{ind}$) and repulsive ($\Delta\nu_{rep}$). The rare gas matrices are assumed to be weakly interacting with the sample molecules; therefore electrostatic ($\Delta\nu_{elec}$) and inductive ($\Delta\nu_{ind}$) interactions are minimal, leaving the rare gas matrix-molecule interaction dominated by long range London dispersion ($\Delta\nu_{disp}$) and short range repulsive ($\Delta\nu_{rep}$) forces. The frequency of a particular species trapped in the matrix can show blue or red shift with respect to gas phase frequencies. This behaviour was explained theoretically by Pimental and Charles using the Buckhingham equation, which can predict the effect of size of cage cavity on the direction of the frequency shift (red or blue).

$$\Delta\upsilon = (\upsilon_{matrix} - \upsilon_{gas}) = (B_e/hc\omega_e)(U" - 3AU'/\omega_e)$$

$B_e = h/8\pi^2 c\mu r_e^2$ is the rotational constant,

a = Anharmonicity constant,

U = Energy due to solute-solvent interaction,

$U' = \{\partial U/\partial r_{BC}\}$ and $U'' = \{\partial^2 U/\partial^2 r_{BC}\}$, r_{BC} = equilibrium distance between atom B and C of molecule ABC as shown in Fig.2.3.

ω_e = Harmonic oscillator frequency
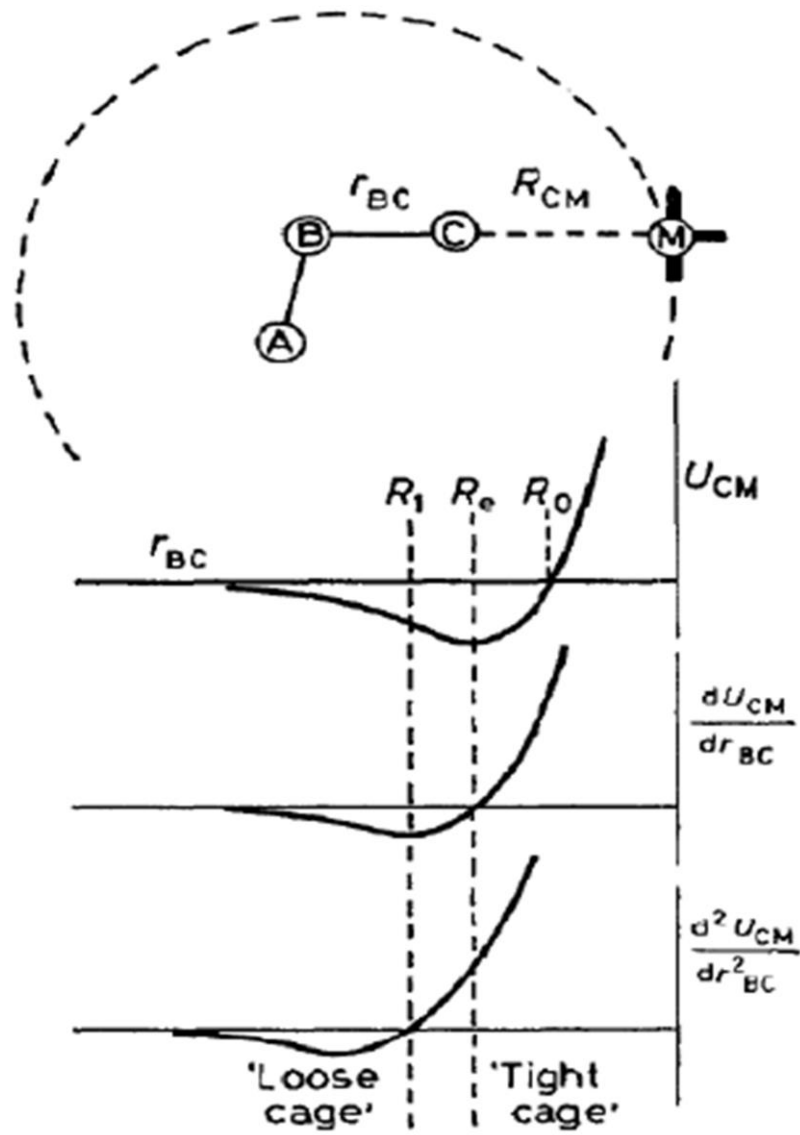
Fig.2.3 Plot showing the dependence of U, U' and U" on matrix cage size

Figure 2.3 shows the effect of matrix cage size on U, U' and U". A tight cage would imply that the distance between the atom C and matrix atom M i.e. R_{CM} is less than R_e, therefore U' and U" are positive, which results in positive value of $\Delta \upsilon$ and hence a blue shift. When host atoms are placed at a larger distance from matrix atoms, i.e they are held in a loose cage, the resultant $\Delta \upsilon$ is negative and it results in a red shift. Thus the red shift observed in high frequency vibrations such as stretching modes of a polyatomic molecule and blue shift in low frequency vibrations such as bending and rocking modes are rationalized. The high frequency modes, such as stretching, are small amplitude modes and mimic the loose cage effect. Consequently, they show red shifts; while large amplitude low frequency modes, which mimic a tight cage effect, show blue shifts. Thus it is important to understand the matrix effects to interpret the spectra of matrix isolated species accurately.

b. Multiple Trapping Sites

The matrix gas when solidified adopts either hexagonal close packed (hcp) or face centred cubic (fcc) crystal structure, depending on the matrix gas used. The sample molecules may get trapped in either the interstitial sites or substitutional holes in which case the same molecule faces environment of slightly different geometries, possibly inducing different shifts. This results in either broadening or splitting of single vibrational mode into multiplet structure. The intensity of each band corresponding to different site varies according to the stability of each trapping site. This phenomenon of trapping of sample molecule in different sites leading to multiplet structure of a vibrational mode is usually termed as site effect. The identification of the site effect can be recognised by changing the matrix, since it is highly unlikely that two different matrices will give rise to exactly similar sites. Annealing the matrix at elevated temperature causes the unstable sites to vanish, thus generally sharpening the spectral features. Molecules trapped in stable sites persist even on annealing. The distribution of different sites can also be varied by varying the rate of deposition, and the effect can be used to study the problem of multiple sites.

c. Molecular Rotation in Trapping Sites

Matrix isolated species are immobilized in the rigid matrix, essentially inhibited to rotate freely. However some small molecules like water, ammonia, methane and alkali halides show quantised rotations in some matrices. In general, unsymmetrical matrix sites hinder rotational motion but there are exceptions such as H_2 in nitrogen matrix. Temperature cycling can clearly reveal the rotational features by reversible intensity changes. The reversible intensity changes occur due to change in population of rotational energy levels.

d. Aggregation

Matrix isolation of an analyte molecule is assured only at very high dilutions, where the matrix/analyte (M/A) ratio is greater than 1000:1. At lower M/A ratios, the possibility of trapping the molecular aggregates like dimers, trimers along with the monomeric species increases considerably. Hence it becomes necessary to do concentration dependence studies, which give us insight on aggregation of the solute molecules in the matrix. The probability of isolation can be calculated as shown below for a molecule such as carbon monoxide, which occupies a single substitutional site. The probability of interaction is simply the chance of finding another molecule occupying one of the 12 nearest neighbour sites, that form the cage. The chance for the absence of the second CO molecule is given by the formula $P = (1 - r)^{12}$, where r is the reciprocal of the matrix ratio. For very small values of r, the expression becomes, $P = 1 - 12r$. From this it is clear that a matrix ratio of 1000 is needed to ensure 99% isolation. It is found experimentally, for example, that carbon monoxide forms dimers or higher aggregates to the extent of several percent at a matrix ratio of 1000 in argon, rather than the 1% expected on the basis of the above analysis. Lithium atoms will dimerize completely even with matrix to analyte ratios of 10,000:1, unless matrixes that rigidify at a very fast rate are used. Aggregation effects can be eliminated by carefully choosing the concentration window of solute molecules without compromising on the intensity of monomeric spectral feature.

e. Lifting of degeneracy of Vibrational Levels

The symmetry of the site occupied by molecules can also contribute towards matrix effects. The different vibrational modes of molecules experience varied perturbations in the different sites. In case of degenerate vibrational modes, the asymmetry of the trapping site can cause the lifting of degeneracy of the vibrational levels, leading to a splitting of the degenerate vibrational modes, such as in CO_2 and C_2H_2, in N_2 matrices. Between N_2 and Ar, N_2 has been reported to interact more strongly with the sample molecules relative to Argon.

2.5 Matrix isolation Infrared Set up

The instrumentation of matrix isolation set up involves the following components:

1. Cryostat and Associated Units
2. Vacuum System
3. Sample Introduction
4. FTIR Spectrometer

a. Cryogenic Assembly

The cryostat producing a temperature of 12 K is the heart of the matrix isolation set up.

In all our experiments, we used a closed cycle helium compressor cooled cryostat CH-202w/HC4E1 Model (Sumitomo Heavy Industries Ltd.) which can attain a temperature of ~12K. Such refrigerators are commercially available with helium as working fluids. The cryostat used in our setup works on the principle of Gifford-McMahon (GM) cycle. The important constituents of a closed cycle cryostat are:

1) Compressor   2) Expander   3) Vacuum Shroud   4) Radiation Shield

The GM refrigeration cycle takes place at the expander, commonly known as the cold head or cold finger. It is connected to a compressor through two gas lines for the flow of the working fluid (He). One of the gas lines supplies high pressure helium gas to the expander, the other gas line returns low pressure helium gas from the expander. The helium gas flow is maintained by the compressor. The vacuum shroud surrounding the cold end of the expander in vacuum, limits the heat load on the expander caused by conduction and convection. The radiation shield is actively cooled by the first stage of the expander and insulates the second stage from the room temperature thermal radiation being emitted from the vacuum shroud. In addition to these major components, the closed cycle cryocooler is often accompanied by an instrumentation skirt, which provides a vacuum port, electrical feedthroughs, as well as a temperature controller to measure and adjust the sample temperature.

The other associated components include an electronically controlled temperature controller unit (Lakeshore Instruments-Model 335) which helps to maintain temperatures between 12 K to 300 K, using a heater mounted on the cold finger. Regulation of the temperature is achieved by using a closed loop PID (Proportional-Integral-Derivative) controller, coupled to a heater unit. A silicon diode sensor is used for monitoring the temperature. Temperatures above 12 K are required to anneal the matrix, to promote diffusion of the trapped species, resulting in complex formation. Temperature variation is also required to study the effect of multiple sites on the vibrational features of the trapped species. The compressor is cooled by 3kW water chiller system (Werner Finley) that maintains flowing water at an approximate temperature of 17°C. Fig. 2.4 and 2.5 shows the cryostat and the associated units.

b. Vacuum System

The cryogenic system to produce very low temperature and the spectroscopic probe both require the setup to function under high vacuum conditions ($\sim 10^{-6}$ mbar or lower). The vacuum obtained in our experimental setup is attained using a diffusion pump. First a mechanical rotary pump (Hind Hivac; ED6), operating at a pumping speed of 200 L/min provides a rough vacuum of about 10^{-2} mbar, which is then followed by a vapour diffusion

pump (Edwards, Diffstak MK2 series 100/300) operating at a pumping speed of 300L/sec. Working of diffusion pump is based on momentum transfer to gas molecules from a directed jet of oil. Vapour is conducted upward through a tower above the boiler to an array of fine nozzles from which the vapour is emitted in a jet directed downward and outward toward the pump walls. The diffusion pump walls are usually water-cooled so that molecules of the working-fluid vapour condense before their motion is randomized by repeated collisions. The walls of the diffusion pump are cooled by water from a chiller (Werner-Finley). The diffusion pump requires to be backed by the rotary pump, and the two pumps together achieve an ultimate pressure of ~1 x 10^{-6} mbar. The vacuum is measured using a digital Penning gauge (Hind Hivac) and a Pirani Gauge 26 (Edwards APG 100 Active Pirani Gauge) (Fig.2.6).

c. Fourier Transform Infrared Spectrometer (FTIR)

The matrix isolated molecules are studied in these experiments using a Bruker-Tensor 27 FTIR Spectrophotometer (Fig. 2.6). The instrument was operated at a resolution of 0.50 cm^{-1}. In all the experiments 8 scans were coadded to obtain a spectra, with a good signal to noise ratio.

d. Sample Introduction

As mentioned above, this technique isolates the sample molecules by diluting them with large excess of matrix gas. The sample/inert gas mixture is prepared in a stainless steel mixing chamber of 1L capacity connected to the cryostat, using quarter inch diameter Cu tubing.The mixing chamber contains 5 ports, which can be connected to sample holders via glass stop cocks, and to the vacuum chamber housing the cryostat through a Cu line fitted with Swagelok connectors and valves (Fig. 2.7). The mixing chamber itself was pumped using a diffusion pump backed by a rotary pump. A pressure gauge is fixed to the mixing chamber, to monitor the pressure in the chamber. In an experiment, the mixing chamber was filled with an appropriate quantity of the species of interest, and the chamber was then topped to about 1000 mbar with the matrix gas, to eventually obtain the desired sample to matrix ratio. The flow of sample and matrix gas mixture to the cold KBr window, during the deposition was was achieved using a needle valve (Model: EVN 116, Pfeiffer Vacuum). Typical flow rates used in an experiment was ~3 mmoles /hr of the matrix gas.

The experiment commences with first pumping down the cryostat chamber and the mixing chamber to a pressure less than ~1 x 10^{-6} mbar. The mixing chamber is then isolated from the cryostat chamber through a bellows valve. The mixing chamber is then filled with the matrix and the sample at the desired ratios. In all the experiments discussed in this thesis,
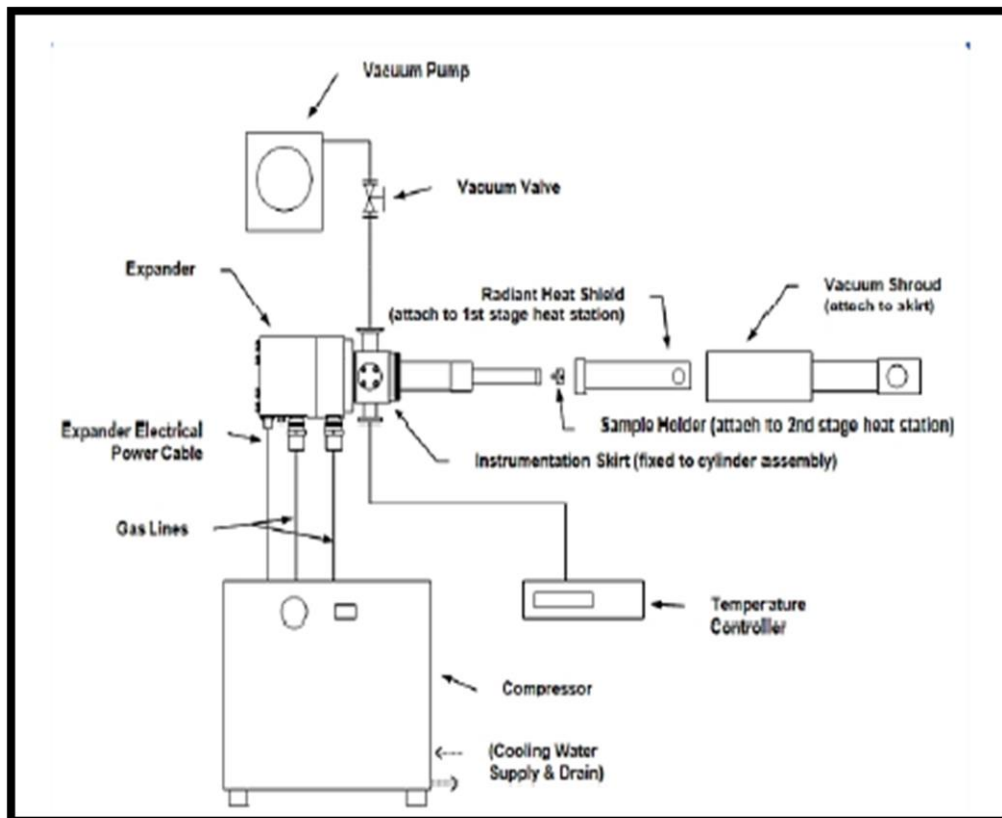
Fig.2.4: (A) The general schematic diagram for the cryosystem assembly
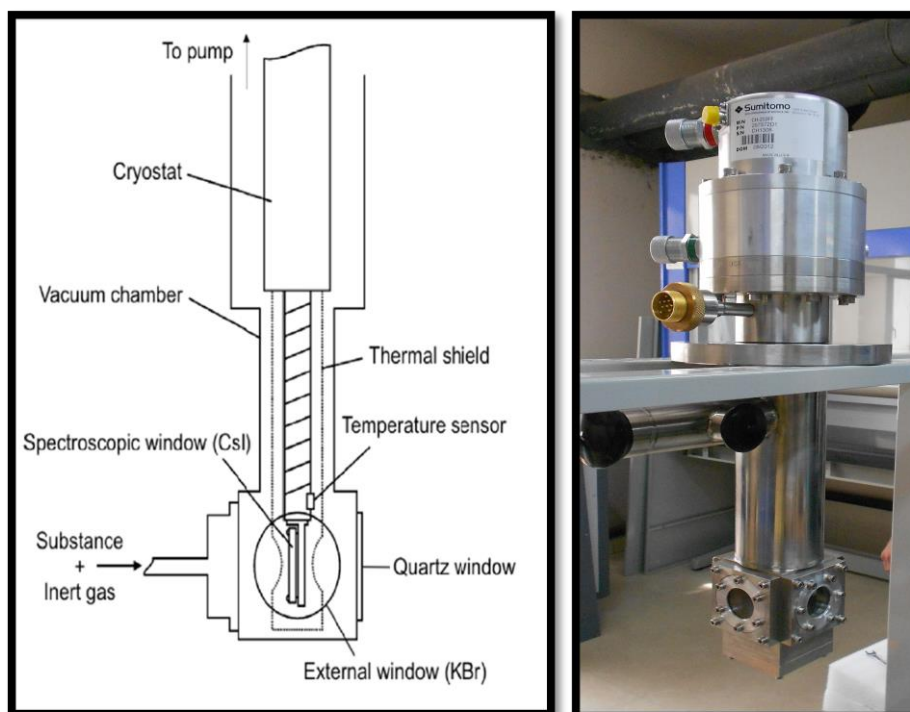
Fig. 2.4: (B) The schematic for the cryostat head mounted on the FTIR Spectrometer

(C) Picture of the cryostat mounted in Matrix Isolation set up at IISER Mohali

Cryostat without thermal shield

Helium Compressor
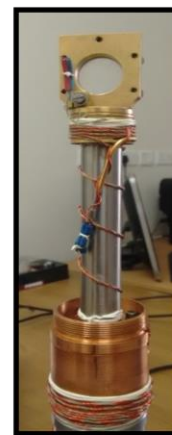
Cryostat without radiation shield

Helium Hoses

Temperature Controller

Fig. 2.5 Cryostat and Associated Units

(A) Penning Gauge
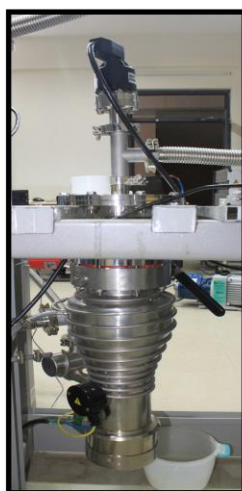
(C) Diffusion Pump

(B) Pirani Gauge
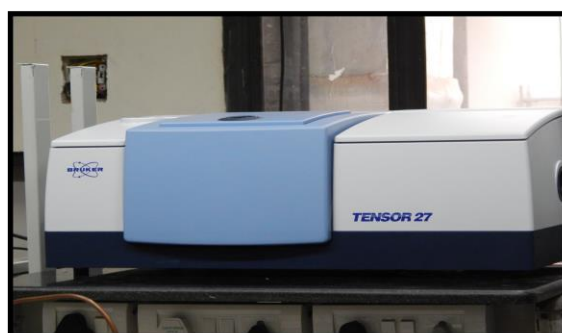
(D) FTIR Spectrometer

Fig. 2.6 Vacuum System (A-C) and (D) FTIR

the compounds had to be cooled, using liquid nitrogen/ethanol slush baths, to appropriate temperatures to obtaine the desired matrix to sample ratios. The temperature required to maintain the vapour pressure was obtained from vapour pressure data of the sample and the use of the Clausius Clayperon equation. The mixture was then introduced to the vacuum system through the needle valve, connected to an effusive nozzle. The effused gas mixture was deposited on a KBr substrate mounted on the 12 K cryotip. In some experiments, a double jet nozzle was used, where it was necessary to codeposit two precursors separately. In the double jet nozzle, one of the samples, say HCl, is effused through one nozzle, while from a second nozzle, the matrix gas together with the second precursor, say N_2/PhAc, is allowed to effuse out. Fig. 2.7 shows different sample introduction assemblies and flow control valve.

After deposition of the matrix/sample onto the cold substrate, a spectrum was recorded. The matrix was then annealed to encourage the diffusion of the trapped species to enable complex formation. The process of annealing was done by raising the matrix temperature to 27K for N_2 and 30 K for Ar, maintained at this temperature for about an hour and then recooled to 12 K. A spectrum was then recorded. New features that were observed following annealing were generally due to the products formed during the annealing process. That the new features really belonged to the products were confirmed by performing concentration dependence studies. In the concentration dependence experiments, the concentration of each precursor was independently varied to ensure that the intensity of the product features depended on the concentration of each of the precursors. Only then, could the features be considered as arising due to complex formation.

2.6 *Ab Initio* **Computations**

The computational study on the hydrogen bonded complexes was carried out using Gaussian-09[73] on a Fujitsur Workstation. Some computations were also performed using the GAMESS suite of programs.[74] The following protocol was followed in the computations.

1) Geometry Optimization

2) Vibrational Frequency Calculations

3) Computation of the Interaction Energy of Complex

4) Zero Point Energy Correction and BSSE Correction for the interaction energy

5) Calculations for the isotopic species, wherever required

6) Analysis of electron density topology using Atoms-in-Molecules (AIM) method

7) Natural Bond Orbital (NBO) Analysis to understand the orbitals involved in the formation of the complex
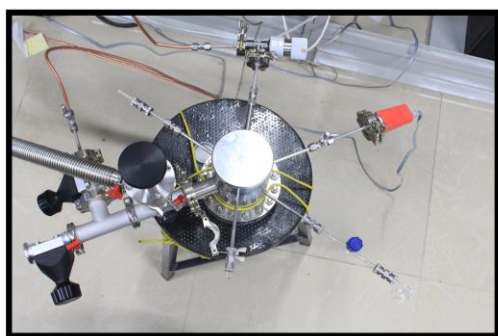
(A) Mixing Chamber (Top View)
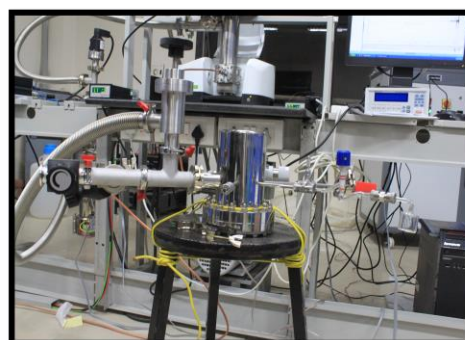
(B) Mixing Chamber (Front View)
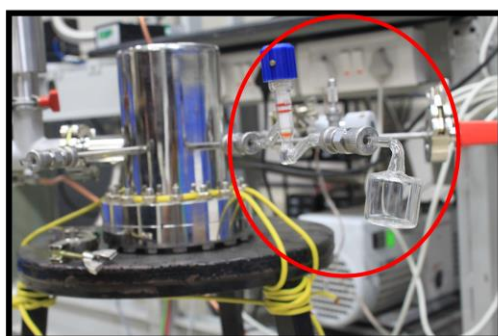
(C)Sample Holder

(D) Needle Valve

Fig. 2.7 Sample Introduction Assembly

A- Cryostat
B- Diffusion Pump
C- FT-IR
D- Mixing Chamber
E- Data Acquisition
F- Sample Container
G-Inert Gas Cylinder
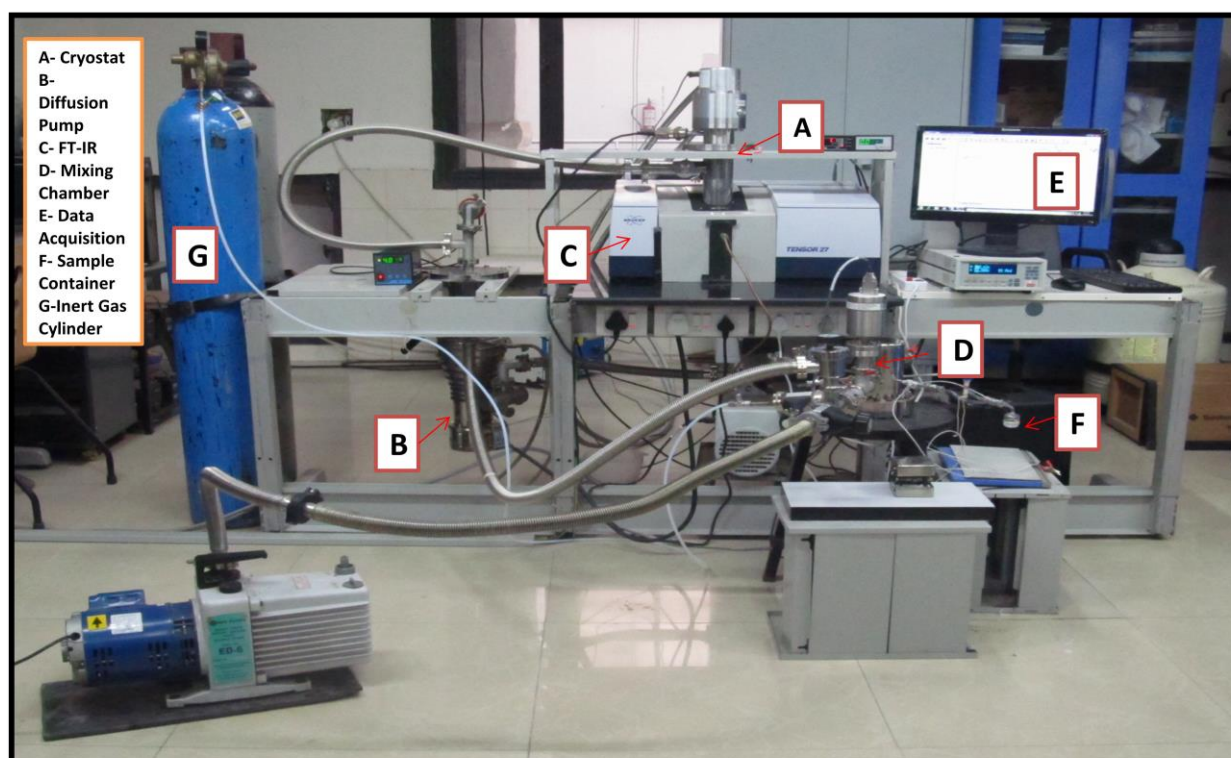
Fig. 2.8 Matrix Isolation Set Up at IISER Mohali

24

8) LMO-EDA analysis to understand the partitioning of the interaction energy into component interactions, such as electrostatic, dispersions etc.

9) Solvent Effect Calculations-Onsager Self Consistent Reaction Field Model and PCM Model

a Geometry Optimization and Vibrational Frequency Calculations: The computational study of non-covalent interactions begins with optimization of the structure of the individual submolecules involved in complex formation. The optimized geometry of the submolecules were then used to obtain the geometry of the complexes subjected to optimization protocol in Gaussian 09 package to construct the hydrogen bonded complexes between the two subunits.[73] Optimization refers to a finding a set of geometrical parameters such as bond length, bond angles and dihedral angles for a molecular species which corresponds to the stationary point on the potential energy surface. This structure could correspond to a minimum on the surface or to a saddle point, which is then characterized using frequency calculations. The optimization protocol starts by giving an initial guess of the molecular structure. The energy and gradient are calculated at the point on the potential surface corresponding to the initial geometry and then this information is used to determine in which direction and to what extent the next step should be taken to improve the geometry. At the minimum in the potential energy curve all the forces will be zero. In the case of Gaussian suite of programmes, the minimum energy structure of the molecules is achieved when the forces, the root mean square of forces, the calculated displacement and the root mean square of the displacement for the subsequent step reach values below specified threshold values. All computations were performed using Møller-Plesset second order perturbation (MP2) and density functional methods such as M06-2X, using 6-311++G(d,p) and aug-cc-pVDZ basis sets. Single point calculations at MP2/aug-cc-pVTZ, MP2/aug-cc-pVQZ, CCSD/aug-cc-pVDZ and CCSD(T)/aug-cc-pVDZ were also performed using optimized geometries at MP2/aug-cc-pVDZ level.

Frequency calculations were performed at the same level of theory as that used for geometry optimization. The second derivative of the energy term at the critical point evaluates vibrational frequencies for that particular geometry. For a minimum on the potential surface, all vibrational frequencies should be positive, whereas for points corresponding to saddle points, there can be imaginary frequencies for one or more modes of vibration. Vibrational frequency computations were done to ensure that the computed structures corresponded to minima on the potential surface and also to assign the vibrational features observed in the experiments. For the M06-2X calculations, the optimization and

harmonic frequency calculations were done using opt=tight and int=ultrafine options in Gaussian 09, as suggested by Vincent *et al.* [75] The computed frequencies of the complexes, were scaled by using appropriate scaling factors to enable a comparison with experimentally observed features. The scale factors were calculated by bringing the computed frequencies of *monomeric* species, in agreement with the observed experimental frequencies, in a given matrix. We generally use different scale factors for different frequency regions as these regions are perturbed differently by matrix. The scale factors were then used to scale the computed features of all the complexes. Details regarding the computation of the scaling factors are given in chapter 3. Vibrational spectra were simulated using the scaled vibrational wavenumbers and the intensity obtained from the vibrational analysis implemented through Gaussian. All computed spectra for the precursors and the complexes were plotted using spectrum synthesis program, Synspec,[76] and were compared with the experimental spectra. Synthetic spectra were obtained using a Lorentzian lineshape and a full width at half maximum (FWHM) of 1.0 cm^{-1}.

b. Stabilization Energy Calculation of Complexes

The interaction energies of the hydrogen bonded complexes are evaluated to characterize the stability of the complex. The interaction energies were calculated by using the supermolecule approach i.e. by subtracting the sum of energies of monomers from the energy of the complex, obtained at the same level of theory.

The Interaction Energy (E) of a complex is given by

$E = E_{AB} - (E_A + E_B)$ ………. (1)

where, E_A, E_B and E_{AB} represent the energies for the monomers A, B and complex AB,

respectively. Negative value of interaction energy signifies that the complex is more stable relative to the precursors. The interaction energy of the complex, E_{ZPE}, corrected for zero point energy (ZPE) was also calculated as follows.

$E_{ZPE} = E_{cal} + ZPE$………. (2)

In our studies, the stabilization energies of the complexes corrected for the basis set superposition errors (BSSE) were also computed. A simultaneous correction for ZPE and BSSE were not performed, as such a simultaneous correction, is known to overcorrect the stabilization values.[77,78] The origin of the BSSE arises from the basis set artifact. When the energy of complex (E_{AB}) is computed, the basis functions used are those of both the monomer subunits. Whereas, for computing the energy of the individual precursors (i.e. E_A and E_B), the basis functions correspond to only one of the precursors used. As the number of basis functions becomes larger in the computation of the complex, the energy obtained will be

lower, simply from the larger basis sets. Interaction energies thus derived from the calculated energies E_A, E_B and E_{AB} will be overestimated and the error is referred to as the basis set superposition error (BSSE). One way to eliminate the BSSE is to increase the basis set sufficiently to offset the above errors, with the tradeoffs of large computation times for even small systems. However, the commonly used method to correct for BSSE is through the use of the counterpoise correction method proposed by Boys and Bernadi.[79] In this scheme, all the energies of monomer E_A, E_B and the complex E_{AB} are computed in the same basis set spanned by the functions of the complex AB.

The Interaction energies are then obtained as follows:

$E = E_{AB}$ (AB) $– \{E_A$ (AB) $+ E_B$ (AB)$\}$ …….. (3)

Where, E_A (AB) = Energy of the monomer A using the basis set of AB

E_B (AB) = Energy of the monomer B using the basis set of AB

E_{AB} (AB) = Energy of the complex AB using the basis set of AB

Single point calculations at MP2/aug-cc-pVTZ, MP2/aug-cc-pVQZ, CCSD/aug-cc-pVDZ and CCSD(T)/aug-cc-pVDZ were also performed using optimized geometries at MP2/aug-cc-pVDZ level. Interaction energies at MP2/CBS limit were calculated using two point extrapolation method by Helgaker $et\ al,$.[80] which employs the MP2/aug-cc-pVXZ level where X represents triple and quadruple zeta basis set, given by Equation (4)

$$\Delta E_{MP2/CBS} = \frac{4^3 \times \Delta E\ (pVQZ) - 3^3 \times \Delta E\ (pVTZ)}{4^3 - 3^3}$$ (4)

We calculated interaction energies at CCSD(T)/CBS limit, as well, using the following equation

$$\Delta E_{CCSD(T)/CBS} = \Delta E_{MP2/CBS} + (\Delta E_{CCSD(T)/aug-cc-pVDZ} - \Delta E_{MP2/aug-cc-pVDZ})$$ (5)

c. Atoms-in-Molecules (AIM)

The presence of hydrogen bonding interaction between interacting molecules can be confirmed using topological analysis of electronic charge density ρ (r). The knowledge of ρ (r), can used to deduce diverse range of molecular properties. Charge-density based criteria for hydrogen bonding is based on "atoms-in-molecules" theory developed by Bader and his co-workers.[81] In the topology of the charge density there are points referred to as critical points, where the gradient of ρ(r) vanishes ($\nabla\rho$ (r_c) = 0). Once the critical points are located, the characteristics of these critical points can be determined by the second derivative $\nabla^2\rho$ and the so called Hessian of ρ. The Hessian is the (3x3) symmetric matrix of partial second derivatives. Diagonalization of this matrix yields three eigenvalues also called the principle

axis of curvature $\lambda_1 < \lambda_2 < \lambda_3$. The sum of the diagonal terms ($\sum_{i=1}^{3} = \lambda_i$) is called Laplacian of ρ ($\nabla^2\rho$) at bond critical point and is of fundamental importance.

The nature of the critical points is defined using the rank and the signature of the Hessian matrix. The rank of critical point, denoted by ω, is equal to the number of non-zero eigenvalues or non-zero curvature of ρ at the critical point. The signature denoted by σ, is the algebraic sum of the signs of the eigenvalues. The critical point (CP) is labelled by giving the values (ω, σ). A (3, -1) CP corresponds to a bond between two atoms, a (3, +1) CP to a ring, a (3, +3) CP to a cage and a (3, -3) CP corresponds to a maximum. The numbers of critical points of all types, which can coexist in a system with a finite number of nuclei, are governed by the Poincare-Hopf relationship.

$$n - b + r - c = 1$$

Where, n is the number of nuclei, b is the number of bond critical points, r is the number of ring critical points and c is the number of cage critical points.

To perform an AIM analysis, wavefunctions of optimized geometries of complexes from Gaussian 09 software are used as input to AIM2000[82] software which can then construct the electron density topology. According to Koch and Poplier,[83] for any interaction to qualify as hydrogen bonded contact, it should have electron density values ρ (r) in the range 0.002-0.034 a.u and $\nabla^2\rho(r_c)$ values within the range 0.024-0.139 a.u at the BCP. The sign of $\nabla^2\rho(r_c)$ at BCP differentiates between closed shell interactions, as found in ionic, hydrogen bonded and van der Waals complexes and shared-shell interaction, as in covalent bonds. A positive sign of $\nabla^2\rho(r_c)$ is indicative of closed shell interaction, where electronic charge is locally depleted between a pair of atoms. On the other hand, a negative sign refers to shared shell type interaction, resulting in concentration of electronic charge between bonded atoms.

One can also compare the ratio $|\lambda_1/\lambda_3|$, and these values should be less than 0.25 for hydrogen bonding interactions. Ellipticity at the bond critical point which is given by [(λ_1/λ_2)-1], where λ_1 and λ_2 are the negative eigenvalues of the Hessian, was also calculated for all the complexes. It ranges from 0 to ∞, and provides a measure of the extent to which charge is preferentially accumulated in a given plane. Employing the topological parameters, we also computed the interaction energy (ΔE_{HB}) for each interaction, through the use of local kinetic density, $G(r_{CP})$ and local potential energy density $V(r_{CP})$ as described by Espinosa et al.[84]

d. Energy Decomposition Analysis

The energy decomposition analysis (EDA) is a valuable analytical tool, which decomposes the interaction energy between two fragments A and B in molecule A-B, into

physically meaningful energy components such as electrostatic, polarization, charge transfer, exchange repulsion, dispersion and correlation. EDA is a popular method to characterise the energy contributions from various terms and hence gives us an insight regarding the dominant terms characterising an intermolecular interaction. The EDA schemes can be categorized by the nature of their underlying theory; variational in which the interaction energy is decomposed by use of intermediate wavefunctions, or alternatively perturbation-based, in which the interaction between the fragments is seen as a perturbation to the non-interacting description, and the interaction is constructed as corrections resulting from different physical effects. Kitaura-Morokuma EDA,[85] Natural EDA (NBO based approach),[85] ALMO-EDA (Absolute-Localised Molecular Orbital-EDA) [85]are some of the methods using variational approach whereas SAPT (symmetry adapted perturbation analysis and Natural Bond Order Second Order perturbation analysis are perturbation based approaches in which interaction energy is constructed as perturbative corrections to the isolated monomers.

In this work, we have used LMO-EDA (Localized Molecular Orbital EDA) to partition the interaction energy of hydrogen bonded complexes of PhAc. This method was implemented through GAMESS, on the basis of single determinant HF (restricted closed shell HF, restricted open shell HF and unrestricted open shell HF) and their density functional theory analogues. For HF methods, total interaction energy can be decomposed into electrostatic, exchange, repulsion and polarization components

$$\Delta E_{int} = \Delta E_{elec} + \Delta E_{ex} + \Delta E_{rep} + \Delta E_{pol}$$

whereas dispersion energy can be calculated using second order Moller–Plesset theory and coupled cluster methods such as CCSD and CCSD(T).

$$\Delta E_{int} = \Delta E_{elec} + \Delta E_{ex} + \Delta E_{rep} + \Delta E_{dis} + \Delta E_{pol}$$

In the case of DFT methods also, the interaction energy is decomposed into above stated components. The various contributing terms are defined as follows:

1. Electrostatic (ΔE_{elec}): the classical electrostatic interaction between occupied molecular orbitals , which does not cause any mixing of molecular orbitals.

2. Polarization (ΔE_{pol}): the interaction which causes the mixing between the occupied and vacant molecular orbitals within each molecule.

3. Exchange (ΔE_{ex}): the interaction between occupied molecular orbitals which causes electron exchange and delocalization between molecules.

4. Repulsion (ΔE_{rep}) : the repulsive interaction due to pauli's exclusion principle.

5. Dispersion(ΔE_{dis}): the interaction due to instantaneous dipole-induced dipole interactions .

A flow chart of the LMO-EDA method is given in Fig. 2.8. To begin with, monomer and supermolecule HF or KS (Kohn-Sham) orbitals and energies at the desired level of theory are calculated. For monomers, the monomer basis sets and, optionally, the supermolecule basis set are used. If MP2 or CC calculations are requested, they will be performed immediately after the HF SCF procedure. Then the intermolecular HF electrostatic and exchange interactions by virtually calculating the intermolecular Coulomb <ii|jj> and exchange <ij|ij> integrals using the monomer HF spin orbitals are determined. This requires an integral transformation from basis functions to molecular spin orbitals. Next, the program orthornormalizes the occupied HF spin orbitals of the monomers using the S^{-1} matrix and then calculates an energy, which is used to derive the HF repulsion energy. DFT interaction energies are determined in a similar manner. Finally, the interaction terms are organized and printed out.

e. Natural Bond Orbital Analysis (NBO)

NBO analysis developed by Weinhold and co-workers, was performed to understand the nature of hydrogen bonding interactions occurring through donor-acceptor orbital overlaps and subsequently to quantify them.[86] NBO analysis is based on a method for transforming a given wave function into localized form, corresponding to the one-centre (lone pair) and two-centre (bond pair) elements of the Lewis structure picture. The NBOs are localized few-centred orbitals that describe the Lewis-like molecular bonding pattern of electron in optimally compact form. More precisely, NBOs are an orthonormal set of localized maximum occupancy orbitals whose leading N/2 members give the most accurate possible Lewis-like description of the total N-electron density. In NBO analysis, the input atomic orbital basis set is transformed via natural atomic orbitals (NAOs) and natural hybrid orbitals (NHOs) into natural bond orbitals (NBOs). The NBOs obtained in this fashion correspond to the widely used Lewis picture, in which two-center bonds and lone pairs are localized.

NBO analysis was performed using Gaussian 09 suite of program with a keyword pop=nbo. The second order perturbation energy E(2) obtained in the output of NBO analysis depends on orbital overlap between donor and acceptor orbitals, denoted by F(i,j) and electron occupancy in donor orbital, whereas it is inversely proportional to energy difference between donor-acceptor orbitals [E(j)-E(i)]. The electron occupancies in acceptor orbitals were used to explain the different vibrational shifts in isoenergetic complexes.

f. Solvent Effect Calculations

The effect of matrix gases which act like a solvent for the trapped molecular species (solute)
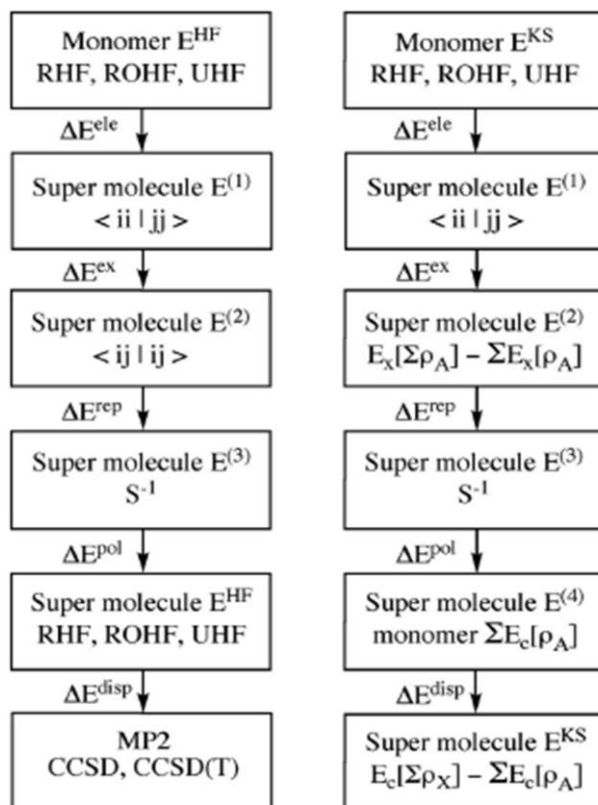
Fig. 2.8 Scheme of EDA Analysis

can be described quantitatively using models such as Onsager Self Consistent Reaction Field (SCRF) Solvation Model and PCM Solvation Model.[87-89] These models basically assumes solvent as a polarizable continuum medium. The influence of solvent (matrix) on the equilibrium geometries and energies of the monomers as well as complexes were calculated and implemented through Gaussian.

1. Onsager Self Consistent Reaction Field Model: This model is based on the assumption that the solute molecules (trapped analyte molecules) are placed in a spherical cavity in a solvent. The later is a homogenous and polarizable medium having a constant dielectric constant. The dipole moment (or instantaneous dipole moment) of the solute induces dipole moment in opposite direction in the surrounding medium. The polarized medium in turn polarizes the charge distribution in solvent molecules. The mutual polarization can be treated in self consistent manner to produce the reaction field. The reaction field produced is directly proportional to the dielectric constant of the medium and is inversely proportional to the third power of radius of spherical cavity housing the solute molecule. The radius of the spherical cavity is dependent on the size of the trapped species, and it was estimated based on molecular volumes obtained from Gaussian calculations, using the command int=finegrid volume. This is a dipole induced-dipole model and the calculation can be done using SCRF=dipole keyword in Gaussian. The solvent model calculation essentially requires the input of dielectric constant of the matrix gas used, along with radius of the spherical cavity.

2. Polarizable Continuum Model: The Polarized Continuum Model by Tomasi and co-workers, defines the cavity in which the solute molecule is placed, as the union of a series of interlocking van der Waals spheres centered on the atoms.[88] The reaction field is represented through point charges located on the surface of the molecular cavity. The model can be implemented through Gaussian using keyword SCRF=PCM. This calculation also requires dielectric constant of the medium in addition to the eps and eps infinity values. Another variation of PCM model; CPCM (Conductor like Polarizable Continuum Model) is also available which is used for polar solvents.[90] Since the matrix gases used were non-polar, PCM model was preferred for calculating solvent effects.

The PCM model is available for calculation of energies, optimizations and frequencies at Hartree-Fock, DFT and MP2 levels, whereas Onsager Model calculates only energies at these levels in addition to frequency calculations at HF and DFT levels.

Use of the solvation model showed that while the 'inert matrix' does influence the energies and spectra of the trapped species and the complexes, the effects are only marginal and do not affect any of the conclusions that we have made assuming the matrix to be inert.

Chapter 3

Phenylacetylene-Water complex: Is it n⋯σ* or H⋯π in the Matrix?

3.1 Introduction

The various hydrogen bonded complexes in the PhAc-H_2O system fall under the category of weak hydrogen bonded systems having energies less than 5 kcal/mol. In PhAc-H_2O complexes both the precursors can serve as amphoteric molecules, thereby resulting in a number of possible structures for the hetero dimer.

Patwari and coworkers studied the hydrogen bonded interactions in PhAc and H_2O, using IR-UV double resonance spectrosocopy.[28] Arunan *et al.* studied the same system using gas phase microwave spectroscopy.[29] Both groups concluded that the global minimum corresponded to a cyclic quasi planar structure having dual interactions involving the O-H⋯π and C-H⋯O interactions. Computations indicated two other structures which were local minima. One of these local minima, was a structure where the water donated the proton to the phenyl π system, while the second minima corresponded to a structure where the acetylenic hydrogen of PhAc was the proton donor; an n⋯σ* structure. Both the local minima were not observed in the gas phase experiments. The n⋯σ* complex is an interesting minima in that it is a local minimum in the PhAc-H_2O system, but turns out to be the global minimum in the C_2H_2-H_2O heterodimer. The n⋯σ* structure has been experimentally observed in the C_2H_2-H_2O system.[91] The question that we asked in this work is whether the hydrogen bonded structures corresponding to local minima in PhAc-H_2O can at all be observed in matrix isolation experiments; a technique which is known to trap local minima.[92] In fact, the O-H⋯π complex in the case of the C_2H_2-H_2O system has not even observed experimentally. Clearly the PhAc and C_2H_2 present two very contrasting scenarios with respect to their complexes with H_2O. The relative acidities of PhAc (pKa =26) and C_2H_2 (pKa = 25) does not provide the explanation for this difference.[105] This chapter attempts to understand this difference which forms the main theme of this chapter.

3.2 Experimental Details

The details of experimental procedure have been discussed in Chapter 2. We only present a brief experimental procedure followed in the study PhAc-H_2O system. Ar and N_2 (Sigma & Gases, 99.999%) were used as matrix gases. Phenylacetylene (Sigma Aldrich, 98%), Phenylacetylene-D (Sigma Aldrich, 99% Atom-D), H_2O (millQ, 16-18 Ω) and D_2O

(Sigma Aldrich, 99 %) were used without further purification. However before the preparation of the mixture of sample and matrix gases, the precursors were subjected to several freeze-pump-thaw cycles.

To begin with, experiments were performed with phenylacetylene (PhAc) and H_2O separately, to record the spectrum of the precursor molecules. Experiments were also performed with isotopically substituted PhAc in which acetylenic hydrogen was replaced by deuterium ($PhAc_D$). To observe the isotopic effect for shifts corresponding to the OH stretch in H_2O, experiments were performed with D_2O, which helped to confirm vibrational assignments of the water submolecule in the adducts. In short, all combinations of experiments corresponding to PhAc-H_2O, PhAc-D_2O, $PhAc_D$-H_2O, $PhAc_D$-D_2O systems were conducted, to investigate hydrogen bonding between PhAc and H_2O.

Sample to matrix ratios were typically varied from 0.25:1000 to 3:1000 individually for both precursors PhAc (or $PhAc_D$) and H_2O (or D_2O), using standard manometric procedures. Sample and the matrix gas were deposited on a cold KBr substrate, using a single jet effusive nozzle. A deposition rate of typically ~3mmol/hr of matrix gas, was employed, which yielded a uniform matrix film. A few experiments were also performed using a double jet nozzle, where the water was premixed with nitrogen in the mixing chamber and deposited using one nozzle. PhAc was deposited through a second nozzle.

Infrared spectra of matrix isolated species were recorded using a Bruker Tensor 27 FTIR spectrometer at a spectral resolution of 0.5 cm^{-1}. After recording a spectrum of the matrix isolated species at 12 K, the matrix was annealed at 27-30 K in the case of N_2 and 32 K in the case Ar, using a temperature controller unit (Lakeshore, Model No.335). Since the results obtained using N_2 and Ar matrices were similar, only the results obtained using a N_2 matrix are reported, to avoid a repetitive display of spectra.

3.3 Computational Details

We performed *ab initio* electronic structure calculations on PhAc-water system using Gaussian 09 suite of program on a Fujitsu Workstation to obtain molecular properties, such as structures, energies and frequencies, of the precursor molecules and the complexes. The computations were done at M06-2X and MP2 levels of theory employing 6-311++G** and aug-cc-pVDZ basis sets. Single point calculations were also done at the MP2/aug-cc-pVTZ , MP2/aug-cc-pVQZ and CCSD(T)/aug-cc-pVDZ level on the optimized geometries obtained at the MP2/aug-cc-pVDZ level of theory. Interaction energies at MP2/CBS and CCSD(T)/CBS limits were also calculated. The computational details have already been discussed in Chapter 2.

The potential surface of the PhAc–H_2O system was searched for locating the structures of the complex corresponding to the stationary points. Structures of PhAc and H_2O were first optimized individually and these structures were used as starting geometries for optimization of the supermolecule geometry. To ensure that the molecular structure obtained was indeed a minimum, vibrational frequency calculations were done to ascertain that all frequencies were positive. The vibrational frequency calculations were also used to assign the experimentally observed features. Zero point vibrational energies were obtained from frequency calculations which were used to calculate ZPE corrected energies. Frequency calculations for the isotopically substituted substrates were also performed.

The computed frequencies were scaled to enable a comparison with the experimentally measured frequencies. The scaling factor was determined as follows. The strongest feature observed experimentally for the *precursor* molecule was correlated with the strongest computed feature for the same *precursor*, in a given spectral region. For example in case of PhAc spectra recorded in N_2, matrix the highest intensity feature is observed at 3323.2 cm^{-1} which corresponds to ≡C-H stretch of PhAc. The same feature was computed to occur at 3481.2 cm^{-1} at MP2/aug-cc-pVDZ level of theory. The ratio of the experimentally observed feature to calculated feature comes out to be 0.9546. This factor brings the computed feature in agreement with the experimental feature for PhAc submolecule ; in other words the *precursor* data was used as a calibration for determining the scaling factor. This scaling factor obtained using the PhAc data, was then used to scale the computed features of the ≡C-H stretch in *complex*. In matrix isolation experiments, due to the matrix effects, modes occurring in different frequency regions are perturbed differently, which therefore calls for a different scaling factor for modes in different spectral regions.[93] We believe that mode-by-mode scaling is appropriate for matrix isolation experiments. The computed frequencies for the various modes for the PhAc-H_2O complexes were also simulated as a vibrational spectrum using SYNSPEC program.[94] The simulated vibrational spectra were generated assuming a Lorentzian line profile with full width at half maximum (FWHM) of 1 cm^{-1}.

3.4 Results

a) Experimental

Figure 3.1 shows the matrix isolated spectra of PhAc in a N_2 matrix, at 12 K, over spectral regions corresponding to the ≡C-H stretch (3340-3300 cm^{-1}) and phenyl -CH out-of-plane bending (770-750 cm^{-1}) region of PhAc.[95] The ≡C-H stretch is particularly explored as it is sensitive to hydrogen bond formation.[96] As can be seen from Fig. 3.1, ≡C-H stretch of

PhAc was observed in the N_2 matrix, at 3323.2 cm^{-1} with its Fermi resonance diad appearing at 3309.2/3310.8 cm^{-1}; this doublet being due to site splitting. The Fermi resonance has been reported to occur between the $\equiv$C-H stretch and a combination of one quantum of C$\equiv$C stretch and two quanta of C$\equiv$C-H out-of-plane bend.[97] The phenyl-CH out-of-plane bending was observed at 758.7 cm^{-1} with multiple site effects (Fig. 3.1). Likewise, Fig. 3.2 shows the infrared features of PhAc$_D$, which will be discussed later.

On co-deposition of PhAc and H_2O followed by annealing, new product vibrational bands were observed at 3254.0/3258.5 cm^{-1}, 760.2 and 763.3 cm^{-1} (Fig. 3.3). That these bands are due to the products, was confirmed by the observation that these bands increased in intensity when the concentration of either of the monomers was increased (Fig. 3.4).

Experiments were done by depositing PhAc alone (without H_2O) to ensure that the product features were not due to the dimer of PhAc. However, since H_2O is an unavoidable impurity in any matrix isolation experiments, the product features were still observed with very small intensities. Increase in the concentration of any of the monomers, PhAc or H_2O, resulted in an increase in intensity of these product features, which confirms their origin to PhAc-H_2O complex (Fig. 3.4). Furthermore, appearance of these product features at very low concentrations of PhAc and H_2O (0.25:0.5:1000) indicated that these adducts had a 1:1 PhAc-H_2O stoichiometry. The concentrations of PhAc being as low as they are (PhAc/N_2=0.25:1000), it is unlikely that these product features could be due to PhAc dimer.

To obtain shifts in the vibrational frequencies for the isotopic species, for corroborating our assignments, experiments were also conducted using PhAc$_D$. While Fermi resonance was a source of multiplet peaks in PhAc, PhAc$_D$ was free from Fermi resonance effects due to the shift to smaller wavenumbers of the $\equiv$C-D stretch and consequent suppression of Fermi resonance which involved this mode. However, the PhAc$_D$ manifested site splitting as can be seen in Fig. 3.2. An intense feature due to the $\equiv$C-D stretch was observed at 2599.9 cm^{-1} in the N_2 matrix, with site split features at 2602.6 and 2604.7 cm^{-1}. In experiments where PhAc$_D$ and H_2O were co-deposited, new product features were observed at 2565.7/2568.0 cm^{-1} and 759.6 cm^{-1}, corresponding to the $\equiv$C-D stretch and phenyl-CH out-of-plane bending, respectively, of the PhAc$_D$ submolecule in the complex (Fig. 3.5).

Experiments were also performed using D_2O in place of H_2O. The feature due to the antisymmetric O-D stretch of free D_2O was observed at 2766.1 cm^{-1} in the N_2 matrix.[98] On complex formation, with PhAc (PhAc$_D$), this mode was red shifted by about 1.9 cm^{-1} in PhAc-D_2O and PhAc$_D$-D_2O complexes (Fig. 3.6) and is observed at 2764.2 cm^{-1}.
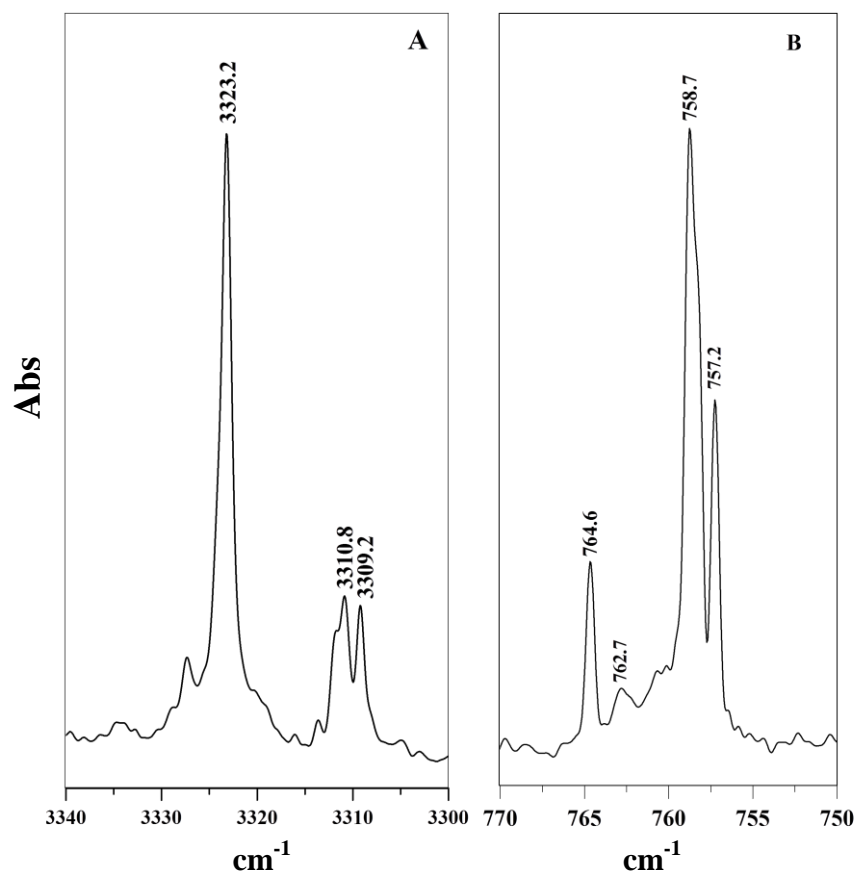
Fig.3.1. Infrared spectrum of PhAc trapped in a N_2 matrix at 12 K. Concentration of PhAc:N_2 is 0.25:1000. The spectral regions shown are A) 3340-3300 cm^{-1} corresponding to the $\equiv$CH stretch of PhAc and B) 770-750 cm^{-1} which corresponds to the phenyl -CH out-of-plane bend of PhAc.
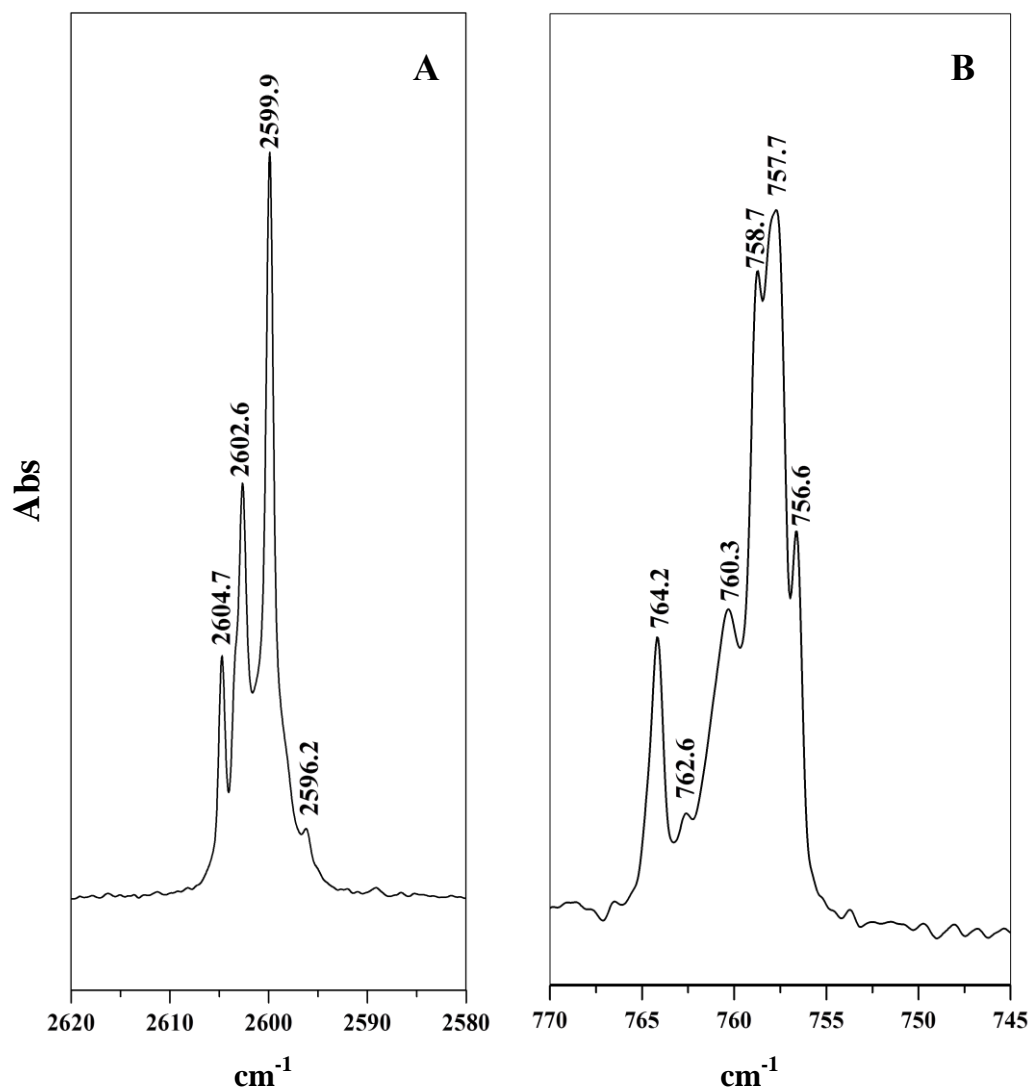
Fig.3.2. Infrared spectrum of PhAc$_D$ trapped in a N$_2$ matrix at 12 K. Concentration of PhAc$_D$:N$_2$ is 1.0:1000. The spectral regions shown are A) 2620-2580 cm^{-1}, corresponding to the $\equiv$CD stretch of PhAc$_D$ and B) 770-745 cm^{-1} which corresponds to the phenyl -CH out-of-plane bend of PhAc$_D$.
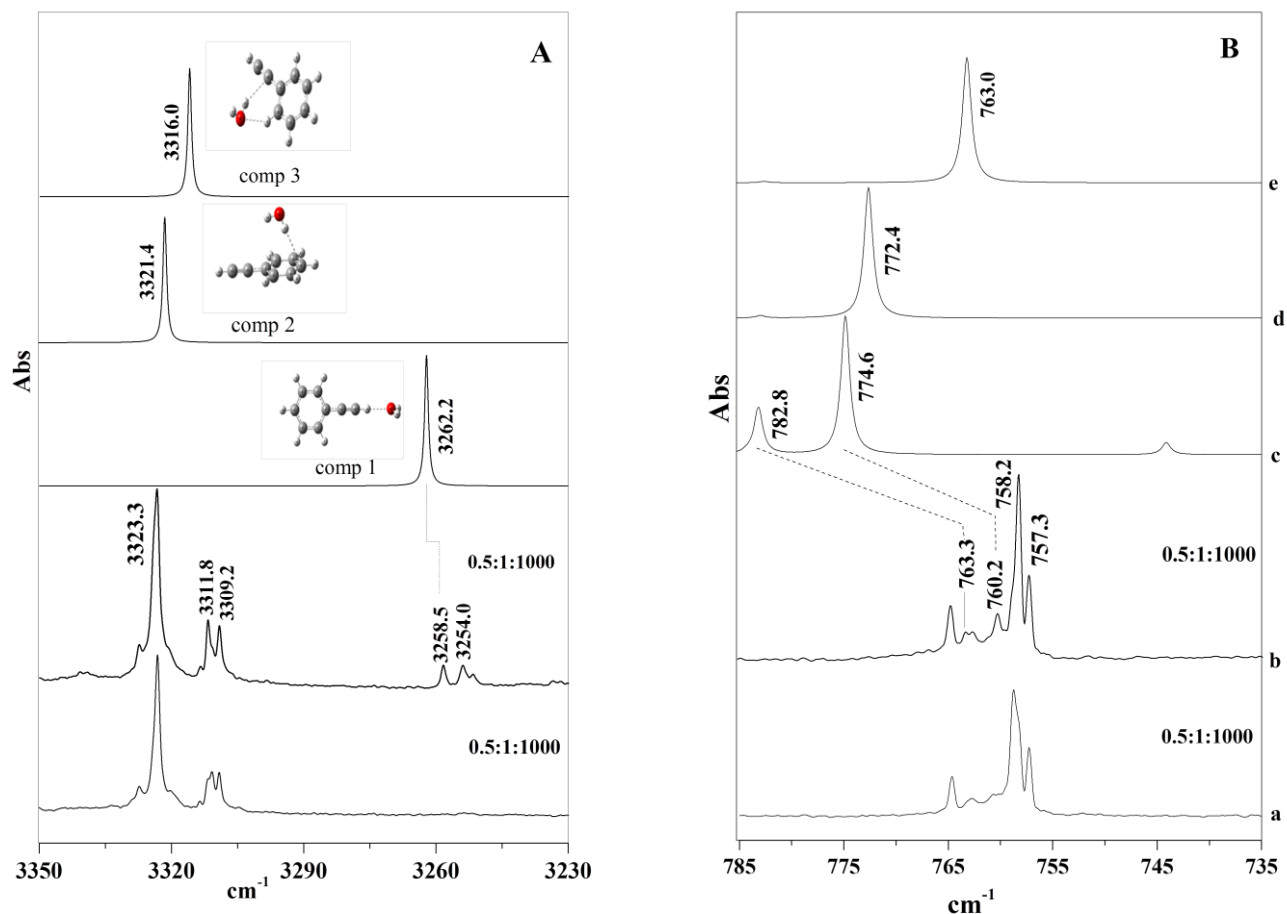
Fig.3.3. Experimental and computed infrared spectrum of PhAc-H₂O complexes over the spectral regions (A) 3350-3230 cm^{-1} ($\equiv$CH stretch of PhAc) and (B) 785-735 cm^{-1} (phenyl out-of-plane bend of PhAc)

(a) Experimental spectrum of PhAc-H₂O (0.5 : 1: 1000) recorded at 12 K in a N₂ matrix
(b) Spectrum of (a) annealed at 27 K
(c) Computed spectra of complex 1
(d) Computed spectra of complex 2
(e) Computed spectra of complex 3
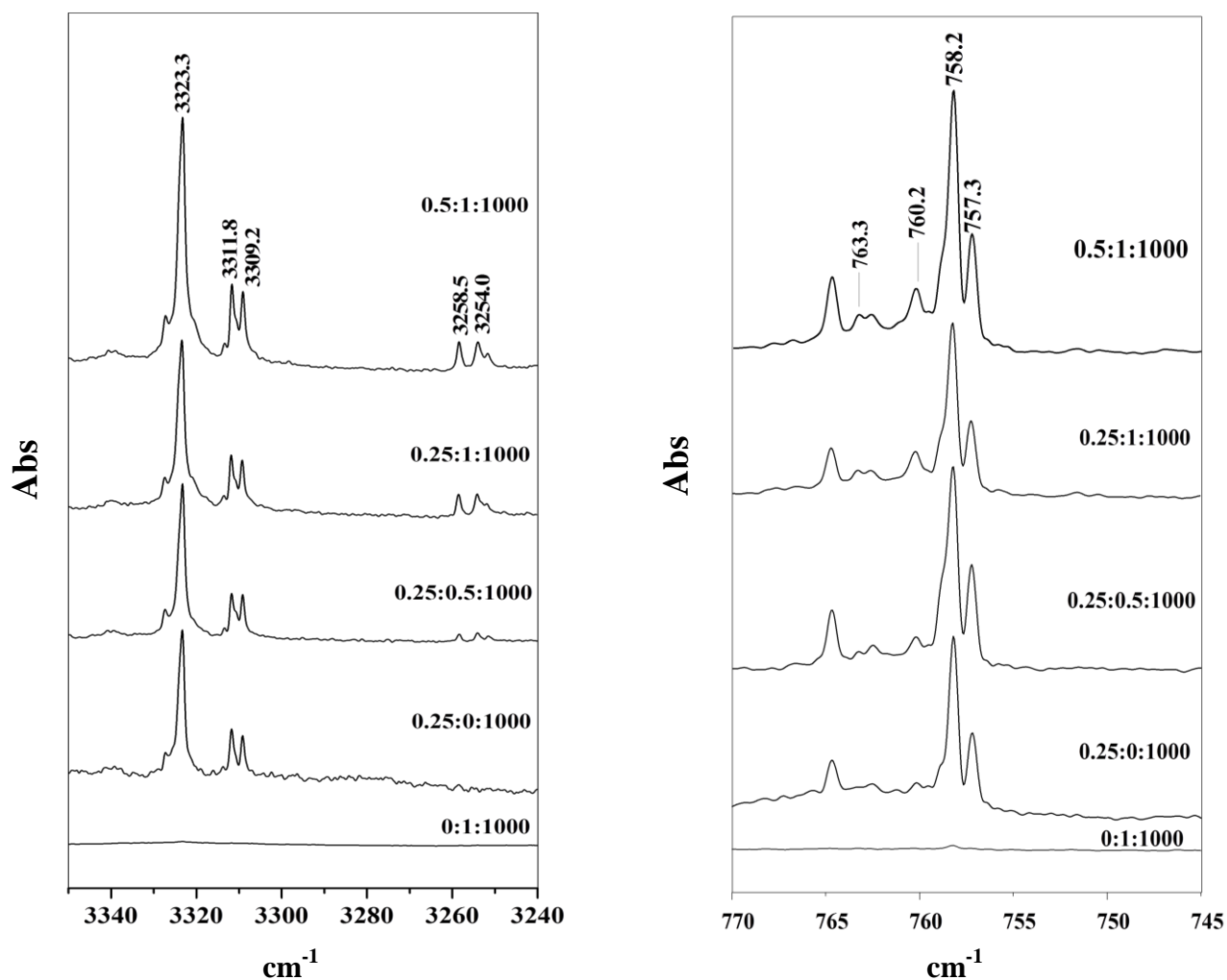
Fig.3.4. 27 K annealed spectra of PhAc-H$_2$O complexes in a N$_2$ matrix at various concentrations of the precursors, over the spectral region A) 3350-3240 cm^{-1} corresponding to the $\equiv$CH stretch of PhAc and B) 770-745 cm^{-1} which corresponds to the phenyl -CH out-of-plane bend of PhAc. Concentrations of precursors are shown alongside each trace as PhAc:H$_2$O:N$_2$

b) Computational

At the outset geometry optimization of the precursors was done using DFT (M06-2X) and post Hartree Fock perturbation methods (MP2), employing 6-311++G** and aug-cc-pVDZ basis sets. Starting with the optimized monomer geometries, the structures of PhAc and H_2O complexes were then computed. At all levels of theories, we obtained three minima for the hydrogen bonded structures, which are shown in Fig. 3.7. Important geometrical parameters defining the complexes are given in Table 3.1. The complexes can be classified as $n\cdots\sigma^*$ (complex 1), where H_2O was the proton acceptor, or $H\cdots\pi$, where H_2O was the proton donor. Two types of $H\cdots\pi$ structures were indicated computationally. One of them, referred to as a $H\cdots\pi_{Ph}$ (complex 2), was a structure where H_2O forms a hydrogen bond with the π cloud of the phenyl ring, much like in benzene-H_2O. In the second complex, referred to as a $H\cdots\pi_{Ac}$ (complex 3), H_2O forms a hydrogen bond with the acetylenic π system of PhAc. In this complex, H_2O in fact shows dual interactions; one is a $O-H\cdots\pi$ hydrogen bond, while at the same time it also serves as a proton acceptor by interacting with hydrogen of the phenyl ring ortho to the acetylenic group, forming a $C-H\cdots O$ type of hydrogen bond. The resulting structure is a near planar cyclic structure. All the three structures, identified computationally, were also reported independently, by Patwari and Arunan.[28,29] Table 3.2, which gives the interaction energies of the various PhAc-H_2O complexes, shows all of them to be weak hydrogen bonded complexes, with interaction energies less than -5 kcal/mol. At the MP2/aug-cc-pVDZ level of theory, it is seen that the complex 3 ($H\cdots\pi_{Ac}$) is the global minimum, whereas complex 2 ($H\cdots\pi_{Ph}$) and complex 1 ($n\cdots\sigma^*$) correspond to local minima, given in order of increasing energy. It may be noted that the BSSE corrected energy difference at the MP2/aug-cc-pVDZ, between the two $H\cdots\pi$ structures is only about 0.4 kcal/mol. Earlier reports have shown that complex 3 ($H\cdots\pi_{Ac}$) was the one observed in molecular beam experiments, which seemed to imply that this structure must be the global minimum, as indicated by the computations at the MP2 level.

While harmonic frequency calculations were performed at various levels of theory, we present the results of our MP2/aug-cc-pVDZ frequency calculations (Table 3.3 & 3.4), which best agreed with our experimental observations. The scaling factors to scale the computed frequencies are also shown in this table.
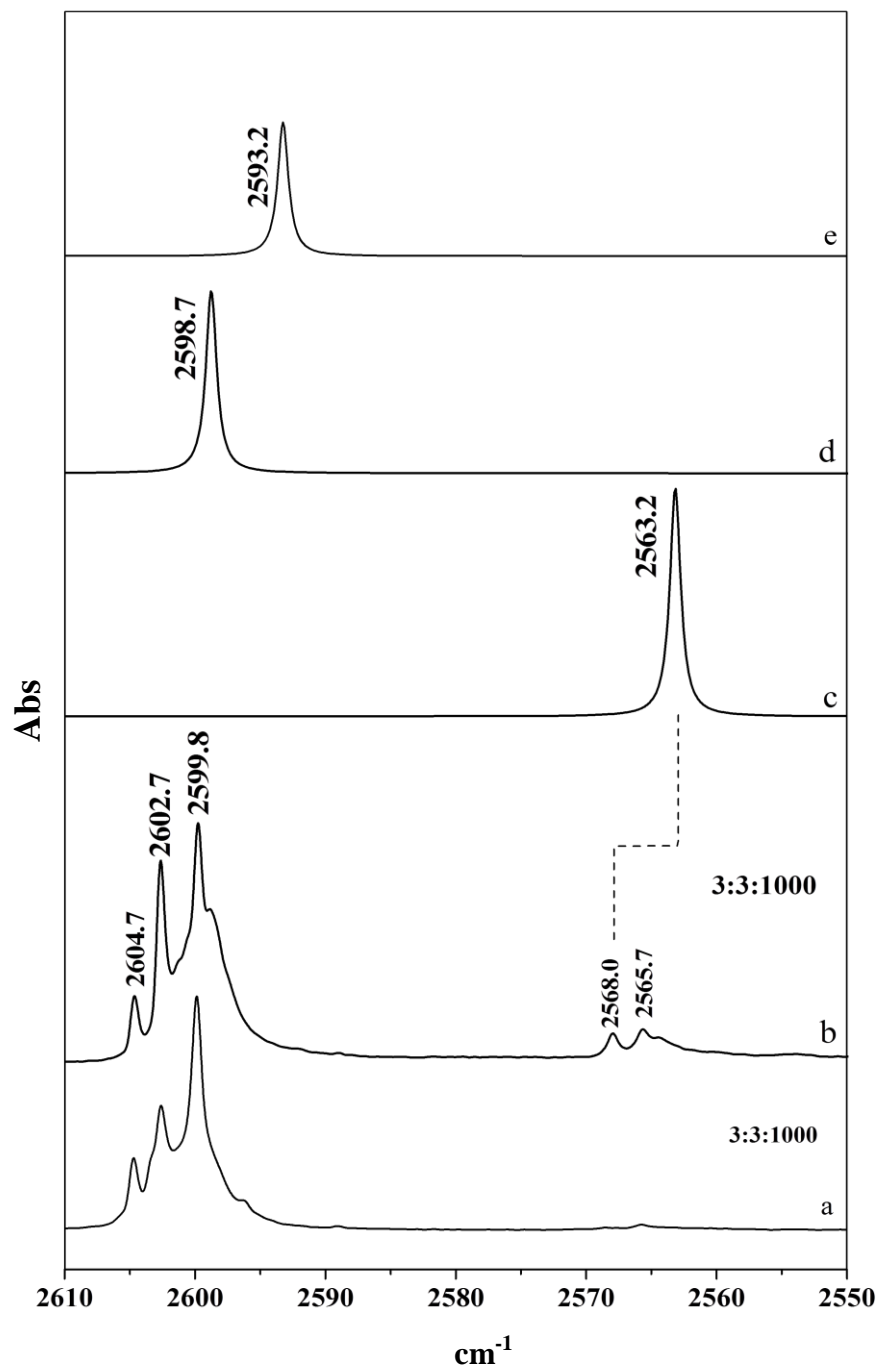
Fig.3.5. Experimental and computed infrared spectrum of PhAc$_D$-H$_2$O complexes over the spectral region 2610-2550 cm^{-1} ($\equiv$CD stretch of PhAc$_D$).

 (a) Spectrum of PhAc$_D$-H$_2$O (3:3:1000) recorded at 12 K in a N$_2$ matrix

 (b) Spectrum of (a) annealed at 27 K

 (c) Computed spectra of complex 1

 (d) Computed spectra of complex 2

 (e) Computed spectra of complex 3
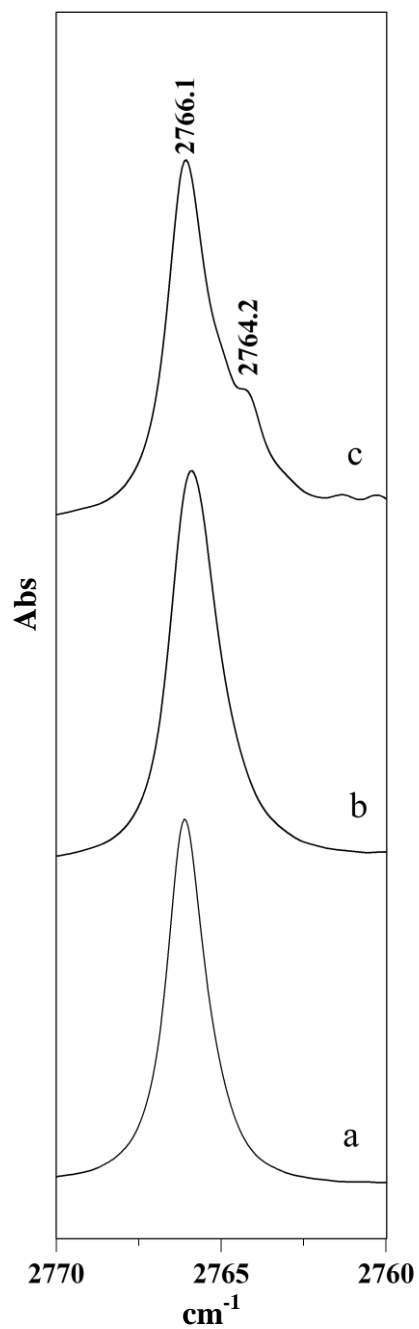
Fig. 3.6. Infrared spectra of PhAc$_D$:D$_2$O complexes in a N$_2$ matrix, over the spectral region 2770-2760 cm^{-1}, corresponding to OD stretch. (a) Spectrum recorded after annealing at 27 K of D$_2$O:N$_2$ (6:1000), (b) As-deposited spectrum at 12 K of PhAc$_D$:D$_2$O:N$_2$ (3:6:1000) and (c) Spectrum of (b) annealed at 27 K.
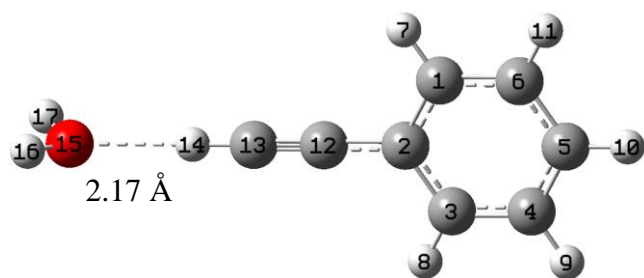
Complex 1
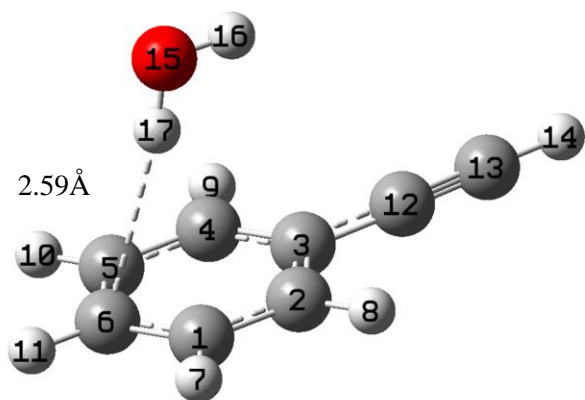
Complex 2
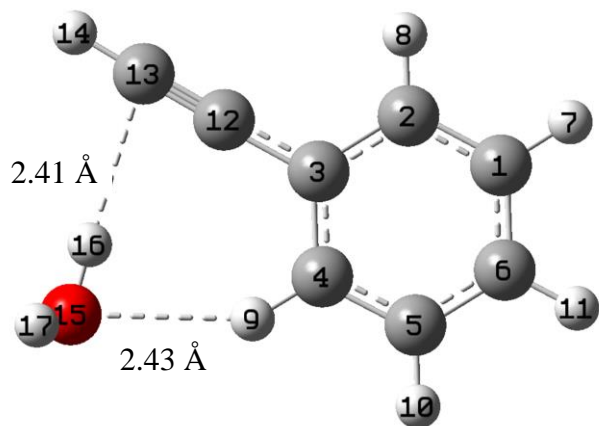
Complex 3

Fig.3.7. Optimized structures of 1:1 PhAc:H_2O complexes at MP2/aug-cc-pVDZ level of theory.

Table. 3.1. Important geometrical parameters, bond lengths (Å), bond angles (˚), dihedral angles* (˚), for PhAc-H₂O complexes computed at the MP2/aug-cc-pVDZ level. Labelling of atoms is shown in Fig. 3.7.

Complex 1	
O15-H14	2.17
H16-O15-H14	125.8
H16-O15-H14-C13	-84.1
Complex 2	
H17-C6	2.59
H17-centre of phenyl ring	2.31
O15-H17-C6	170.3
H17-C6-H11	115.1
H16-O15-H17-C6	179.9
H16-O15-H17-C5	-78.6
Complex 3	
H16-C13	2.41
H16-C12	2.46
O15-H9	2.43
H17-O15-H9	120.9
O15-H16-C12	148.1
O15-H9-C4	146.5
H16-C12-C3	108.2
O15-H16-C13-H14	119.2
O15-H16-C12-C13	172.6
H17-O15-H9-C4	-90.5
H17-O15-H16-C13	174.8

*Dihedral angle ABCD implies the angle between two planes ABC and BCD

3.5 Discussions

Vibrational assignment

a) ≡C-H stretch of the PhAc submolecule in the PhAc-H$_2$O complex

The identification of the nature of the PhAc-H$_2$O complexes rely significantly on the observation of shifts in the ≡C-H stretch, as this feature is very sensitive to hydrogen bonding interactions. This mode shows a red shift, the extent of shift depending on the nature and strength of the hydrogen bonding interaction. As mentioned earlier, the product band due to PhAc-H$_2$O complex was observed at 3254.0 cm^{-1}, which amounts to a red shift of 69.3 cm^{-1}. This band can be assigned to the ≡C-H stretch in the n···σ* complex (Fig 3.3 and Table 3.3). The red shift for the n···σ* complex is computed to be 61.0 cm^{-1}, which is significantly larger than the shift of 1.8 cm^{-1} calculated for H···π 'complex 2' and 7.2 cm^{-1} for the H···π 'complex 3' (Table 3.3). The excellent agreement of our experimentally observed shift in the ≡C-H stretch with the computed value for the n···σ* complex, therefore provides unequivocal evidence for the occurrence of the n···σ* complex in the matrix. It must be mentioned, that the n···σ* complex of PhAc-H$_2$O was not observed in any of the earlier studies and this is the first observation of this complex. We searched hard for evidence of the H···π complex, particularly complex 3, in our experiments, as this was observed in the gas phase experiments. However, we did not observe any clear evidence for this complex, though a weak shoulder is observed at around the region where the H-π complex 3 is expected to occur.

In our experiments on the complexes of PhAc-MeOH and PhAc-DEE, which will be discussed in Chap 4, we found that ≡C-H stretch of PhAc in these complexes are shifted from the uncomplexed PhAc, by 90.5 and 88.6 cm^{-1} respectively, comparable to the shift of about 69 cm^{-1} observed in the PhAc-H$_2$O complex. The shifts observed for the methanol and ether complexes agree with an earlier report on these complexes.[96] Clearly in the case of PhAc-diethylether, only the n···σ* complex can be produced, thereby confirming that these large shifts in the ≡C-H stretch of PhAc are clearly indicative of an n···σ* complex. We believe that these results provide further evidence that what we have observed in the matrix for the PhAc-H$_2$O system is an n···σ* complex.

b) ≡C-H bending and phenyl C-H bending of the PhAc submolecule

It is necessary to look at these bending modes together. The feature at 758.7 cm^{-1} corresponds predominantly to the phenyl -CH out-of-plane bending mode in PhAc. The ≡C-H

Table. 3.2. Interaction energies Raw/ZPE/BSSE at various levels of theory for the PhAc-H_2O complexes. Energies are given in kcal/mol.

	M06-2X		MP2			CCSD(T)	
	6-311++G(d,p)	aug-cc-pVDZ	6-311++G(d,p)	aug-cc-pVDZ	CBS	aug-cc-pVDZ	CBS
1(n-σ*)	-3.68/-2.37/-2.96	-3.04/-2.04/-2.59	-3.93/-0.94/-2.40	-3.61/-2.55/-2.53	-2.74	-3.63	-2.76
2(H-π_{Ph})	-4.66/-3.51/-3.85	-4.11/-2.90/-3.65	-4.65/-2.71/-2.41	-4.89/-4.01/-2.81	-3.40	-4.67	-3.17
3(H-π_{Ac})	-4.56/-3.19/-4.10	-4.42/-2.98/-4.01	-4.43/-1.25/-2.64	-4.79/-3.39/-3.24	-3.95	-4.77	-3.93

Table. 3.3. Experimental, scaled computed vibrational wavenumbers (cm^{-1}) and vibrational mode assignments for PhAc and its complexes with H_2O and D_2O. Computations were done at the MP2/aug-cc-pVDZ level of theory.

	Experimental		Scaled Computed Wavenumbers				Vibrational Mode assignment
	PhAc	**1:1 complex**	**Monomer**	**Complex 1**	**Complex 2**	**Complex 3**	
PhAc-H₂O	3323.2	**3254.0/3258.5 (-69.3/-64.8)**[a]	3323.2	**3262.2 (-61.0)**	3321.4 (-1.8)	3316.0 (-7.2)	≡CH stretch
	758.7	760.2	758.7	774.6[b]	772.4	763.0	phenyl -CH out-of-plane bend and ≡CH out-of-plane bend
	655.1	**763.3 (108.2)**	622.5	**782.8 (160.3)**	628.5 (6.0)	637.7 (15.2)	≡CH in-plane bend
	H₂O	**1:1 complex**					
	3727.6	-	3758.8	3755.6 (-3.2)	3728.2 (-30.6)	3722.2 (-36.3)	OH antisymmetric stretch
	3635.1	-	3630.7	3628.9 (-1.8)	3606.5 (-24.2)	3574.6 (-56.1)	OH symmetric stretch
	1597.5	-	1597.5	1599.1 (1.6)	1593.6 (-3.9)	1601.5 (4.0)	OH bend
PhAc-D₂O	**PhAc**	**1:1 complex**		**Complex 1**	**Complex 2**	**Complex 3**	
	3323.2	**3254.0/3258.5 (-69.3/-64.8)**[a]	3323.2	**3262.2 (-61.0)**	3321.4 (-1.8)	3316.0 (-7.2)	≡CH stretch
	758.7	760.2	758.7	773.8[b]	772.3	762.9	phenyl -CH out-of-plane bend and ≡CH out-of-plane bend
	655.1	**763.3 (108.2)**	622.5	**782.8 (160.3)**	628.5 (6.0)	635.8 (13.3)	≡CH in-plane bend
	D₂O	**1:1 complex**					
	2766.1	**2764.1 (-2.0)**	2801.7	**2799.6 (-2.1)**	2777.1 (-24.6)	2771.6 (-30.2)	OD antisymmetric stretch
	2655.6	-	2663.8	2662.4 (-1.4)	2647.3 (-16.5)	2625.8 (-37.9)	OD symmetric stretch
	1178.9	-	1168.9	1170.6 (1.7)	1165.3 (-3.6)	1169.6 (0.7)	OD bend

[a]Δν = ν(complex)-ν(monomer), is given in parenthesis

[b]Strong coupling between ≡CH out-of-plane bend of PhAc + phenyl -CH out-of-plane bend of PhAc

Scaling Factor : 4000-3000 cm^{-1} = 0.95461 ; 3000-2200 cm^{-1} = 0.97136; 2200-1000 cm^{-1} = 0.98470 ; 1000-200 cm^{-1} = 1.0277 .

Table. 3.4. Experimental, scaled computed vibrational wavenumbers (cm^{-1}) and vibrational assignments for PhAc$_D$ and its complexes with H_2O and D_2O. Computations were done at the MP2/aug-cc-pVDZ level of theory.

	Experimental		Scaled Computed Wavenumbers				Vibrational Mode assignment
	PhAc$_D$	1:1 complex	Monomer	Complex 1	Complex 2	Complex 3	
PhAc$_D$ -H$_2$O	2599.9	**2565.7/2568.0 (-34.1/-31.8)** [a]	2599.9	**2563.2 (-36.7)**	2598.8 (-1.1)	2593.3 (-6.6)	≡CD stretch
	757.5	759.6	757.5	757.2	771.4	762.0	phenyl -CH out-of-plane bend
	487.4	-	475.5	589.2 (113.8)	480.4 (4.9)	488.9 (13.4)	≡CD in-plane bend
	H$_2$O						
	3727.6	-	3758.8	3755.6 (-3.2)	3728.2 (-30.6)	3722.2 (-36.3)	OH antisymmetric stretch
	3635.1	-	3630.7	3628.8 (-1.8)	3606.5 (-24.2)	3574.6 (-56.1)	OH symmetric stretch
	1597.5	-	1597.5	1599.1 (1.6)	1593.6 (-3.9)	1601.4 (3.9)	OH bend
PhAc$_D$ -D$_2$O	PhAc$_D$	1:1 complex		Complex 1	Complex 2	Complex 3	
	2599.8	**2565.3/2567.5 (-34.5/-32.3)** [a]	2599.9	**2563.2 (-36.7)**	2598.8 (-1.1)	2593.3 (-6.6)	≡CD stretch
	757.6	759.5	757.5	757.2	771.4	761.9	phenyl -CH out-of-plane bend
	487.6	-	475.5	589.2 (113.8)	480.4 (4.9)	483.6 (8.2)	≡CD in-plane bend
	D$_2$O	1:1 complex					
	2766.1	**2764.2 (-1.9)**	2801.7	**2799.6 (-2.1)**	2777.1 (-24.6)	2771.6 (-30.2)	OD antisymmetric stretch
	2655.6	-	2663.8	2662.5 (-1.3)	2647.3 (-16.5)	2625.9 (-37.9)	OD symmetric stretch
	1178.9	-	1168.9	1170.5 (1.6)	1165.3 (-3.6)	1169.6 (0.6)	OD bend

[a] Δν = ν(complex)-ν(monomer), is given in parenthesis

Scaling Factor : 4000-3000 cm^{-1} = 0.95461; 3000-2200 cm^{-1} = 0.97136 ; 2200-1000 cm^{-1} = 0.98470 ; 1000-200 cm^{-1} = 1.0277.

bending occurs as an in-plane bend at 655.1 cm^{-1} and an out-of-plane bend at 619.3 cm^{-1}. Clearly the three different bending modes in PhAc occur in different spectral regions.

When an n···σ* complex is formed, a feature is computed to occur at 774.6 cm^{-1}, which is due to the phenyl -CH out-of-plane bending, but which is now mixed with the ≡C-H out-of-plane bending. The in-plane ≡C-H bending, is computed to occur at 782.8 cm^{-1}, thereby showing a large blue shift of ~160 cm^{-1} in the n···σ* complex. In other words, in the n···σ* complex, two of the bending modes are computed to occur at 774.6 and 782.8 cm^{-1}, separated from each other by barely 8 cm^{-1}. Formation of the n···σ* complex must therefore result in two product bands in the 770 cm^{-1} region. In our experiments, we clearly see *two* product bands in this region at 760.2 and 763.3 cm^{-1} (Fig 3.3 & 3.4 and Table 3.3). The in-plane ≡C-H bend shows the largest shift in the n···σ* complex and its occurrence in the experiments in the 760 cm^{-1} region, manifesting an experimental blue shift of almost 108 cm^{-1} confirms the presence of the n···σ* complex. We believe that the more intense 760.2 cm^{-1} feature can be assigned to the mode that is predominantly phenyl -CH out-of-plane bend, and the less intense 763.3 cm^{-1} feature to the ≡C-H in-plane bend, in the n···σ* complex, which is in keeping with the intensities obtained in our calculations. The above discussion is summarized in Fig. 3.3B, which shows the experimental spectra together with the computed spectra for the three complexes, in the region 735-785 cm^{-1}. Only the n···σ* complex is computed to show two bands in this region; the other two H···π complexes show only one band. This computational prediction is corroborated by our experiments, which shows two product bands in this region, lending support to our assertion that the n···σ* complex is trapped in the matrix.

c) Vibrational features of the H$_2$O submolecule

The antisymmetric (v_3) and symmetric (v_1) stretch in H$_2$O appears at 3727.6 cm^{-1} and 3635.1 cm^{-1} in the N$_2$ matrix.[99] Both v_3 and v_1 were computed to show a red shift of 3.2 cm^{-1} and 1.8 cm^{-1} for the n···σ* complex 1, as shown in Table 3.3. In this complex, water acts as proton acceptor, and hence is not surprising that the shifts are small and not discernible from the features of the water monomer. The intensity of these features were also small, which therefore adds to the difficulty in observing them. Likewise, the bending mode of water is computed to show just a blue shift of about 1.6 cm^{-1}, which also could not be discerned.

For the H···π complexes, the shifts in the H$_2$O features are large and are computed to be about 30 cm^{-1}, since H$_2$O is a proton donor in this case. We searched for evidence for this

complex, particularly complex 3, which was observed in the gas phase experiments. However, the region where this feature is expected to occur is masked by water multimers, making it difficult to discern these features. We can only conclude that while we do not have clear evidence for the H···π complex 3, we do not rule out the occurrence of this complex, in the matrix. However, the occurrence of the n···σ* complex is unambiguous.

Experiments with isotopic substitution

PhAc-D$_2$O complexes

In experiments where PhAc and D$_2$O were codeposited to form the PhAc-D$_2$O complexes, the shifts in the PhAc submolecule were identical to those observed in the PhAc-H$_2$O (Table 3.3) complexes, as the isotopic substitution was only in the water submolecule. Reassuringly, the shift in the ≡C-H, on complexation with D$_2$O again provided evidence for the n···σ* complex. The following discussion will be presented only for the D$_2$O features.

d) OD stretching features of D$_2$O submolecule in the PhAc-D$_2$O complex

As mentioned earlier, the small red shift in the antisymmetric stretch of H$_2$O was not clearly discernible. In experiments with D$_2$O, a very small shoulder was barely observable at 2764.1 cm^{-1}; a feature that is assignable to D$_2$O submolecule in the n···σ* complex (Fig.3.6). This shoulder appears only on annealing and not in the as-deposited spectrum. This experimentally observed feature agrees well with that computed for this submolecule (Table 3.3). The shifts in the same mode for the complex 2 and complex 3 were not observable, as the region where they are computed to occur is again masked by the multimer features of D$_2$O.

PhAc$_D$-H$_2$O

e) ≡C-D stretch of PhAc$_D$ in the PhAc$_D$-H$_2$O complex

The shift in the ≡C-D stretch, in the PhAc$_D$ submolecule in the PhAc$_D$-H$_2$O complex (Table 3.4 and Fig. 3.5), provides further evidence for the formation of the n···σ* complex. The ≡C-D stretch in the complex appeared at 2568.0/2565.7 cm^{-1}, which amounts to a red shift of ~34 cm^{-1} from the corresponding feature in uncomplexed PhAc$_D$. This shift agrees well with the computed red shift of 36.7 cm^{-1}, for this feature, in the n···σ* complex (complex 1) of PhAc$_D$-H$_2$O. Once again we find that the matrix experiments provide unambiguous evidence for the n···σ* complex.

As in the case of PhAc-H$_2$O complex where a shoulder was tentatively assigned to complex 3, in the PhAc$_D$-H$_2$O experiments also, a feature was observed at 2598.7 cm^{-1}, which can be tentatively assigned to complex 3.

The phenyl -CH out-of-plane bend in $PhAc_D$ occurs at 757.7 cm^{-1}; in the same region as it does in PhAc, as the substitution is only in the acetylenic hydrogen. The $\equiv$C-D bend, on the other hand, occurs to smaller wavenumbers compared with the $\equiv$C-H bend. Following complex formation, the phenyl C-H bend is shifted to the blue and is observed at 759.6 cm^{-1}, in agreement with the computed value(Table 3.4). This mode does not mix with the $\equiv$C-D bend, a phenomenon that was discussed earlier with PhAc. It must be also noted that due to isotopic exchange, samples of $PhAc_D$ have PhAc as an impurity, and hence show features of the PhAc.

f) OD stretching features of D_2O submolecule in the $PhAc_D$-D_2O complex

Similar to our experiments using PhAc and D_2O, we observed a discernible shoulder at 2764.2 cm^{-1} in the region of the OD antisymmetric stretch of D_2O, which is shown in Fig. 3.6. This feature is assigned to the D_2O submolecule in the n$\cdots\sigma$* complex. This experimentally observed feature agrees well with that computed for this submolecule (Table 3.4).

3.6 AIM Analysis

AIM theory, developed by Bader,[81] has become a very powerful tool to study hydrogen bonding interactions, like C-H$\cdots$O and O-H$\cdots\pi$. The theory was used to characterize the nature of interactions through topological analysis of electronic density, $\rho(r)$. Wave functions generated from optimized structures of PhAc-H_2O complexes at MP2/aug-cc-pVDZ level of theory were used to locate (3, -1) bond critical points (BCP), where they existed. The electron density $\rho(r_c)$ and $\nabla^2\rho(r_c)$ (defined as sum of the Hessian eigenvalues, λ_1, λ_2 and λ_3) were analysed, at the bond critical point, for all the three complexes (Fig 3.8, Table 3.5).

In all the three PhAc-H_2O complexes, the values of $\rho(r_c)$ and $\nabla^2\rho(r_c)$ and the sign of $\nabla^2\rho(r_c)$ were consistent with the suggested values for hydrogen bonds by Koch and Poplier[83] (Table 3.5). In all the cases, positive values of $\nabla^2\rho(r_c)$ indicated the interactions to be of the closed shell type.

Complex 1, which has been clearly identified in our experiments, has the largest values for $\rho(r_c)$ and $\nabla^2\rho(r_c)$ amongst all the three complexes. Complex 3 (H$\cdots\pi$ acetylenic), the global minimum, which was identified in the gas phase experiments, enjoyed two interactions, O-H$\cdots\pi$ and C-H$\cdots$O. Both interactions had similar values of $\rho(r_c)$ and $\nabla^2\rho(r_c)$. As discussed in earlier works, the presence of dual interactions likely stabilizes this complex,

enough to cause this to be the global minimum.[28,29] Complex 2 has the smallest values for both the above parameters.

We have also compared the ratio $|\lambda_1/\lambda_3|$, and these values are similar and less than 0.25 for all the three complexes. This observation indicates that all the complexes demonstrate a closed shell interaction.[100] Ellipticity at the bond critical point which is given by $[(\lambda_1/\lambda_2)-1]$, where λ_1 and λ_2 are the negative eigenvalues of the Hessian, was also calculated for all the complexes. It ranges from 0 to infinity and provides a measure to which charge is preferentially accumulated in a given plane. The two interactions present in complex 3, show different ellipticities, with the C-H⋯O showing a smaller ellipticity than the O-H⋯π interaction. The O-H⋯π interaction in complex 2, in turn, showed an ellipticity which was about 7 times larger than the O-H⋯π interaction in complex 3. This indicates a difference in the nature of interaction between the π cloud in two systems. Similarly, the C-H⋯O interaction in complex 3 had a marginally larger ellipticity than the C-H⋯O in complex 1. However, it must be borne in mind that the values of λ_1 and λ_2 for the complexes are rather small, and hence small variations in these values can result in significant changes in the ratio of λ_1/λ_2. Hence conclusions based on ellipticities must be made with abundant caution.

In summary, while all the hydrogen bonded interactions in the PhAc-H_2O system, had one thing in common, in that they all showed closed-shell type of interactions, the detailed topological behaviour of every interaction seemed unique in themselves.

3.7 Energy Decomposition Analysis

Energy Decomposition analysis was done for all three complexes to understand the components of total interaction energy in terms of electrostatic, exchange, repulsion, polarization and dispersion energies. LMO-EDA scheme of analysis was implemented through GAMESS.[74] Table 3.6 shows different components of interaction energy in all the complexes. All the complexes have significant electrostatic component. In complex 1, which is an n⋯σ* system, polarization and dispersion interactions were also present but were less dominant than electrostatic. In complex 2, which is a H⋯π_{Ph} complex, dispersion contributed as much as electrostatic, with a lesser contribution from polarization, and not surprisingly so, as this system involved a π system, which is a soft base. In complex 3, which is a H⋯π_{Ac} complex, electrostatic interaction was again the main contributor, with smaller but sizable contributions from dispersion and polarization. It must be borne in mind that complex 3, manifests a dual H⋯π and n⋯σ* interaction.

It is reassuring to note that the conclusions reached from an LMOEDA analysis that electrostatic component makes a dominant contribution in all the three complexes, is consistent with the AIM analysis, which through an analysis of $\nabla^2\rho$ (r_c) and $|\lambda_1/\lambda_3|$, yields a similar conclusion.

3.8 NBO Analysis

NBO analysis on the PhAc-H_2O system was also performed, the results of which are shown in Table 3.7[86]. In this table, we have shown the second order perturbation energies E(2), the energy difference between the donor and acceptor orbitals [E(j)-E(i)] and the overlap between the two orbitals [F(i,j)]. The perturbation energy is directly proportional to orbital occupancy and the square of the overlap integral between the donor and acceptor orbitals and inversely proportional to the difference in energy of the donor and acceptor orbitals (D-A).

The dominant orbital interaction in the n$\cdots\sigma^*$ (complex 1) was between the lone-pair on oxygen of H_2O to the σ^* orbital of the acetylenic C-H of PhAc. In the H$\cdots\pi_{Ac}$ complex which was the global minimum (complex 3), NBO analysis showed two dominant interactions. One was the π to σ^* overlap between the acetylenic π cloud and the O-H antibonding orbital, which corresponds to the primary H$\cdots\pi$ interaction. In addition there was also another orbital delocalization corresponding to the C-H$\cdots$O interaction, between the lone pair of oxygen of H_2O to the σ^* orbital of C-H of the phenyl group. Both these interactions individually showed smaller second order perturbation energies than that corresponding to the n$\cdots\sigma^*$ interaction in complex 1. However, as mentioned earlier, the two interactions together make for complex 3 to be more stable than complex 1. As will be discussed in Chapter 7, it is the presence of this secondary interaction in PhAc-H_2O complex that enables the O-H$\cdots\pi$ complex to assume the status of a global minimum in this case, and the lack of it in C_2H_2-H_2O, that probably relegates it to a local minima in the latter case. It may also be noted that the n$\cdots\sigma^*$ interaction in complex 1 showed a larger second order perturbation energy, due to the larger overlap between the donor and acceptor orbitals. In the case of the C_2H_2-H_2O complex, the H$\cdots\pi$ complex, does not enjoy the secondary interaction and in the absence of the secondary interaction, the n$\cdots\sigma^*$ complex turns out to be the global minimum. The dominant orbital interactions, in the H$\cdots\pi$ and n$\cdots\sigma^*$ complexes, of the C_2H_2-H_2O system, are shown in Table 3.7.
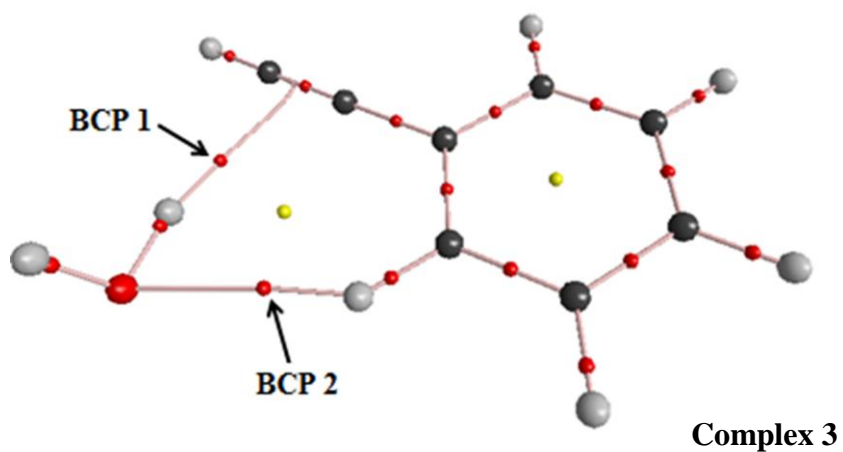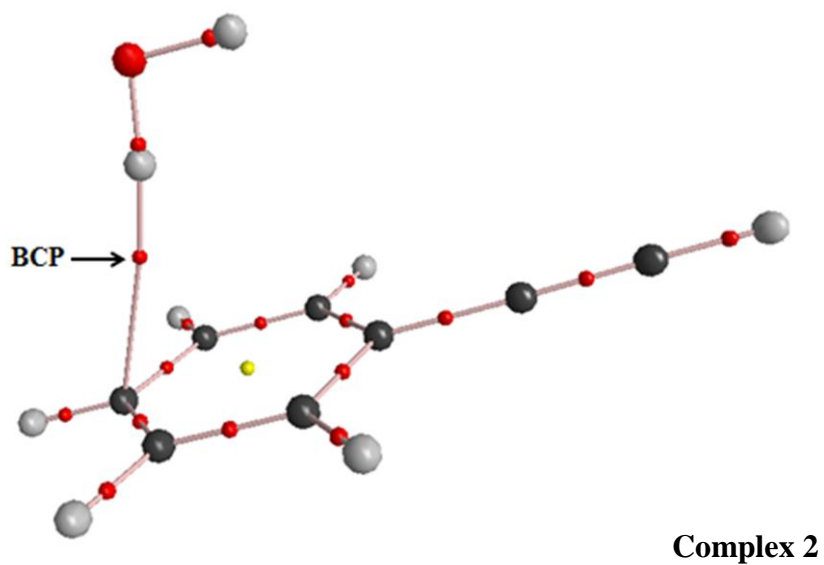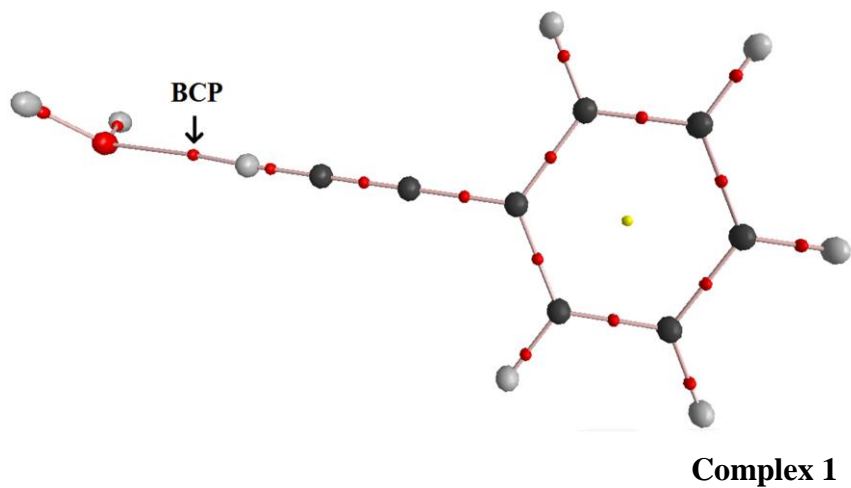
Fig.3.8. AIM calculations for the three PhAc:H_2O complexes shown in Fig. 3.7, performed at the MP2/aug-cc-pVDZ level, showing the bond critical points.

Table. 3.5. AIM calculations performed using wavefunctions obtained at MP2/aug-cc-pVDZ for 1:1 PhAc-H_2O complexes.

Complex	$\rho(r_c)$	$\nabla^2\rho(r_c)$	λ_1	λ_2	λ_3	$|\lambda_1/\lambda_3|$	$(\lambda_1/\lambda_2)-1$	ΔE_{HB}
1 **C-H···O**	0.0143	0.0505	-0.0162	-0.0151	0.0817	0.198	0.073	-2.84
2 **O-H···π**	0.0096	0.0258	-0.0058	-0.0013	0.0329	0.176	3.46	-1.46
3 **O-H···π**	0.0129	0.0353	-0.0112	-0.0074	0.0539	0.208	0.514	-2.20
3 **C-H···O**	0.0108	0.0326	-0.0108	-0.0098	0.0533	0.203	0.102	-1.80

Table 3.6: Energy Decomposition analysis of complexes 1, 2 and 3 at MP2/aug-cc-pVDZ[a]

Complex	E_{ES}	E_{ER}	E_{Pol}	E_{Disp}	E_{Total}	E_{ES}/E_{Total}	E_{Disp}/E_{Total}	E_{Pol}/E_{Total}
Complex 1	-4.31	3.52	-1.55	-1.30	-3.63	1.19	0.36	0.43
Complex 2	-3.45	4.21	-1.55	-4.14	-4.92	0.70	0.84	0.32
Complex 3	-6.54	7.30	-2.41	-3.19	-4.85	1.35	0.66	0.50

[a]All energies are in kcal/mol.

3.9 Why was only the n⋯σ* observed in our experiments?

While gas phase experiments did not observe the local minimum corresponding to the n⋯σ* PhAc-H_2O adduct, the matrix isolation experiments in both N_2 and Ar matrixes, gave unambiguous evidence for the presence of this local minimum. The local minimum was produced during the annealing process and was trapped and preserved due to the cage effect. Without the cage effect, this structure may have likely interconverted to the global minimum, as it probably did in the gas phase experiments. Trapping of the local minima in the matrix isolation experiments is well documented, in various studies involving weak interactions and conformations.[101,102] In reality, the search for the local minimum in this system was the motivation of the present study.

While one would have expected to observe the global minimum corresponding to the H⋯π complex also, it probably eluded detection due to interferences from other species in the region of absorption of this complex, as explained earlier.

We also explored the possibility if the general solvent effect provided by the inert gas matrix had altered the energy ordering of the three complexes, thus making the n⋯σ* complex a global minimum in the matrix. It may be noted from Table 3.2, that the difference in energy between the O-H⋯π complex, the global minimum, and the n⋯σ* complex, the local minimum, was only ~0.8 kcal/mol. We therefore performed calculations by including the solvent effect, using the Onsager Self Consistent Reaction Field (SCRF) continuum model.[87,88] In these computations we used the reported values for the dielectric constant of 2.00 for N_2.[103,104] However, introduction of the solvent effect preserved the energy ordering, as observed for the vacuum calculations, as it simply reduced the energies of all the complexes uniformly by ~22%.

3.10 H⋯π as the global minima in the PhAc system

In order to probe if this secondary interaction was the reason for the transformation from an n⋯σ* system in C_2H_2-H_2O to a H⋯π system in PhAc-H_2O, we computationally investigated some model systems, which afforded this secondary interaction. The systems studied were: propyne-H_2O, but-1-yne-H_2O and but-1-en-3-yne-H_2O (Fig. 3.9), for an eventual comparison with C_2H_2-H_2O and C_6H_6-H_2O, which do not have the possibility of any secondary interaction. Stabilization energies were computed for the H⋯π and n⋯σ* complexes for the series of systems mentioned above (Table 3.8). AIM analysis was also performed on all the systems to analyse the nature of interactions (Table 3.9).

Table.3.7 NBO analysis for C_2H_2-H_2O and PhAc-H_2O complexes performed at MP2/aug-cc-pVDZ level of theory. The atom numbering indicated in table is as shown in Fig.3.7and 3.9. E(2) is the second order perturbation energy (kcal/ mol), E(j)-E(i) is the donor-acceptor energy difference and F(i,j) is the overlap between the donor and acceptor orbitals.

Complex	Orbital Involved		E(2) (kcal/mol)	E(j)-E(i) a.u.	F(i,j) a.u.	Electron occupancy donor orbital	Electron occupancy acceptor orbital
Acetylene-water	**Donor**	**Acceptor**					
H···π	C_1-C_3 (π)	O_5-H_6(σ*)	3.27	1.19	0.056	1.99448	0.00501
n···σ*	O_5 (n)	C_3-H_4(σ*)	5.97	1.67	0.089	1.98992	0.01216
PhAc-water							
H···$π_{Ac}$ (O-H···π)	C_{12}-C_{13}(π)	O_{15}-H_{16}(σ*)	3.68	1.15	0.058	1.98131	0.00577
H···$π_{Ac}$ (C-H···O)	O_{15}(n)	C_4-H_9(σ*)	2.42	1.26	0.049	1.99165	0.01180
n···σ*	O_{15}(n)	C_{13}-H_{14}(σ*)	6.43	1.65	0.092	1.98951	0.01211

Table 3.8. Comparison of Interaction Energies, Raw/ZPE/BSSE (kcal/mol) at MP2/aug-cc-pVDZ level for various water complexes.

	Complex	n···σ*	H···π
1.	Acetylene-H_2O	-3.61/-2.57/-2.64	-3.04/-1.88/-2.16
2.	Propyne-H_2O	-3.12/-2.12/-2.12	-4.50/-3.08/-3.28
3.	But-1-yne-H_2O	-3.12/-1.93/-2.12	-4.92/-3.56/-3.48
4.	But-1-en-3-yne-H_2O	-3.52/-2.37/-2.52	-4.46/-3.05/-3.18
5.	Phenylacetylene-H_2O [a]	-3.61/-2.55/-2.53	-4.79/-3.39/-3.24
6.	Benzene-H_2O	-	-4.84/-3.85/-2.85

[a] In the case of H-π complex for Phenylacetylene-H_2O, energies of complex 3 are given.

In C_2H_2-H_2O complex, the ZPE corrected stabilization energy of the n···σ* complex was lower than the H···π complex by ~0.7 kcal/mol (Table 3.8). On the other hand, in all the other systems, propyne-H_2O, but-1-yne-H_2O and but-1-en-3-yne-H_2O, the H···π complex was the global minimum. All these systems have the possibility of a secondary interaction. That a secondary interaction was in fact involved in all these complexes, is confirmed by an AIM analysis (Table 3.9). Furthermore, the $\rho(r_c)$ and $\nabla^2\rho(r_c)$ values at the bond critical points of O-H···π interactions in all the systems are comparable. Likewise, the corresponding values for the C-H···O interactions are also comparable. Even though the secondary C-H···O interaction showed significantly lower ρ_c values at its bond critical point in all the complexes, this weak interaction together with the primary O-H···π interaction results in the O-H···π complex to be more stable than the n···σ*.

In the systems that we chose as model system, but-1-en-3-yne resembled the PhAc-H_2O system the closest (Fig. 3.9). Both systems showed an O-H···π interaction together with a secondary C-H···O interaction. The difference between these systems, is that the C-H···O interaction in but-1-en-3-yne involved hydrogen attached to an *aliphatic* sp^2 carbon, while in PhAc, this interaction involved a hydrogen attached to an *aromatic* sp^2 carbon. In but-1-yne-H_2O and propyne-H_2O systems, the secondary C-H···O interaction involved hydrogen attached to an sp^3 carbon. As the sp^3 carbon is less electronegative than an sp^2 carbon, the hydrogen attached to an sp^2 carbon is more disposed to form a C-H···O interaction. All these arguments are supported by the $\rho(r_c)$ values of C-H···O interaction obtained from AIM analysis (Table 3.9). It is therefore interesting to observe that in all the systems studied, irrespective of whether they involve hydrogens attached to sp^2 or sp^3 carbons, the secondary interaction seemed to influence sufficiently as to cause the H···π complex to be lower in energy than the n···σ complex. Hence small structural changes in interacting precursors have a significant effect on the geometry of the global minima.

In the case of C_2H_2-H_2O system, the occurrence of the n···σ* complex as the global minimum presents a question. The pKa values of acetylene is ~25 while that of water is 15.7 ; the higher acidity of water should therefore have led to water being the proton donor, forming the H···π complex, which should have been global minimum[105]. However, contrary to this argument, the n···σ* complex, employing the less acidic acetylenic proton is the
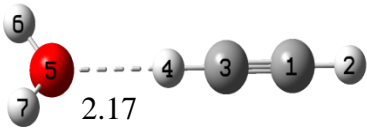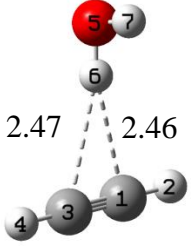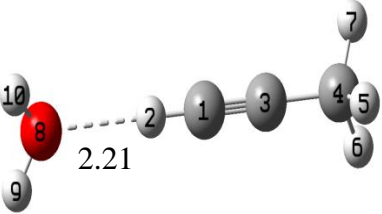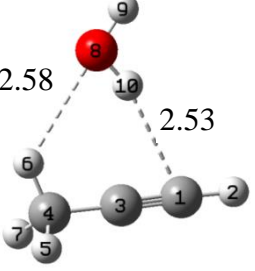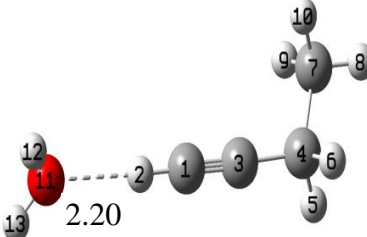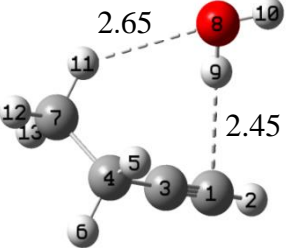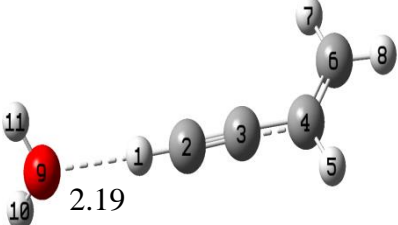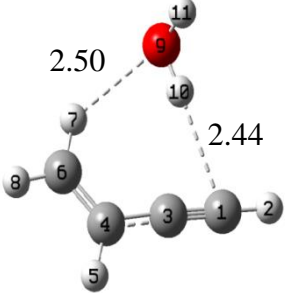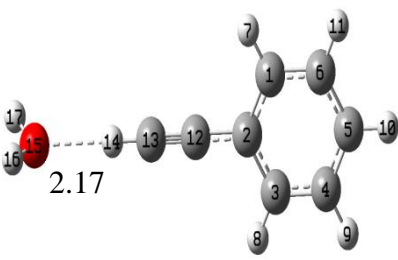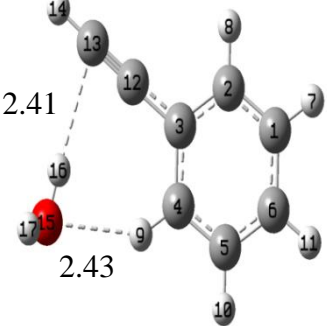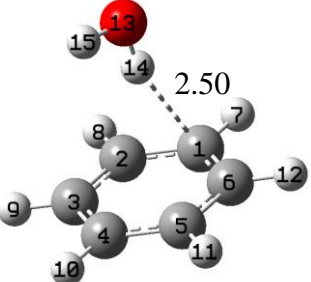
System	n···σ*	H···π
Acetylene-H$_2$O	2.17	2.47 2.46
Propyne-H$_2$O	2.21	2.58 2.53
But-1-yne-H$_2$O	2.20	2.65 2.45
But-1-en-3-yne-H$_2$O	2.19	2.50 2.44
Phenylacetylene-H$_2$O	2.17	2.41 2.43
Benzene-H$_2$O		2.50

Fig.3.9. Optimized structures of the various water complexes of model systems, obtained at MP2/aug-cc-pVDZ level of theory. (Hydrogen bond distances are shown in Å.)

Table. 3.9. AIM calculations performed using wavefunctions obtained at MP2/aug-cc-pVDZ for the various H$_2$O complexes.

System	$\rho(r_c)$	$\nabla^2\rho(rc)$	λ_1	λ_2	λ_3	$|\lambda_{1/}\lambda_3|$	$(\lambda_{1/}\lambda_2)$-1
Acetylene-H$_2$O							
H$\cdots\pi$	0.0116	0.0319	-0.0098	-0.0065	0.0482	0.203	0.508
n$\cdots\sigma$*	0.0144	0.0492	-0.0164	-0.0153	0.0809	0.203	0.072
Propyne-H$_2$O							
H$\cdots\pi$ (O-H$\cdots\pi$)	0.0118	0.0352	-0.0101	-0.0073	0.0526	0.192	0.384
H$\cdots\pi$ (C-H$\cdots$O)	0.0071	0.0285	-0.0062	-0.0047	0.0394	0.157	0.319
n$\cdots\sigma$*	0.0137	0.0461	-0.0154	-0.0144	0.0758	0.203	0.069
But-1-yne-H$_2$O							
H$\cdots\pi$ (O-H$\cdots\pi$)	0.0143	0.0408	-0.0129	-0.0092	0.0629	0.205	0.402
H$\cdots\pi$ (C-H$\cdots$O)	0.0059	0.0244	-0.0050	-0.0042	0.0335	0.149	0.190
n$\cdots\sigma$*	0.0137	0.0466	-0.0154	-0.0144	0.0763	0.202	0.069
But-1-en-3-yne-H$_2$O							
H$\cdots\pi$ (O-H$\cdots\pi$)	0.0126	0.0346	-0.0110	-0.0074	0.0531	0.207	0.486
H$\cdots\pi$ (C-H$\cdots$O)	0.0093	0.0294	-0.0091	-0.0084	0.0467	0.195	0.083
n$\cdots\sigma$*	0.0145	0.0482	-0.0165	-0.0155	0.0802	0.206	0.065
PhAc-H$_2$O							
H$\cdots\pi$ (O-H$\cdots\pi$)	0.0129	0.0353	-0.0112	-0.0074	0.0539	0.208	0.514
H$\cdots\pi$ (C-H$\cdots$O)	0.0108	0.0326	-0.0108	-0.0098	0.0533	0.203	0.102
n$\cdots\sigma$*	0.0143	0.0505	-0.0162	-0.0151	0.0817	0.198	0.073
Benzene-H$_2$O							
H$\cdots\pi$ (O-H$\cdots\pi$)	0.0098	0.0285	-0.0079	-0.0030	0.0394	0.201	1.633

global minimum. It can be seen from Table 3.7, which presents the results of the NBO analysis, that the dominant delocalization interaction in the H···π system in the C_2H_2-H_2O system, involves the C_1-C_3 (π) to O_5-H_6 (σ^*) delocalization, while the strongest delocalization in the n···σ complex occurs between the lone pair of O_5 (n) to the σ^* of C_3-H_4 (Table 3.7). In the former interaction, the D-A energy difference is smaller than in the latter; however, the latter interaction enjoys a larger overlap, which results in the n···σ^* interaction being the favoured complex. It is the dominance of the overlap integral in the case of n···σ^* complex that results in it being the preferred complex in the C_2H_2-H_2O system. In short, it is not necessarily the strongest acid that serves as the proton donor; the most stable structure is one where both proton donor and acceptor affinities are optimized.

While we have addressed the question of relative strengths of the hydrogen bonds, through D-A energy differences and overlaps, Gilli *et al.*[18] have addressed the same question, by examining the pK_a values of the proton donor and the conjugate acid of the proton acceptor. They concluded that systems with small differences in these two values, show strong interactions. Based on the 'slide rule' concept that they proposed, the ≡C-H···O interaction (n···σ^* complex) in C_2H_2-H_2O and PhAc-H_2O, falls under the category of "medium/weak" interaction. Since the pK_a values for π bond acceptors are not known, their arguments could not be extended to O-H···π system in C_2H_2-H_2O and PhAc-H_2O.

3.11 Conclusions

This study has identified for the first time the n···σ^* complex, a local minimum, in the PhAc-H_2O system. The PhAc-H_2O complex provides a rich landscape of structures, with the H···π structure being predicted to be the global minimum and which was observed in cold molecule gas phase experiments. The local minimum, the n···σ^* complex, was however not observed in those experiments. Hence it was thought interesting to see if the n···σ^* structure, which is reasonably bound, could be observed in the matrix, as the matrix isolation technique is known to trap local minima. Our experiments using N_2 and Ar matrix, have provided unambiguous evidence, through shifts in the ≡C-H stretch and the phenyl -CH out-of-plane bending modes, for the formation of the n···σ^* complex. This conclusion was further confirmed through experiments using PhAc$_D$ and D_2O. The observed experimental wavenumbers were corroborated by computations performed at MP2/aug-cc-pVDZ level. AIM and LMOEDA analysis were performed on all the complexes. We were, however,

unable to obtain evidence for the H⋯π structure, the global minimum, in our experiments. It appears likely that features due to the H⋯π structure were masked by spectral interferences.

This work has exploited a feature of matrix isolation experiments, which is to trap local minima. This study has thrown light on the local minimum in the PhAc-H_2O complex. Interestingly, the n⋯σ* complex which is a local minimum in the PhAc-H_2O system, is the global minimum in the C_2H_2-H_2O system, thereby highlighting the influence of the structure of the precursors on the structure of the complex.

Chapter 4

Another Look at the Elusive ≡C-H··O Complex in the Hydrogen Bonded Systems of Phenylacetylene: A Study of PhAc-DEE and PhAc-MeOH Complexes

4.1 Introduction

This chapter attempts to further confirm the presence of the n-σ* complex, a local minimum, observed in the PhAc-H$_2$O system. In the previous chapter, we studied PhAc-H$_2$O system and observed the n-σ* complex, which was a local minimum and which in gas phase experiments was not observed . The molecular beam studies identified the global minimum, which was an O-H···π$_{Ac}$ complex (additionally stabilized by a phenyl C-H···OH$_2$ interaction), wheras matrix isolation studies unambiguously trapped an n-σ* (≡C-H···O) complex, which was a local minimum.[28-27] The study of PhAc-methanol (MeOH) and PhAc-Diethylether (DEE) systems, in which the former can potentially show H···π and n-σ* structures while the latter is constrained to form only n-σ* contacts with PhAc, was undertaken, to independently confirm the experimental observation of n-σ*structure in PhAc-H$_2$O system.

Computation on PhAc-MeOH indicated two types of nearly degenerate O-H··π complexes, where MeOH donates a proton to the π system of either the phenyl ring or the acetylenic π system of PhAc. Gas phase studies, using UV-IR double resonance as the probe, clearly identified the O-H···π complex.[59] It was inferred in these experiments that the observed complex was one where MeOH donated its hydroxyl proton to the phenyl ring of PhAc. Furthermore, the n-σ* complex, where PhAc donates a proton to the oxygen of MeOH was not observed in their experiments, though computations indicated this complex to be a local minimum, which was only marginally less stable than the O-H··π global minimum. It was therefore thought interesting to examine if this local minimum could be observed in the matrix, much like in the PhAc-H$_2$O system.Some preliminary work on PhAc-MeOH system was performed by Mariyam using PhAc$_D$ and a low resolution spectrometer.[106]

To independently confirm the presence of the n-σ* complex in the matrix, and hence unambiguously corroborate the infrared spectra of such complexes, we performed experiments with diethylether (DEE), to study the hydrogen bonded complex of PhAc-DEE. This system can be expected to manifest only the n-σ* complex. A comparison of the shifts in the ≡C-H vibrational frequency in PhAc-DEE with that observed for PhAc-H$_2$O and PhAc-

MeOH would unambiguously confirm the presence of this type of interaction in these complexes, which was the motivation for our studies with DEE.

4.2 Experimental Details

The details of the experiments are described in chapter 2. In particular, the present set of experiments was performed using N_2 and Ar (Sigma Gases and Services, 99%) as matrix gases. Phenylacetylene (Sigma Aldrich, 98%), Phenylacetylene-D (Sigma Aldrich, 99% Atom-D), MeOH (Merck ≥99.8) and diethylether (Merck ≥99.8) were used without further purification. All liquid samples were used after subjecting them to several freeze-pump-thaw cycles, before preparation of the matrix gas-sample mixture.

Matrix gas–sample mixture was deposited on the cold substrate using a single jet effusive nozzle . The concentration of matrix gas–sample was varied typically from 0.5:1000 to 3:1000 individually, for both precursors using manometric procedures.

Experiments were performed in both Ar and N_2 matrices, both of which showed evidence for the formation of the PhAc-MeOH and PhAc-DEE complexes. However, since the spectra were well resolved in the N_2 matrix, we show the spectra obtained in this matrix.

4.3 Computational Details

The computational study was carried out using Gaussian-09 suite of programs.[73] All computations were performed using M06-2X and MP2 methods, using 6-311++G(d,p) and aug-cc-pVDZ basis sets. Single point calculations were also done at the MP2/aug-cc-pVTZ, MP2/aug-cc-pVQZ and CCSD(T)/aug-cc-pVDZ level on the optimized geometries obtained at the MP2/aug-cc-pVDZ level of theory. The computational details have already been discussed in Chapter 2.

The computed frequencies of the complexes, PhAc-MeOH and PhAc-DEE were scaled by using appropriate scaling factors to enable a comparison with experimentally observed features. The scale factors were computed as explained in Chapter 3 and have been mentioned in tables listing the experimental and computed vibrational wavenumbers. The interaction energies of the complexes were calculated from the energies of the complexes and the monomers. These interaction energies were corrected separately for basis set superposition error (BSSE), using counterpoise method proposed by Boys and Bernardi[79] and ZPE (zero point energies). Interaction energies using single point calculation at the CCSD/6-311++G(d,p) and CCSD/aug-cc-pVDZ level were also calculated using the geometry optimized at the MP2 level and the respective basis sets. Interaction energies at MP2/CBS and CCSD(T)/CBS limits were also calculated. An examination of electron density topology was performed using the atoms-in-molecules analysis implemented through AIM2000,[81] to

understand bonding characteristics in the complex. NBO and LMOEDA analysis, implemented using Gaussian-09 and GAMESS,[74] respectively, were also performed to understand the nature of bonding in these non-covalent interactions.

We will first present our results on PhAc-Methanol and then PhAc-DEE complexes.

4.4 Results- PhAc-MeOH

a) Experimental

When PhAc and MeOH were codeposited and the matrix then annealed, new product features were observed at 3235.1/3232.6 cm^{-1} in the region of the $\equiv$CH stretch of PhAc (Fig. 4.1) and 3593.9/3590.6 cm^{-1} in the region of MeOH O-H stretch (Fig. 4.2). These features were observed only when both precursors were codeposited and the matrix was annealed. Furthermore, on increasing the concentration of either monomer, the intensity of the product features increased, thereby confirming them to be due to the PhAc-MeOH complex. Experiments were also performed at very low concentration of both the monomers thereby excluding the possibility of these features being due to dimers or other higher aggregates of the monomeric species. Furthermore low concentration experiments also confirmed these complexes as 1:1 adducts rather than larger hydrogen bonded clusters. Experiments with isotopically substituted PhAc with acetylenic hydrogen replaced with deuterium (PhAc$_D$) were also performed to observe isotopic shifts. Product features were observed at 2554.7 and 2593.6 cm^{-1} in N_2 matrix (Fig. 4.3).

b) Computational

Ab-initio calculations performed at MP2/6-311++G(d,p) and MP2/aug-cc-pVDZ level of theory yielded three hydrogen bonded complexes as a minima on potential energy surface.The structures of PhAc-MeOH complexes at MP2/aug-cc-pVDZ level are shown in Fig 4.4 and agree with those reported by Patwari and coworkers.[59] Table 4.1 gives the details of geometrical parameters of PhAc-MeOH complexes at MP2/aug-cc-pVDZ level of theory. Complex 1 represents an n-σ* complex in which PhAc acts as proton donor through acetylenic C-H to oxygen of MeOH. The two other structures represent O-H··π systems, where the MeOH serves as a proton donor, to the π system of the phenyl ring (Complex 2) or the acetylenic system (Complex 3). At this level of theory, Complex 2 is the global minimum, while Complex 3 is only marginally higher in energy, by about 0.1 kcal/mol. At the M06-2X level of theory in addition to these three complexes a fourth complex (Complex 4) was also located. This complex has an interaction between the O-H group of MeOH and the acetylenic
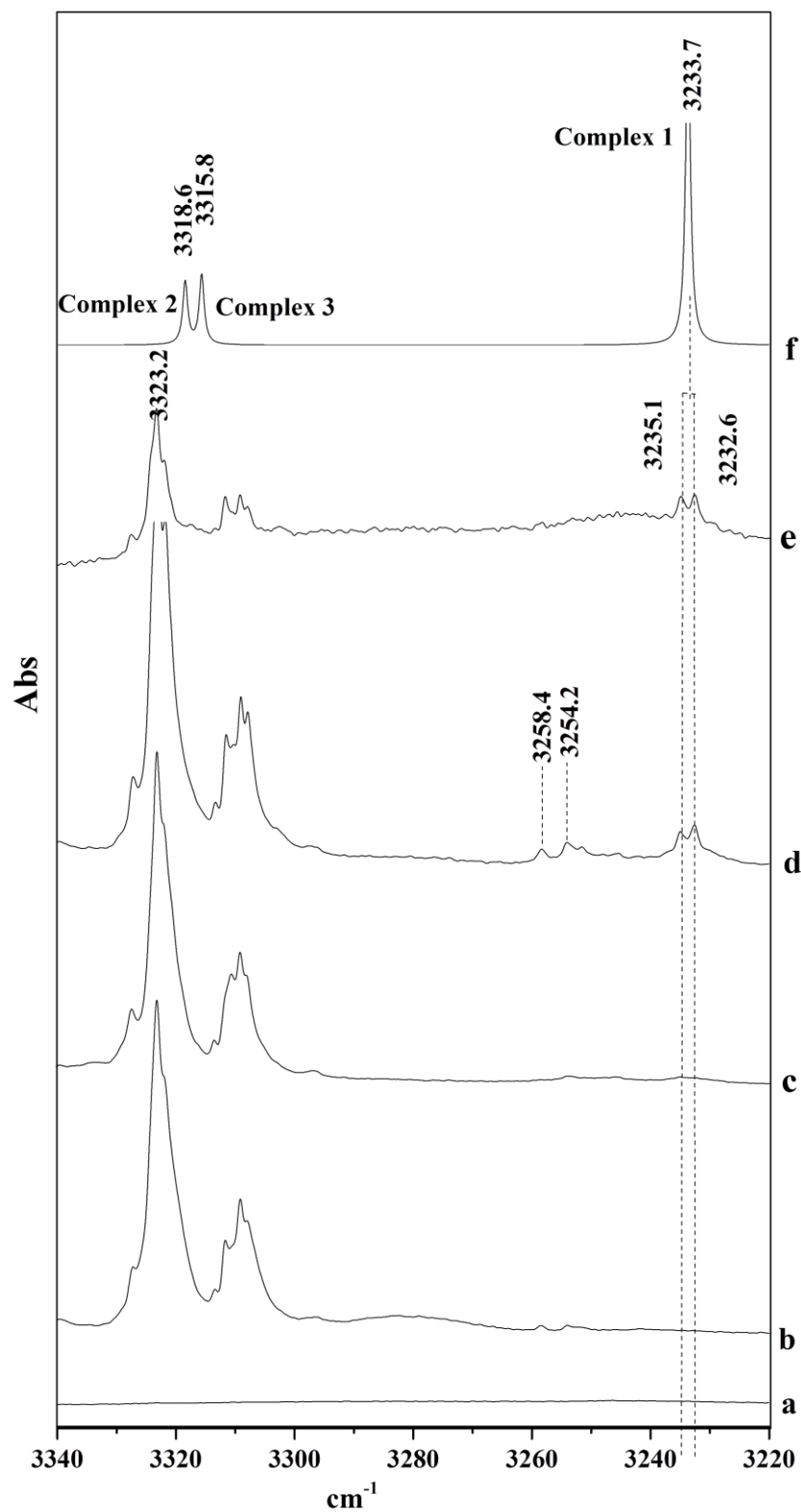
Figure 4.1: Annealed spectra of PhAc, MeOH and PhAc-MeOH complex in ≡CH stretching region of PhAc (3440-3220 cm^{-1}).(a) MeOH:N$_2$ (1:1000) (b) PhAc :N$_2$ (3:1000) (c) 12 K spectrum of PhAc:MeOH:N$_2$ (3:1:1000) (d) PhAc:MeOH:N$_2$ (3:1:1000). (e) PhAc:MeOH:N$_2$ (0.5:1:1000) (f) Computed Spectra of Compex 1,2 and 3 at MP2/aug-cc-pVDZ level of theory.

Figure 4.2: Annealed spectra of PhAc, MeOH and PhAc-MeOH complex in OH stretching region of PhAc (3700-3550 cm^{-1}).(a) MeOH:N_2 (1:1000) (b) PhAc :N_2 (3:1000) (c) 12 K spectrum of PhAc:MeOH:N_2 (3:3:1000) (d) PhAc:MeOH:N_2 (3:3:1000). (e) PhAc:MeOH:N_2 (3:1:1000) (f) Computed Spectra of Compex 1,2 and 3 at MP2/aug-cc-pVDZ level of theory.

Figure 4.3: Annealed spectra of PhAc$_D$, MeOH and PhAc$_D$-MeOH complex in $\equiv$CD stretching region of PhAc$_D$ (2650-2500cm^{-1}).(a) MeOH:N$_2$ (1:1000) (b) PhAc$_D$:N$_2$ (3:1000) (c) 12 K spectrum of PhAc$_D$:MeOH:N$_2$ (3:3:1000) (d) PhAc$_D$:MeOH:N$_2$ (3:3:1000). (e) PhAc$_D$:MeOH:N$_2$ (3:1:1000) .
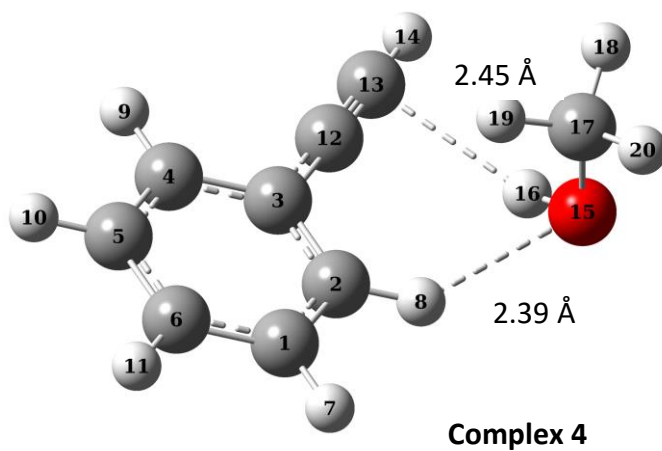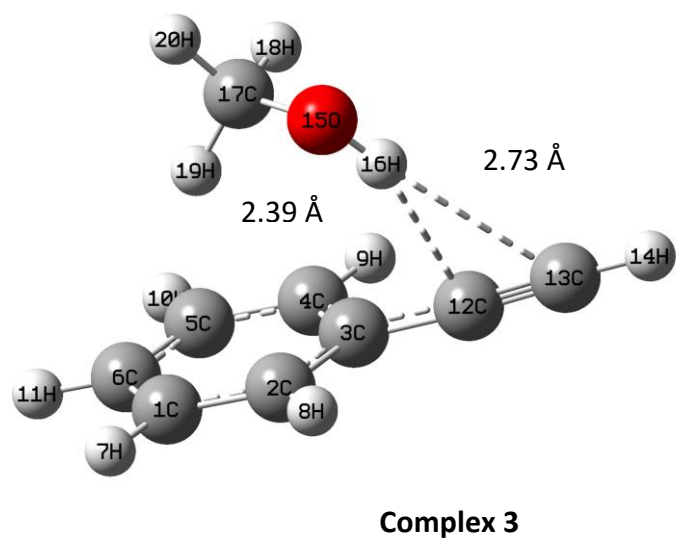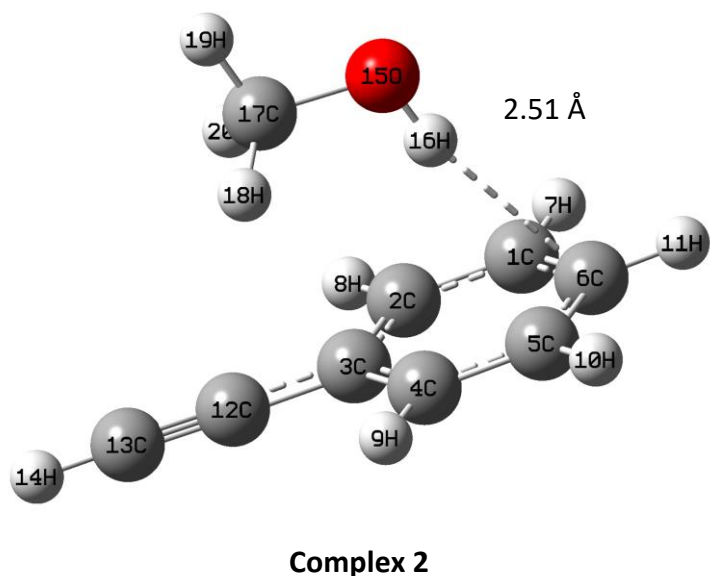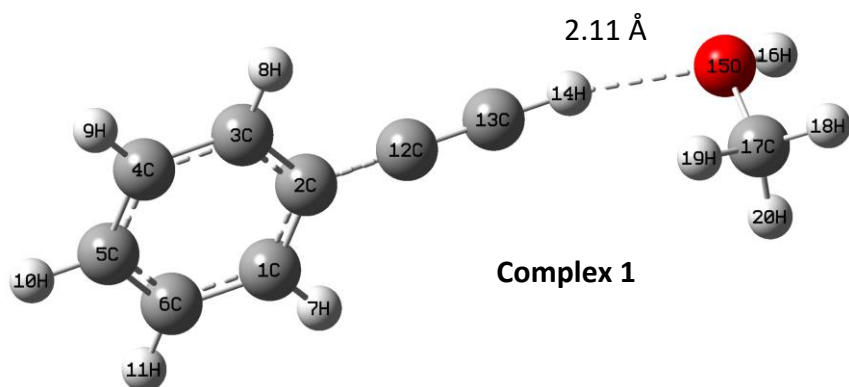
Figure 4.4. Optimized geometries of PhAc-MeOH complexes at MP2/aug-cc-pVDZ level of theory. Note that the structure of Complex 4 shown, was obtained at M06-2X/aug-cc-pDVZ level of theory. See text for details.

Table 4.1: Important structural complex parameters, bond lengths (Å), bond angles (°) and dihedral angles (°), of PhAc-MeOH complexes, computed at MP2/aug-cc-pVDZ level of theory.

Complex 1	
O15-H14	2.11
C17-O15-H14	102.37
O15-H14-C13	165.64
H16-O15-H14	132.01
H20-C17-O15-H14	82.52
H16-O15-H14-C13	143.71
Complex 2	
H16-C6	2.51
O15-H16	0.97
C17-O15-H16	107.43
O15-H16-C6	167.80
H19-C17-O15-H16	179.99
C17-O15-H16-C6	179.77
Complex 3	
H16-C13	2.73
O15-H16	0.97
H16-C12	2.39
C13-H14	1.07
C17-O15-H16	107.62
O15-H16-C13	173.71
O15-H16-C12	159.18
H19-C17-O15-H16	64.77
C17-O15-H16-C13	150.48
C17-O15-H16-C12	-45.59
Complex 4*	
H16-C12	2.49
H16-C13	2.45
O15-H16	0.96
H8-O15	2.39
C2-H8-O15	140.86
H8-O15-H16	77.00
C12-H16-O15	135.54
C2-H8-O15-C17	51.40
C13-H16-O15-C17	-10.06
H16-O15-C17-H19	58.89

*The parameters of Complex 4 obtained at M06-2X/aug-cc-pVDZ level of theory are shown. See text for details

π cloud of PhAc, together with a C-H··O interaction between hydrogen atom attached to ortho C of PhAc and O of MeOH; very similar to the PhAc-H_2O structure, which was the global minimum (Fig.4.4). This structure was not found at the MP2 level. The Raw/ZPE/BSSE corrected interaction energies of PhAc-MeOH complexes at various levels of theory are given in Table 4.2. Table 4.2 shows that at the M06-2X level of theory, complex 4 is the lowest energy structure whereas at the MP2 level, complex 2 is the global minima. Since complex 4 occurs only at the M06-2X level and not at the MP2, we refrain from discussing this structure further. It is clear that in systems with weakly interacting contacts, a number of isomers are possible and the energy ordering amongst these structures can often be ambiguous and a function of the level of theory employed. Only with experimental results together with computations, can answers to energy ordering of the various isomers, be provided. In the case of PhAc-MeOH, but for the experimental data of Patwari[59], the issue of the global minimum would have been an open question. Experiments, such as ours, which probe local minima, lead to an enhanced understanding of the system.

4.5 Discussions

Vibrational Assignments

a) ≡C-H stretch of PhAc in PhAc-MeOH

The PhAc in N_2 matrix shows ≡C-H frequency at 3323.2 cm^{-1} [95] with Fermi resonance diad appearing at 3309.2/3310.8 cm^{-1}; this doublet being due to site splitting. The Fermi resonance has been reported to occur between the ≡C-H stretch and a combination of one quantum of C≡C stretch and two quanta of C≡C-H out-of-plane bend.[97] New product features at 3235.1 cm^{-1}/3232.6 cm^{-1} were seen when PhAc and MeOH were codeposited in the matrix. These product features were assigned to the ≡C-H stretch of PhAc in PhAc-MeOH complex (Fig. 4.1). Table 4.3 shows that this feature was red shifted from ≡C-H stretch of monomer PhAc by 88.1 cm^{-1}. This shift is in good agreement with the computed wavenumber shift of ~87 cm^{-1} for Complex 1. PhAc being the proton donor shows large red shift which is in agreement with our previous work on PhAc-H_2O complexes where also the n-σ* complex showed a red shift of ~ 60 cm^{-1}. The n-σ* complex, which is unambiguously observed in our experiments, was not observed in the gas phase experiments.

In O-H··π complexes, PhAc acts as a proton acceptor; and as is well known, in such complexes, the ≡C-H frequency shows significantly smaller red shifts than that observed in ≡C-H··O (n-σ*) complexes.[101] Our computations for the H-π complexes indicated red shifts

Table 4.2: Computed interaction energies Raw/ZPE/BSSE (kcal/mol) of the complexes of PhAc-MeOH, at various levels of theory and basis sets. CCSD(T) values are uncorrected interaction energies obtained using single point energy calculations at the geometries optimized at the MP2 level and the corresponding basis sets.

Complex	M06-2X		MP2			CCSD(T)	
	6-311++G**	aug-cc-pVDZ	6-311++G**	aug-cc-pVDZ	CBS	aug-cc-pVDZ	CBS
1	-3.96/-3.14/-3.53	-3.56/-2.50/-3.09	-4.28/-1.61/-2.74	-4.36/-3.57/-3.08	-3.35	-4.27	-3.26
2	-5.62/-4.85/-4.84	-5.55/-4.97/-4.65	-6.18/-4.55/-3.17	-7.59/-6.74/-4.04	-4.92	-6.84	-4.16
3	-5.56/-4.63/-4.77	-5.47/-4.64/-4.64	-6.28/-4.24/-3.13	-7.36/-6.31/-3.94	-4.80	-6.68	-4.12
4	-5.64/-4.50/-5.07	-5.69/-4.55/-5.02	----	---	---	---	---

Table 4.3: Experimental and scaled[1] computed wavenumbers (cm^{-1}) for PhAc-MeOH complexes at MP2/aug-cc-pVDZ level of theory.

Experimental (N_2)		Scaled Computed Wavenumbers (cm^{-1})				Mode Assignment
PhAc	Complex	Monomer	Complex 1	Complex 2	Complex 3	
3323.2	**3235.1/3232.6 (-88.1)[2]/(-90.6)**	3320.5	**3233.7 (-86.9)**	3318.6 (-2.0)	3315.8 (-4.8)	≡CH stretch
CH_3OH						
3664.2	**3593.9/3590.6 (-70.3/-73.6)**	3664.3	3660.7 (-3.6)	**3623.7 (-40.6)**	**3617.1 (-47.2)**	OH stretch
$PhAc_D$						
2599.7	**2554.7 (-45.0)**	2652.2	**2599.9 (-52.3)**			≡CD stretch
	2593.6 (-6.1)			**2650.7 (-1.5)**	**2647.7 (-4.5)**	

[1]Scaling Factor (500-3000 cm^{-1}) = 0.99089 ; Scaling Factor (3000-3900 cm^{-1}) = 0.95385

[2]$\Delta\nu = \nu_{complex} - \nu_{monomer}$

of 2 cm^{-1} and 5 cm^{-1} for complexes 2 and 3, respectively, which were not evident in our experiments. It is possible that these features were probably masked by the Fermi resonance bands of PhAc occurring at 3309.2/3310.8 cm^{-1}. It must be recalled that the O-H··π complex was observed in the gas phase experiments.[59] Hence experiments with isotopically substituted PhAc with deuteriated acetylenic hydrogen (PhAc$_D$) were performed to see if the features of the O-H··π complex could be observed in the isotopic molecule, which will be presented next.

b) ≡C-D stretch of PhAc$_D$ in PhAc$_D$-MeOH

The ≡C-D stretch of PhAc$_D$ occurs at 2599.7 cm^{-1} in N$_2$ matrix. The deuterium substituted PhAc (PhAc$_D$) does not show a Fermi resonance, as seen in PhAc, due to the shift in ≡C-D stretch to a lower wavenumber and consequent suppression of Fermi resonance which involved the ≡C-H stetching mode. However, the PhAc$_D$ manifested site splitting as can be seen in Fig.4.3 . An intense feature due to the ≡C-D stretch was observed at 2599.7 cm^{-1} in the N$_2$ matrix, with site split features at 2602.6 and 2604.7 cm^{-1}. With the absence of Fermi resonance diads, it was explored if the small shift in the ≡C-D stretch as a result of the formation of the H-π complex, could be observed.

Complex 1

When PhAc$_D$ and MeOH were codeposited, new product features were observed in the ≡C-D stretching region at 2554.7 cm^{-1}, which was red shifted from the ≡C-D stretch of uncomplexed PhAc$_D$ by 45 cm^{-1}. The computational studies predict a feature for n-σ* complex at 2599.9 cm^{-1} which is red shifted by 52.3 cm^{-1} (Table 4.3). The experimental and computational observations agree very well so this feature was assigned to Complex 1 (n-σ*). This assignment further reassures the formation of the n- σ* (Complex 1).

Complex 2/3

In the annealed matrices containing *both* PhAc$_D$ and MeOH, a new feature at 2593.6 cm^{-1} was observed. This feature is red shifted from the feature due to uncomplexed PhAc$_D$ by ~6 cm^{-1}, and agrees with the computed shift of 2 cm^{-1} (Complex 2) or 3 cm^{-1} (Complex 3) for it to be due to a O-H··π complex (Fig. 4.3). Our data does not unambiguously point to Complex 2 or 3, and we therefore refrain from making a firm assignment other than to say that the O-H··π complex was observed.

c) O-H stretch of MeOH in PhAc-MeOH

Complex 1

The O-H stretching frequency of MeOH occurs at 3666.2 cm^{-1} in a N$_2$ matrix. In Complex 1, the O-H stretch of MeOH was computed to occur at 3660.7 cm^{-1} which amounts

to a red shift of 4 cm^{-1} from that of uncomplexed MeOH. However, we did not discern any feature that could be assigned to this feature in the matrix, even though the formation of Complex 1 was unambiguously indicated through the shifts in the ≡C-H stretch.

Complex 2/3

In the codeposition experiments of PhAc and MeOH, new product bands in O-H stretching region were observed at 3593.9 and 3590.6 cm^{-1} which are respecitively red shifted by 70.3 and 73.6 cm^{-1} from the O-H stretch of uncomplexed MeOH at 3666.2 cm^{-1} (Fig 4.2 , Table 4.3). Such large red shifts are generally indicative of complexes where MeOH is a proton donor, which in this case would imply the formation of a O-H··π complex. It can be observed from Table 4.3 that the observed shifts are in agreement with the O-H··π type complexes, which are computed to show a red shift of 40.6 and 47.2 cm^{-1} for Complex 2 and 3 respectively. Hence these product features can be assigned to O-H··π complex of PhAc-MeOH adducts. However, once again it is impossible for us to assign these features firmly to either Complex 2 or 3. We only assert that the O-H··π complexes are observed in the matrix in addition to the n-σ*.

4.6 Results-PhAc-DEE Complex

While the computed and observed frequency shifts were in agreement, for the n-σ* complex of PhAc-MeOH, we looked for an independent confirmation for the presence of this complex. Towards this end, we studied the PhAc-DEE system, which can be expected to manifest only an n-σ* (≡C-H··O) complex. A comparison of the shift of the ≡C-H frequency observed in this system with that observed for the systems studied earlier, PhAc-MeOH and PhAc-H$_2$O, would provide unequivocal proof for the existence or not of the n-σ* complex in these experiments. Diethylether (DEE) was used in these experiments owing to its more ready availability than dimethylether.

a) Experimental

When PhAc and DEE were codeposited and the matrix then annealed, new product bands were observed at 3194.2 cm^{-1} and 1123.9 cm^{-1} (Fig 4.5). Concentration dependence of these features further proved their assignment to a 1:1 PhAc-DEE complex. Experiments with PhAc$_D$ and DEE yielded product features at 2554.7/2552.8 cm^{-1} and 1123.9 cm^{-1} (Fig 4.6).

b) Computational

DEE can serve only as a hydrogen bond acceptor, since it has only one basic site at the oxygen atom, with no sufficiently acidic proton for proton donation. Incidentally, the

presence of two ethyl chains on oxygen, leads to the possibility of conformers in DEE. At the MP2/aug-cc-pVDZ level four conformers of DEE were found, as shown in Fig. 4.7. It can be seen that the conformers arise due to the relative orientation of the terminal carbon atoms; the four conformers being labelled as TT , TG , G^+G^- , $G^\pm G^\pm$. In the TT conformer all the carbon atom and the oxygen, adopt an all-trans orientation, while in the gauche conformer the terminal carbon atom has a staggered orientation. The TT conformer is the global minimum, while progressive change of the terminal carbon to adopt a gauche orientations raises the energy, as shown in Fig. 4.7, which shows both the structures and the relative energies of the various conformers. While the TT structure is the global minimum as it experiences the least steric interaction, the TG and GG conformers adopt a gauche orientation, stabilized by a n→σ_{C-C}* delocalization, as revealed through an NBO analysis. A similar effect, referred to as the anomeric effect, operates in many compounds with heteroatoms such as dimethoxymethanes, where the anomeric stabilization is so strong, that it dominates over the steric interaction, leading to the molecule adopting a GG conformer as the ground state.[107]

Based on the relative energies and the conformational degeneracies of the different confomers of DEE, the population of the TT , TG , G^+G^- , $G^\pm G^\pm$ can be calculated to the in the ratio of 79.4:17.5:1.6:1.6. Since the dominant population is due to the TT conformer all computations were done for the complexes with DEE in this conformation.

Fig. 4.8 shows the structure of the PhAc-DEE complex with DEE in the TT conformation. As expected, the PhAc-DEE complex turns out to be an n-σ* complex with PhAc acting as proton donor through ≡C-H to the oxygen atom of DEE. Table 4.4 gives structural parameters of this complex. The interaction energies of the PhAc-DEE complex at various levels of theory are given in Table 4.5.

Vibrational Assignments

c) ≡C-H stretch of PhAc$_H$ in PhAc$_H$-DEE

Fig 4.5 shows the ≡CH stretching region of PhAc spanning from 3360-3150 cm^{-1}. The vibrational feature observed at 3234.1 cm^{-1} shows a red shift of 89.0 cm^{-1} from the same mode in uncomplexed PhAc, which agrees reasonably well with the computed shift (Table 4.6). The shift observed for PhAc-DEE n-σ* complex is similar in magnitude and direction to the red shift observed for the n-σ* complex of PhAc-MeOH and PhAc-H$_2$O. (Table 3.3and 4.3), which independently and convincingly proves the existence of the n-σ* complex in the matrix; a structure that eluded observation in the molecular beam studies.
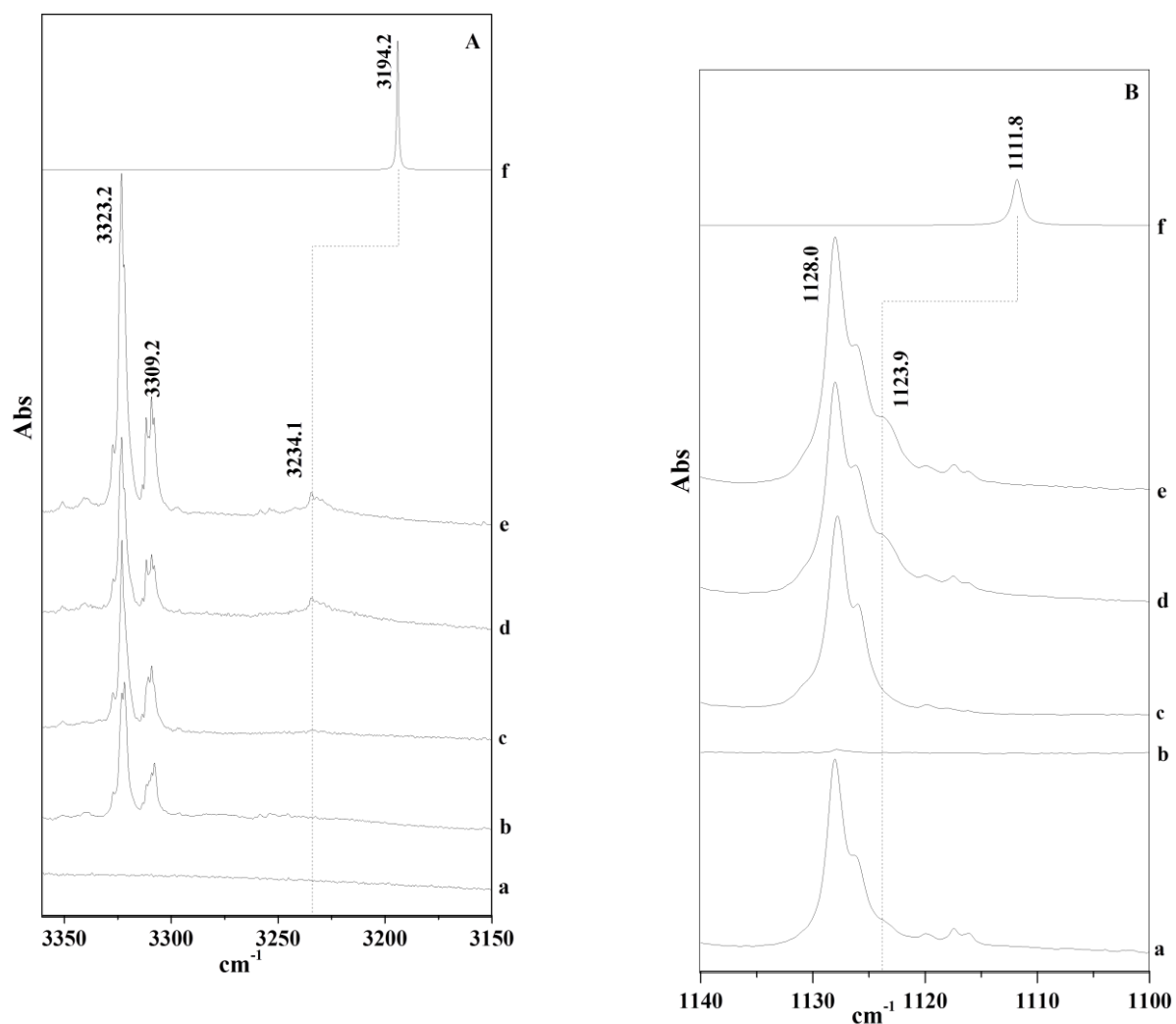
Figure 4.5: Annealed spectra of PhAc, DEE and PhAc-DEE complex in ≡CH stretching region of PhAc (3360-3150cm^{-1}) in Grid A and C-O stretching region of DEE (1140-1100 cm^{-1}) in Grid B.(a) DEE:N$_2$ (0.25:1000) (b) PhAc:N$_2$ (1:1000) (c) 12 K spectrum of PhAc:DEE:N$_2$ (1:1:1000) (d) PhAc:DEE:N$_2$ (1:1:1000). (e) PhAc:DEE:N$_2$ (2:1:1000) (f) Computed Spectra of n-σ* complex at MP2/aug-cc-pVDZ level of theory.
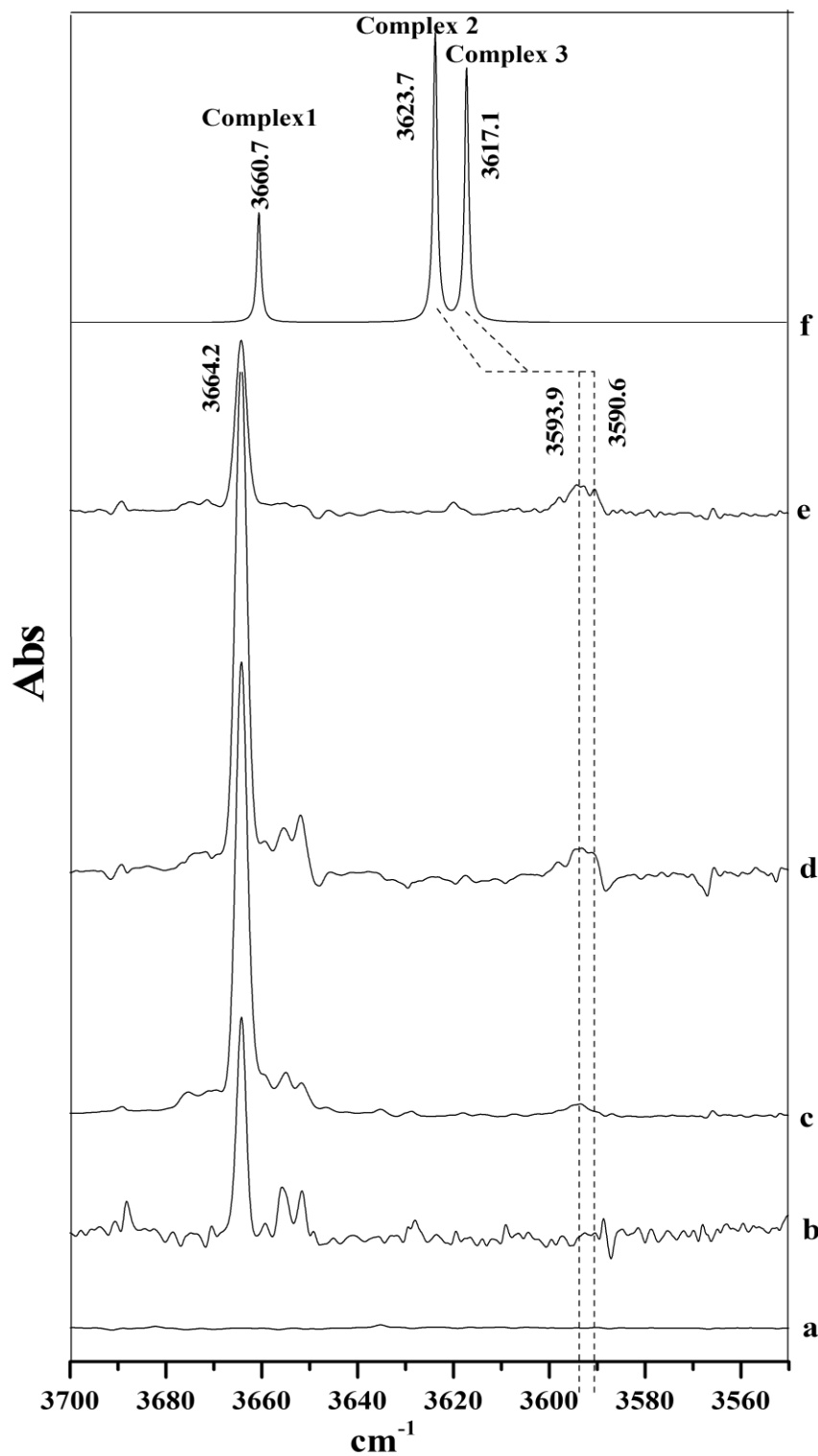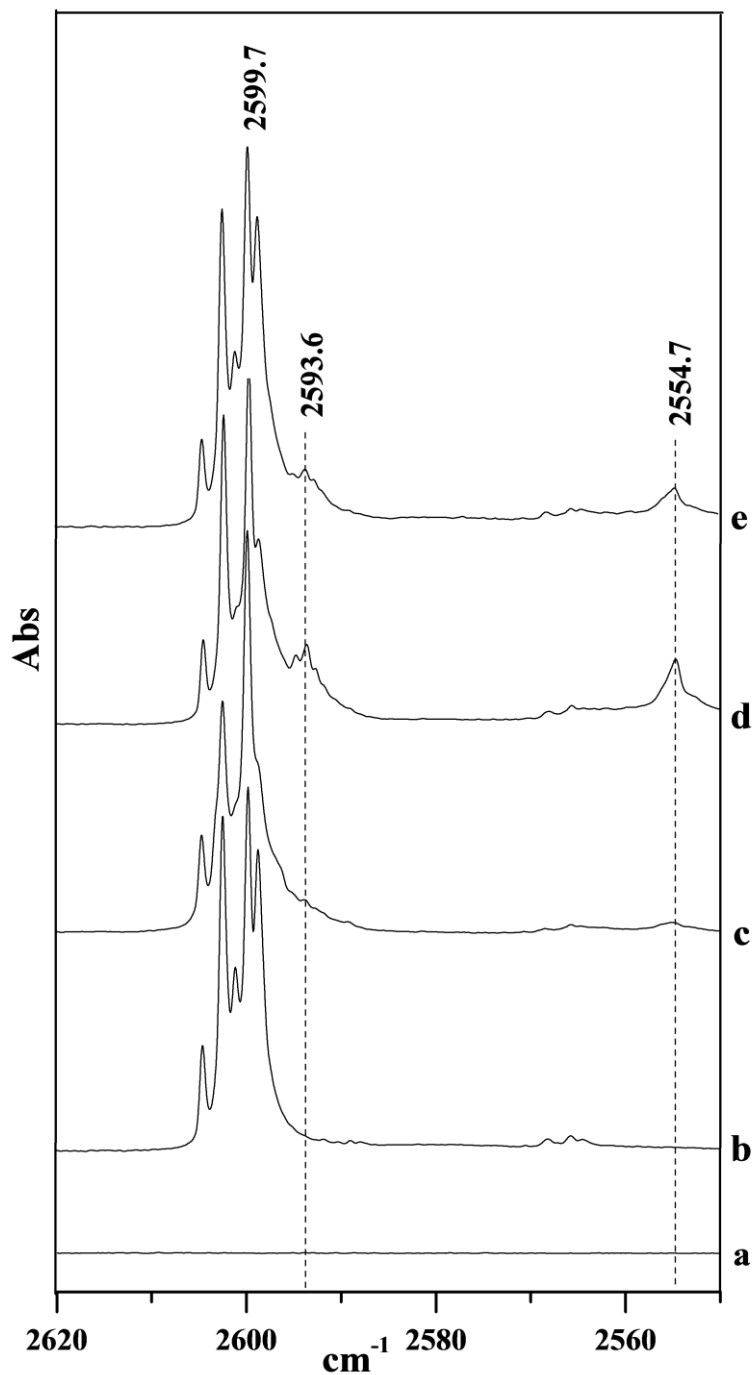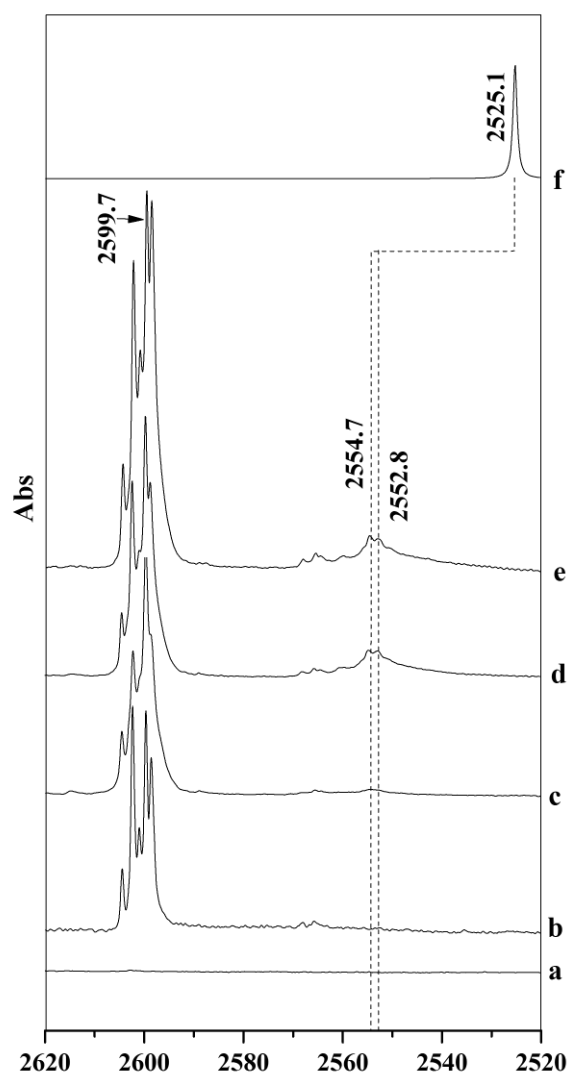
Figure 4.6: Annealed spectra of PhAc$_D$, DEE and PhAc$_D$-DEE complex in ≡CD stretching region of PhAc$_D$ (2620-2520cm^{-1}).(a) DEE:N$_2$ (0.25:1000) (b) PhAc$_D$:N$_2$ (3:1000) (c) 12 K spectrum of PhAc$_D$:DEE:N$_2$ (3:0.5:1000) (d) PhAc$_D$:DEE:N$_2$ (3:0.5:1000). (e) PhAc$_D$:DEE:N$_2$ (3:1:1000) (f) Computed Spectra of n-σ* complex at MP2/aug-cc-pVDZ level of theory

G[±]G[±] 3.04

G⁺G⁻ 2.63

TG   1.31

TT 0.0
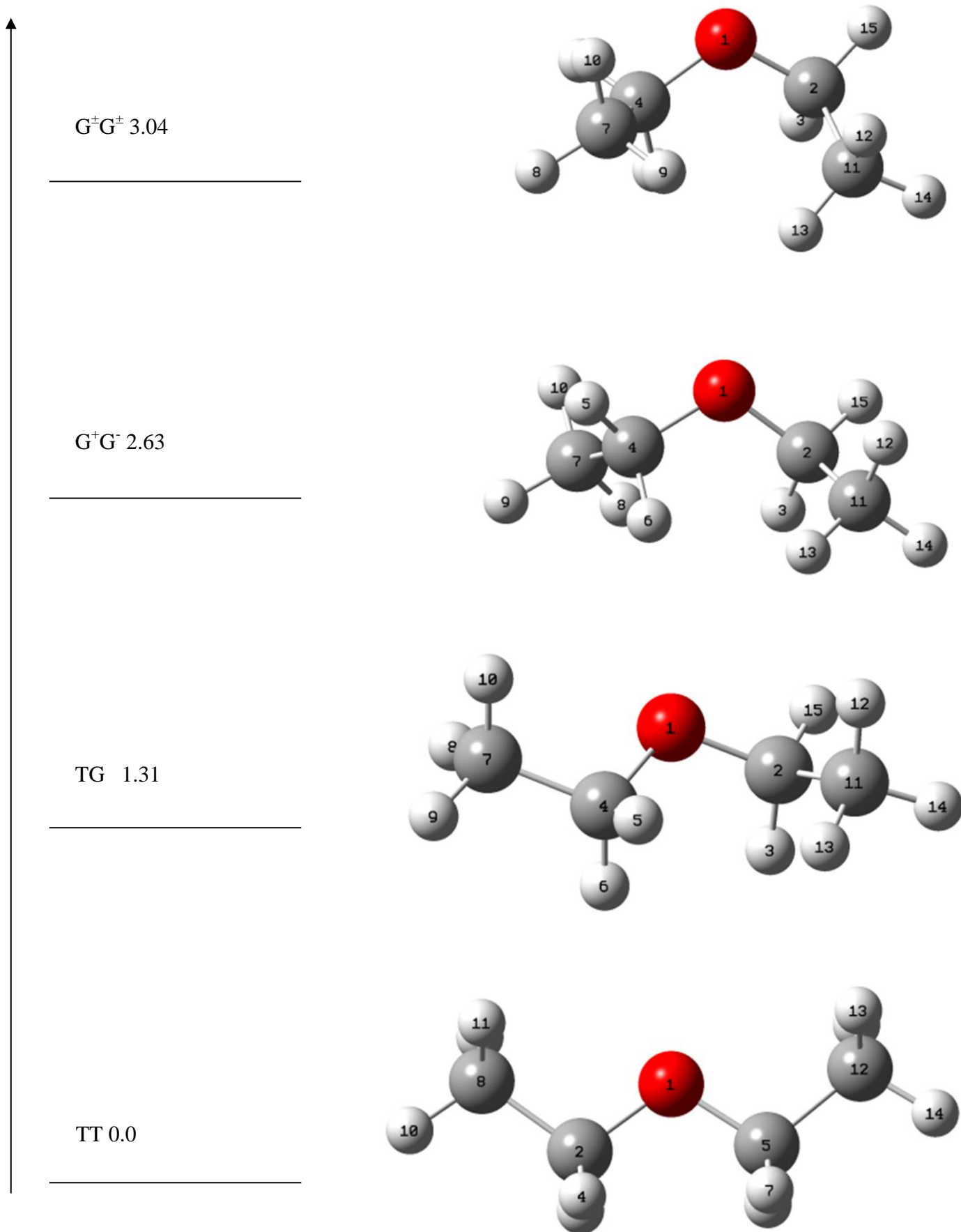
Figure 4.7: Conformations of Diethylether (DEE) with relative energies in kcal/mol at MP2/aug-cc-pVDZ level of theory.

d) C-O stretch of DEE in PhAc-DEE complex

The C-O stretch of the TT conformer of DEE in TT in the N_2 matrix is oserved at 1128.0 cm^{-1} (Fig 4.5). The product feature corresponding to the PhAc-DEE complex was observed as a shoulder at 1123.9 cm^{-1} (Fig 4.5), amounting to a red shift of 4.1 cm^{-1}. This observation corrobrates well with the computed value for the n-σ* complex thereby further confirming the observation of n-σ* complex (Table 4.6).

e) ≡C-D stretch of PhAc$_D$ in PhAc$_D$-DEE

Fig. 4.6 shows the spectrum over the region of the ≡C-D stretch of PhAc$_D$. The product feature for the PhAc$_D$-DEE was observed at 2554.7/2552.8 cm^{-1}, which amounts to a red shift of ~45 cm^{-1}, from the feature of ≡C-D stretch of uncomplexed PhAc$_D$ at 2599.7 cm^{-1} in agreement with the computations (Table 4.6) .The isotopic shift further corroborates the trapping of the n-σ* complex in the matrix.

4.7 AIM analysis

An examination of charge density topology was performed using the atoms-in-molecules (AIM) theory of Bader,[81] with wavefunctions generated at the MP2/aug-cc-pVDZ level of theory. (3,-1) bond critical points corresponding to the weak intermolecular interactions in Complex 1, 2 and 3 of PhAc-MeOH and the n-σ* complex of PhAc-DEE are shown in the Fig. 4.9. Values of electron density $\rho(r_c)$, eigenvalues of the Hessian, $\lambda_1, \lambda_2, \lambda_3,$ the Laplacian ($\nabla^2\rho$) of electron density (defined as the sum of the eigenvalues), the ellipticity, $[(\lambda_1/\lambda_2)-1]$ and $|\lambda_1/\lambda_3|$, for all the complexes, computed at the bond critical points, are shown in Table 4.7.

PhAc-MeOH Complexes

Complex 1 shows a bond critical point (BCP 1) having ≡C-H···O type of interaction. (Fig 4.9). It can be seen that the electron density at BCP of the n-σ* complex is the largest amongst all three complexes. While Complex 2 shows more than one BCP between PhAc and MeOH, the interaction between the O-H of MeOH and the carbon of phenyl appears to be the dominant interaction as revealed by its electron density.This parameters corresponding to this BCP alone is presented in Table 4.7. Complex 3 show two simultaneous interactions between PhAc and MeOH which have comparable electron densities at both the BCPs. It can be seen that the values of $\rho(r_c)$ for all these systems fall in the range of hydrogen bonding complexes proposed by Koch and Popelier.[83]
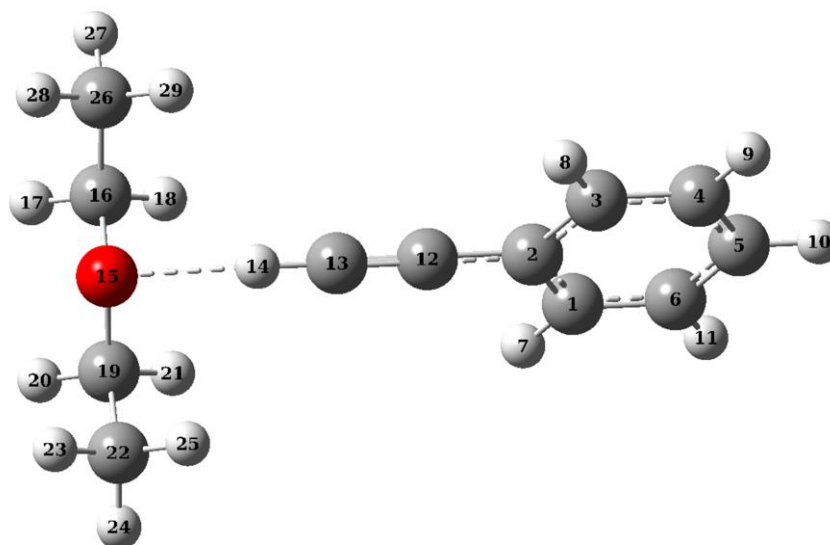
Fig. 4.8 PhAc-DEE complex optimized at MP2/aug-cc-pVDZ level of theory

Table 4.4: Important structural complex parameters, bond lengths (Å), bond angles (°) and dihedral angles (°), of PhAc-DEE complex, computed at MP2/aug-cc-pVDZ level of theory.

n-σ* complex	
O15-H14	2.05
C13-H14	1.08
O15-H14-C13	161.13
C19-O15-H14	96.30
C16-O15-H14	96.28
C19-O15-H14-C13	58.52
C16-O15-H14-C13	-53.83

Table 4.5 : Computed interaction energies Raw/ZPE/BSSE (kcal/mol) of PhAc-DEE n-σ* complex , at various levels of theory and basis sets**.**

Complex	M06-2X		MP2	
	6-311++G**	**aug-cc-pVDZ**	**6-311++G****	**aug-cc-pVDZ**
1	-4.30/-3.60/-3.92	-4.31/-3.60/-3.62	-5.02/-2.82/-3.19	-6.53/-5.69/-4.02

Table 4.6: Experimental and scaled computed wavenumbers (cm^{-1}) of PhAc/PhAc$_D$ and DEE in PhAc-DEE and PhAc$_D$-DEE complex computed at the MP2/aug-cc-pVDZ level of theory.

Experimental (N$_2$ matrix)			Scaled	Mode Assignment
PhAc	Complex	Monomer	n-σ* Complex	
3323.2	**3234.1 (-89.0)[1]**	3323.2	**3194.2 (-129.0)**	≡C-H stretch
DEE				
1128.0	**1123.9 (-4.1)**	1128.0	**1111.8 (-16.2)**	C-O stretch
Phac$_D$				
2599.7	**2554.7/2552.8 (-45.0)/(-46.8)**	2599.7	**2525.1 (-74.6)**	≡CD stretch

Scaling Factor (1630-500 cm^{-1}) = 0.97992

Scaling Factor (3500-2000 cm^{-1}) = 0.95460

Scaling Factor = 0.97128 for PhAc$_D$-DEE complex

[1]$\Delta \nu = \nu_{complex} - \nu_{monomer}$

We have also compared the ratio $|\lambda_1/\lambda_3|$, and these values are approximately equal to but less than 0.25 (Table 4.7), which is indicative of a closed shell interaction. Ellipticity at the bond critical point which is given by $[(\lambda_1/\lambda_2)-1]$, was also calculated for all the complexes. In complex 1, the ellipticity is close to zero for the $\equiv$C-H$\cdot\cdot$O interaction , indicating a bond with a cylindrical symmetry, while the large values of ellipticity for Complex 2 and C-H$\cdot\cdot\cdot$C interaction in Complex 3 , indicating the accumulation of charge in a plane.

PhAc-DEE Complex

It can be seen that in PhAc-DEE the electron density at the only BCP corresponding to the n-σ* intermolecular interaction is 1.3 times larger compared with that in the n-σ* complex of PhAc-MeOH (Table 4.7), indicating the DEE complex to be stronger than the MeOH complex, which is consistent with the larger interaction energy computed for the DEE complex compared with the MeOH complex of PhAc at the same level of theory.

4.8 NBO Analysis

NBO analysis on the PhAc-MeOH and PhAc-DEE systems was also performed, to understand the nature of bonding interactions between donor-acceptor orbitals the results of which are shown in Table 4.8[86.] In this table, we have shown the second order perturbation energies E(2), the energy difference between the donor and acceptor orbitals [E(j)-E(i)] and the overlap between the two orbitals [F(i,j)].

PhAc-MeOH Complexes

Complex 1, with an n-σ* interaction, involves the delocalization of electron density from the lone pair on oxygen to the antibonding orbital on $\equiv$C-H of PhAc (proton donor). The value of second order perturbation energy for this complex shows that it is the strongest interaction, possibly because of higher value of overlap integral . Complex 2 and Complex 3 both have comparatively smaller second order perturbation values as compared to Complex 1 (n-σ*) indicating that $\equiv$C-H$\cdot\cdot$O interaction to be stronger than O-H$\cdot\cdot\pi$ interaction. However, the O-H$\cdot\cdot\pi$ complexes turn out to be stronger and represent the global minima, probably due to multiple contacts.

PhAc-DEE Complex

Table 4.8 shows the results for PhAc-DEE n-σ* complex. The large value for the second order perturbation energy indicates a stronger n-σ* interaction in the PhAc-DEE complex than in the MeOH complex, consistent with the fact that DEE is a stronger proton acceptor than MeOH.
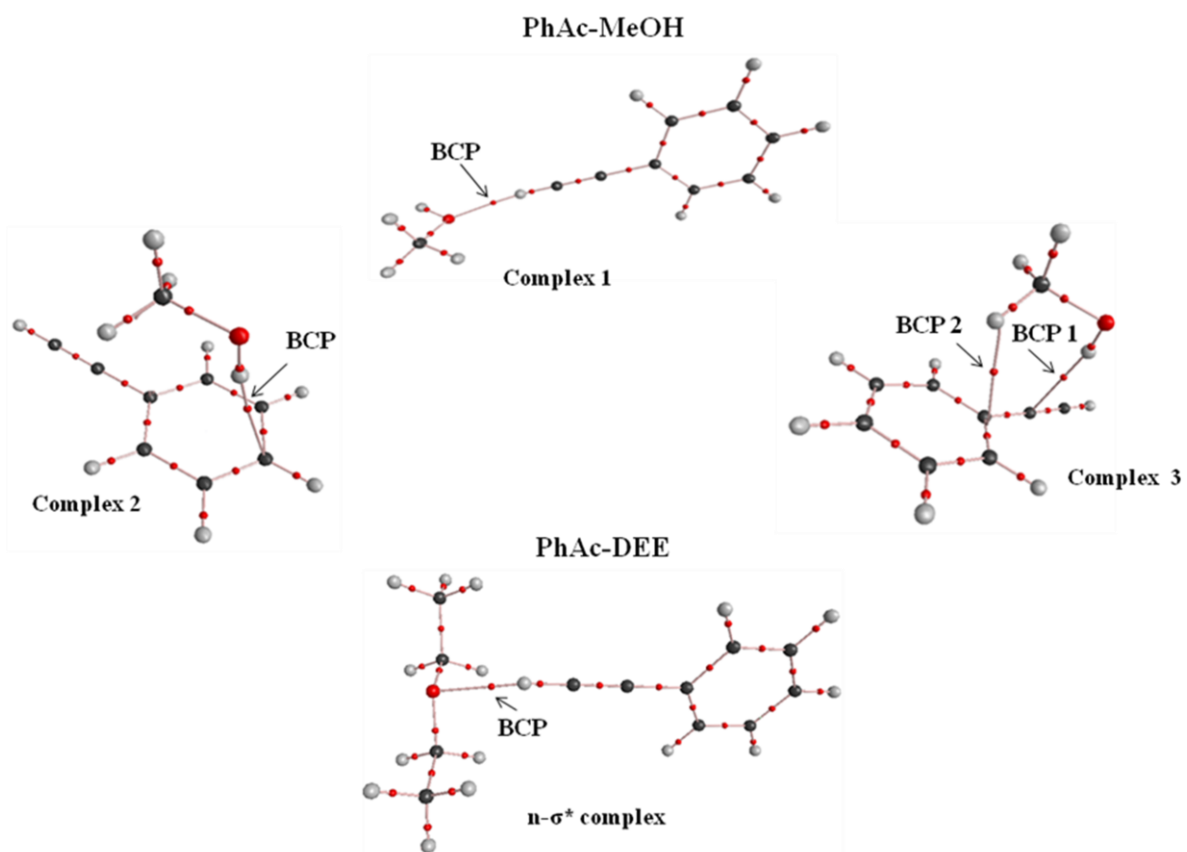
Figure 4.9: AIM analysis of PhAc-MeOH and PhAc-DEE complexes showing Bond Critical Points (BCP) at MP2/aug-cc-pVDZ level of Theory.

Table. 4.7. AIM calculations performed using wavefunctions obtained at MP2/aug-cc-pVDZ for 1:1 PhAc-MeOH and PhAc-DEE complexes.

Complex	$\rho(r_c)$	$\nabla^2\rho(r_c)$	λ_1	λ_2	λ_3	$|\lambda_1/\lambda_3|$	$(\lambda_1/\lambda_2)-1$	ΔE_{HB}	Total ΔE_{HB}
PhAc-MeOH									
Complex 1 C-H⋯O	0.0176	0.0573	-0.0207	-0.0196	0.0976	0.2124	0.0601	-3.30	-3.30
Complex 2 C⋯H-O	0.0101	0.0296	-0.0076	-0.0022	0.0394	0.1935	2.5386	-1.51	-1.51
Complex 3 C⋯H-O	0.0111	0.0326	-0.0097	-0.0062	0.0486	0.1998	0.5554	-3.71	-4.61
Complex 3 C-H⋯C	0.0084	0.0280	-0.0057	-0.0010	0.0347	0.1637	4.4725	-0.90	
PhAc-DEE									
n-σ* C-H⋯O	0.0224	0.0688	-0.0276	-0.0262	0.1226	0.2250	0.0520	-3.30	-3.30

Table 4.8: NBO analysis for PhAc-MeOH and PhAc-DEE complexes, performed at MP2/aug-cc-pVDZ level of theory. The atom numbering indicated in table is as shown in Fig. 4.4 and 4.7. E is the second order perturbation energy (kcal/mol), E(j)-E(i) is the donor-acceptor energy difference and F(i,j) is the overlap between the donor and acceptor orbitals.

System	Orbitals involved		E (kcal/mol)	E(j)-E(i) a.u.	F(i,j) a.u.	Electron occupancy in σ* orbital
	Donor	Acceptor				
PhAc-MeOH						
Complex 1	$O_{15}(n)$	C_{13}-H_{14}(σ*)	4.26	1.32	0.067	0.01424
Complex 2	C_5-C_6 (σ)	O_{15}-H_{16}(σ*)	1.51	1.07	0.039	0.0078
Complex 3	C_{12}-C_{13} (σ)	O_{15}-H_{16}(σ*)	1.71	1.16	0.040	0.00723
PhAc-DEE						
n-σ* complex	$O_{15}(n)$	C_{13}-H_{14}(σ*)	6.06	1.27	0.079	0.01882

4.9 Energy Decomposition Analysis

Localised Molecular Orbital Energy Decomposition Analysis Scheme (LMOEDA) was done to partition interaction energy of the various complexes of PhAc-MeOH and PhAc-DEE into individual contributing energy component, electrostatic E_{ES}, exchange-repulsion E_{ER}, polarization E_{POL} and dispersion E_{DIS}. Table 4.9 lists the contribution of various energy components to the total interaction energy .

In complex 1 of PhAc-MeOH adduct, the major contribution to the interaction energy is from the electrostatic component while polarization and dispersive components have smaller contributions. This picture is similar to that computed for the n- σ* complexes of PhAc-H$_2$O. Complex 2 and Complex 3 present an interesting scenario; both are isoenergetic O-H··π complexes but the energy decomposition pattern of both complexes show contrasting features. In Complex 2 dispersion interaction is the major component followed by electrostatic, while in Complex 3 both dispersive and electrostatic components are almost equal contributors to the total interaction energy. In the PhAc-DEE n-σ* complex too, the electrostatic component is the largest contributor to the interaction energy. It therefore appears that all the n-σ* type complexes observed in our studies receive contributions from the electrostatic components, wheras the O-H··π complexes show dispersive interactions.

4.10 Conclusions

Hydrogen bonded complexes of PhAc-MeOH and PhAc-DEE were studied using matrix isolation infrared spectroscopy and *ab initio* calculations. Gas phase studies on the PhAc complexes with H$_2$O and MeOH identified only the O-H··π complexes which was the global minimum and not the n-σ* complex that was a local minimum. In our experiments, we clearly identified the n-σ* complex in both PhAc-H$_2$O and PhAc-MeOH. In the case of PhAc-MeOH both n-σ* and O-H··π complex were observed in N$_2$ and Ar matrices. The n-σ*complex was identified through the large shifts in the ≡C-H vibrational wavenumbers, which corroborated with our computations. However, in an effort to independently verify this observation, we performed experiments with PhAc-DEE which is contrained to form only the n- σ* complex. The ≡C-H shift observed in the PhAc-DEE was ~90 cm^{-1} to the red. Reassuringly, the shift in the same mode in both the H$_2$O and MeOH complexes was comparable, ~60 cm^{-1} and 88 cm^{-1} respectively thus providing unequivocal evidence for the observation of the n-σ* complex. It might not be out of place to mention that in the case of

Table 4.9: Energy Decomposition analysis of PhAc-MeOH and PhAc-DEE complexes at MP2/aug-cc-pVDZ**.** All energies are given in kcal/mol.

Complex	E_{ES}	E_{ER}	E_{Pol}	E_{Disp}	E_{Total}	E_{ES}/E_{Total}	E_{Pol}/E_{Total}	E_{Disp}/E_{Total}
PhAcH-MeOH								
Complex 1	-5.25	5.06	-1.52	-1.40	-3.12	1.68	0.49	0.45
Complex 2	-4.39	8.27	-1.63	-6.33	-4.08	1.08	0.40	1.55
Complex 3	-5.01	8.66	-1.69	-6.01	-4.06	1.23	0.42	1.48
PhAcH-DEE								
n-σ* Complex	-6.67	8.81	-2.23	-4.01	-4.1	1.63	0.54	0.98

C$_2$H$_2$, complexes with H$_2$O and MeOH yield the n-σ* complex as the global minimum. The dual interactions observed in the case of the H-π complex in PhAc, causes a reversal in the energy ordering in the O-H··π and n-σ* complex compared with C$_2$H$_2$. The PhAc complexes with MeOH and DEE were also studied using AIM, NBO and EDA methodologies, to understand the nature of the interactions.

It may also be noted that the n-σ* complex was the strongest in PhAc-DEE in keeping with the increased basicity of the ether compared with the other precursors studied.

Chapter 5

H-π Landscape of the Phenylacetylene-HCl System:
Does this Provide the Gateway to the Markovnikov Addition?

5.1 Introduction

We present here the results of our study on the phenylacetylene (PhAc)-HCl complexes. The interaction between PhAc and HCl provides an opportunity to study a landscape of structures involving mainly H-π contacts. Furthermore, this system also presents the possibility of halogen-π bonding.

Experimental studies on HCl-acetylene in low temperature matrices were performed by Barnes *et al.* and Mcdonald *et al.*.[108,109] Later Legon, Aldrich and Flygare studied HCl-acetylene heterodimer using Fourier Transform Microwave Spectroscopy in the gas phase and observed a T-shaped complex with HCl lying along the C_2 axis of C_2H_2.[110] Kelsell *et al.* also performed matrix isolation experiments in Ar and observed the C_2H_2-HCl complex, where the HCl stretch was red shifted by approximately 125 cm^{-1}, from that of the uncomplexed HCl.[111] Computations were also performed by Pople *et al.* to corroborate experimental findings on the H-π complexes.[112] The non-aromatic π electrons studied in these systems, gave a fair estimate of the strength, geometry and spectral changes occurring in these H-π interactions. Investigations on π-bonded complexes, with C_6H_6 as an aromatic π electron donor were also performed. Experiments and theoretical studies undertaken by various groups, to understand the H-π interaction between C_6H_6 and HCl concluded that HCl lies on the C_6 axis of benzene with the hydrogen pointing towards centre of the ring.[113-115]

The combination of aromatic and acetylenic π clouds in a single molecule such as PhAc poses an interesting question as to which of the two π electron systems will preferentially interact with HCl, to form the most stable isomer. Furthermore, HCl, in addition to manifesting hydrogen bonding interactions, may also exhibit halogen bonding contacts, an interaction that has been increasingly explored in recent times.[116,117] PhAc-HCl system, which therefore promises to be an interesting puzzle, was studied using matrix isolation infrared spectroscopy and *ab-initio* computations.

5.2 Experimental Details

The details of the experiments are described elsewhere in chapter 2. In particular, the present set of experiments were performed using N_2 and Ar (Sigma Gases and Services, 99%) as matrix gases. Phenylacetylene (Sigma Aldrich, 98%), phenylacetylene-D (Sigma Aldrich,

99% Atom-D) were used without further purification, except to subjecting them to several freeze-pump-thaw cycles before use. Concentrated H_2SO_4 (Merck) and HCl solution (Merck 37%) were used in the preparation of gaseous HCl. Benzoyl chloride (Sigma Aldrich) and D_2O (Sigma Aldrich,) were used to prepare gaseous DCl. HCl gas was prepared using conc. H_2SO_4 and HCl (~37%), and DCl was prepared using the method described by Brown and Groot.[118] The detailed preparation method for gaseous HCl and DCl is described as follows:

HCl Preparation : A 3 necked glass container of 125 mL capacity was used for preparing pure gaseous HCl. One of the 3 outlets of the container was connected to rotary pump for evacuation, the second to the sample bottle to store the HCl and the third outlet was stoppered using rubber septum. At the outset the whole assembly was evacuated using a rotary pump. 5-10 ml of conc. H_2SO_4 was injected through the rubber septum into the empty evacuated container followed by 0.1 ml of 35% HCl solution. The HCl gas evolved was collected in sample container kept in liq. N_2 trap.

DCl Preparation : DCl gas was prepared using a method described by Brown and Groot. 18 mL of Benzoyl Chloride was taken in a 3 necked 100 mL round bottom flask. Through one of the inlets of the flask, 0.5mL D_2O was injected. The mixture was heated to about 110-120° C for about 20 minutes. Approximately 750 mbar of DCl gas was collected in glass sample holder which was used for the matrix isolation experiments.

Gaseous HCl, collected in a glass sample container, was attached to one port of the mixing chamber. Freeze-pump-thaw was performed on the HCl gas before use. Various mixtures of matrix gas and HCl, with relative concentrations ranging from 1000:0.5 to 1000:1.2, were prepared using standard manometric procedures. The concentrations of HCl and DCl were kept low in all these experiments to avaoid formation of the aggregates of HCl or DCl. Typical deposition rates of ~3 mmol/hr of the matrix gas was employed, using a needle valve (Model: EVN 116, Pfeiffer Vacuum). DCl experiments were done using a double jet assembly, in which $PhAc/N_2$ mixture was introduced through one nozzle and DCl through another. In such sample introduction geometries, sample to matrix concentrations were uncertain, hence we have indicated the concentration in the figure captions as x:1000.

The spectra of the matrix isolated species, were recorded in the region 4000-400 cm^{-1} using a Bruker Tensor 27 FTIR spectrometer, at a resolution 0.5 cm^{-1}. The matrix was then annealed at 27 K (N_2) or 32 K (Ar), and the spectrum again recorded after recooling the matrix to 12 K, to observe the product bands. Experiments were performed in both Ar and N_2 matrices, both of which showed evidence for the formation of the PhAc-HCl complexes.

However, since the spectra were well resolved in the N_2 matrix, we have shown the spectra obtained in this matrix.

5.3 Computational Details

The computational study was carried out using Gaussian-09 suite of programs. All computations were performed using M06-2X and MP2 methods, together with a 6-311++G(d,p) and aug-cc-pVDZ basis sets. The computed frequencies of the PhAc-HCl complexes, were scaled by using appropriate scaling factors to enable a comparison with experimentally observed features. The scale factors have been mentioned in the footnote of each of the tables, listing the experimental and computed vibrational wavenumbers. Vibrational spectra were simulated using the scaled vibrational wavenumbers and the intensity obtained from the vibrational analysis implemented through Gaussian.

The details of computational procedure followed is given in chapter 2 in detail.

To understand the effect of the matrix, we performed computations using the PCM solvation model invoked through Gaussian 09. A value of 1.47 was used for the dielectric constant of N_2[119]. Structures of complexes obtained in the vaccum calculations were used as starting geometries for the optimization in the N_2 solvent. Frequency calculations were performed on these optimized geometries.

Electron density topology was examined using the atoms-in-molecules analysis implemented through AIM2000,[82] to identify and characterize the nature of the non-covalent interactions in the complex. NBO and LMO-EDA analysis, implemented using Gaussian-09 and GAMESS,[73,74] respectively, were performed to understand the nature of bonding in these complexes.

5.4 Results

PhAc-HCl Complexes

a. Experimental

In the N_2 matrix, the HCl stretch occurs at 2855.0 cm^{-1}. Codeposition of PhAc and HCl at 12 K and subsequent annealing resulted in the appearance of new product features centred at 2731.0 and 2775.0 cm^{-1} which corresponds to the HCl stretch in the complexes (Fig. 5.1). A difference spectrum was obtained by subtracting the annealed spectrum from spectrum of the as-deposited matrix at 12 K (Fig.5.1 inset). This difference spectrum clearly revealed the product features, which appeared as negative going peaks, at 2733.4, 2730.7, 2725.9 and 2722.4 cm^{-1}. These features appeared consistenly in every single spectra that we recorded, thus establishing the reproducibility of these features. It was also confirmed that the presence of both monomers was necessary for these product features to be observed.

Furthermore, on increasing the concentration of either monomer, the intensity of these features increased, as can be seen in traces 'e' and 'f' of Fig. 5.1, thereby confirming them to be due to the PhAc-HCl complexes. As these product features were observed even at low concentration of the two monomers, we believe that they must be due to a 1:1 complex of PhAc-HCl. No product peaks

were observed in the acetylenic ≡C-H stretch region of PhAc. Experiments with isotopically substituted PhAc, where the acetylenic hydrogen was replaced with deuterium (PhAc$_D$), and DCl were also performed to observe isotopic shifts. With the isotopic species, spectral features due to complex formation were observed at 2593.8 cm^{-1} in ≡C-D stretching region of PhAc$_D$ (Fig.5. 2) and 1979.6 cm^{-1} for the DCl stretch in N$_2$ matrix (Fig. 5.3).

b. Computational

Ab-initio calculations performed at M06-2X/6-311++G(d,p) and M06-2X/aug-cc-pVDZ levels of theory yielded four geometries, while at the MP2/6-311++G(d,p) and MP2/aug-cc-pVDZ levels we obtained six isomers of the PhAc-HCl complexes, as minima on the potential energy surface.The structures of PhAc-HCl complexes at MP2/aug-cc-pVDZ level are shown in Fig 5.4. The potential energy landscape of PhAc-HCl heterodimer exhibits two types of non covalently bonded structures – hydrogen bonded (1a, 1b, 2 and 5) and possibly Cl-π bonded complexes (complexes 3 and 4).

In structures 1a, 1b and 2, HCl serves as a proton donor, to the π cloud of the acetylenic system (complex 1a and 1b) and the phenyl ring (complex 2) of PhAc. Complex 1a and 1b differ in the orientation of the HCl molecule relative to PhAc. In complex 1a, the HCl is located in a plane, inclined at 54.0^o to the plane containing the phenyl ring, while in the isomeric complex 1b, the HCl is in the plane of the phenyl ring. (All these structures were also located at the M06-2X/aug-cc-pVDZ level.)

In these two complexes, the H-π hydrogen bond distance is ~ 2.3 Å. Both these complexes were nearly isoenergetic, displaying computed red shifts in the HCl stretch that are different by ~10 cm^{-1}. The multiplet seen in the 2731 bunch of features in the difference spectra, may well arise from the two different complexes, 1a and 1b. A transition state connecting structures 1a and 1b (TS1) was located, having a dihedral angle of ~22° with the plane of the molecule. It must be noted that complex 1a, has, by symmetry, another equivalent structure (1a*) where the HCl is located inclined at an angle of 126.0^o to the plane of the phenyl ring.
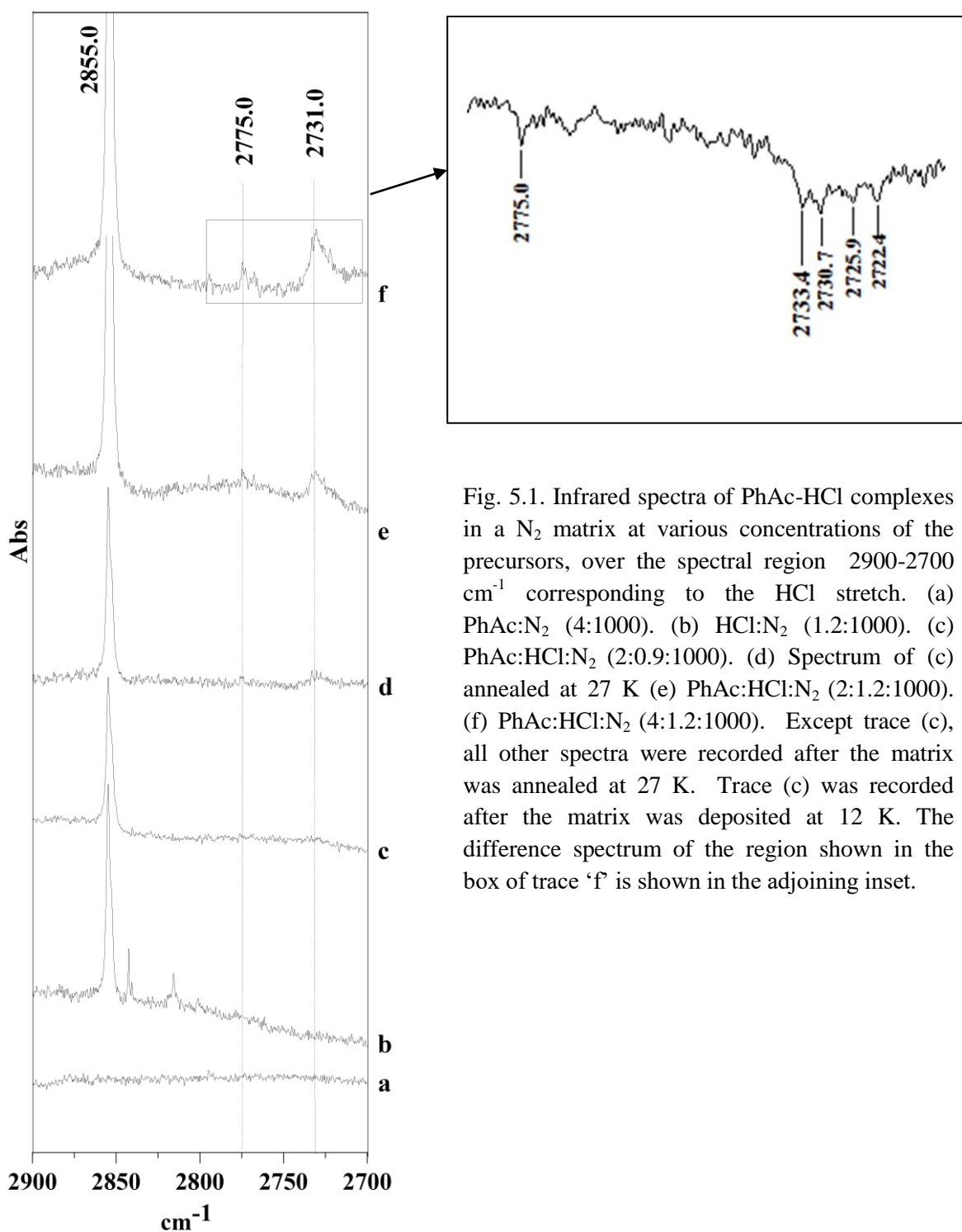
Fig. 5.1. Infrared spectra of PhAc-HCl complexes in a N_2 matrix at various concentrations of the precursors, over the spectral region 2900-2700 cm^{-1} corresponding to the HCl stretch. (a) PhAc:N_2 (4:1000). (b) HCl:N_2 (1.2:1000). (c) PhAc:HCl:N_2 (2:0.9:1000). (d) Spectrum of (c) annealed at 27 K (e) PhAc:HCl:N_2 (2:1.2:1000). (f) PhAc:HCl:N_2 (4:1.2:1000). Except trace (c), all other spectra were recorded after the matrix was annealed at 27 K. Trace (c) was recorded after the matrix was deposited at 12 K. The difference spectrum of the region shown in the box of trace 'f' is shown in the adjoining inset.

We have also calculated the transition state structure (TS2) connecting the minima corresponding to 1a and 1a*, where the HCl lies above the acetylenic π system in a plane that is perpendicular to the plane containing the phenyl ring. Fig.5 depicts all these minima together with the associated transition states. The barrier between all the minima, around the acetylenic moiety shown in Fig.5.5, are less than 0.2 kcal/mol. This extremely small value of the barrier height makes it almost a barrierless rotation for the HCl around the acetylenic π electron cloud. This leads to the possibility that the HCl may be freely rotating around the acetylenic π cloud. Such floppiness has been discussed before in complexes involving water and benzene and other weakly bonded complexes.[120]

In complex 2 (Fig. 5.4), the hydrogen of HCl, is directed towards the carbon of the phenyl ring in PhAc, which is attached to the acetylenic moiety. However, at the MP2/6-311++G** level, in addition to the above structure, another isomer was also obtained, where the HCl was oriented towards the carbon para to the carbon referred to above. This raises the possibility of the HCl gliding on the surface of the phenyl ring. Furthermore, the ZPE corrected barrier for the conversion of structure 1a to 2 is negligibly small (~0.01 kcal/mol) and therefore feasible, while the barrier for the reverse process (2→1a) is somewhat large (~1 kcal/mol).

Structures 3 and 4, show an intermolecular bond distance of 3.3 and 3.4 Å, respectively, between the Cl atom and the π cloud, leading to possible Cl-π interaction, a class of weak interactions dominated by dispersion forces and operating over distances larger than typical hydrogen bonding interactions.[121,122] In complex 3, the Cl is directed towards the phenyl π system, while in complex 4, the Cl points towards the acetylenic π system. Complex 4 also appears to have a second interaction between the Cl and the phenyl hydrogen, as is evident from AIM analysis, discussed later.

In structure 5, which shows a n-σ* interaction, PhAc serves as the proton donor, through its acetylenic hydrogen to H-Cl, with a hydrogen bond distance of 2.71 Å and an interaction energy of -1.2 kcal/mol. HCl in this complex is oriented perpendicular to H-C≡ bond of PhAc.Experimentally we could observe only structures 1a, 1b and 2, and no evidence was seen for the formation of complexes 3, 4 and 5.

The important geometrical parameters of the complexes are given in Table 5.1 at MP2/aug-cc-pVDZ level of theory.Table 5.2 gives the interaction energies of the PhAc-HCl complexes at various levels of theories. It can be seen that complex 1a,1b and 2 are nearly isoenergetic and are the strongest of all the complexes mentioned above.
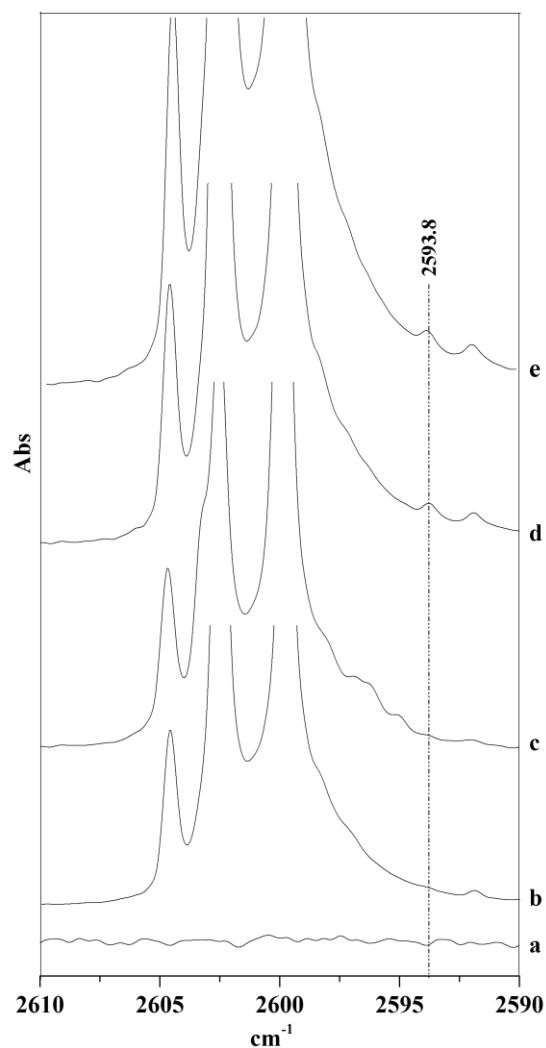
Fig. 5.2. Infrared spectra of PhAc$_D$-HCl complexes in a N$_2$ matrix at various concentrations of the precursors, over the spectral region 2610-2590 cm^{-1} corresponding to the ≡C-D stretch of PhAc$_D$. (a) HCl:N$_2$ (1.2:1000). (b) PhAc$_D$:N$_2$ (4:1000). (c) PhAc$_D$:HCl:N$_2$ (4:0.9:1000). (d) Spectrum of (c) annealed at 27 K. (e) PhAc$_D$:HCl:N$_2$ (4:1.2:1000). Except trace (c), all other spectra were recorded after the matrix was annealed at 27 K. Trace (c) was recorded after the matrix was deposited at 12 K.
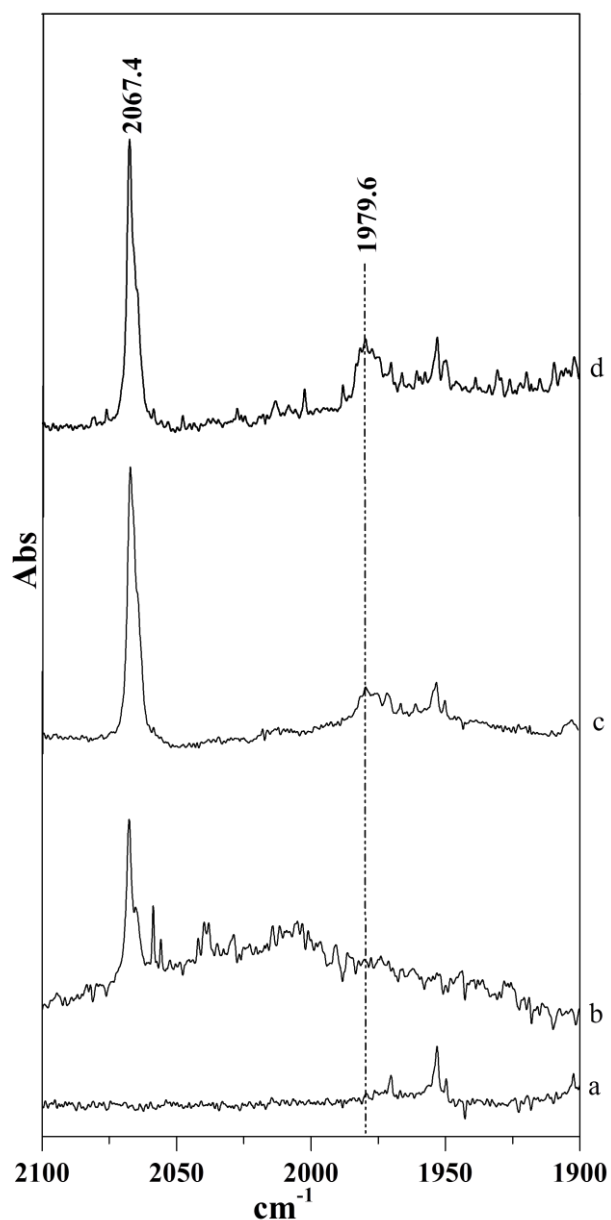
Fig.5.3 Infrared spectra of PhAc-DCl complexes in a N$_2$ matrix at various concentrations of the precursors, over the spectral region 2100-1900 cm^{-1} corresponding to the D-Cl stretch. (a) PhAc:N$_2$ (3:1000). (b) DCl:N$_2$ (x:1000). (c) PhAc:DCl:N$_2$ (3:x:1000). (d) Spectrum of (c) annealed at 27 K Except trace (c), all other spectra were recorded after the matrix was annealed at 27 K. Trace (c) was recorded after the matrix was deposited at 12 K.
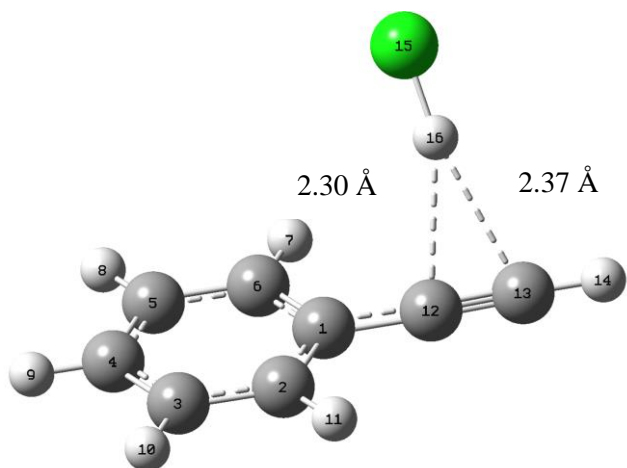
Complex 1a
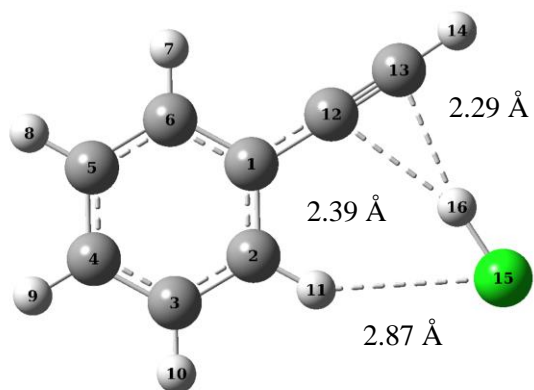
Complex 1b
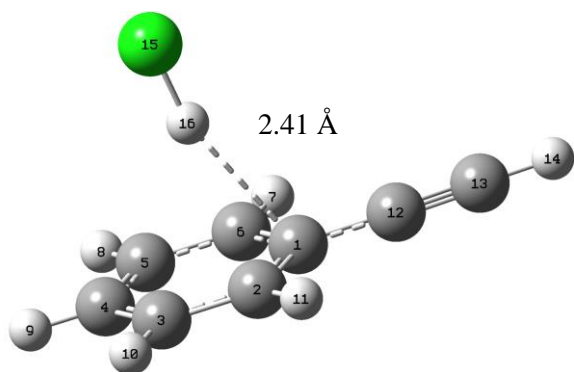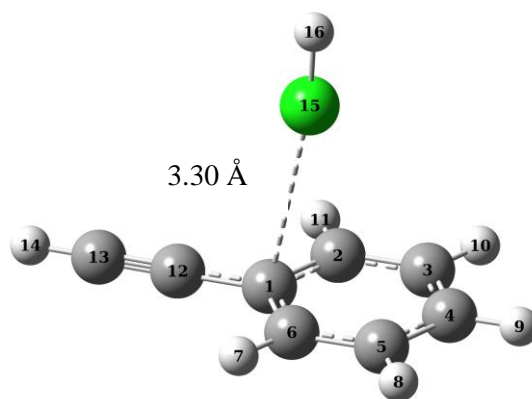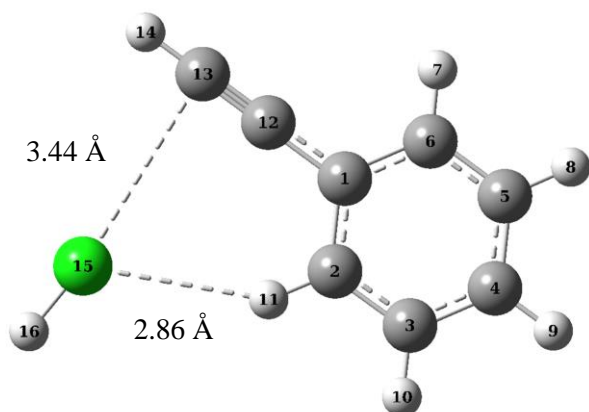
Complex 2
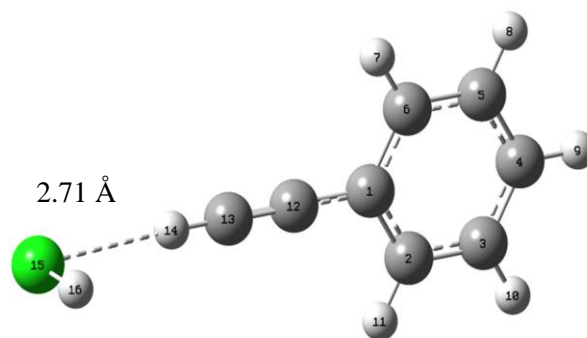
Complex 3

Complex 4

Complex 5

Fig. 5.4. Optimized structures of 1:1 PhAc:HCl complexes at MP2/aug-cc-pVDZ level of theory

The energy difference between the three complexes being as small as they are, which of the structures is a global minimum is not unambiguous, and depends on the level of theory employed. Interaction energies at the complete basis set limit were also calculated. At both MP2/CBS and CCSD(T)/CBS levels, complex 1a was indicated to the the global minima, but only barely, with complex 2 lying higher by 0.13 and 0.49 kcal/mol, respectively, at the two levels.

5.5 Discussions

PhAc-HCl Complexes

a. H-Cl stretch

H-Cl stretch in the monomer occurs at 2855.0 cm^{-1} in N$_2$ matrix. A broad product feature centred at 2731.0 cm^{-1} was observed, which is red shifted by 124.0 cm^{-1} from the HCl monomer feature. The computed shifts for complex 1a and 1b were found to be 148.3 cm^{-1} and 158.8 cm^{-1} respectively, at MP2/aug-cc-pVDZ level of theory (Table 5.3, Fig. 5.6). It is likely that the broad feature centred at 2731 encompasses features due to both complexes, 1a and 1b. In fact, a difference spectrum (Fig. 5.6) shows the presence of four peaks, at 2733.4, 2730.7, 2725.9, 2722.4 cm^{-1} with concomitant red shifts of 121.6, 124.3, 129.1 and 132.6 cm^{-1} from the feaure of uncomplexed HCl. The multiplicity of the peaks in this region may possibly be due to the presence of the two isomeric structures trapped in multiple sites.

In addition to these features, we also observed a product feature at 2775.0 cm^{-1} with a red shift of 80 cm^{-1}, which can be assigned to complex 2, involving the phenyl system. The experimentally observed shift of 80 cm^{-1} agrees well with the computed red shift of 83.7 cm^{-1} for this complex. Fig.5.6 compares the spectra computed at the MP2/aug-cc-pVDZ level of theory with the experimental spectra, which summarizes the above assigments.

We have looked at the effect of solvent (N$_2$) on the individual monomers and on the complexes, using the PCM solvation model. The calculated red shifts in the vibrational frequency for HCl, following complex formation, changes only minimally, in the N$_2$ solvent, compared with vacuum. For example, for complex 1b, the computed shift ($\nu_{complex} - \nu_{monomer}$) in vacuum is 158.8 cm^{-1} to the red, while in the N$_2$ solvent, we obtain a red shift of 165.3 cm^{-1}. The change in shift due to solvation is therefore only 6.5 cm^{-1}, in a ~160 cm^{-1} shift due to complex formation. This scenario holds for all the complexes. Likewise, the ZPE corrected interaction energy of complex 1b, changes from -4.21 kcal/mol in vacuum to -3.92 kcal/mol
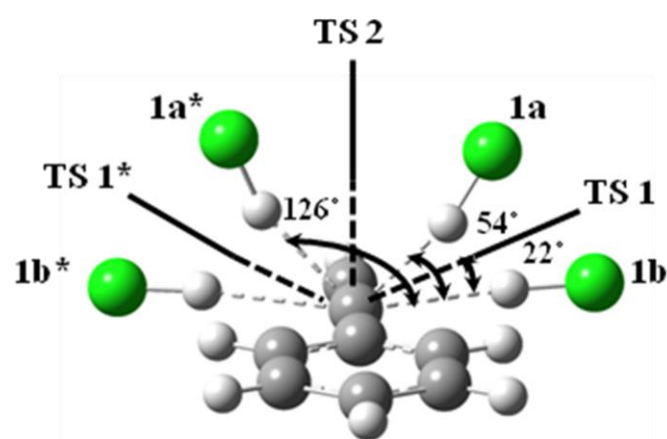
Fig.5.5 Depiction of various isomers of the PhAc-HCl (H-π_{Ac}) complexes together with the associated transition states, indicated by black solid lines.The angles indicate the orientation of the HCl internuclear axis with respect to the plane containing the phenyl ring.

Table. 5.1. Important geometrical parameters, bond lengths (Å), bond angles (˚), dihedral angles (˚), for PhAcHCl complexes computed at the MP2/aug-cc-pVDZ level. Labelling of atoms is shown in Fig.5. 4.

Parameter	1a	1b	2	3	4	5	PhAc	HCl
C_{12}-H_{16}	2.30	2.39						
C_{13}-H_{16}	2.29	2.29						
C_{12}-C_{13}	1.24	1.24	1.27	1.24	1.24	1.24	1.27	
C_{13}-H_{14}	1.08	1.08	1.07	1.07	1.07	1.08	1.07	
Cl_{15}-C_2				3.48				
H_{16}-Cl_{15}	1.30	1.30	1.29	1.29	1.29	1.29		1.29
Cl_{15}-H_{11}		2.87		3.92	2.86			
C_1-H_{16}			2.41					
Cl_{15}-C_1			3.67	3.30				
Cl_{15}-C_{13}			---		3.44			
Cl_{15}-C_{12}					3.56			
Cl_{15}-H_{14}			---			2.71		
H_{16}-H_{14}						3.07		
H_{16}-C_{12}-C_1	100.90							
Cl_{15}-C_{12}-C_1	93.78							
Cl_{15}-C_{13}-C_{12}				85.38				
H_{16}-C_1-C_6			78.80					
H_{16}-C_{13}-C_{12}		79.40	---					
C_{12}-H_{16}-C_{13}		30.58	---					
Cl_{15}-H_{16}-C_{12}		159.65	---					
H_{16}-Cl_{15}-H_{11}		60.61	---	146.18	119.13			
Cl_{15}-H_{11}-C_2					146.57			
Cl_{15}-H_{16}-C_1			164.01					
H_{16}-C_1-C_{12}			112.40					
H_{16}-Cl_{15}-C_1			---	171.96				
Cl_{15}-C_1-C_{12}			---	99.63				
H_{16}-Cl_{15}-C_4				143.36				
H_{16}-Cl_{15}-C_{13}			---		172.52			
C_{13}-Cl_{15}-H_{11}			---		68.35			
H_{16}-Cl_{15}-H_{14}			---			93.62		
Cl_{15}-H_{14}-C_{13}			---			172.85		
H_{16}-C_{12}-C_1-C_2	---	0.00						
H_{16}-Cl_{15}-H_{11}-C_2		0.00			---			
Cl_{15}-C_{12}-C_1-C_2	---				0.00			
H_{14}-C_{13}-C_{12}-C_1	---	-0.03	---	179.96	179.98	-0.18	---	
H_{16}-C_{13}-C_{12}-C_1	---	179.99						
Cl_{15}-C_{13}-C_{12}-C_1	---	179.99			179.98			
Cl_{15}-H_{16}-C_1-C_6			---					
H_{16}-Cl_{15}-H_{14}-C_{13}					179.99	-0.00		
Cl_{15}-C_1-C_{12}-C_{13}				-0.00	-179.99			
H_{16}-Cl_{15}-C_1-C_2				119.92	0.00			

Table. 5.2. Interaction energies Raw/ZPE/BSSE at various levels of theory for the PhAc-HCl complexes. Energies are given in kcal/mol.

	M06-2X		MP2			CCSD(T)		
	6-311++G(d,p)	aug-cc-pVDZ	6-311++G(d,p)	aug-cc-pVDZ	CBS	6-311++G(d,p)	aug-cc-pVDZ	CBS
1a (H-π_{Ac})	-4.39/-3.08/-3.87	-4.32/-3.14/-4.03	-5.18/-4.10/-2.25	-5.39/-4.39/-3.81	-4.81	-4.69	-4.70	-4.13
1b (H-π_{Ac}) in plane	---	-4.15/-3.05/-3.77	---	-5.34/-4.21/-3.56	-4.61	---	-4.80	-4.07
2 (H-π_{Ph})	-4.58/-3.55/-3.89	-4.28/-3.25/-3.70	-5.69/-5.13/-2.68	-6.30/-5.51/-3.80	-4.68	-4.97	-5.26	-3.64
3 (Cl-π_{Ph})	-2.08/-1.04/-1.42	-1.91/-0.94/-1.55	-3.48/-2.91/-0.41	-3.11/-2.53/-1.70	-2.38	-2.68	-2.24	-1.51
4 (Cl-π_{Ac})	-1.60/-0.67/-1.12	---	-2.29/-1.68/-0.35	-2.35/-1.61/-1.25	-1.81	-2.22	-2.06	-1.52
5 (n-σ*)	---	---	-2.12/-1.44/-0.46	-1.93/-1.22/-0.91	-1.16	-2.16	-1.92	-1.16

in the N_2 solvent, which is a nominal change of 0.29 kcal/mol. Hence, while the solvent does have a small influence, it does not alter the conclusions.

b ≡CH stretch of PhAc

There was no discernible spectral feature in ≡CH stretch region of PhAc which could be assigned to complex 1a and 1b. Complex 1a and 1b are computed to show red shifts of 8.4 cm^{-1} and 11.1 cm^{-1} respectively. But the presence of multiplet features of PhAc in this region due to Fermi resonance makes it difficult to discern any product feature even if it were present. Experiments were therefore performed with isotopically substituted PhAc$_D$ to probe the ≡CD region for complex formation, as this region is free from any features due to Fermi resonance.

PhAc$_D$-HCl Complexes

a H-Cl stretch

In experiments where PhAc$_D$ and HCl were codeposited and annealed, we observed features corresponding to the H-Cl stretch in the complex around 2731.0 and 2775.0, as was observed for the H-isotopomer of the PhAc-HCl complexes; thereby confirming the presence of complex 1a, 1b and 2.

b ≡CD stretch of PhAc$_D$

Fig. 5.2 shows the spectra of PhAc$_D$-HCl complexes in the ≡CD stretch region of PhAc$_D$. Since the region to the red of the ≡CD stretch of PhAc$_D$ (occurring at 2599.7 cm^{-1}) is free from the multiplet structure, a feature due to the complex was observed at 2593.8 cm^{-1}. This amounts to a red shift of 5.9 cm^{-1} in the ≡CD stretch, which agrees well with the computed shift of 6.8 cm^{-1} for complex 1a/1b. This observation lends credence for the observation of complex 1a/1b.

PhAc-DCl Complexes

Experiments were also performed with DCl and PhAc. Codeposition of PhAc with DCl, yielded a product feature at 1979.6 cm^{-1} corresponding to the DCl stretch in the D-π bond of complex 1a/1b(Fig. 5.3). This shift agrees well with the computed feature for complex 1a and/or 1b. Furthermore, the experimental wavenumbers for DCl and HCl in the complex occurs at 1979.6 and 2731 cm^{-1}, respectively. The ratio of $\omega_{HCl}/\omega_{DCl}$ (experimental) works out to 1.39, which is in excellent agreement with the value of $(\mu_{DCl}/\mu_{HCl})^{1/2}$, where μ refers to reduced mass of the corresponding species, thus confirming our assignment.

Table.5.3. Experimental (N_2 matrix), scaled computed vibrational wavenumbers (cm^{-1}) and vibrational mode assignments for PhAc/ PhAc$_D$ and its complexes with HCl/DCl. Computations were done at the MP2/aug-cc-pVDZ level of theory.

	Experimental		Scaled Computed Wavenumber							Modes
	Monomer	**Complex**	**Monomer**	**1a**	**1b**	**2**	**3**	**4**	**5**	
HCl	2855.0	**2731.0 (-124.0)** **2775.0 (-80.0)**	2855.0	**2706.7 (-148.3)**	**2696.2 (-158.8)**	**2771.2 (-83.7)**	2842.5 (-12.4)	2842.2 (-12.8)	2845.6 (-9.4)	H-Cl stretch
DCl	2067.5	**1979.6 (-87.9)**	2046.8	**1939.7 (-107.1)**	1932.2 (-114.6)	1986.5 (-60.3)	2037.7 (-9.1)	2037.5 (-9.3)	2040.0 (-6.8)	D-Cl stretch
PhAc	3323.2	-	3323.2	3314.8 (-8.4)	3312.1 (-11.1)	3321.9 (-1.3)	3323.5 (0.3)	3321.7 (-1.5)	3306.1 (-17.1)	≡C-H stretch
PhAc$_D$	2599.7	**2593.8 (-5.9)**	2527.7	**2520.9 (-6.8)**	2518.7 (-9.0)	2527.2 (-0.5)	2527.6 (-0.1)	2526.2 (-1.5)	2516.9 (-10.8)	≡C-D stretch

[a] $\Delta\nu = \nu$(complex)- ν(monomer), is given in parenthesis
Scaling Factors : 0.944390967 (3000-2000 cm^{-1}) , 0.954613221 (3500-3000 cm^{-1})
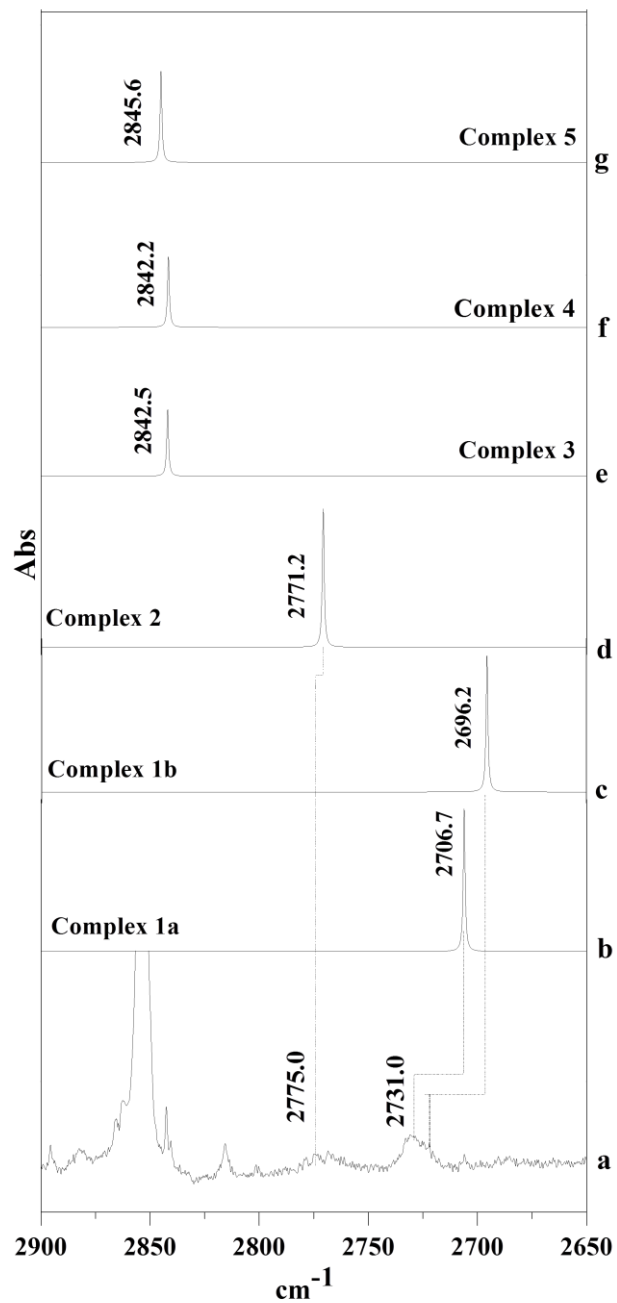
Fig. 5.6 Experimental and computed spectra of PhAc-HCl complexes at MP2/aug-cc-pVDZ level of theory.(a) Annealed spectrum; (b)-(g) Computed spectra of various complexes indicated along each trace.

103

5.6 AIM Analysis

The atoms-in-molecules (AIM) theory of Bader[81], was used to study the charge density topology of the PhAc-HCl complexes, using the wavefunctions generated at the MP2/aug-cc-pVDZ level of theory. (3,-1) bond critical points obtained for the various complexes are shown in Fig. 5.7. Values of topological parameters, such as electron density $\rho(r_c)$, eigenvalues of the Hessian, λ_1, λ_2, λ_3, and the Laplacian ($\nabla^2\rho$) of electron density (defined as the sum of the eigenvalues), computed at the bond critical points, are shown in Table 5.4. The values of $\rho(r_c)$ and $\nabla^2\rho$ for complex 1a, 1b, 2 and 5 lie in the range of hydrogen bonding interactions as proposed by Koch and Popelier.[83] The positive values of $\nabla^2\rho$ in the range of 0.024-0.139 a.u. are typical of closed shell interactions, such as hydrogen bonds. Complexes 1a and 1b have the largest value of $\nabla^2\rho$ and $\rho(r_c)$ in keeping with them being the global minima. The three complexes, 3,4 (Cl-π) and 5 (n-σ*) interactions have amongst them, similar values of for electron density and Laplacian and these values are all less than those for the H-π complexes. The topological parameters calculated using AIM analysis for structures 3 and 4 are rougly in the realm of values for the Cl-π interactions discussed by Arunan et al.[100] In complex 4, in addition to the bond critical point for the Cl-π interaction, another interaction involving the Cl of HCl and the H of the C-H phenyl group was also indicated, which has been labelled as 'bcp2' in Fig. 5.7 and Table 5.4. It can be seen from this table that the Cl···H-C interaction was not insignificant in magnitude compared with the Cl···π interaction. Employing the topological parameters, we also computed the interaction energy (ΔE_{HB}) for each interaction, through the use of local kinetic density, $G(r_{CP})$ and local potential energy density $V(r_{CP})$.[84] Though the values of interaction energies obtained through a topological analysis do not exactly match with the numbers presented in Table 5.2, it does provide a consistent trend. Both analysis predict complexes 1a and 1b to be the global minima.

5.7 NBO Analysis

Different complexes between PhAc-HCl involve different donor acceptor orbital interactions. These intereactions were quantified using NBO analysis at MP2/aug-cc-pVDZ level of theory which helped us to understand the role of stabilizing interactions between two monomers, during the complex formation (Table 5.5). The second order perturbation energy E(2) depends on orbital overlap between donor and acceptor orbitals, denoted by F(i,j) and

Table 5.4: Summary of AIM calculations for PhAc-HCl complexes at MP2/aug-cc-pVDZ level of theory. All quantities are expressed in a.u. See text for definition of each of the quantities.

Complex		$\rho(r_c)$	$\nabla^2\rho(r_c)$	$G(r_{CP})$	$V(r_{CP})$	ΔE_{HB}
1a (H-π_{Ac})		0.0165	0.0427	0.010166	-0.00967	-3.03
1b (H-π_{Ac} in plane) bcp1		0.0166	0.0415	0.010004	-0.00964	-3.02
	bcp2	0.0071	0.0223	0.004459	-0.00335	-1.05
2 (H-π_{Ph})		0.0129	0.0344	0.007761	-0.00693	-2.17
3 (Cl-π_{Ph})		0.0073	0.0241	0.004808	-0.0036	-1.13
4 (Cl-π_{Ac}) bcp1		0.0059	0.0180	0.003549	-0.00261	-0.82
	bcp2	0.0067	0.0215	0.004253	-0.00314	-0.99
5 (n-σ^*)		0.0084	0.0261	0.00534	-0.00416	-1.31
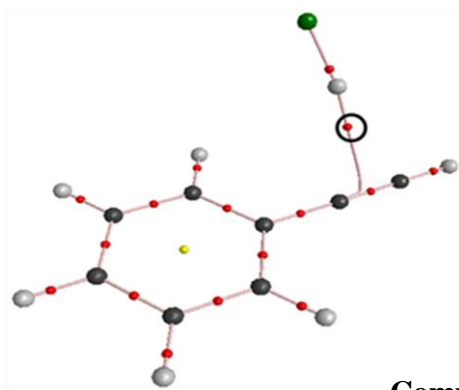
Complex 1a
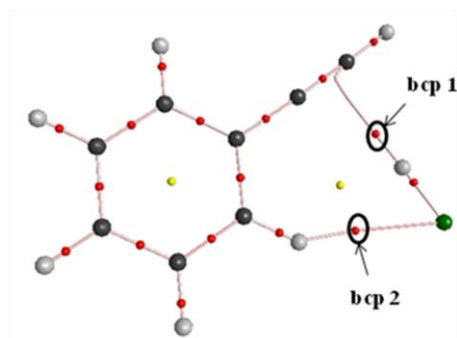
Complex 1b
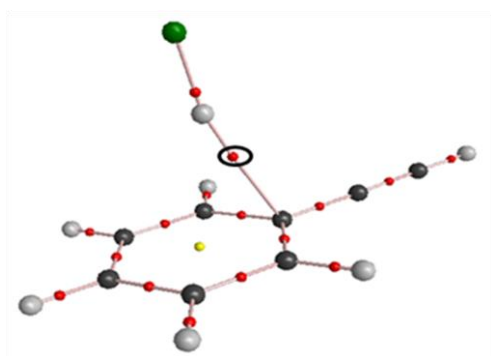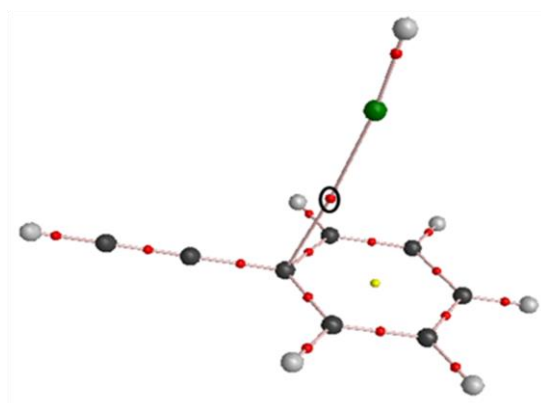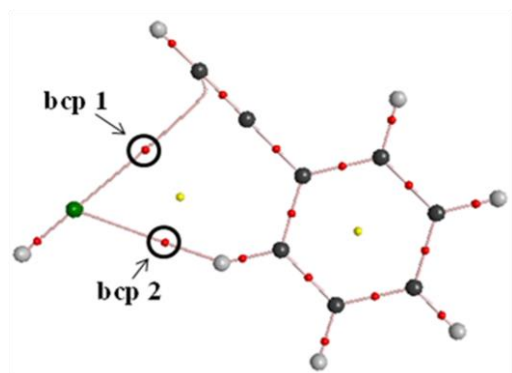
Complex 2
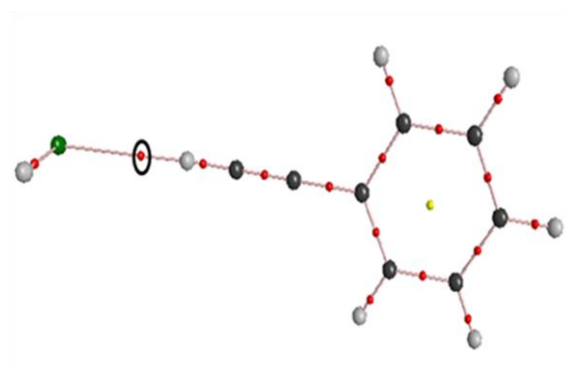
Complex 3

Complex 4

Complex 5

Fig.5.7. Aim analysis of PhAc-HCl complexes at MP2/aug-cc-pVDZ level of theory .

electron occupancy in donor orbital, whereas it is inversely proportional to energy difference between donor-acceptor orbitals [E(j)-E(i)]. All the complexes involve delocalization of electrons, either from π bonding orbital or lone pairs, to the antibonding orbitals (σ^*), resulting in $\pi \rightarrow \sigma^*$ or $n \rightarrow \sigma^*$' interactions. The global minima i.e. the H-π_{Ac} complex 1 (a & b) involved electron transfer from the π orbital of C_{12}-C_{13} to σ^* acceptor orbital of H-Cl, and has the maximum value for second order perturbation energy E(2) amongst all other complexes. Transfer of electron density to the σ^* orbital of H-Cl results in the red shift of the HCl stretch. It can be seen that complexes 1a and 1b have larger occupancies, of 0.0180e and 0.0197e in the acceptor σ^* orbital of H-Cl, relative to complex 2 which has an occupancy of 0.0088e. The greater occupancy of the σ^* HCl orbital results in a larger red shift and marginally longer HCl bond lengths for complex 1 (a& b). This argument rationalizes the larger red shift seen in complex 1a/1b, even though complexes 1 and 2 are nearly isoenergetic.

Complex 5 which involves transfer of electrons between lone pair on Cl to σ^* orbital of $\equiv$CH of PhAc has slightly larger E(2) than complex 2 owing to larger overlap as well as electron occupancy in σ^* orbital. We had alluded to the possibility of complexes 3 and 4 being of the Cl-π type, based on their geometries and AIM parameters. However, NBO calculations do not reveal any significant orbital interactions that can be considered typical of Cl-π bonding. In fact all the orbital interactions in complexes 3 and 4 had second order perturbations < 2 kcal/mol and hence have not been listed in Table 5.5. Our conclusions regarding complexes 3 and 4 being of the Cl-π type are therefore made with caution.

5.8 LMO-EDA

LMO-EDA of PhAc-HCl complexes at MP2/aug-cc-pVDZ level was performed using GAMESS to partition the total interaction energy of the complexes into various energy terms such as electrostatic, exchange-repulsion, dispersion and polarization. Complex 1 (a & b) shows a dominance of electrostatic component whereas isoenergetic complex 2 has dispersion as a major contributor to the total interaction energy. Complexes 3 and 4, involving the halogen interactions, are dispersion dominated (Table 5.6).

5.9 A comparison of the Benzene-HCl, Acetylene-HCl and Phenylacetylene-HCl Complexes

It is relevant to compare the hydrogen bonded interactions in the PhAc-HCl system with the benzene-HCl and acetylene-HCl, since benzene and acetylene are component moieties in the PhAc molecule. As mentioned earlier, the H-π interaction in the acetylene-

Table.5.5 NBO analysis of PhAc-HCl complexes at MP2/aug-cc-pVDZ level of theory. The atom numbering indicated in table is as shown in Fig.5.4. E(2) is the second order perturbation energy (kcal/ mol), E(j)-E(i) is the donor-acceptor energy difference and F(i,j) is the overlap between the donor and acceptor orbitals.

Complex	Orbital Involved		E(2) (kcal/mol)	E(j)-E(i) a.u.	F(i,j) a.u.	Electron occupancy donor orbital	Electron occupancy acceptor orbital
	Donor	Acceptor					
1a (H-π_{Ac})	C_{12}-C_{13} (π)	Cl_{15}-H_{16} (σ*)	7.31	0.83	0.070	1.949	0.0180
1b (H-π_{Ac} in plane)	C_{12}-C_{13} (π)	Cl_{15}-H_{16} (σ*)	9.18	0.83	0.078	1.968	0.0197
2 (H-π_{Ph})	C_1-C_2 (π)	Cl_{15}-H_{16} (σ*)	3.34	0.73	0.048	1.647	0.0088
3 (Cl-π_{Ph})	-	-	-	-	-	-	-
4 (Cl-π_{Ac})	-	-	-	-	-	-	-
5 (n-σ*)	Cl_{15} (n)	C_{13}-H_{14} (σ*)	3.89	1.32	0.064	1.993	-
Ac-HCl	C_1-C_2 (π)	Cl_4-H_5 (σ*)	7.44	0.85	0.071	1.984	0.0156
Bz-HCl	C_2-C_3 (π)	Cl_{12}-H_{13} (σ*)	2.62	0.72	0.043	1.665	0.0071

Table 5.6: LMO-EDA of PhAc-HCl complexes at MP2/aug-cc-pVDZ.All energies are given in kcal/mol.

Complex	E_{ES}	E_{ER}	E_{Pol}	E_{Disp}	E_{Total}	E_{ES}/E_{Total}	E_{Disp}/E_{Total}	E_{Pol}/E_{Total}
1a (H-π_{Ac})	-5.94	8.91	-3.34	-3.48	-3.85	1.54	0.90	0.87
1b (H-π_{Ac} in plane)	-6.59	9.88	-3.53	-3.39	-3.63	1.82	0.93	0.97
2 (H-π_{Ph})	-3.69	7.16	-2.46	-4.83	-3.81	0.97	1.27	0.65
3 (Cl-π_{Ph})	-1.31	4.41	-0.6	-4.26	-1.75	0.75	2.43	0.34
4 (Cl-π_{Ac})	-2.04	3.84	-0.56	-2.53	-1.29	1.58	1.96	0.43
5 (n-σ*)	-1.48	2.03	-0.48	-0.98	-0.92	1.61	1.07	0.52

HCl and benzene-HCl complexes have been thoroughly studied in the literature, both experimentally and computationally. A comparison of the HCl stretching frequencies in the various complexes reveals the following order in the computed red shifts: ~160 cm^{-1} for PhAc-HCl (H-π_{Ac}) which is greater than the red shift of 112 cm^{-1} for the acetylene-HCl complex. Likewise the red shift of 89 cm^{-1} for the PhAc-HCl (H-π_{Ph}) > 78 Benzene-HCl (Table 5.7). The order of the red shifts mentioned above is consistent with the electron occupancies in the $\sigma*$ orbital of the HCl for two sets of complexes mentioned above. Clearly the PhAc-HCl complex 1a has the largest occupancy in $\sigma*$ orbital whereas Benzene-HCl has the smallest (Table 5.5). The former therefore shows the largest red shift and the later the smallest. It is also reassuring to note that although benzene-HCl and the different PhAc-HCl H-π complexes are almost isoenergetic (Table 5.7), they show variable spectral red shifts in keeping with $\sigma*$ occupancy. These trends shown by the computed shifts are in agreement with the experimental shifts reported for these systems.[108,111]

5.10 Is the H-π_{Ac} Complex the Prereaction Complex for the Markovnikov Addition?

Unsaturated compounds such as alkenes and alkynes are known to show addition reactions with hydrogen halides across the multiple bonds. This addition reaction has been shown to add in a Markovnikov fashion, through the intermediacy of a carbocation, the stability of which is believed to favour the Markovnikov pathway. Complex 1b manifests the characteristics of the incipient Markovnikov intermediate. We believe this H-π_{Ac} complex (structure 1b) could be a *prereaction* complex leading to the Markovnikov product. Analysis of the charges on the atomic centres was performed through NBO analysis (using keyword Density=Current) to validate the above hypothesis. Table.5.7 shows charges on atoms in the HCl complexes as well as free monomer. In uncomplexed PhAc, C_{12} with a charge of -0.032e is more positive than C_{13} which carries a charge of -0.201e. On complexation with HCl (complex 1b) C_{12} becomes more positive relative to that in uncomplexed PhAc, indicating the incipient formation of the carbocation on C_{12}, as required for a Markovnikov addition. It was also observed that only complex 1b shows the decrease in charge on C_{12} and a corresponding increase of negative charge on C_{13}, whereas complex 1a shows increase in negative charges on both C_{12} and C_{13} atoms as compared to uncomplexed PhAc. This observation indicates that only 1b must be the complex that serves as the prereaction complex. Furthermore, the HCl being in the plane of the phenyl ring in complex 1b, it would easily facilitate the alkene product to be planar, as required. However, the product formed

Table 5.7: Comparison of interaction energies (Raw/ZPE/BSSE) and calculated shifts of the HCl stretch in PhAc-HCl , Benzene-HCl and Acetylene-HCl complexes, at the MP2 /aug-cc-pVDZ level of theory.

Complex	Interaction Energy (kcal/mol)	Computed shift (unscaled) (cm^{-1})
PhAc-HCl		
1a (H-π_{Ac})	-5.39/-4.39/-3.81	-157.0
1b (H-π_{Ac}) in plane	-5.34/-4.21/-3.56	-168.2
2 (H-π_{Ph})	-6.30/-5.51/-3.80	-88.7
Ac-HCl	-3.74/-2.69/-2.72	-111.7
Bz-HCl	-6.38/-5.57/-4.06	-78.2

Table 5.8. NBO analysis showing the charge distribution on various atom in PhAc-HCl complexes at MP2/aug-cc-pVDZ level of theory. Numbering on carbon atoms is shown in Fig.5.4.

Complex	Charge (C_{12})	Charge (C_{13})	Charge (C_1)
Monomer (PhAc)	-0.03187	-0.20104	-0.12504
1a	-0.03234	-0.21230	-0.13633
1b	-0.01654	-0.22603	-0.13315

from 1a would require a rotation of the phenyl ring to attain the necessary planarity for the alkene. Hence, even if 1a were to be initially formed, it may have to convert to 1b before Markovnikov addition can take place. As discussed earlier, the facile rotation of HCl around the acetylenic triple bond, would facilitate the conversion to complex 1b, if required. In short, 1b appears to be the 'gateway complex' through which the addition reaction actually takes place.

5.11 Conclusions

Matrix isolation FTIR and *ab initio* calculations were used to study PhAc-HCl complexes. Experimentally, we observed H-π complexes involving H-π_{Ac} and H-π_{Ph} contacts, which were unambiguously discerned by shifts in the infrared frequencies of the HCl vibration. The H-π_{Ac} complex showed two isomers, complex 1a and 1b. This was corroborated by computations which indicated all the H-π complexes to be near-isoenergetic minima, with the H-π_{Ac} complex 1a being the global minimum, both at MP2/CBS and CCSD(T)/CBS limits. The experimentally observed complex 1a and 1b, had multiple minima on the potential surface delineated by very small barriers, which allows for the possibility of the HCl molecule conducting a free rotation around the acetylenic triple bond. Furthermore, these H-π_{Ac} complexes also appeared to be prereaction complexes for Markovnikov addition, with complex 1b actually serving as a gateway complex. It was also interesting to note that while the H-π_{Ac} and H-π_{Ph} complexes had nearly equal interaction energies, they manifested different vibrational wavenumbers of the HCl submolecule. This observation was explained based on the occupancies of the σ^* orbital of HCl in the complex. The ZPE corrected barrier for the conversion of H-π_{Ac} (complex 1a) to H-π_{Ph} (complex 2) was negligibly small, while the barrier for the reverse interconversion was somewhat larger (~1 kcal/mol).

In addition, computations also predicted interactions involving the chlorine of HCl. One of these was an n-σ^*complex where the PhAc was the proton donor to the Cl of HCl, through its acetylenic hydrogen. Two other complexes were also optimized, which were likely Cl-π contacts, with bond distances between 3-3.5 Å. All the complexes computed in this study had interaction energies in the range of -1 to -5 kcal/mol at CCSD(T)/CBS limit.

Through the use of the PCM solvation model, we also showed that the matrix has only a marginal effect on the energetics and vibrational frequencies of the various complexes.

Chapter 6
The Many Facets of Phenylacetylene-Formic Acid Hydrogen Bonded Complexes

6.1 Introduction

Formic acid (FA)-the simplest organic carboxylic acid, is an interesting model system to study non-covalent interactions. Even though it is a small molecule, it presents multiple bonding sites for weak interacions and therefore lends sufficient complexity to make its study challenging. For instance, the OH group of FA can play the dual role of proton donor as well as a proton acceptor, through the H or O, respectively. The C=O group provides a proton acceptor site on the O, while the C-H group can serve as a proton donor. In addition, FA exists in two isomeric forms, cis and trans, with the cis lying about 4 kcal/mol, above the trans, which adds to the complexity.[123] The study of FA has been of interest since it has been identified in interstellar medium[124,125,126] and its aqueous reactions on aerosols and cloud droplets affect halogen activation and ozone concentrations.[127,128]Hence understanding its bonding characteristic is imperative in understanding many of its functions. Consequently, a number of reports exist in the literature, where this molecule has been studied from the point of view of its weak non-covalent interactions.[129-132]

Techniques such as supersonic jet spectroscopy and matrix isolation have been employed to study non-covalent interactions. Using such techniques, FA has been studied for its interactions with precursors such as H_2O, C_2H_2, C_6H_6, to name a few.[133-135] Lisa *et. al.* performed matrix isolation experiments in Ar, to study the interactions of FA with C_2H_2, which is a nonaromatic π system.[134] FA was shown to act as a bidentate hydrogen bonding ligand, forming two contacts. They observed three isomeric structures, having either an OH···π or a CH···π contact as a primary interaction, together with a C-H···O as a secondary interaction. Among all complexes, a structure having an OH···π interaction was the global minimum (-4.9 kcal/mol) and showed an experimental red shift of 137 cm^{-1} in the OH stretch of FA, relative to that observed in uncomplexed FA. Recently Banerjee *et. al.* studied hydrogen bonded complexes of C_6H_6-FA which involves an aromatic π electron system.[135] They observed a T-shaped complex, having an OH···π interaction with the C_6H_6 ring along with a C-H···O interaction, involving C=O of FA and C-H of C_6H_6. The complex was evidenced by a red shift of 120 cm^{-1} in the O-H stretch of FA. Both these studies gave an insight into the dominant O-H···π interaction of FA.

With an aim to deduce the competitive preference of FA towards a system having multifunctional π system, we studied hydrogen bonded complexes of FA with PhAc. FA falls in between the highly acidic HCl and the less acidic H_2O, MeOH and DEE, employed in this study and hence serves to complete the panorama of hydrogen bonded complexes of PhAc. It was also found interesting to compare this sytem with the FA complexes of C_2H_2 and C_6H_6, the two constituent moieties in PhAc.

6.2 Experimental Details

The details of the experiments are described in chapter 2. In particular, the present set of experiments were performed using N_2 and Ar (Sigma Gases and Services, 99%) as matrix gases. Phenylacetylene (Sigma Aldrich, 98%), Phenylacetylene-D (Sigma Aldrich, 99% Atom-D), Formic-Acid (Sigma-Aldrich) were used after subjecting them to several freeze-pump-thaw cycles, before preparing the matrix gas/sample mixture.

Matrix gas to sample ratios were varied from 0.5:1000 to 3:1000 using manometric procedures, for each of the two precursors. Only low concentrations of FA and PhAc were used in all the experiments, to avoid self aggregation. Typical deposition rates of ~3 mmol/hr of the matrix gas was employed for the experiments.

The spectra of the matrix isolated species, were recorded in the region 4000-400 cm^{-1} using a Bruker Tensor 27 FTIR spectrometer, operating at a resolution of 0.5 cm^{-1}. The matrix was then annealed at 27 K (N_2) or 32 K (Ar), typically for 1 hr, and the spectrum again recorded after recooling the matrix to 12 K. Experiments were performed in both Ar and N_2 matrices, both of which showed evidence for the formation of the PhAc-FA complexes. However, since the spectra were well resolved in the Ar matrix, we show the spectra obtained in this matrix.

6.3 Computational Details

The computational study was carried out using Gaussian-09 suite of programs.[73] All computations were performed using M06-2X and MP2 methods, using 6-311++G(d,p) and aug-cc-pVDZ basis sets. Fig. 6.1-6.3 show the optimized structures of complexes at MP2/aug-cc-pVDZ level of theory. The computed frequencies of the complexes, PhAc-*t*FA, were scaled by using appropriate scaling factors to enable a comparison with experimentally observed features. These scale factors have been mentioned in the tables listing the experimental and computed vibrational wavenumbers.

The interaction energies of the complexes were calculated and corrected separately for basis set superposition error (BSSE), and ZPE (zero point energies). Single point calculations at MP2/aug-cc-pVTZ, MP2/aug-cc-pVQZ, CCSD/aug-cc-pVDZ and
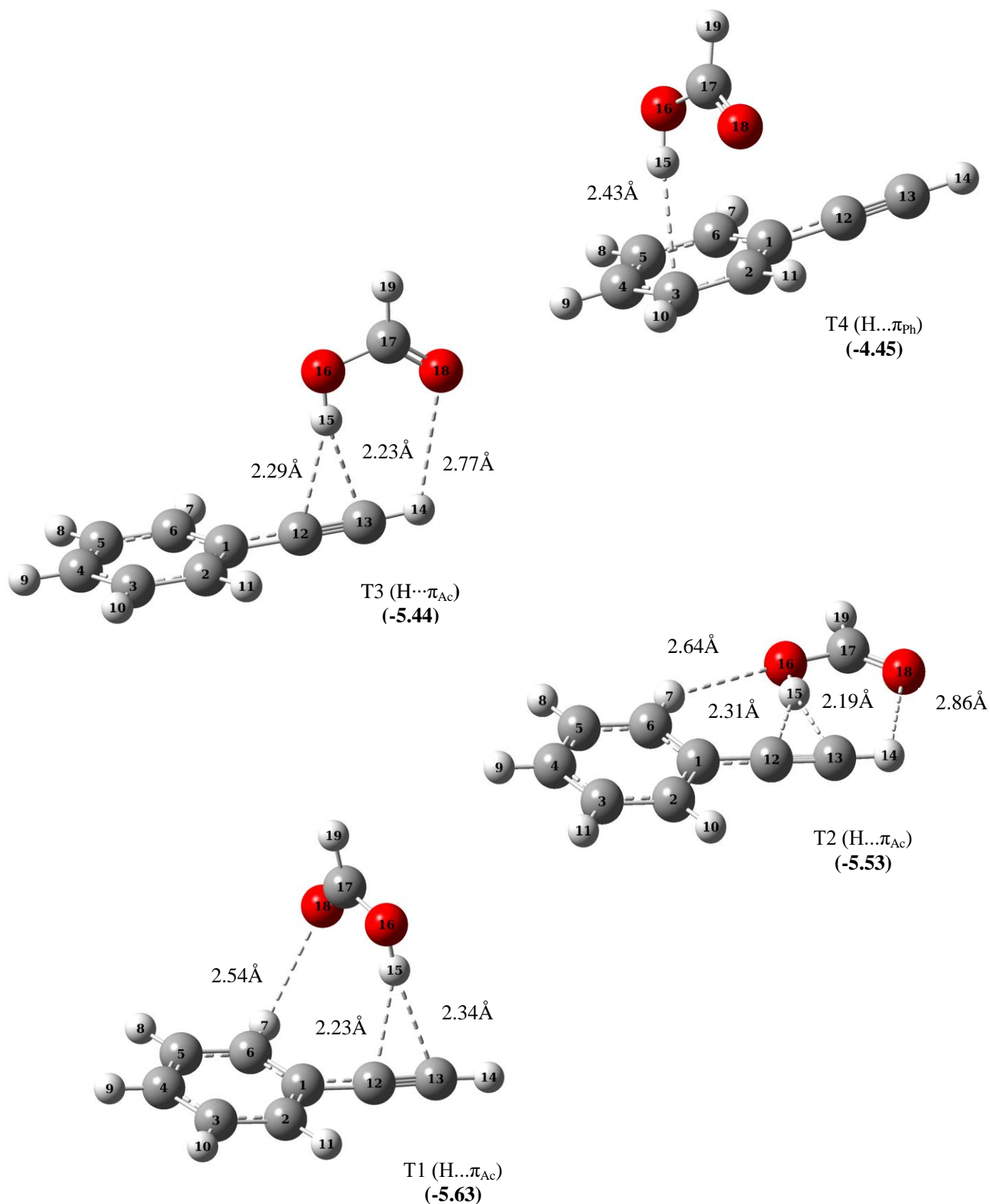
Fig.6.1. Optimized geometries of PhAc-tFA complexes of Group 1 manifesting an O-H···π interaction. Geometry optimizations were done at MP2/aug-cc-pVDZ level of theory. Interaction energies computed at CCSD(T)/CBS limit (kcal/mol) are given in parenthesis. (See text for details.)

T7 (H···π_{Ac})
(-3.25)

T6 (H...π_{Ph})
(-3.19)
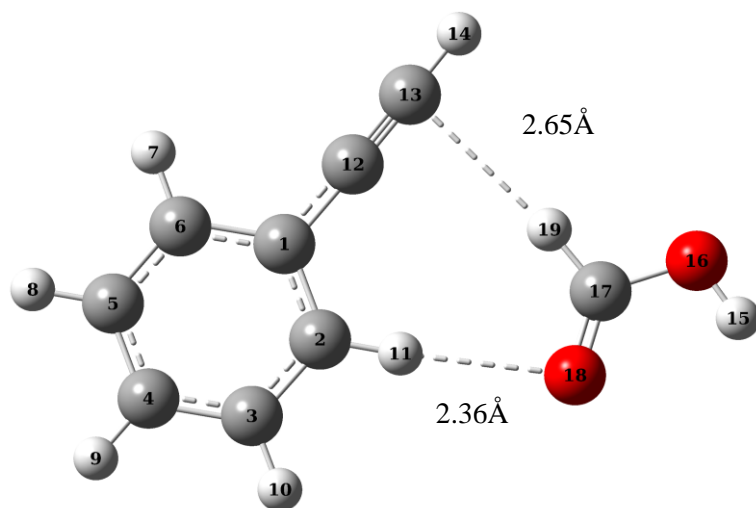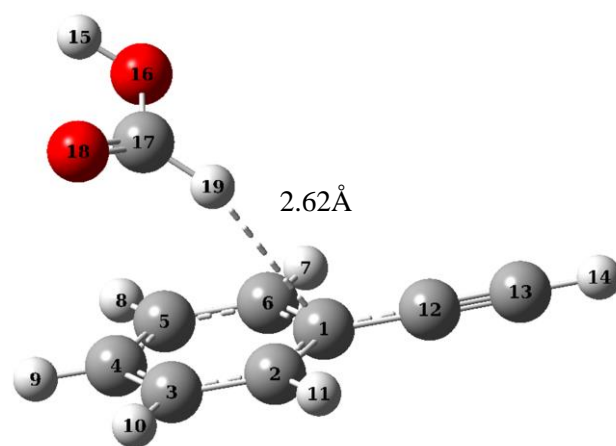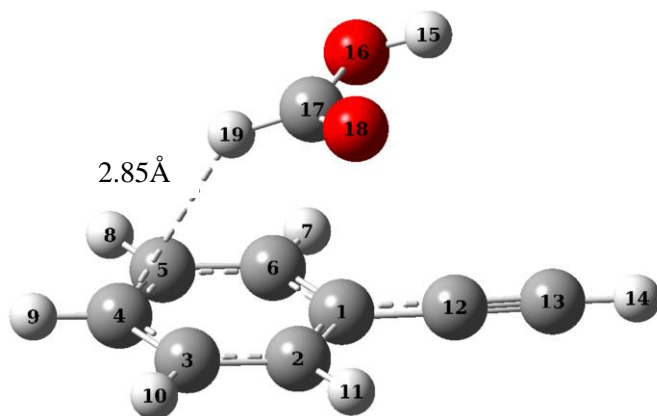
T5 (H...π_{Ph})
(-3.36)

Fig.6.2. Optimized geometries of PhAc-*t*FA complexes of Group 2 manifesting a C-H···π interaction. Geometry optimizations were done at MP2/aug-cc-pVDZ level of theory. Interaction energies computed at CCSD(T)/CBS limit (kcal/mol) are given in parenthesis. (See text for details.)

2.26Å

T8 (C-HAc...OH)
(-1.57)

2.16Å

T9 (C-HAc...O=C)
(-3.07)
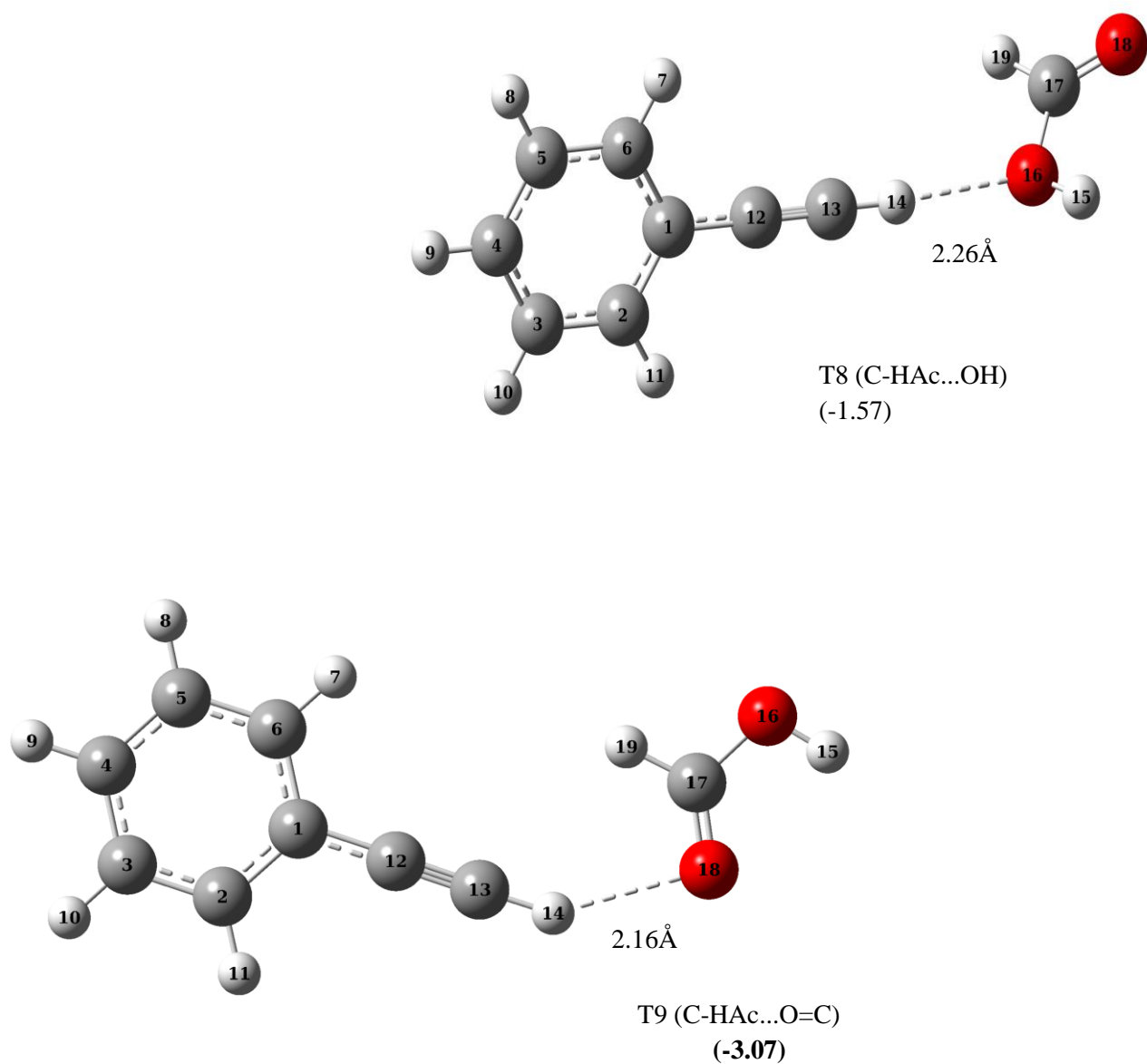
Fig.6.3.Optimized geometries of PhAc-*t*FA complexes of Group 3 manifesting a C-H···O interaction. Geometry optimizations were done at MP2/aug-cc-pVDZ level of theory. Interaction energies computed at CCSD(T)/CBS limit (kcal/mol) are given in parenthesis. (See text for details.)

CCSD(T)/aug-cc-pVDZ were performed using optimized geometries at MP2/aug-cc-pVDZ level. Some preliminary computations on these complexes at the MP2/6-311++G** were perfomed by Gaurav.[136]

An examination of electron density topology was performed using the atoms-in-molecules analysis implemented through AIM2000,[82] to characterize the hydrogen bonding interactions in the complex. NBO and LMOEDA analysis,[73,74] respectively, were also performed to understand the nature of bonding in these non-covalent interactions.

6.4 Results

PhAc-tFA Complexes

a) Experimental

The OH stretch of tFA appears as a doublet at 3350.7 cm^{-1} and 3548.6 cm^{-1} (Fig. 6.4). The doublet is due to site splitting in the Ar matrix. The ≡C- H stretch of PhAc appears as a multiplet in Ar matrix due to Fermi resonance. Codeposition of PhAc and tFA, in an Ar matrix, at 12 K, followed by annealing at 32 K for 1 hr, resulted in the appearance of two strong product features in the O-H stretching region of tFA, at 3375.1 and 3368.1 cm^{-1}. In addition, two weak features at 3439.7 and 3394.9 cm^{-1} were also observed

In the C-O stretching region of tFA, a strong product feature was observed at 1131.3 cm^{-1}, in addition to weak features at 1123.4, 1120.2 cm^{-1}, as shown in Fig. 6.5 (Block A). The C-O stretch in uncomplexed FA occurs at 1103.6 cm^{-1}. In the C=O stretching region of FA, product features were observed at 1751.8 and 1758.2 cm^{-1} , while the corresponding feature in uncomplexed FA occurs at 1767.8 cm^{-1} (Fig. 6.5, Block B). In the ≡CH stretching of PhAc, weak product features were observed at 3306.6, 3304.7and 3290.8 cm^{-1} (Fig, 6.6).

All the features mentioned above were assigned as product features of the PhAc-tFA complexes, as these features were not observed when only one of the precursors was present. On increasing the concentration of either monomer, the intensity of the product bands increased, confirming them to be features due to complexes of PhAc-tFA . These features were due to 1:1 complexes of PhAc-tFA, as they were seen at very low concentration of both the monomers. Experiments with isotopic PhAc$_D$ (acetylenic hydrogen substituted by deuterium) were also performed to observe isotopic shifts . The feature observed at 2586.1 cm^{-1} in ≡C-D stretching of PhAc$_D$ corresponds to PhAc$_D$-tFA adduct (Fig. 6.7).

It should be noted that cis-FA (cFA) was not observed in the matrix due to the large energy difference (~4 kcal/mol) between cis and trans FA isomers. Hence only complexes of PhAc-tFA were observed in the matrix. It is interesting to note that some of the complexes of PhAc-cFA had the largest interaction energies, but the higher energy of the cis isomer of FA,

rendered these complexes inaccessible to experiments. Fig. 6.8 shows the correlation diagram between the energy asymptote of the monomers and the energy of the complexes to clearly indicate that the complexes involving the cis-isomers were indeed placed well above the energies of the complexes involving the tFA.

b.Computational

Several hydrogen bonded structures were indicated as minima by our calculations. Figures 6.1-6.3 shows the structures calculated at MP2/aug-cc-pVDZ level of theory. Table 6.1 gives important geometrical parameters at MP2/aug-cc-pVDZ level of theory.Table6.2 summarizes the interaction energies of the PhAc-tFA complexes at various levels of theory. On the basis of primary interactions in the complex, we can classify the various structures into three groups. Group 1 (O-H$\cdots\pi$) consists of structures having an O-H$\cdots\pi$ contact as the primary interaction, involving the O-H of tFA as the proton donor (Fig. 6.1). In some cases, as will be explained below, the O-H$\cdots\pi$ interaction, involved the π system of the acetylenic group as the proton acceptor, which is denoted as an O-H$\cdots\pi_{Ac}$ interaction. In cases where the O-H$\cdots\pi$ interaction involved the phenyl π system as the proton acceptor, the interaction was indicated as O-H$\cdots\pi_{Ph}$. In addition to this primary interaction, some structures also show a secondary n-σ* interaction. Structures T1, T2 and T3 belong to the O-H$\cdots\pi_{Ac}$ category, while T4 shows an O-H$\cdots\pi_{Ph}$ interaction. Group 2 (C-H$\cdots\pi$) consists of structures, which are dominated by a C-H$\ldots\pi$ contact between, the C-H moiety of tFA and acetylenic/phenyl π cloud of PhAc as observed in complexes T5 , T6 and T7 (Fig. 6.2) . In complex T5, C-H of tFA points towards C4 of phenyl ring whereas complex T6 involves C-H pointing towards the carbon C1 of PhAc. Structure T7 shows two contacts simultaneously - a C-H$\cdots\pi_{Ac}$ contact with acetylenic π cloud of PhAc and a n-σ* interaction involving C=O of tFA and C-H of phenyl ring. We also obtained complexes, T8 and T9, having n-σ* interaction as the only contact between tFA and PhAc. In both complexes PhAc acts as proton donor through $\equiv$C-H group. In T8 the proton acceptor is the oxygen in O-H group of tFA, while in complex T9, C=O group of tFA is the proton acceptor. Of all these structures, (which were restricted to tFA) the complexes belonging to group 1 have the largest BSSE corrected interaction energies, with T1 as a global minimum followed by T2,T3 and T4 as local minima. It must be however said that all the three structures (T1,T2 &T3) are nearly isoenergetic, with energy differences between them being as small as ~0.2 kcal/mol. All the three structures vary in the orientation of tFA with respect to plane of the PhAc .
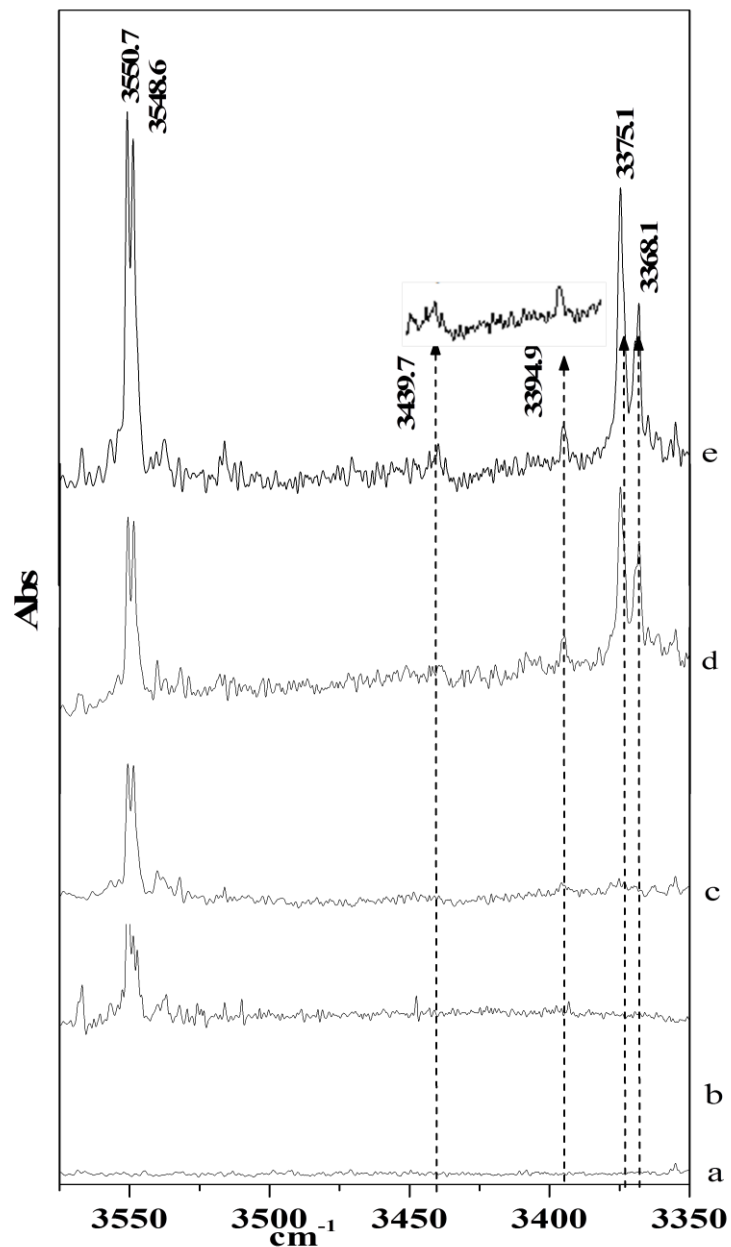
Fig. 6.4. Spectra of PhAc-*t*FA complexes in an Ar matrix in OH stretching region of Formic acid (3575-3350 cm^{-1}) (a) PhAc:Ar (3:1000) (b) FA:Ar (0.6:1000) (c) PhAc:FA:Ar(3:0.6:1000) (as deposited) (d) PhAc:FA:Ar (3:0.6:1000) (e) PhAc:FA:Ar(3:0.9:1000). All spectra, except that shown in trace (c), were recorded after annealing the matrix at 32 K. Spectrum in trace 'c' was recorded after depositing the matrix (before annealing.)
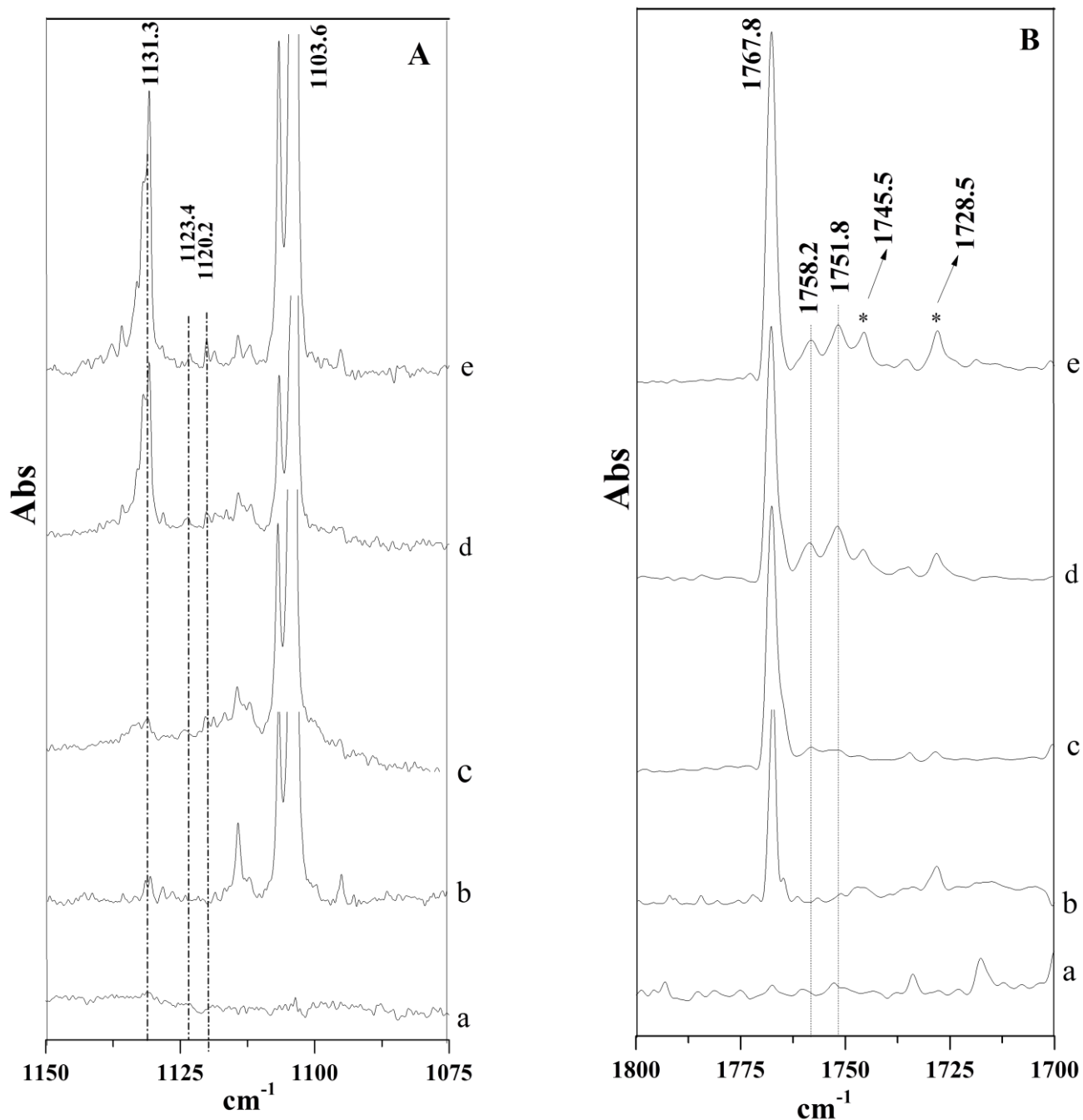
Fig.6.5. Spectra of PhAc-tFA complexes in an Ar matrix in (**A**) C-O stretching region of FA (1150-1075 cm^{-1}) (**B**) C=O stretching region of FA (1700-1800 cm^{-1}) (a) PhAc:Ar (3:1000) (b) FA:Ar (0.6:1000) (c) PhAc:FA:Ar (3:0.6:1000) (as deposited) (d) PhAc:FA:Ar (3:0.6:1000) (e)PhAc:FA:Ar (3:0.9:1000). All spectra, except that shown in trace (c), were recorded after annealing the matrix at 32 K. Spectrum in trace 'c' was recorded after depositing the matrix (before annealing.)
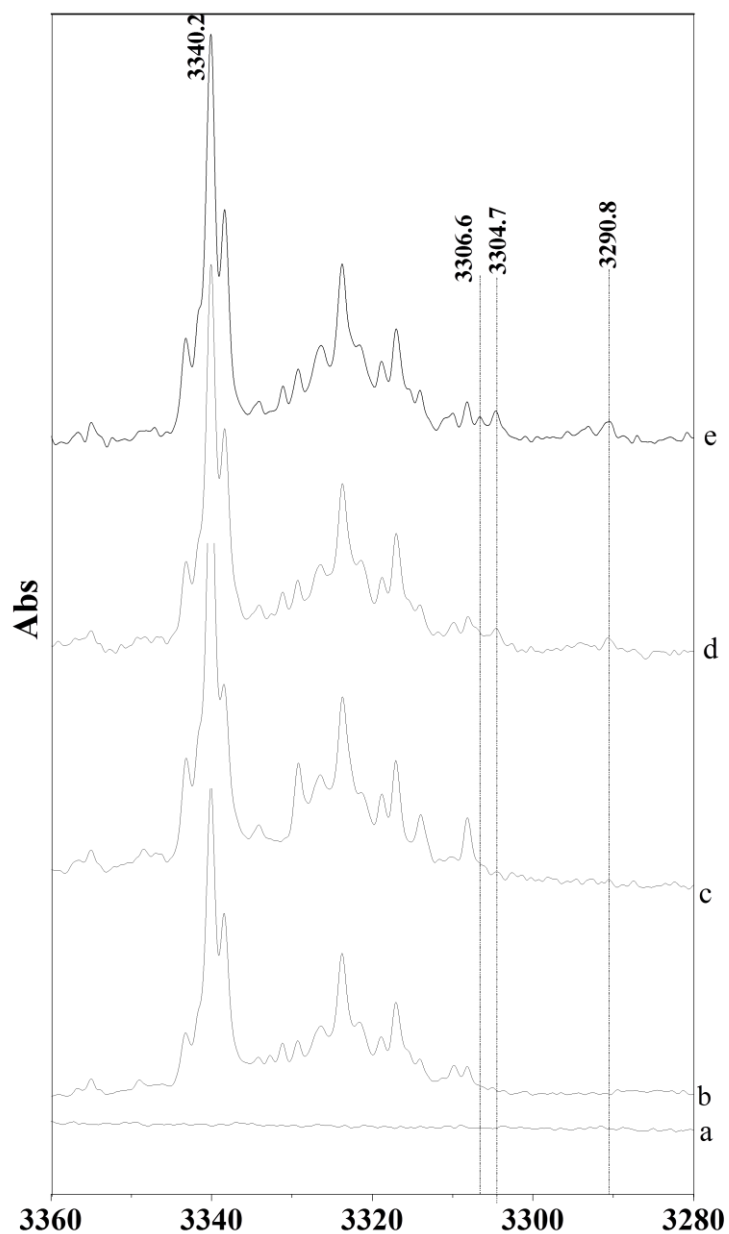
Fig 6.6 Spectra of PhAc-*t*FA complexes in an Ar matrix in the ≡CH stretching region of PhAc (3360-3280 cm^{-1}) (a) FA:Ar (0.6:1000) (b) PhAc:Ar (3:1000) (c) PhAc:FA:Ar (3:0.6:1000) (as deposited) (d) PhAc:FA:Ar (3:0.6:1000)(e) PhAc:FA:Ar (3:0.9:1000). All spectra, except that shown in trace (c), were recorded after annealing the matrix at 32 K. Spectrum in trace 'c' was recorded after depositing the matrix (before annealing.)
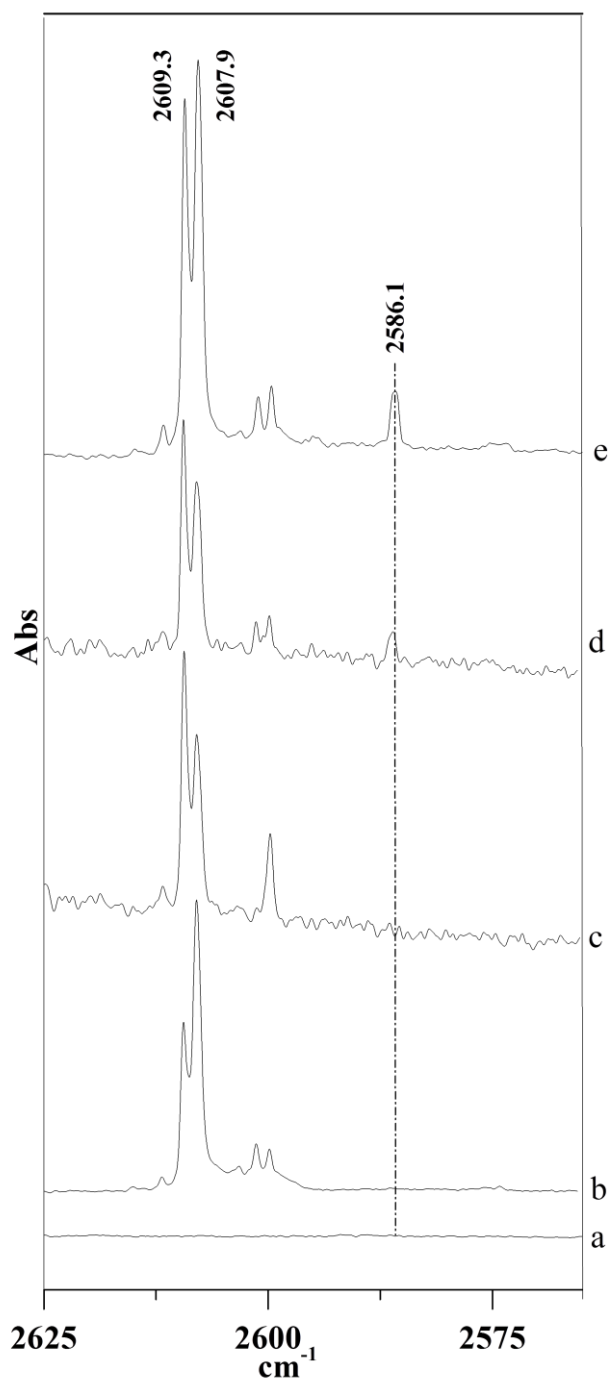
Fig 6.7. Spectra of PhAc-tFA complexes in an Ar matrix in the ≡CD stretching region of PhAcD (2625-2575 cm^{-1}) (a) FA:Ar (0.6:1000) (b) PhAcD:Ar (3:1000) (c) PhAcD:FA:Ar(1:0.6:1000) (as deposited). (d) PhAcD:FA:Ar (1:0.6:1000) (e) PhAcD:FA:Ar (3:0.6:1000). All spectra, except that shown in trace (c), were recorded after annealing the matrix at 32 K. Spectrum in trace 'c' was recorded after depositing the matrix (before annealing.)
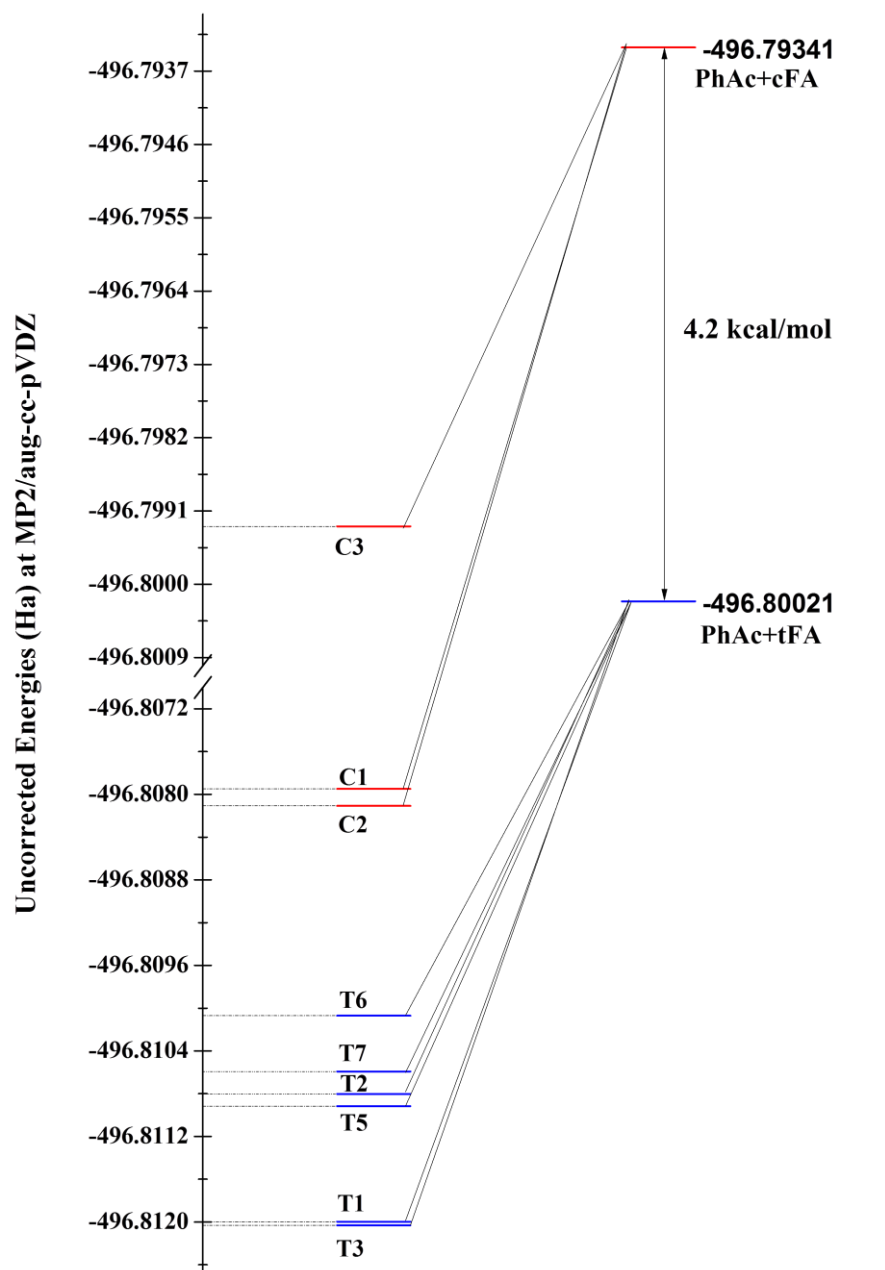
Fig 6.8. Correlation diagram showing uncorrected energies of the PhAc-FA complexes involving both cis and trans FA.

Table. 6.1. Important geometrical parameters, bond lengths (Å), bond angles (°), dihedral angles (°), for PhAc-*t*FA complexes computed at the MP2/aug-cc-pVDZ level. Labelling of atoms is shown in Fig. 6.1, 6.2 and 6. 3.

Parameter	T1	T2	T3	T4	T5	T6	T7	T8	T9
C_{13}-H_{14}	1.07	1.08	1.08	1.07	1.074	1.074	1.074		
O_{16}-H_{15}	0.98	0.98	0.98	0.98	0.97				
O_{18}-H_7	2.54								
C_{12}-H_{15}	2.23	2.31	2.29						
C_{12}-H_{15}-O_{16}	155.06	159.0	163.70						
C_6-H_7-O_{18}	118.29								
O_{16}-H_{15}-C_{12}-C_1	21.60	0.03	0.01						
C_1-C_6-H_7-O_{18}	-75.97								
O_{18}-H_{14}		2.86	2.77						
H_7-O_{16}		2.64	--						
C_{13}-H_{14}-O_{18}		107.7	107.35						
C_6-H_7-O_{16}		141.1	81.03						
H_{15}-O_{16}-H_7-C_6		0.00	---						
C_{17}-O_{18}-H_{14}-C_{13}		0.00	-0.00						
C_{17}-O_{16}-H_{15}-C_{13}		0.03							
H_{15}-C_3				2.43					
C_3-H_{15}-O_{16}				172.19					
C_3-H_{15}-O_{16}-C_{17}				-16.66					
H_{19}-C_4					2.85				
C_{17}-H_{19}-C_4					140.56				
O_{18}-C_{17}-H_{19}-C_4					-79.35				
H_{19}-C_1						2.62			
H_{19}-C_1-C_{17}						152.77			
H_{11}-C_2-C_1-H_{19}						-110.11			
H_{19}-C_{13}							2.65		
O_{18}-H_{11}							2.36		
H_{19}-C_{17}-O_{18}-H_{11}							0.00		
C_2-H_{11}-O_{18}							176.89		
C_{13}-H_{19}-C_{17}							173.78		
O_{16}-C_{17}-O_{18}-H_{11}							-		
C_{17}-H_{19}							1.10		
O_{16}-H_{11}									
C_2-H_{11}-O_{16}									
H_{11}-O_{16}-C_{17}-H_{19}									
O_{18}-H_{14}									2.26
C_{17}-O_{18}-H_{14}-C_{13}									0.00
C_{13}-H_{14}-O_{18}									146.76
H_{14}-O_{16}								2.26	
C_{13}-H_{14}-O_{16}								175.94	
C_{13}-H_{14}-O_{16}-C_{17}								-19.43	

In T1, *t*FA is at an angle of ~71˚ with the plane of PhAc, manifesting two interactions; an OH···π between the OH of tFA and the acetylenic π system of PhAc, with a secondary interaction between carbonyl of *t*FA and a hydrogen of the phenyl ring . Complex T2 is a complex with a three point contact, as shown in the Fig. 6.1, where PhAc and *t*FA are coplanar. In this case, an OH···π_{Ac} interaction is the primary interaction, accompanied by two secondary interactions. Complex T3 is similar to T2, the difference being in the orientation of the FA relative to PhAc. The perpendicular orientation allows only two hydrogen bonded contacts – an OH···π and a ≡C-H···O=C. Table 6.2 shows the interaction energies of PhAc-*t*FA complexes.

It must be mentioned that when uncorrected or only ZPE corrected interaction energies are considered at the MP2/aug-cc-pVDZ level, T4 which is a phenyl bonded complex shows the largest interaction energy followed by structures T1, T5, T2, T3 and T6, with the difference between the strongest and weakest bound complexes being just ~1.2 kcal/mol. When BSSE correction is applied, the ordering changes, as follows; T1, T3, T2, T4, T5 and T6, given in order of decreasing stability, with the difference between the strongest and weakest bound complex being ~1.9 kcal/mol. The same ordering was also obtained when the interaction energies were computed by extrapolation to the complete basis set limit. We therefore consider this ordering as being reliable, which is used for comparison with experiments. With the difference between the various structures, being as small as they are and dependent on the computational methodology, experimental evidences, as presented in this work, are necessary to corroborate the computational findings.

6.5 Discussions

PhAc-*t*FA complexes

a) OH stretch of *t*FA

The OH group of *t*FA is the most favourable site for hydrogen bonding in the molecule. In Ar matrix OH stretch of *t*FA occurs as a site split doublet at 3550.7 cm^{-1} and 3548.6 cm^{-1} (Fig. 6.4). The codeposition of PhAc and FA at 12 K and annealing to 32 K produces strong product features at 3375.1 and 3368.1 cm^{-1}, which are red shifted from the OH stretch in uncomplexed *t*FA by 175.6 cm^{-1} and 182.6 cm^{-1} respectively. These are in agreement with the computed red shifts for complex T3 and T2 respectively, thereby confirming the presence of O-H…π bonded PhAc-*t*FA complexes (Table 6.3). In addition, there is a weak product feature at 3394.9 cm^{-1}, which amounts to red shifts of 155.8 cm^{-1}. This observed red shift for the weak feature corroborates well with the calculated red shift of

148.5 cm^{-1}, for complex T1. A feature at 3439.7 cm^{-1} was also observed, particularly at higher concentrations of FA, whose shift of 110 cm^{-1}, is in agreement with the shift computed for T4, which is an O-H$_{Ph}$ complex. We conclude that in the Ar matrix, complexes T2 and T3, which are near isoenergetic global minima were unambiguously identified, together with probably complexes T1 and T4. It may be seen from Table 6.2 that the three complexes, T1, T2 and T3 are nearly isoenergetic structures with T4 being less stable by ~1.2 kcal,/mol at CCSD(T)/CBS level. Experimental results are consistent with the energy ordering predicted by MP2/CBS, CCSD(T)/CBS levels and BSSE corrected MP2 and M06-2X methods using aug-cc-pVDZ basis sets.

b) C-O stretch of *t*FA

A strong product feature, in the C-O stretching region, due to the PhAc-*t*FA complex, was observed at 1131.3, with weaker features at 1123.4 and 1120.2 cm^{-1} (Fig. 6.5, Block A) . Assignment of the feature at 1131.3 to the PhAc-FA complex, requires to be made with caution, as a feature at this wavenumber has already been reported in the literature to belong to an acyclic dimer of *t*FA.However, in our experiment, the feature at 1131.3 shows a strong dependence on both PhAc and *t*FA concentration, indicating it to be due to a PhAc-*t*FA complex. We also confirmed it to be a product feature of the hetero complex, by performing experiments at very low concentrations of FA when the feature at 1131.3 was barely visible.

At the same concentration of *t*FA, when PhAc was added, this feature grew in strength, indicating it to be due to PhAc-*t*FA complex. This feature is blue shifted by 27.7 cm^{-1} from the monomer feature at 1103.6 cm^{-1} and once again can be assigned to any of the three PhAc-*t*FA complexes, T1, T2 or T3, confirming that O-H⋯π complexes are indeed prepared in the matrix . No experimental feature was observed that could be assigned to the T4 complex.

c) C=O stretch of tFA

The C=O stretch of uncomplexed *t*FA in Ar is observed at 1767.8 cm^{-1} (Fig. 6.5, Block B). FA is known to show association extensively either in the form of dimers or water complexes.[137] It is already reported in the literature and which was also observed in our experiments, that *t*FA on annealing yields features at 1728.5 cm^{-1} and 1745.5 cm^{-1} which correspond to cyclic and acyclic dimer of *t*FA respectively.[137] In our experiments, new features at 1751.8 cm^{-1} and 1758.2 cm^{-1} were observed, only in the presence of *both* *t*FA and PhAc . These feature are red shifted from the monomer feature by ~16 and 10 cm^{-1} respectively , which agree well with the computed shifts of all three acetylenic complexes of

PhAc-*t*FA,T1, T2 and T3, more so with T2 and T3 (Table 6.3). Hence, while the product features in the C=O region indicate the formation of the PhAc-*t*FA complex, it does not allow for an unambiguous assignment to any particular complex, but confirms the presence of complexes T2, T3 and T7. No evidence was observed for the T4, which was barely observable in the O-H stretching region.

d) ≡C-H stretch of PhAc

In Ar matrix, ≡C-H stretch of PhAc occurs as a Fermi resonance diad at 3340.2 and 3323.9 cm^{-1} (Fig. 6.6). These peaks also suffer from site effects and as a result the ≡C-H stretch of PhAc occurs as bunch of sharp peaks spread between 3343.4 and 3308.3 cm^{-1}. The product features appear as weak peaks at 3306.6, 3304.8 and 3290.8 cm^{-1}. It is rather difficult to compute the red shifts as the feature for the monomer occurs as a bunch of multiplets. Computations show this feature to be red shifted by ~18 cm^{-1} for complexes T2 and T3. It should be noted that due to spectral congestion in this region the assignment of these features is at best tentative (Table 6.3). The shifts in the T4 complex was too small to be observed. A feature observed at 3290.8 cm^{-1} which was red shifted by ~60 cm^{-1} can be tentatively assigned to an n…σ* structure (T9) involving carbonyl oxygen of *t*FA.(Fig. 6.6, Table 6.3)

e) ≡C-D stretch of PhAc$_D$

Spectra were also recorded with PhAc$_D$, where the acetylenic hydrogen was replaced with deuterium, to confirm the vibrational assignment in the complexes through isotopic shifts. It was observed that although PhAc$_D$ was free of any Fermi resonance, it still suffered from site effects . The ≡C-D stretch of PhAc$_D$, occurs as a doublet at 2609.3 and 2607.9 cm^{-1} (Fig. 6.7). The product feature occurs at 2586.1 cm^{-1} which amouts to a red shift of 21.8 cm^{-1}. The computed red shifts for complex T3 and T2, are 12.4 and 14.3 cm^{-1} (Table 6.3) which is in general agreement with the experimental value for complexes T3 and T2.

The experimental observation therefore clearly point to the presence of complexes T2 and T3 in the matrix. As indicated by the features in the O-H region (Fig. 6.4) it is likely that complex T1 may be present in minor amounts. The shift in the feature for the T4 complex was computed to be negligible and hence not observed.

6.6 AIM Analysis

Hydrogen bonding interactions between multifunctional PhAc and *t*FA were examined by the charge density topology, performed using the atoms-in-molecules (AIM) theory of Bader.[81] This analysis require wavefunctions, which were generated at the MP2/aug-cc-pVDZ level of theory and subsequently (3,-1) bond critical points were located

Table 6.2: Interaction energies for the various PhAc-*t*FA complexes at different levels of theory. Interactions energies have been given as Raw/ZPE/BSSE (kcal/mol). Where only one entry is given, they are uncorrected energies.(See text for details.)

Complex	M06-2X		MP2			CCSD(T)	
	6-311++G(d,p)	aug-cc-pVDZ	6-311++G(d,p)	aug-cc-pVDZ	CBS	aug-cc-pVDZ	CBS
(O-H⋯π)							
T1(H⋯π$_{Ac}$)	-6.14/-5.33/-5.64	-6.10/-5.32/-5.63	-6.71/-4.23/-3.96	-7.40/-6.57/-4.88	-5.98	-7.05	-5.63
T2(H⋯π$_{Ac}$)	-5.90/-5.11/-5.56	-6.03/-5.14/-5.47	-5.93/-3.95/-3.78	-6.55/-5.88/-4.66	-5.72	-6.45	-5.53
T3(H⋯π$_{Ac}$)	---	-5.86/-5.11-5.49	---	-6.52/-5.82/-4.70	-5.68	-6.28	-5.44
T4(H⋯π$_{Ph}$)	-5.51/-4.88/-4.75	-5.44/-4.84/-4.66	-6.36/-4.67/-3.09	-7.42/-6.73/-4.11	-5.07	-6.80	-4.45
(C-H⋯π)							
T5 (H⋯π$_{Ph}$)	-4.86/-4.20/-4.02	---	-5.74/-4.06/-2.27	-6.72/-5.94/-3.24	-4.10	-5.98	-3.36
T6 (H⋯π$_{Ph}$)	---	-4.04/-3.35/-3.27	---	-6.19/-5.36/-3.00	-3.76	-5.61	-3.19
T7 (H⋯π$_{Ac}$)	---	---	---	-4.56/-3.86/-2.60	-3.13	-4.67	-3.25
(n⋯σ*)							
T8 (C-H$_{Ac}$⋯OH)	-1.84/-1.25/-1.48	---	-2.41/-0.16/-1.32	-2.62/-1.86/-1.46	-1.51	-2.68	-1.57
T9 (C-H$_{Ac}$⋯O=C)	---	---	-3.06/-0.90/-2.08	-3.82/-3.12/-2.64	-3.04	-3.85	-3.07

Table .6.3 Experimental (Ar matrix) and scaled computed wavenumbers (MP2/aug-cc-pVDZ) for the different PhAc-*t*FA complexes.

	Experimental		Scaled Computed Wavenumbers										Modes
	Monomer	Complex	Monomer	1	2	3	4	5	6	7	8	9	
PhAc	3340.2	**3304.8 (-35.4)**[a] **3306.6 (-33.6)** **3290.8 (-49.4)**	3316.9	3309.2 (-7.7)	**3297.1 (-19.8)**	**3299.9 (-17.0)**	3316.0 (-0.8)	3315.3 (-1.6)	3315.7 (-1.1)	3311.0 (-5.9)	3288.9 (-27.9)	**3256.0 (-59.9)**	≡C-H stretch
*t*FA	3550.7	**3368.1 (-182.6)** **3375.1 (-175.6)** **3394.9 (-155.8)** **3439.7 (-110.0)**	3550.7	**3402.2 (-148.5)**	**3373.5 (-177.2)**	**3385.0 (-165.7)** **3467.3 (-83.4)**	3544.5 (-6.2)	3545.1 (-5.6)	3546.7 (-3.9)	3538.9 (-11.8)	3547.6 (-3.1)		O-H stretch
	1103.6	**1131.3 (+27.7)**	1103.6	**1134.5 (30.9)**	**1133.9 (30.3)**	**1138.2 (34.6)**	1112.5 (8.9)	1097.7 (-5.9)	1095.5 (-8.1)	1105.4 (1.8)	1092.9 (-10.7)	1114.3 (10.7)	C-O stretch
	1767.8	**1751.8 (-16.0)** **1758.2 (-9.6)**	1751.8	**1738.2 (-13.6)**	**1737.2 (-14.6)**	**1736.0 (-15.8)**	1739.9 (-11.9)	1744.8 (-7.0)	1743.4 (-8.4)	1738.5 (-13.3)	1753.9 (2.1)	1741.8 (-10.0)	C=O stretch
PhAc$_D$	2607.9	**2586.1 (-21.8)**	2607.9	2600.9 (-7.0)	**2593.6 (-14.3)**	**2595.5 (-12.5)**	2607.6 (-0.3)	2606.4 (-1.6)	2607.1 (-0.9)	2602.9 (-5.0)	2590.2 (-17.8)	2571.8 (-36.2)	≡C-D stretch

[a] Numbers in parenthesis are Δν =ν(complex)- ν(monomer)

Scaling Factors : 0.959487991 (3800-3000 cm^{-1}) , 0.974366064 (3000-2500 cm^{-1}), 0.98917262 (2500-1000 cm^{-1})

theory of Bader. This analysis require wavefunctions, which were generated at the MP2/aug-cc-pVDZ level of theory and subsequently (3,-1) bond critical points were located (Fig. 6.9). Values of topological parameters, such as electron density $\rho(r_c)$, eigenvalues of the Hessian, $\lambda_1, \lambda_2, \lambda_3$, the Laplacian ($\nabla^2\rho(r_c)$) of electron density (defined as the sum of the eigenvalues), the ellipticity, $[(\lambda_1/\lambda_2)-1]$ and $|\lambda_1/\lambda_3|$, for all the complexes, computed at the bond critical points, are shown in Table 6.4. The positive value of ($\nabla^2\rho$) in the range of 0.024-0.139 a.u. indicate a closed shell interaction, as is seen in hydrogen bonds . Furthermore, the values of $\rho(r_c)$ and ($\nabla^2\rho$) for all the contacts lie in the range of hydrogen bonding interactions as proposed by Koch and Popelier.[83] The nearly isoenergetic complexes T1, T2 & T3 have O-H$\cdots\pi_{Ac}$ as the primary interaction, and have similar values of $\rho(r_c)$ and ($\nabla^2\rho$). These complexes also show a secondary interaction as shown in Fig. 6.9. Using the topological parameters, we also computed the interaction energy for each contact, through the use of local kinetic energy density, $G(r_{CP})$ and local potential energy density $V(r_{CP})$, as proposed by Espinosa et al[84]. Though the values of interaction energies obtained through a topological analysis do not exactly match with the values presented in Table 6.2, they still indicate complexes T1, T2 and T3 to be the most stable. Clearly the most stable complexes in the PhAc-*t*FA system manifest bi or tridentate ligation in the hydrogen bonded complexes.

6.7 NBO Analysis

We used natural bond orbital analysis (NBO analysis) implemented through Gaussian 09, to quantify interactions between donor and acceptor orbitals of PhAc-*t*FA complexes (Table 6.5).[73] The acetylenic π system is the donor orbital in complex T1, T2 and T3, whereas in case of complex T4 the phenyl π system acts as donor orbital. In all the complexes mentioned above, σ* O-H orbital of *t*FA acts as acceptor of electron density. Electron transfer to the σ* OH orbital of *t*FA corroborate the observed and computed red shifts in the O-H stretch discussed earlier. For example, it can be seen that complex T2 has the largest red shift amongst all the three acetylenic complexes and it can be related to the largest electron occupancy in the acceptor σ* OH, followed by complex T3. Complex T1 which manifests a smaller shift in the O-H frequency can also be seen to have smaller occupancies in the σ* OH relative to complexes T2 and T3. (Table 6.5).

6.8 LMOEDA

The interaction energy of various PhAc-*t*FA complexes was partitioned into contributions from various interactions, such as electrostatic, exchange-repulsion,dispersion

Table 6.4: Summary of AIM calculations (MP2/aug-cc-pVDZ level) for the PhAc-*t*FA complexes. All quantities are expressed in a.u. See text for definition of each of the quantities.

Complex	$\rho(r_c)$	$\nabla^2\rho(rc)$	λ_1	λ_2	λ_3	$\lambda|_1/\lambda_3|$	$(\lambda_1/\lambda_2)-1$	ΔE_{HB}	Total ΔE_{HB}
T1 bcp1	0.0171	0.0482	-0.0169	-0.0111	0.0762	0.2218	0.5278	-3.30	-4.81
bcp2	0.0088	0.0316	-0.0078	-0.0066	0.0460	0.1700	0.1899	-1.51	
T2 bcp1	0.0187	0.0512	-0.0187	-0.0136	0.0835	0.2244	0.3821	-3.71	-5.57
bcp2	0.0058	0.0239	-0.0051	-0.0037	0.0327	0.1553	0.3684	-0.96	
bcp3	0.0058	0.0214	-0.0044	-0.0015	0.0274	0.1621	1.9601	-0.90	
T3 bcp1	0.0179	0.0494	-0.0175	-0.0121	0.0791	0.2218	0.4450	-3.49	-4.59
bcp2	0.0068	0.0251	-0.0054	-0.0026	0.03313	0.1632	1.0949	-1.10	
T4 bcp1	0.0118	0.0334	-0.0094	-0.0032	0.04601	0.2043	1.9357	-1.97	-3.00
bcp2	0.0072	0.0213	-0.0041	-0.0033	0.02868	0.1434	0.2550	-1.03	
T5	0.0089	0.0315	-0.0034	-0.0022	0.03701	0.0915	0.5592	-1.51	-1.51
T6 bcp1	0.0097	0.0295	-0.0073	-0.0015	0.03823	0.1900	3.8009	-1.56	-2.79
bcp2	0.0074	0.0276	-0.0022	-0.0005	0.03031	0.0719	2.9626	-1.23	
T7 bcp1	0.0085	0.0228	-0.0062	-0.0051	0.0346	0.1913	0.2899	-1.23	-3.24
bcp2	0.0119	0.0342	-0.0123	-0.0120	0.0584	0.2103	0.0259	-2.01	
T8	0.0125	0.0410	-0.0138	-0.0130	0.0677	0.2032	0.0620	-2.28	-2.28
T9	0.0142	0.0422	-0.0149	-0.0148	0.0718	0.2069	0.0079	-2.61	-2.61

and polarization. LMOEDA analysis was performed at MP2/aug-cc-pVDZ level of theory using GAMESS. Complex T1, T2 and T3 having O-H$\cdots\pi_{Ac}$ as major interaction receive the largest contribution from electrostatic interactions, whereas complex T4, T5 and T6 have nearly equal contributions from dispersion and electrostatic components (Table 6.6).

6.9 Conclusions

Hydrogen bonded interactions in PhAc-tFA heterodimer were explored using matrix isolation FTIR spectroscopy and *ab initio* calculations. PhAc and FA both being multifunctional molecules gave rise to a large number of hydrogen bonded geometries. Our computations reveal that 9 isomeric complexes were possible on the PhAc-tFA potential surface, a situation that is a theorists' delights but an experimentalists' nightmare. Amongst PhAc-tFA complexes – the structures constituting the global minima were composed of primary O-H$\cdots\pi$ interaction together with a secondary C-H$\cdots$O interaction. In our experiments we observed clearly two of the three nearly isoenergetic structures (complexes T2 and T3) , in which OH of FA interacts with acetylenic π cloud of PhAc. The secondary C-H$\cdots$O interactions involved either the C=O or the OH group of FA on the one hand and –C-H of phenyl or the CH of the acetylenic grouop of PhAc on the other. A third strucrure (complex T1) was also tentavely observed. The interaction energy in these structures were approximately -5.5 kcal/mol computed at the CCSD(T)/CBS limit. In all these complexes, AIM calculations show that these structures are multiply bonded. The LMO-EDA calculations indicate these complexes to be dominated by electrostatic contributions. As in the case of our earlier work on PhAc-HCl, where HCl was indicated to have a free rotation around the acetylenic π system, here too it was found that the energy varied little as the FA was rotated around the cylindrical π acetylenic system. This phenomenon may have implications in the experimental observation of structures T2 and T3 showing large intensities compared with T1, even though all the three structures are isoenergetic. It is likely that structures T2 or T3 are produced by the approach of FA along any plane, while T1 may require the approach of FA along specific directions. In other words, the trapping of T2 and T3 is kinetically directed and features corresponding to these structures have a greater intensity than T1, even though all of them are nearly isoenergetic.

Local minima having O-H$\cdots\pi_{Ph}$ interaction was also observed with a red shift of ~110 cm^{-1} in the O-H mode, a shift which is significantly lower than that observed in the case of the O-H$\cdots\pi_{Ac}$ structures. It is interesting to compare the 1:1 hydrogen bonded complexes

Table 6.5. NBO analysis of Phac-tFA complexes at MP2/aug-cc-pVDZ level of theory. The atom numbering indicated in the table is as shown in Fig.6.1,6.2 and 6.3. E(j) is the second order perturbation energy (kcal mol^{-1}), E(j)-E(i) is the donor-acceptor energy difference and F(i,j) is the overlap between the donor and acceptor orbitals.

Complex	Orbital Involved		E(kcal mol^{-1})	E(j)-E(i) a.u.	F(i,j) a.u.	Electron occupancy in σ* orbital
	Donor	Acceptor				
T1	C_{12}-$C_{13}(\pi)$	H_{15}-$O_{16}(\sigma*)$	6.94	1.07	0.078	0.02261
T2	C_{12}-$C_{13}(\pi)$	H_{15}-$O_{16}(\sigma*)$	9.49	1.07	0.090	0.02612
T3	C_{12}-$C_{13}(\pi)$	H_{15}-$O_{16}(\sigma*)$	8.33	1.07	0.085	0.02348
T4	C_3-$C_4(\pi)$	H_{15}-$O_{16}(\sigma*)$	3.10	1.00	0.054	0.01695
T5	C_1-$C_2(\pi)$	C_{17}-$O_{18}(\sigma*)$	1.56	0.53	0.027	0.12148
T6	C_4-$C_5(\pi)$	C_{17}-$O_{18}(\sigma*)$	1.27	0.54	0.025	0.1183
T7	C_{12}-$C_{13}(\pi)$	C_{17}-$H_{19}(\sigma*)$	2.75	1.05	0.048	0.04961
T8	$O_{16}(n)$	C_{13}-$H_{14}(\sigma*)$	3.60	1.66	0.069	0.01047
T9	$O_{18}(n)$	H_{14}-$C_{12}(\sigma*)$	2.98	1.22	0.055	0.01079

T1

T2

T3

T4

T5

T6

T7

T8
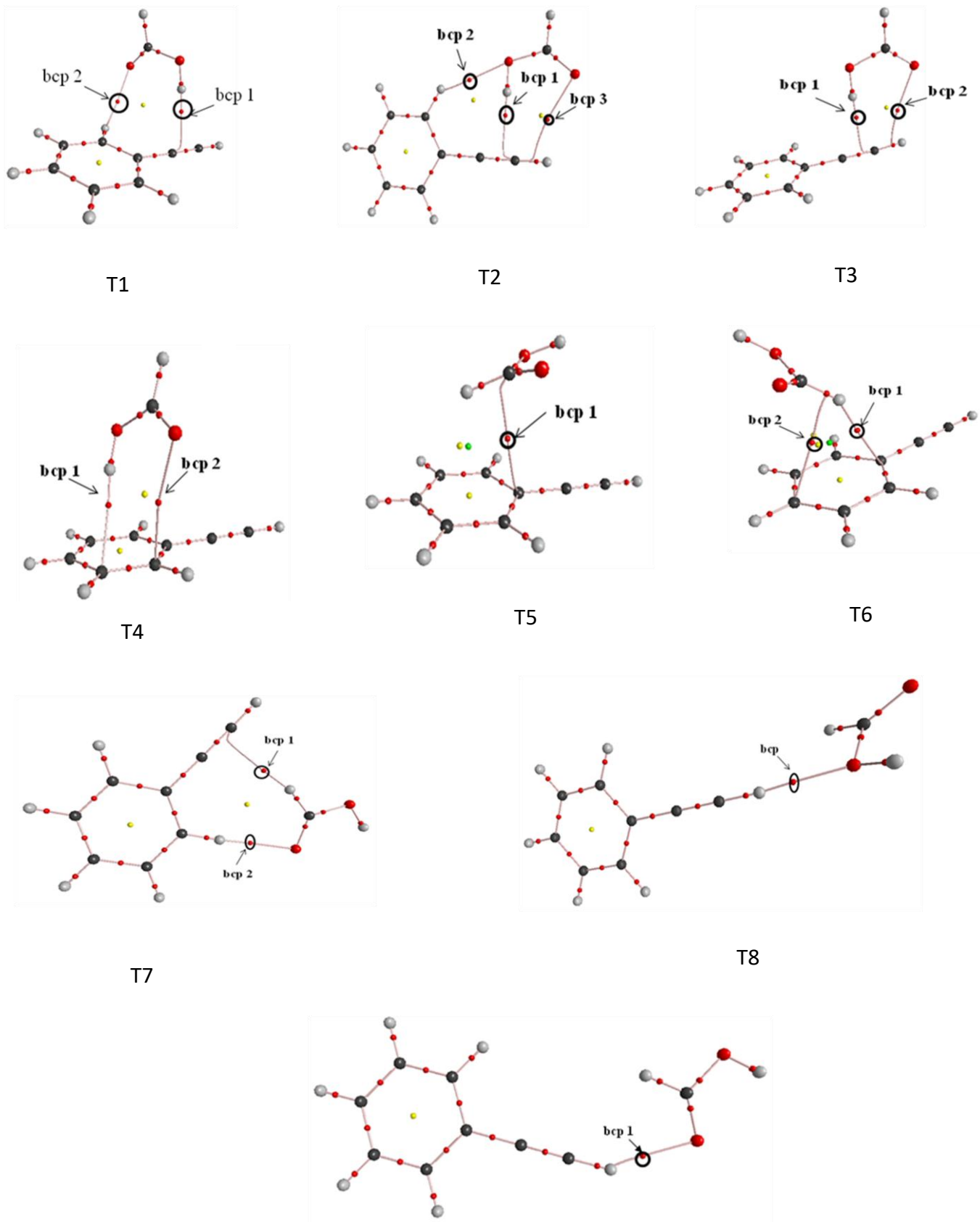
Fig.6. 9. AIM analysis on the optimized geometries of the PhAc-tFA complexes, obtained at MP2/aug-cc-pVDZ level of theory. Bond critical points corresponding to the intermolecular interactions have been indicated.

Table 6.6: LMO-EDA analysis for the various Phac-tFA complexes at the MP2/aug-cc-pVDZ. All energies are given in kcal/mol.

Complex	E_{ES}	E_{ER}	E_{Pol}	E_{Disp}	E_{Total}	E_{ES}/E_{Total}	E_{Disp}/E_{Total}	E_{Pol}/E_{Total}
T1	-7.92	10.43	-3.69	-3.87	-5.05	1.57	0.77	0.73
T2	-8.87	10.67	-3.82	-2.75	-4.78	1.86	0.58	0.80
T7	-8.61	9.84	-3.76	-2.32	-4.86	1.77	0.48	0.77
T3	-4.96	8.74	-2.68	-5.31	-4.22	1.18	1.26	0.64
T5	-4.84	9.02	-1.57	-5.93	-3.31	1.46	1.79	0.47
T6	-4.50	8.03	-1.66	-4.91	-3.04	1.48	1.62	0.55
T7	-5.03	5.73	-1.48	-1.89	-2.68	1.88	0.71	0.55
T8	-2.61	2.70	-0.61	-0.96	-1.48	1.76	0.65	0.41
T9	-4.71	4.37	-1.14	-1.21	-2.68	1.76	0.45	0.43

of FA with C_2H_2, C_6H_6 and PhAc since all three are predominantly π systems. Formic acid essentially shows bidentate hydrogen bonds with acetylene and benzene. In the case of PhAc, it can construct more than two hydrogen bonds in a given structure, as was observed in complex T2. Hydrogen bonded complexes of FA with these π systems have interaction energies in the range of -4 to -5.5 kcal/mol. PhAc:FA can mimic Ac:FA as well as C_6H_6:FA systems. For example , structure T4 is identical to global minimum of C_6H_6:FA heterodimer as it dominated by O-H$\cdots\pi_{Ph}$ interaction whereas structure T2 shows O-H$\cdots\pi_{Ac}$ and $\equiv$C-H$\cdots$O contacts just like global minimum of Ac:FA hydrogen bonded complex. However the low symmetry of PhAc as compared with C_6H_6 or C_2H_2, results in PhAc:FA adopting a number of a different geometries from that observed in C_6H_6:tFA and C_2H_2:tFA. For example, complex T1 has the C-H of the phenyl ring present a secondary C-H$\cdots$O interaction, not seen nor even possible in C_6H_6:FA and C_2H_2:FA. It is also interesting to compare the red shifts in OH stretch of the FA in the above mentioned complexes and which is seen to follow the order : C_6H_6:FA (-120 cm^{-1}) < C_2H_2:FA(-137 cm^{-1}) < PhAc:FA (-155 cm^{-1}). Clearly the PhAc shows the largest red shift as evidenced by the large occupancy of the σ* orbital of O-H.

Chapter 7

Complexes of Phenylacetylene-H$_2$S and Phenylacetylene-CO

7.1 Introduction

In the context of unconventional hydrogen bonding systems, proton donors, such as C-H and proton acceptors such as π systems, have attracted significant attention. In comparison to donors such as O-H, N-H and C-H, the hydrogen bonding interactions of the S-H group have not been explored extensively. We have, therefore, looked at the hydrogen bonding interactions of sulfuhydryl group with PhAc. Sulphur containing amino acids such as cysteine and methionine are actively involved in hydrogen bonding interactions, and the role of S-H group in hydrogen bonding landscape of biomolecules is therefore of great significance.[138]

Arunan and coworkers had earlier studied PhAc-H$_2$S system using microwave spectroscopy. They observed an H···π complex of PhAc-H$_2$S heterodimer, in which H$_2$S served as a proton donor to PhAc.[62] We revisited the PhAc-H$_2$S system in an attempt to understand the vibrational spectroscopy of this complex, which has not been explored. H$_2$S, a prototypical model for molecules containing S-H group, is an interesting candidate for studying the hydrogen bonding contacts containing S-H groups.

CO, which is isoelectronic with N$_2$, also presents an interesting case study in the study of hydrogen bonding interactions, as it has two basic sites. It was interesting to know which of the two sites will prefer to act as proton acceptor, when interacting with PhAc. We have also studied the PhAc-CO system in an attempt to understand the very weak hydrogen bonding landscape involving PhAc and CO.

7.2 Experimental Details

Matrix isolation FTIR experiments and *ab initio* computations were performed to study non-covalently bonded PhAc-H$_2$S and PhAc-CO complexes. The matrix isolation experiments were performed in the N$_2$ matrix. The details of the experimental methodology are given in chapter 2. Phenylacetylene (Sigma Aldrich, 98%), H$_2$S (Sigma-Gases) and CO (Sigma-Gases) were used without any further purification. Liquid sample of PhAc was used after subjecting it to several freeze-pump-thaw cycles, before preparing the matrix gas/sample mixture.

7.3 Computational Details

The computational study was carried out using Gaussian-09 suite of programs. All computations were performed at M06-2X and MP2 levels, using 6-311++G (d,p) and aug-cc-pVDZ basis sets. Fig.7.1 shows the optimized structures of complexes at MP2/aug-cc-pVDZ

level of theory. The interaction energies of the complexes were computed, followed by application of zero point and BSSE corrections separately. The details of the computational procedure followed is mentioned in chapter 2. Harmonic frequency calculations were also performed at the same level of theory, at which optimization of the monomers and complexes was performed. The computed frequencies of the complexes were scaled using scaling factors, derived as explained in Chapter 3. The non-covalent interactions were computationally characterized by AIM, NBO and LMOEDA analysis.

7.4 Results and Discussions

a) Experimental

Matrix isolation studies were performed on both the PhAc-H_2S and PhAc-CO systems, where the concentration of the PhAc, H_2S and CO in codeposition experiments were individually varied over the range 1:1000 to 3:1000. However, in all these experiments, we did not obtain any convincing signatures for the presence of the heterodimers of PhAc-H_2S and PhAc-CO. Hence, in the subsequent sections, we have only discussed our results on the computational exercises, that we have performed on these systems, so as to document these results. We believe that modified experimental methodology, such as employing supersonic jet-matrix isolation experiments may have to be employed to prepare these weakly bound complexes for experimental studies.

b) Computational

PhAc-H_2S System

H_2S, as its oxygen analogue, can behave as amphiprotic molecule, similar to H_2O. Based on our search of the potential surface, at the MP2/aug-cc-pVDZ level of theory, PhAc-H_2S system shows, three different geometries. In complex 1, PhAc acts as a proton donor to H_2S forming an n-σ* complex. This weakly bound complex was a local minimum with hydrogen bonded distance of 2.74Å. The BSSE corrected interaction energy of the complex is -1.43 kcal/mol (Table 7.1). A similar n-σ* complex was also computed and observed in the PhAc-H_2O system. The global minimum for the PhAc-H_2S was complex 2, which is an H⋯π complex, with H_2S serving as a proton donor to the π cloud of the phenyl ring of PhAc. Complex 3, has H_2S serving as proton donor to the acetylenic π cloud of PhAc, while at the same acts as a proton acceptor, involving a phenyl C-H⋯S contact, much like the global minimum in the PhAc- H_2O complex. Complex 3 in PhAc-H_2S system is a local minimum,
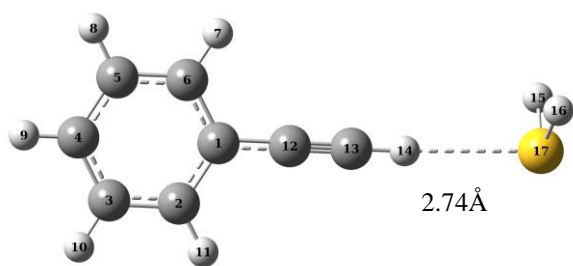
Complex 1 (-2.69/-1.70/-1.44)
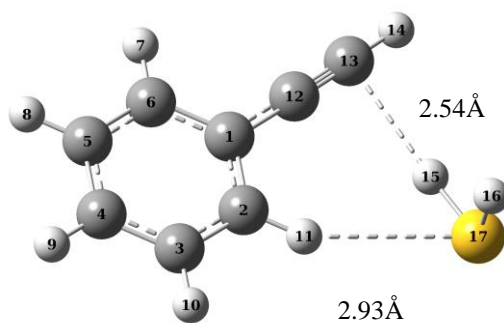
Complex 2 (-5.99/-4.94/-3.47)
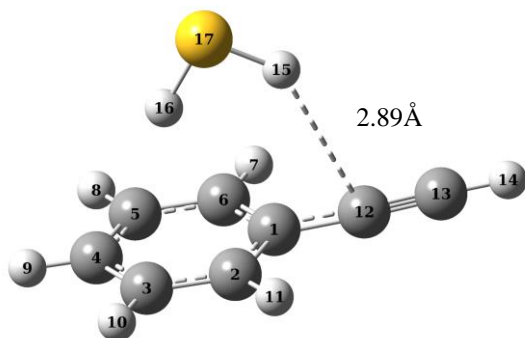
Complex 3 (-4.17/-3.21/-2.45)

Figure 7.1 Optimised geometries of PhAc-H$_2$S complexes at MP2/aug-cc-pVDZ level of theory. Interaction Energies Raw/ZPE/BSSE (kcal/mol) of complexes are given in parenthesis

Table 7.1 Interaction Energies of PhAc-H$_2$S and PhAc-CO complexes Raw/ZPE/BSSE (kcal/mol) at MP2/aug-cc-pVDZ level of theory.

Complex	Raw	ZPE	BSSE
PhAc-H$_2$S			
Complex 1 (n...σ*)	-2.69	-1.70	-1.44
Complex 2 (H...π$_{Ph}$)	-5.99	-4.94	-3.47
Complex 3 (H...π$_{Ac}$)	-4.17	-3.21	-2.45
PhAc-CO			
Complex 1 (O-bonded)	-1.41	-0.77	-0.45
Complex 2 (C-bonded)	-2.03	-1.15	-0.96

located about ~1 kcal/mol above the global minimum. It may be noted that while in PhAc-H_2O system complex 3 was the global minimum, in the PhAc-H_2S system, complex 2 was the global minimum. The point of similarity between the PhAc-H_2O and PhAc-H_2S complexes is that in both cases, an H-π complex was the global minimum, and not the n···σ* complex.

The scaled computed frequencies were obtained by using appropriate scaling factors (Table 7.2). The ≡CH as well as S-H stretching features of PhAc and H_2S submolecules respectively show red shifts as compared to uncomplexed monomers. The ≡CH stretch in complex 1 shows a red shift ~ 50 cm^{-1} which is typical of n…σ* complexes of PhAc. The H_2S submolecule also shows red shift on formation of an H...π adduct which amounts to ~23 cm^{-1}. The computed red shifts in vibrational features of submolecules in PhAc-H_2S system were less in magnitude than PhAc-H_2O. As already mentioned, we were not able to observe any experimental product features in our experiments.

AIM analysis was also performed using the wavefunctions generated at MP2/aug-cc-pVDZ level of theory, to establish the presence of hydrogen bonding interactions in PhAc-H_2S complexes. Values of topological parameters, such as electron density $\rho(r_c)$, eigenvalues of the Hessian, λ_1, λ_2, λ_3, the Laplacian ($\nabla^2\rho(r_c)$) of electron density (defined as the sum of the eigenvalues), the ellipticity, $[(\lambda_1/\lambda_2)-1]$ and $|\lambda_1/\lambda_3|$, for all the complexes, computed at the bond critical points, are shown in Table 7.3 and Fig. 7.2. $\rho(r_c)$ and $\nabla^2\rho(r_c)$ values were analysed for PhAc-H_2S complexes. These values were similar for all the complexes. It was observed that $\rho(r_c)$ and $\nabla^2\rho(r_c)$ values lie within range suggested by Koch and Popelier, though these values lie at lower end of this range, indicating PhAc-H_2S to be very weakly interacting system. In fact, the $\rho(r_c)$ at the intermolecular bond critical points in the PhAc-H_2S complexes are smaller than that observed in the corresponding complexes of PhAc-H_2O.

NBO analysis was also performed on PhAc-H_2S complexes to quantify the hydrogen bonding interactions involved in terms of orbital interactions. Complex 1 involves transfer of electron density from lone pair on S to antibonding orbital of acetylenic C-H of PhAc. The large value of second order perturbation energy E(2) is probably due to large overlap integral. (Table7.4). The H···π complexes involve π orbitals of either the phenyl ring (complex2) or the acetylenic moiety (Complex 3) as donor orbitals and result in transfer of electron density to antibonding S-H orbital of H_2S.

LMOEDA analysis was used to partition the interaction energy of PhAc-H_2S complexes into various components such as electrostatic, exchange-repulsion, polarization

Table 7.2 Experimental (N$_2$ matrix) and scaled computed wavenumbers (cm^{-1}) at MP2/aug-ccpVDZ for the different PhAc-H$_2$S and PhAc-CO complexes. Spectral shifts (cm^{-1}) are given in parenthesis.

	Experimental		Scaled Computed Wavenumbers				Modes
	Monomer	Complex	Monomer	1 (n...σ*)	2 (H...π$_{Ph}$)	3(H...π$_{Ac}$)	
PhAc	3323.2	---	3323.2	3272.9 (-50.3)[a]	3320.7 (-2.5)	3316.3 (-6.9)	≡C-H stretch
H$_2$S	2632.6	---	2632.6	2627.0 (-5.6)	2609.5 (-23.1)	2617.7 (-14.9)	-S-H (*v3*)
	2619.5	---	2609.2	2603.7 (-5.5)	2588.3 (-20.9)	2575.7 (-33.6)	-S-H (*v1*)
	---	---	1174.9	1175.1 (0.27)	1167.0 (-7.9)	1174.5 (-0.4)	-S-H (*v2*)

[a] Δν = ν(complex)- ν(monomer), is given in parenthesis
Scaling Factors : 0.98471(2000-1000 cm^{-1})   0.94712 (3000-2000 cm^{-1}) , 0.95461 (3500-3000 cm^{-1})

PhAc-CO							
	Monomer	Complex	Monomer	1 (O-bonded)	2 (C-bonded)		**Modes**
PhAc	3323.2	---	3323.2	3330.0 (6.8)	3304.3 (-18.8)		≡C-H stretch
CO	2139.9	---	2139.9	2139.5 (-0.4)	2146.9 (7.0)		C≡O stretch

Scaling Factors : 1.03277 (3000-2000 cm^{-1}) , 0.95461 (3500-3000 cm^{-1})

Table 7.3: Summary of AIM calculations for PhAc-H$_2$S and PhAc-CO complexes at MP2/aug-cc-pVDZ level of theory. All quantities are expressed in a.u. See text for definition of each of the quantities.

Complex	$\rho(r_c)$	$\nabla^2\rho(r_c)$	$\lambda\|_1/\lambda_3\|$	(λ_1/λ_2)-1
PhAc-H$_2$S				
1 (n-σ*)	0.0097	0.0254	0.1963	0.018
2 (H-π$_{Ph}$)	0.0079	0.0251	0.1135	1.6968
3 (H-π$_{Ac}$) bcp1	0.0108	0.0277	0.2056	0.4243
bcp2	0.0076	0.0205	0.1880	0.3112
PhAc-CO				
1 (O-bonded)	0.0080	0.0306	0.1817	0.0030
2 (C-bonded)	0.0082	0.0251	0.1854	0.0002

Complex 1
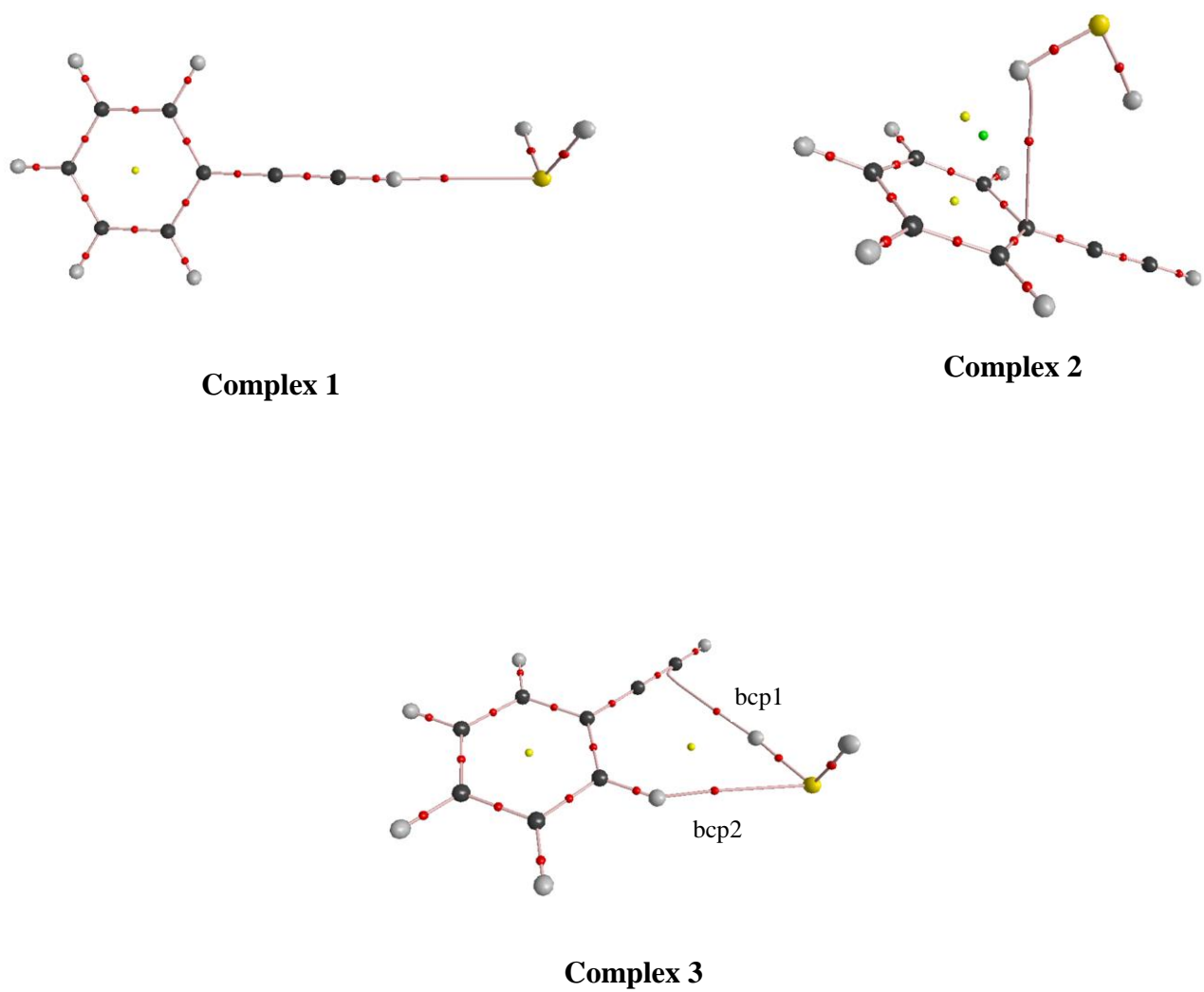
Complex 2

Complex 3

Fig.7.2. Aim analysis of PhAc-H$_2$S complexes at MP2/aug-cc-pVDZ level of theory.

Table.7.4 NBO analysisof PhAc-H$_2$S and PhAc-CO complexes at MP2/aug-cc-pVDZ level of theory. The atom numbering indicated in table is as shown in Fig.7.1 and 7.3. E (2) is the second order perturbation energy (kcal/mol), E(j)-E(i) is the donor-acceptor energy difference and F(i,j) is the overlap between the donor and acceptor orbitals.

Complex	Orbital Involved		E(2) (kcal/mol)	E(j)-E(i) a.u.	F(i,j) a.u.	Electron occupancy donor orbital	Electron occupancy acceptor orbital
	Donor	Acceptor					
PhAc-H$_2$S							
1 (n-σ*)	S$_{17}$ (n)	C$_{13}$-H$_{14}$ (σ*)	5.70	1.21	0.074	1.98789	0.01412
2 (H-π$_{Ph}$)	C$_5$-C$_6$ (π)	S$_{17}$-H$_{16}$ (σ*)	0.91	0.76	0.026	1.65168	0.00362
3 (H-π$_{Ac}$)	C$_{12}$-C$_{13}$ (π)	S$_{17}$-H$_{15}$ (σ*)	4.00	0.84	0.052	1.97917	0.00851
PhAc-CO							
1 (O-bonded)	O$_{16}$ (n)	C$_{13}$-H$_{14}$ (σ*)	2.33	1.81	0.058	1.98983	0.00703
2 (C-bonded)	C$_{15}$ (n)	C$_{13}$-H$_{14}$ (σ*)	5.05	1.43	0.076	1.98864	0.01255

Table7.5: LMO-EDA of PhAc-H$_2$S and PhAc-CO complexes at MP2/aug-cc-pVDZ. All energies are given in kcal/mol.

Complex	E$_{ES}$	E$_{ER}$	E$_{Pol}$	E$_{Disp}$	E$_{Total}$	E$_{ES}$/E$_{Total}$	E$_{Pol}$/E$_{Total}$	E$_{Disp}$/E$_{Total}$
PhAc-H$_2$S								
1 (n-σ*)	-2.70	3.37	-0.88	-1.23	-1.45	1.86	0.61	0.85
2 (H-π$_{Ph}$)	-4.02	7.46	-1.24	-5.73	-3.53	1.14	0.35	1.62
3 (H-π$_{Ac}$)	-4.59	7.07	-1.64	-3.29	-2.45	1.87	0.67	1.34
PhAc-CO								
1 (O-bonded)	-1.13	1.21	-0.26	-0.26	-0.45	2.51	0.58	0.58
2 (C-bonded)	-1.42	1.94	-0.41	-1.08	-0.96	1.48	0.43	1.13

and dispersion. It can be observed from table 7.5 that the complex 1 (n⋯σ*) and complex 3 (H...π_{Ac}) had the largest contributions from the electrostatic component, together with a somewhat smaller contribution from the dispersion component, much like complex 1 and 3 of PhAc-H_2O system. The interaction energy of complex 2 (H⋯π_{Ph}) has the largest contribution from the dispersive component with a comparable, but smaller, component from the electrostatic component.

PhAc-CO System

The complexes of PhAc with CO were studied. Our experiments did not yield signatures of these complexes and we present here onlyour computational results. At the MP2/aug-cc-pVDZ level of theory, two structures were obtained (Fig. 7.3), with CO acting as a proton acceptor in both cases, and PhAc serving as the proton donor through its acetylenic hydrogen. CO has the ability to form hydrogen bonds, with either the C or the O end, which consequently generates two possible orientations. We refer to the complex where PhAc acts as proton donor to O end, as the O-bonded (complex 1), while the the orientation involving the C end of CO, as the C-bonded (complex 2). These complexes were very weak hydrogen complexes having BSSE corrected interaction energy of ~1 kcal/mol (Table 7.1). The global minimum was the C-bonded complex 1, which is consistent with the fact that the carbon is at the negative end in CO. Complex 1, the O-bonded complex, is a local minimum, with the H…O distance of 2.38 Å. Vibrational frequencies were also calculated for these complexes. (Table7.2). Computations indicate that C-bonded complex (complex 2) shows a red shift in the ≡CH stretch of PhAc submolecule in the complex, of ~20 cm^{-1}. The ≡CH stretch of PhAc in the O-bonded (complex 1) was predicted to show an interesting blue shift of ~7 cm^{-1}. The stretch in the CO submolecule is computed to show a blue shift in the C-bonded (complex 2), and a red shift in O-bonded (complex 1).

AIM analysis showed the bond critical points in the intermolecular interaction between PhAc and CO, which as can be seen from Table 7.3 are rather small. The NBO analysis conformed these interactions to be n…σ* interactions involving transfer of electron density from the C or O in CO to the antibonding orbital of the acetylenic C-H in PhAc (Table 7.4). Further LMOEDA analysis predicted C-bonded complex to have an electrostatic component with comparable dispersive contribution, whereas O-bonded complex was dominated by the electrostatic component (Table 7.5).
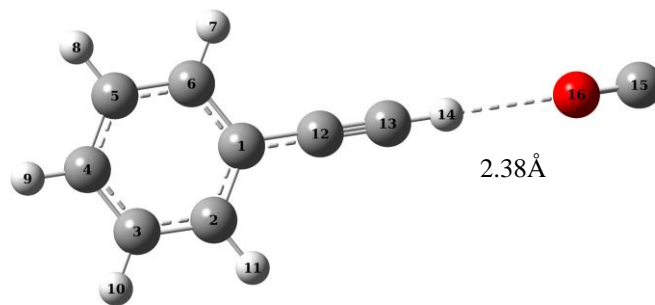
Complex 1 (O-Bonded)
(-1.41/-0.77/-0.45)
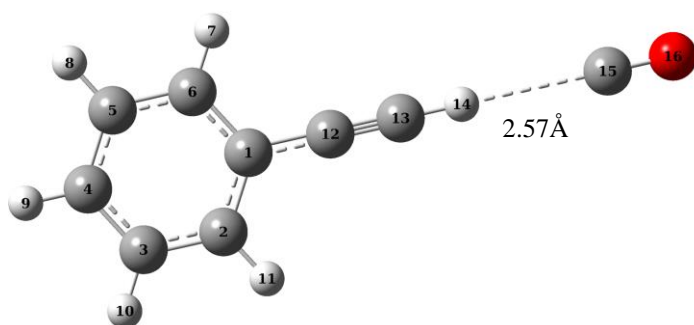
Complex 2 (C-Bonded)
(-2.03/-1.15/-0.96)

Figure 7.3 Optimised geometries of PhAc-CO complexes at MP2/aug-cc-pVDZ level of theory. Interaction Energies Raw/ZPE/BSSE (kcal/mol) of complexes are given in parenthesis

Complex 1 (O-Bonded)

Complex 2 (C-Bonded)
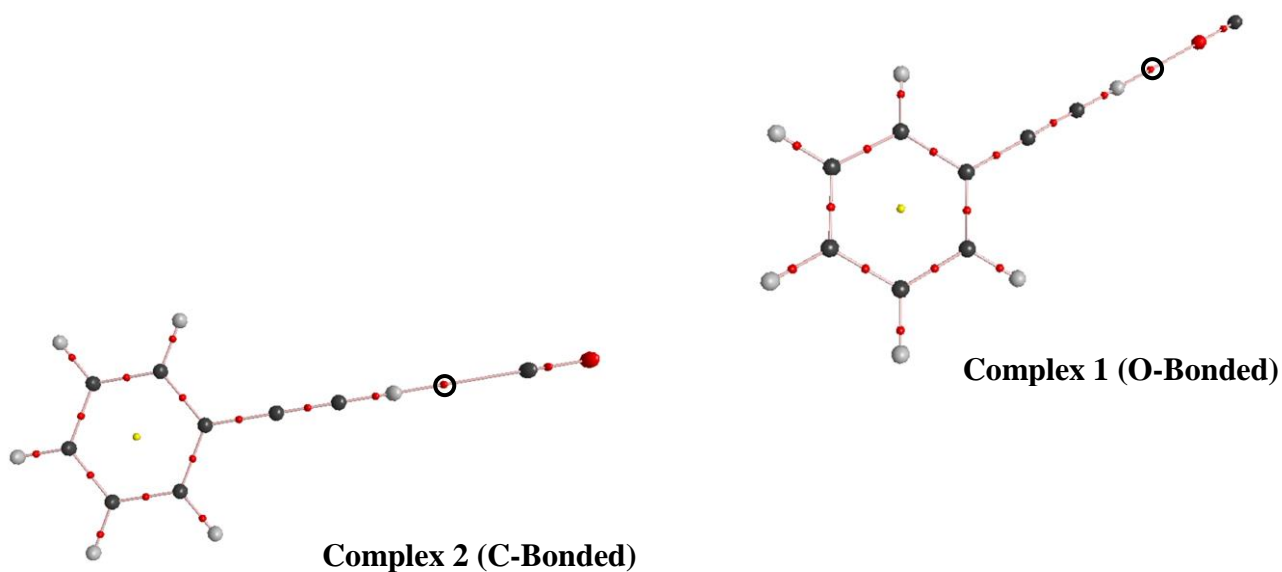
Fig.7.4. Aim analysis of PhAc-CO complexes at MP2/aug-cc-pVDZ level of theory.

7.5 Conclusions

Hydrogen bonded complexes of PhAc-H$_2$S and PhAc-CO were studied using matrix isolation FTIR spectroscopy in N$_2$ matrix and ab initio computations. Experiments on these very weakly bonded complexes did not yield any conclusive evidences of product formation in our matrix isolation experiments. Computations indicated that in the PhAc-H$_2$S, the global minimum was an H…π_{Ph} complex as against the PhAc-H$_2$O system, where the global minimum was a H…π_{Ac} complex. In the case of PhAc-CO system, PhAc exclusively acts as proton donor froming two types of complexes, involving an interaction of the acetylenic hydrogen of PhAc with either the C or the O end of the CO. The complex where the interaction was with the C end was the global minimum, consistent with the negative end of the dipole in CO being at the C end. Both the systems, PhAc-H$_2$S and PhAc-CO were computed to form complexes with very low interactions energies, which were not discerned in our experiments.

Chapter 8

Summary

Hydrogen bonded complexes of PhAc with a variety of partner molecules were studied using matrix isolation infrared spectroscopy and *ab initio* computations. The heterodimer of PhAc consisted of one the following molecules - DEE, H_2O, MeOH, HCl or FA. Each of these systems manifested a different scenario with regard to the hydrogen bonding contacts. In the present study, the transformation of PhAc from being a proton donor to being proton acceptor in above mentioned heterodimers showcased a competition between H-π and n-σ^* contacts.

The systems were, in fact, carefully chosen, to enable us to follow the variation of the global minimum from an exclusively n-σ^* structure to a dominantly H-π structure. For example in PhAc-DEE system only one possibility of hydrogen bonding contact was possible, which corresponded to n-σ^* interaction, because of the presence of only a basic oxygen containing lone pairs, in DEE. This system therefore served as an example of an exclusive n-σ^* system, in which the acetylenic $\equiv$C-H of PhAc acts as a proton donor. The interaction energy of this system was ~-4 kcal/mol at MP2/aug-cc-pVDZ level of theory with a hydrogen bonding distance of 2.05 Å. The n-σ^* PhAc-DEE complex was evidenced by red shift of ~90 cm^{-1} in $\equiv$C-H stretch of PhAc. In this work, the PhAc-DEE was used as a calibrant to identify n-σ^* interactions of PhAc in its complexes with H_2O and MeOH.

On the other hand, in PhAc-HCl system, we observed hydrogen bonded structures dominated by H-π contacts, with the n-σ^* complex being a weakly bound minimum. The global minimum in this case was also computed to have a interaction energy of ~-4 kcal/mol. The PhAc being a proton acceptor resulted in very small red shifts in $\equiv$C-H stretch of PhAc. The large red shifts in H-Cl stretch was instrumental in identifying the PhAc-HCl H-π complexes. The HCl molecule was also shown to possibly execute a barrierless rotation around acetylenic π cloud, resulting in more than one isomer of H-π_{Ac} complex. One of these complexes was identified to be the gateway to Markovnikov reaction.

In between these extremes, Phac-H_2O, Phac-MeOH and PhAc-FA showed structures comprising of both n-σ^* and H-π contacts, with the interaction energies in the range of -1 to -6 kcal/mol, at the CCSD(T) CBS limit.

In this work, we have tried to experimentally observe the global minimum and local minima, wherever possible. We have also attempted to understand the factors which

determine the relative stability of the n-σ* and H-π interactions, in molecules like PhAc, which have the capability to indulge in both these type of contacts.

To rationalize the propensity for the formation of complexes where both the above types of interactions are possible, we have used gas phase acidities, derived from experimental data, of the molecules involved in hydrogen bonding interactions. The gas phase acidities correspond to ΔH°_{acid} of the reaction.[139]

$$A\text{-}H \longrightarrow A^{-} + H^{+}$$

which is a measure of the proton donating ability of the A-H molecule. Higher the value of ΔH°_{acid}, less is the acidity of the molecule.

Figure 8.1 gives the ΔH°_{acid} values (in kcal/mol) for various molecules indicating their proton donating ability. As we go from HCl, through PhAc and C_2H_2, to C_6H_6, the ΔH°_{acid} increases and the acidity correspondingly decreases. This essentially implies that between HCl and PhAc, HCl should serve as the proton donor with PhAc as the proton acceptor in the complex. In general, molecules to the right on acidity line, should serve as proton donors to molecules on the left, in the corresponding hydrogen bonded systems.

In systems that manifest only a primary interaction, as in PhAc-DEE, C_2H_2-H_2O and C_2H_2-HCl, gas phase acidities, as shown in the series in Fig. 8.1, determine the structure of the global minimum. When this gas phase acidity series is applied to H_2O-MeOH, or C_6H_6-H_2O, system, it yields the correct prediction that MeOH and H_2O, respectively, would be proton donors in each of the two systems.

However, when the PhAc-H_2O system is considered, we run into difficulties. While gas phase acidities indicate that here again one should observe the n-σ* complex, rather counter-intuitively calculations show H-π complex to be the global minimum, which implies that H_2O is the proton donor to PhAc. The global minimum in the case of PhAc-H_2O complex (complex 3) consists of a primary O-H···π interaction; incidentally this complex also manifests a secondary C-H$_{phenyl}$···O contact. It was explained in chapter 3, that secondary interaction played a crucial role, due to which H-π structure turn out to be the global minimum instead of n-σ* (Complex 1), clearly signalling a role reversal on the part of PhAc. Experimentally, both complexes have been reported; the global minimum through molecular beam and matrix isolation experiments, and the n- σ* local minimum in our matrix isolation experiments.

A similar dichotomy was observed in case of PhAc-MeOH complexes. According to acidity values, PhAc should act as proton donor in PhAc-MeOH complex but due to the
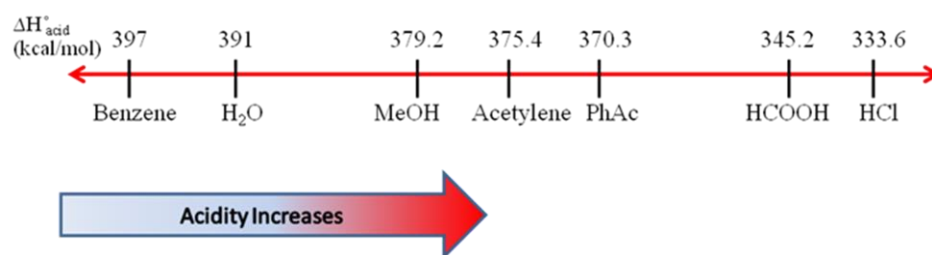
Fig 8.1 Gas Phase Acidity Scale

stabilizing secondary interaction, H-π structure wins the competition and global minimum assumes the H-π structure. From above discussion it can be concluded, where the system can manifest only the primary interaction, as in PhAc-DEE or C_2H_2-H_2O, gas phase acidities, as shown in the series in Fig. 8.1, can predict as to which of the two submolecules will be the proton donor. This series also correctly predicts the global minimum, in C_2H_2-HCl, C_2H_2-H_2O system and C_6H_6-H_2O, all of which manifest a single interaction. However, in cases where a secondary interaction becomes possible, the structure of the complex is determined by the interplay between acidity and supporting secondary interactions.

We further explored the use of gas phase acidities in cases of complexes that manifest multiple interactions, as in PhAc-H_2O and PhAc-MeOH. These systems manifest both n-σ* and H-π structures and we examined the energy difference between these two structures. It can be observed that as acidity increases from H_2O to HCl, the energy difference between n-σ* and H-π structures also increases (Fig.8.2). PhAc-HCl system shows the largest difference between the n-σ* and H-π complexes, while molecules with smaller gas phase acidities, such as H_2O show a much smaller difference in energy between the two competing systems. A plot of energy difference between n-σ* and H-π structures against the gas phase acidity values of the partner molecule of PhAc, in their respective complexes shows a linear plot (Fig.8.3). The presence of secondary interaction in PhAc-H_2O and PhAc-MeOH complexes forces the PhAc to show a role reversal from proton a donor to proton acceptor- i.e. H_2O and MeOH which lie to the left of PhAc, behave like molecules to the right, in the gas phase acidity scale.

It might be relevant to quote an excerpt from the book by Desiraju and Steiner[4] named "The Weak Hydrogen Bond In Structural Chemistry and Biology" on the role of weak interactions like C-H⋯O and O-H⋯π in proteins. "Ubiquitous C-H⋯O contacts are present in large number in proteins (α-helix and β-sheets). …Most of these interactions are weak to very weak and their functions are normally *supportive* at best whereas unambiguous O-H⋯π hydrogen bonds occur relatively rarely in proteins; however they play an important role in protein-ligand recognition. In this sense C-H⋯O and O-H⋯π hydrogen bonds have opposite characteristics of abundance and individual importance." Our work shows that the weak C-H⋯O interactions were not playing just a supportive role but a decisive role in determining the global minimum in PhAc-H_2O and PhAc-MeOH systems. It might not be wrong to say that though weak, these interactions can cause participating molecules to reverse their roles, just like the characters Dr. Jekyl and Mr. Hyde, in the R. L. Stevenson novel. Recognizing that these weak interactions are more than just supportive, can lead to new perceptions in the
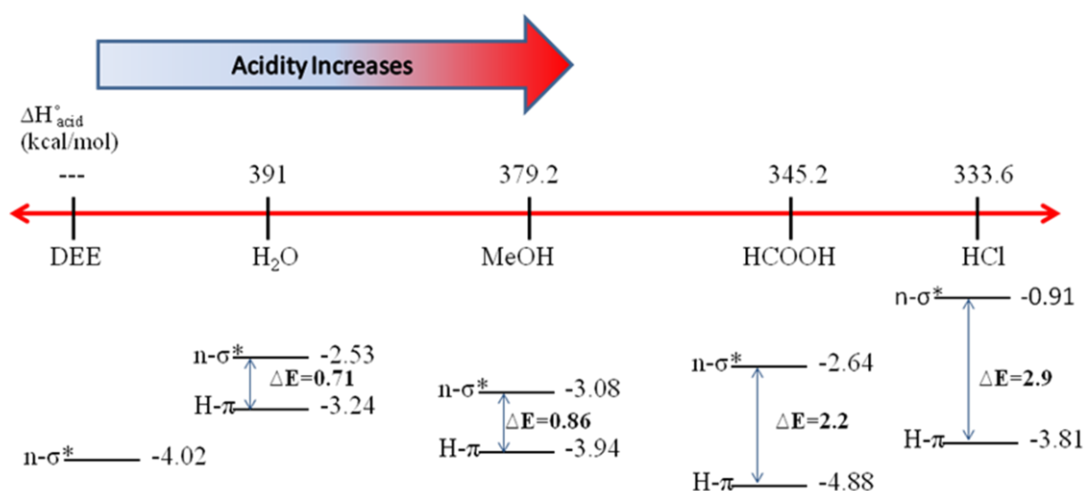
Fig. 8.2 Gas phase acidity scale. Energy difference (ΔE) between n-σ* and H-π structures of hydrogen bonded complexes of PhAc in kcal/mol are shown below the scale. BSSE corrected interaction energies were used to compute the energy difference (ΔE) at MP2/aug-cc-pVDZ level of theory.

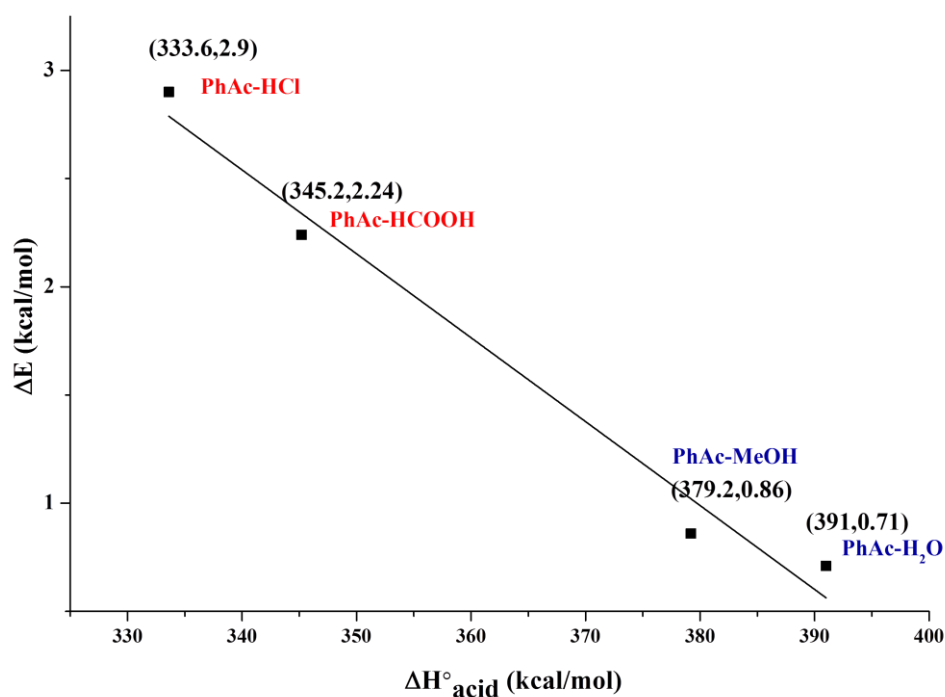Fig. 8.3 Plot of energy difference (ΔE) between n-σ* and H-π structures of hydrogen bonded complexes of PhAc in kcal/mol and gas phase acidities (ΔH°_acid) of the partner molecule of PhAc. The first entry in each parenthesis is ΔH°_acid values and the second entry is ΔE values.

chemistry of interactions!

In addition, the PhAc-H$_2$S and PhAc-CO systems were also studied, both experimentally and computationally. No experimental features, that could be firmly assigned to the complexes were observed and hence we did not discuss experimental aspects of this work. Computations were done, essentially to provide information on the structure of the complexes and estimates of the vibrational shifts in the complexes, as an aid for searching the product features in the experiments. PhAc-H$_2$S system behaved much like the PhAc-H$_2$O system, in that both showed an H-π system as the global minimum. There were some differences, though, between the sulphur and oxygen analogues. While the PhAc-H$_2$O system showed an H-π_{Ac} system as a global minimum, the PhAc-H$_2$S manifested an H...π_{Ph} contact as the global minimum. The PhAc-CO system showed two complexes as minima, with both showing an n-σ* interactions. One complex had a $\equiv$C-H$\cdots$OC interaction, while the second had a $\equiv$C-H$\cdots$CO contact, with the latter complex being the global minimum. Again neither of these complexes were observed in our experiments. It is likely that we may have to employ the hyphenated technique of supersonic jet-matrix isolation to observe these weak complexes.

Future Directions: Recently aromatic noble gas hydrides (C$_6$H$_5$CCXeH) have been prepared by 250 nm photolysis of PhAc and was isolated in Xe matrix.[140] The characteristic H–Xe stretching mode of C$_6$H$_5$CCXeH is observed at about 1500 cm^{-1}. It would be interesting to investigate the competitive hydrogen bonding interactions between H-π and n-σ* contacts in such compounds.

References :

1.Bernstein, J.; Davis, R. E.; Shimoni, L.; Chang, N. L. Patterns in Hydrogen Bonding : Functionality & Graph Set Analysis in Crystals. *Angew. Chem. Int. Ed. Engl.* **1995**, *34*, 1555-1573.

2.Fujii, A.; Ebata, T.; Mikami, N. Direct Observation of Weak Hydrogen Bonds in Microsolvated Phenol: IR of OH Stretching Vibrations of Phenol-CO and -CO2 in S_0 and D_0. *J. Phys. Chem. A*. **2002**, *106*, 10124-10129.

3.Nishio, M. The CH/π Hydrogen Bond in Chemistry. Conformation, Supramolecules, Optical Resolution and Interactions involving Carbohydrates. *Phys.Chem.Chem.Phys.* **2011**, *13*, 13873-13900.

4. Steiner, T. The Hydrogen Bond in the Solid State. *Angew. Chem. Int. Ed.* **2002**, *41*, 48−76.

5.Jeffrey, G. A.; Saenger, W. Hydrogen Bonding in Biological Structures. Springer: Berlin, **1991**.

6. Altnöder, J.; Lee, J. J.; Otto, K. E.; Suhm, M. A. Molecular Recognition in Glycoaldehyde, the Simplest Sugar: Two Isolated Hydrogen Bonds Win Over One Cooperative Pair. *ChemistryOpen.* **2012**, *1*, 269 -275.

7. Desiraju, G.R.; Steiner, T. The Weak hydrogen Bond In Structural Chemistry and Biology. **1999**, Oxford University Press Inc., New York

8. Rozas, I. On the Nature of Hydrogen Bonds: An Overview on Computational Studies and a Word about Patterns. *Phys.Chem.Chem.Phys.* **2007**, *9*, 2782–2790.

9. Dethlefs, K. M.; P. Hobza. Noncovalent Interactions: A Challenge for Experiment and Theory. *Chem. Rev.* **2000**, *100*, 143-167.

10. Hobza,P.; Zahradník, R.; Müller-Dethlefs, K. The World of Non-Covalent Interactions. *Collect. Czech. Chem. Commun.* **2006**, *71*, 443–531.

11. Melandri, S. Union is Strength: How Weak Hydrogen Bonds become Stronger. *Phys. Chem. Chem. Phys.* **2011**, *13*, 13901–13911.

12. Scheiner, S. Hydrogen bonding. A Theoretical Perspective.**1997,**Oxford University press, Oxford.

13.Latimer, W.M.; Rodebush, W. H. Polarity and Ionisation from the Standpoint of the Lewis Theory of Valence.*J. Am. Chem. Soc.* **1920,** *42,* 1419-1433.

14. Sutor, D.J. The C-H…O Hydrogen Bonds in Crystals.Nature **1962,** *195,* 68-69.

15. Arunan, E.; Desiraju, G. R.; Kline, R. A.; Sadlej, J.; Schreiner, S.; Alkorta, I.; Clary, D.C.; Crabtree, R.H.; Dannenberg, J. J.; Hobza, P.; Kjaergaard, H. G.; Legon, A. C.; Mennucci B.; Nesbitt, D.J. Defination of Hydrogen Bond (IUPAC Recommendations). *Pure. Appl. Chem.* **2011,** *83*, 1637-1641.

16. Pearson, R.G. *J. Chem. Educ.* **1968,** *45*, 81-587.

17. Pearson, R.G.The HSAB Principle-More Quantitative Aspects. *Inorg. Chim. Acta*. **1995**, *240*, 93-98.

18. Gilli, P.; Pretto, L.; Bertolasi, V.; Gilli, G. Predicting Hydrogen Bonding Strengths from Acid-Base Molecular Properties. The pKa Slide Rule: Toward the Solution of a Long-Lasting Problem. *Accts. Chem. Res*. **2009**, *42*, 33-44.

19. Steiner, S. Weak H-bonds. Comparisons of CH...O to NH...O in Proteins and PH...N to Direct P...N Interactions. *Phys. Chem. Chem. Phys*. **2011**, *13*, 13860–13872.

20. Kim, Y. S.; Hoschstrasser, R. M. Applications of 2D IR Spectroscopy to Peptides, Proteins and Hydrogen Bond Dynamics. *J. Phys. Chem B*. **2009**, *113*, 8231-8251.

21. Mori, Y.; Masuda, Y. Effect of Solvent on Proton Location and Dynamic Behaviour in Short Intramolecular Hydrogen Bonds Studied by Molecular Dynamics Simulations and NMR Experiments. *Chem. Phys*. **2015**, *458*, 18-29.

22. Sundararajan, K.; Sanskaran, K.; Viswanathan, K. S.; Kulkarni, A. D.; Gadre, S. R. H-π Complexes of Acetylene-Ethylene : A Matrix Isolation and Computational Study. *J. Phys. Chem. A*. **2002**, *106*, 1504-1510.

23. Viswanathan, K. S.; Sankaran, K.; Sundararajan, K. *Encyclopedia of Analytical Chemistry*, edited by J. B. Myers, Wiley, New York **2000.**

24. Dows D. A.; Whittle E.; Pimentel G. C. Infrared Spectrum of Solid Ammonium Azide: A Vibrational Assignment. *J. Chem. Phys.* **1954**, *22,* 1475-.

25. Khriachtchev, L. Matrix-Isolation Studies of Noncovalent Interactions: More Sophisticated Approaches. *J. Phys. Chem. A*. **2015**, *119*, 2735-2746.

26. Karir, G.; Viswanathan, K. S. The elusive ≡C-H· · ·O complex in the hydrogen bonded systems of Phenylacetylene: A Matrix Isolation Infrared and *Ab Initio* Study. *J. Chem. Sci.* **2016**, *128,*1557–1569.

27. Karir, G.; Viswanathan, K. S. Phenylacetylene-Water complex: Is it n···σ or H···π in the matrix? *J. Mol. Struct.* **2016**, *1107*, 145-156.

28. Singh, P. C.; Bandyopadhyay, B.; Patwari, G. N. Structure of Phenylacetylene-Water Complex as Revealed by IR-UV Double Resonance Spectroscopy. *J. Phys. Chem. A.* **2008**,*112*, 3360-3363.

29. Goswami, M.; Arunan, E. Microwave Spectroscopic and Theoretical Studies on the Phenylacetylene...H_2O complex: C-H···O and O-H···π Hydrogen Bonds as Equal Partners *Phys. Chem. Chem. Phys.* **2011**, *13,* 14153-14162.

30. Vidya, V.; Sankaran, K.; Viswanathan, K.S. Matrix Isolation-Supersonic Jet Infrared Spectroscopy: Conformational Cooling in Trimethyl Phosphate. *Chem. Phys. Lett.* **1996**, *258*, 113-117.

31. Pauling, L. The Nature of Chemical Bond and The Structure of Molecules and Crystals. **1960**, Cornell University Press, United States of America.

32. Dewar, M. J. S. The Kinetics of Some Benzidine Rearrangements, and a Note on the Mechanism of Aromatic Substitution, *J. Chem. Soc*. **1946**, *406*, 777-781.

33. Wulf, O. R.; Liddel, U.; Hendricks, S. B. The Effect of Ortho Substitution on the Absorption of the OH Group of Phenol in the Infrared. *J. Am. Chem. Soc.* **1936**, *58,* 2287-2293.

34. Barnes, A. J. Molecular Complexes of the Hydrogen Halides Studied by Matrix Isolation Infrared Spectroscopy. *J. Mol. Struct.* **1983**, *100*, 259-280.

35. McDonald, S. A.; Johnson, G. L.; Keelan, B. W.; Andrews, L. Infrared Spectra of Hydrogen-Bonded π Complexes Between Hydrogen Halides and Acetylene. *J. Am. Chem. Soc.* **1980**, *102*, 2892-2896.

36. Legon, A. C.; Aldrich, P. D.; Flygare, W. H. The Rotational Spectrum and Molecular Structure of the Acetylene-HCl dimer. *J. Chem. Phys.* **1981**, *75*, 625-630.

37. Andrews, L.; Johnson, G. L; Kelsall, B. J. Fourier Transform Infrared Spectra of the C_2H_2-HX and C_2HX-HX Hydrogen-Bonded Complexes in Solid Argon. *J. Phys. Chem.* **1982**, *86*, 3374-3380.

38. Vidya, V.; Sankaran, K.; Viswanathan, K.S. Trimethyl Phosphate-Benzene Complex : A Matrix Isolation Infrared Study and Semiempirical (AM1) Computations. *J.Mol. Struct.* **1998**, *442*, 251-258.

39. Sundararajan, K.; Sankaran, K.; Viswanathan, K.S. H-π Complexes of Acetylene-Ethylene: A Matrix Isolation and Computational Study. *J. Phys. Chem. A.* **2002**,*106*,1504-1510.

40. Sundararajan, K.; Viswanathan, K. S. A Matrix Isolation and *Ab Initio* Study of the C_2H_2 - MeOH Complex. *J. Mol. Struct.* **2006**, *798*, 109−116.

41.Sundararajan, K.; Viswanathan, K. S.; Kulkarni, A. D.; Gadre, S.R. H-π Complexes of Acetylene−Benzene: A Matrix-Isolation and Computational Study. *J. Mol. Struct.* **2002**, *613*, 209−222.

42. Gotch, A. J.; Zwier, T. S. Multiphoton Ionization Studies of Clusters of Immiscible Liquids. I. C_6H_6–$(H_2O)n$, *n*=1,2. *J. Chem. Phys.* **1992**, *96*, 3388-3401.

43. Rodham, D. A.; Suzuki, S.; Suenram, R. D.; Lovas, J. F.; Dasgupta, S. Goddard III, W. A.; Blake, G. A. Hydrogen Bonding in the Benzene-Ammonia Dimer. *Nature*, **1993**, *362*, 735-737.

44. Engdahl, A.; Nelander, B. The Acetylene-Water Complex. A Matrix Isolation Study. *Chem. Phys. Lett*. **1983**, *100*, 129-132.

45.Verma, K.; Dave, K.; Viswanathan, K. S. Hydrogen-Bonded Complexes of Phenylacetylene-Acetylene: Who is The Proton Donor ? *J. Phys. Chem. A*. **2015**,119, 126566-12664.

46. McDonald, S. A.; Johnson, G. L.; Keelan, B. W.; Andrews, L. Infrared Spectra of Hydrogen-Bonded π Complexes between Hydrogen Halides and Acetylene. *J. Am. Chem. Soc.* **1980**, 102, 2892−2896.

47. Biswal, H.S.; Wategaonkar, S. Sulphur, Not Too Far Behind O, N, and C: S-H...π Hydrogen Bond. *J. Phys. Chem. A.* **2009**, *113*, 12774-12782.

48. Barnes, A. J. Blue Shifting Hydrogen Bonds- Are They Improper or Proper ? *J. Mol. Struct.* **2004**, *704*, 3-9.

49. Gu, Y.; Kar, T.; Scheiner, S. *J. Mol. Struct.* **2000**, *552*, 17.

50. Scheiner, S.; Gu, Y.; Kar, T. *Theochem.* **2000**, *500*, 441.

51. Scheiner, S.; Grabowski, S. J.; Kar, T. *J. Phys. Chem. A* **2001**, *105*, 10607

52. Pejov, L.; Hermansson, K. *J. Chem. Phys*. **2003**, *119*, 313.

53. Hobza, P. *Phys. Chem. Chem. Phys*. **2001**, *3*, 2555

54. Alabugin, I. V.; Manoharan, M.; Peabody, S.; Weinhold, F. *J. Am. Chem. Soc.* **2003**, *125*, 5973.

55. Hobza, P.; Havlas, Z. *Chem. Rev.* **2000**, *100*, 4253, and references therein.

56 Van der Veken, B. J.; Herrebout, W. A.; Szostak, R.; Shchepkin, D. N.; Havlas, Z.; Hobza, P. *J. Am. Chem. Soc*. **2001**, *123*, 12290.

57. Joseph, J.; Jemmis, E.D. Red-, Blue-, or No-Shift in Hydrogen Bonds: A Unified Explanation. *J. Am. Chem. Soc.* **2007**, *129*, 4620-4632.

58.Maity, S., Guin, M., Singh, P. C. and Patwari, G. N. Phenylacetylene : A Hydrogen Bonding Chameleon . *Chem Phys Chem.* **2011,** *12*, 26-46.

59.Singh, P. C. and Patwari, G. N.. IR-UV Double Resonance Spectroscopic Investigation of Phenylacetylene-Alcohol Complexes. Alkyl Group Induced Hydrogen Bond Switching.*J. Phys. Chem. A.* **2008,***112,* 5121-5125.

60. Reid, S. A; Nyambo, S.; Muzangwa, L.; Uhler, B. π-stacking, C-H/π, and Halogen Bonding Interactions in Bromobenzene and Mixed Bromobenzene-Benzene Clusters. *J. Phys. Chem. A.* **2013**, *117,* 13556-13563.

61. Metrangolo, P.; Neukirch, H.; Pilati, T.;Resnati, G. Halogen Bonding based Recognition Processes : A World Parallel to Hydrogen Bonding. *Acc. Chem. Res.***2005**, *38,* 386-395.

62. Goswami, M. Rotational Spectroscopic and *Ab Initio* Studies On The Weakly Bound Complexes Containing O-H...π And SH...π Interactions. Diss. G23520, **2010.**

63.https://giphy.com/gifs/spongebob-spongebob-squarepants-nickelodeon-so-cold-KaW6fNYZf6eSk

64 .Norman, I.; Porter, G. *Nature,* **1954**, *174,*508 Whittle, E.; Dows, D.A.; Pimentel, G.C. J. Chem. Phys. **1954**, *22*, 1943.

65 .Becker, E.D.; Pimentel, G.C. Spectroscopic Studies of Reactive Molecules by the Matrix Isolation Method. *J. Chem. Phys.* **1956**, *25,*224-228.

66. Thiel, M.V.; Becker, E.D.; Pimentel, G.C. Infrared studies of Hydrogen Bonding of Water by the Matrix Isolation Technique. *J. Chem. Phys.* **1957**, *27,*486-490.

67. Milligen, D.E.; Pimentel, G.C. Matrix isolation studies: Possible Infrared Spectra of Isomeric Forms of Diazomethane and of Methylene, CH2. *J. Chem. Phys.* **1958**, *29,*1405-1412.

68. Thiel, M.V.; Becker, E.D.; Pimentel, G.C. Infrared studies of Hydrogen Bonding of Methanol by the Matrix Isolation Technique. *J. Chem. Phys.* **1957**, *27*, 95-99.

69. Hobe, M. von; Stroh, F.; Beckers, H.; Benter, T.; Willner, H. The UV/Vis Absorption Spectrum of Matrix-Isolated Dichlorine Peroxide, ClOOCl. **2009**, 11, 1571-1580.

70. Bondybey, V. E.; English, J. H. *J. Chem. Phys.* **1977**, *67*, 3405.

71. Sander, W.; Costa, P. Hydrogen Bonding Switches the Spin State of Diphenylcarbene from Triplet to Singlet. *Angew. Chem. Int. Ed.* **2014,** *53*, 1-5.

72. Majkut; A. O.; Ahokas, J.; Lundell, J.; Petterson, M. Raman Spectroscopy of Formic Acid and its Dimers Isolated in Low Temperature Argon Matrices. **2009**, *468*, 176-183.

73. Frisch, M. J.; Trucks, G. W.; Schlegel, H. B.; Scuseria, G. E.; Robb, M. A.; Cheeseman, J. R.; Scalmani, G.; Barone, V.; Mennucci, B.; Peterson, G. A.; *et al.* GAUSSIAN 09, Revision C.01,Gaussian Inc., Wallingford CT, **2010**.

74. Schmidt, M. W.; Baldridge, K. K.; Boatz, J. A.; Elbert, S. T.; Gordon, M. S.; Jensen, J. H.; Koseki, S.; Matsunaga, N.; Nguyen, K. A.; Su, S., *et al.* General Atomic and Molecular Electronic Structure System. *J. Comp. Chem.* **1993**, *14*, 1347-1363.

75. Vincent, M. A.; Hillier, I. H. The Structure and Interaction Energies of the Weak Complexes of $CHClF_2$ and CHF_3 with HCCH : A Test of Density Functional Theory Methods. *Phys. Chem. Chem. Phys.* **2011**, *13,* 4388-4392.

76. The Spectra were Simulated using SYNSPEC made Available by Irikura K., National Institute of Standards and Technology, Gaithesburg, MD 20899, USA, 1995.

77. Turi, L.; Dannenberg, J. J. Molecular Orbital Studies of the Nitromethane-Ammonia Complex. An Unusually Strong CH…N Hydrogen Bond. *J. Phys. Chem.* **1995**, *99*, 639-641.

78.Wong, N.B.; Cheung, Y.S; Wu, D. Y.; Ren, Y.; Wang, X.; Tian, A. M..; Li, W.K. A Theoretical Study of the C-H …N Hydrogen Bond in the Methane-Ammonia Complex. *J. Mol. Struct.* **2000**, *507*, 153-156.

79. Boys, S. F.; Bernardi, F. The Calculation of Small Molecular Interactions by the Differences of Separate Total Energies. Some Procedures with Reduced Errors. *Mol. Phys.* **1970**, *19*, 553-566.

80. Helgaker, T.; Klopper, W.; Koch, H.; Noga, J. Basis-Set Convergence of Correlated Calculations on Water. *J. Chem. Phys*. **1997**, 106, 9639-9646.

81. Bader R. F. W., Atoms in Molecules. A Quantum Theory, Clarendon Press, Oxford, **1994.**

82. Blieger-König, F.; Bayles, D.; Schönbohn, J. AIM2000 (Version 1.0); Chemical Adviser: Bader, R. F. W.

83. Koch, U.; Popelier,P. L. A. Characterization of C–H···O Hydrogen Bonds on the Basis of the Charge Density. *J. Phys. Chem.* **1995**, *99*, 9747-9754.

84. Espinosa, E.; Molins, E.; Lecomte, C. Hydrogen Bond Strengths Revealed by Topological Analyses of Experimentally Observed Electron Densities. *Chem. Phys. Lett.* **1998**, *285,* 170-173.

85. Su, P. F.; Li, H. Energy Decomposition Analysis of Covalent Bonds and Intermolecular Interactions. *J. Chem. Phys.* **2009**, *131*, 014102-014115.

86. Glendening, E. D.; Carpenter, J. E.; Weinhold, F. NBO (Version 3.1).

87. Onsager, L. Electric Moments of Molecules in Liquid. *J. Am. Chem. Soc.* **1936**, *58*, 1486-1493.

88.Wong, M. W.; Frisch, M. J.; Wiberg, K. B. Solvent Effects. 1. The Mediation of Electrostatic Effects by Solvents. *J. Am. Chem. Soc*. **1991**, *113*, 4776-4782.

89. Tomasi, J.; Mennucci, B.; Cammi, R. Quantum Mechanical Continuum Solvation Models. *Chem. Rev.* **2005**, *105*, 2999-3094.

90. Takano, Yu; Houk, K. N. Benchmarking the Conductor-like Polarizable Continuum Model (CPCM) for Aqueous Solvation Free Energies of Neutral and Ionic Organic Molecules. *J. Chem. Theory Comput.* **2005**,1,70-77.

91. Engdahl, A.; Nelander, B. The Acetylene-Water Complex. A Matrix Isolation Study. *Chem. Phys. Lett*. **1983**, *100*, 129-132.

92. Sundararajan, K.; Sanskaran, K.; Viswanathan, K. S.; Kulkarni, A. D.; Gadre, S. R. H-π Complexes of Acetylene-Ethylene : A Matrix Isolation and Computational Study. *J. Phys. Chem. A*. **2002**, *106*, 1504-1510.

93. George, L.; Viswanathan, K.S.; Singh, S. *Ab Initio* Study of Trimethyl Phospate : Conformational Analysis, Dipole Moments, Vibrational Frequencies, and Barriers for Conformer Interconversion. *J. Phys. Chem. A*. **1997**, *101*, 2459-2464.

94. The spectra were simulated using SYNSPEC made available by K. Irikura, National Institute of Standards and Technology, Gaithesburg, MD 20899, USA, 1995.

95. King, G. W.; So, S. P. Ethynylbenzene: The Vibrational Spectra of Some Deuterated Isomers. *J. Mol. Spectrosc.* **1970**, *36*, 468-487.

96. Delaat, A. M.; Ault, B. S. Infrared Matrix Isolation Study of Hydrogen Bonds Involving C-H Bonds : Alkynes with Oxygen Bases. *J. Am. Chem. Soc.* **1987**, *109*, 4232-4236.

97. Stearns, J. A.; Zwier, T. S. Infrared and Ultraviolet Spectroscopy of Jet-Cooled ortho-, meta-, and para-Diethynylbenzene. *J. Phys. Chem. A*. **2003**, *107*, 10717-10724.

98. Bentwood, R. M.; Barnes, A. J.; Thomas, W. J. O. Studies of Intermolecular Interactions by Matrix Isolation Vibrational Spectroscopy: Self Association of Water . *J. Mol. Spectrosc.* **1980**, *84*, 391-404.

99. Perchard, J. P. Anharmonicity and Hydrogen Bonding II-A Near Infrared Study of Water Trapped in Nitrogen Matrix. *Chem. Phys.* **2001**, *266*, 109-124.

100. Shahi, A.; Arunan, E. Hydrogen bonding, Halogen Bonding and Lithium Bonding: An Atoms in Molecules and Natural Bond Orbital Perspective towards Conservation of Total Bond Order, Inter- and Intra-Molecular Bonding. *Phys. Chem. Chem. Phys.* **2014**, *16*, 22935-22952.

101. Jose, K. V. J; Gadre, S. R.; Sundararajan, K; Viswanathan, K. S. Effect of Matrix on IR frequencies of Acetylene and Acetylene-Methanol Complex: Infrared Matrix Isolation and *Ab Initio* Study. *J. Chem. Phy.* **2007**, *127*, 104501-104510

102. Kar, B. P.; Ramanathan, N.; Sundararajan, K.; Viswanathan, K. S. Matrix Isolation FTIR Studies of Non-Planar Trans-Stilbene. *J. Mol. Struc.* **2011**, *994*, 364-370.

103. Jacox, M. E. *J. Phys. Chem. Ref.* Data, Monograph No. 3, **1994**.

104. Jordan, M. J. T.; Bene, J. E. D. Unraveling Environmental Effects on Hydrogen-Bonded Complexes: Matrix Effects on the Structures and Proton-Stretching Frequencies of Hydrogen−Halide Complexes with Ammonia and Trimethylamine. *J. Am. Chem. Soc.* **2000**, *122*, 2101-2115.

105. Jones, M., Jr. Organic Chemistry, 2nd ed.; W. W. Norton & Company: New York, **2000**.

106. Fatima, M. Matrix Isolation Infrared Spectroscopy and Computational Study of Complexes between Phenylacetylene with Methanol and Methylamine. Dissertation , IISER Mohali, 2014.

107. Venkatesan V.,Sundararajan K., Sankaran K.;Viswanathan K. S.Conformations of Dimethoxymethane : Matrix Isolation Infrared and Ab Initio Studies. *Spectrochim. Acta Mol. Biomol. Spectrosc.* **2002**,*58*, 467-478.

108. Barnes, A. J. Molecular Complexes of the Hydrogen Halides Studied by Matrix Isolation Infrared Spectroscopy. *J. Mol. Struct.* **1983**, *100*, 259-280.

109. McDonald, S. A.; Johnson, G. L.; Keelan, B. W.; Andrews, L. Infrared Spectra of Hydrogen-Bonded π Complexes between Hydrogen Halides and Acetylene. *J. Am. Chem. Soc.* **1980**, *102*, 2892-2896.

110. Legon, A. C.; Aldrich, P. D.; Flygare, W. H. The Rotational Spectrum and Molecular Structure of the Acetylene-HCl Dimer. *J. Chem. Phys.* **1981**, *75*, 625-630.

111. Andrews, L.; Johnson, G. L; Kelsall, B. J. Fourier Transform Infrared Spectra of the C_2H_2-HX and C_2HX-HX Hydrogen-Bonded Complexes in Solid Argon. *J. Phys. Chem.* **1982**, *86*, 3374-3380.

112. Pople, J. A.; Frisch, M. J.; Bene J. D. E. Hydrogen Bonds between Hydrogen Halides and Unsaturated Hydrocarbons. *Chem. Phys. Lett.* **1982**, *91,* 185-189.

113. Tarakeshwar, P.; Lee, S. J.; Lee, J. Y; Kim, S. K. Benzene-Hydrogen Halide Interactions : Theoretical Studies of Binding Energies, Vibrational Frequencies , and Equilibrium Structures. *J. Chem. Phys*. **1998**, *108*, 7217-7223.

114. Read, W. G.; Campbell, E. J.; Henderson, G. The Rotational Spectrum and Molecular Structure of the Benzene-Hydrogen Chloride Complex. *J. Chem. Phys.* **1983**, *78*, 3501- 3508.

115. Gotch, A. J.; Zwier, T. S. The Spectroscopy and Dynamics of π Hydrogen-Bonded Complexes: Benzene-HCl/DCl and Toluene-HCl/DCl. *J. Chem. Phys.* **1990**, *93,* 6977-6986.

116. Reid, S. A; Nyambo, S.; Muzangwa, L.; Uhler, B. π-stacking, C-H/π, and Halogen Bonding Interactions in Bromobenzene and Mixed Bromobenzene-Benzene Clusters. *J. Phys. Chem. A*. **2013**, *117,* 13556-13563.

117. Metrangolo, P.; Neukirch, H.; Pilati, T.;Resnati, G. Halogen Bonding based Recognition Processes : A World Parallel to Hydrogen Bonding. *Acc. Chem. Res.***2005**, *38,* 386-395.

118. Brown, H. C.; Groot, C. A Convenient Procedure for the Preparation of Deuterium Chloride. *J. Am. Chem. Soc*., **1942**, *64*, 2223-2224.

119. Ebert, L.; Keesom, W. H. Preliminary Measurements of the Dielectric Constants of Liquid and Solid Nitrogen. Communication N˚. 182d from the Physical Laboratory at Leyden, **1926**, 1188-1192.

120. Gotch, A. J.; Zwier, T. S. Multiphoton Ionization Studies of Clusters of Immiscible Liquids. I. C_6H_6–$(H_2O)_n$, n=1,2. *J. Chem. Phys.* **1992**, *96*, 3388-3401.

121. Amezaga, N. J. M.; Pamies, S. C.; Peruchena, N. M.; Sosa, G. L. Halogen Bonding : A Study based on Electronic Charge Density. *J. Phys. Chem. A*. **2010**, *114,* 552-562.

122. Hill, J. G.; Legon, A. C. On the Directionality and Non Linearity of Halogen and Hydrogen Bonding. *Phys. Chem. Chem. Phys*. **2015**, *17*, 858-867.

123. Marushkevich, K.; Khriachtchev, L.; Lundell, J.; Domanskaya A., Ra¨sa¨nen M. Matrix Isolation and *Ab Initio* Study of Trans-Trans and Trans-Cis Dimers of Formic Acid. *J. Phys. Chem. A* **2010**, *114,* 3495–3502.

124. Crovisier J.; Bockele´e-Morvan, D. *Space Sci. Rev*. **1999**, *90*, 19–32.

125. Ehrenfreund, P. E.; Charnley, S. B. *Annu. Rev. Astron. Astrophys*., **2000**, *38,* 427–483.

126. Andrade, D. P. P.; Boechat-Roberty, H. M.; da Silveira, E. F.; Pilling, S.; Iza, P.; Martinez, R.; Farenzena, L. S.; Homem, M. G. P.; Rocco, M. L. M. *J. Phys. Chem. C***, 2008**, *112*, 11954–11961

127. Jacob, D. J. Heterogeneous Chemistry and Tropospheric Ozone. *Atmos. Environ.* **2000**, 34, 2131−2159.

128. Lelieveld, J.; Crutzen, P. J. The Role of Clouds in Tropospheric Photochemistry. *J. Atmos. Chem.* **1991**, *12*, 229−267.

129. Miyazawa, T.; Pitzer, K. S. Internal Rotation and Infrared Spectra of Formic Acid Monomer and Normal Coordinate Treatment of Out-of-Plane Vibrations of Monomer, Dimer, and Polymer. *J. Chem. Phys.* **1959**,*30*,1076-1086.

130. Lopes, S.; Domanskaya, A. V.; Fausto, R.; Räsänen, M.; Khriachtchev, L. Formic Acid and Acetic Acids in a Nitrogen Matrix : Enhanced Stability of the Higher Energy Conformer. *J. Chem. Phys.* **2010**,*133*,144507-14414.

131. Tsuge, M.; Marushkevich, K.; Rasä nen, M.; Khriachtchev, L.¨Infrared Characterization of the HCOOH···CO_2 Complexes in Solid Argon: Stabilization of the Higher-Energy Conformer of Formic Acid. *J. Phys. Chem. A,* **2012**, *116*, 5305−5311.

132. Lundell, J.; Rasanen, M.; Latajka, Z. Complexes between Formic Acid and Carbon Monoxide: An ab Initio Investigation. *J. Phys. Chem.* **1993**, *97*, 1152−1157.

133. George, L.; Sander, W. Matrix Isolation Infrared and Ab Initio Study of the Hydrogen Bonding between Formic-Acid and Water. *Spectrochimica Acta Part A*. **2004,** *60*, 3225-3232.

134. George, L.; Sanchez-Garcia, E.; Sander, W. Matrix Isolation Infrared and *Ab Initio* Study of Formic Acid-Acetylene Interaction: Example of H... π and C-H...O Interaction. *J. Phys. Chem. A.* **2003**, *107*, 6850-6858.

135. Banerjee, P.; Bhattacharya, I.; Charaborty, T. Matrix Isolation Infrared Spectroscopy of an O-H...π Hydrogen Bonded Complex between Formic Acid and Benzene. *J. Phys. Chem. A.* **2016**, *120*, 3731-3739.

136. Kumar, G. Study of Hydrogen Bonded Complexes between Formic Acid and Ohenylacetylene using Matrix Isolation Infrared Spectroscopy and Computations. Dissertation, **2013**, IISER Mohali.

137. Gatenberg, M.; Halupka, M.; Sander, W. Dimerization of Formic Acid-An Example of a "Noncovalent" Reaction Mehanism. *Chem. Eur. J.* **2000**, *6*, 1865-1869.

138. Gregoret, L. M.; Rader, S. D.; Fletterick, R. J.; Cohen, F.E. Hydrogen Bonds Involving Sulphur Atoms in Proteins. *Protein Struct Funct Genet*. **1991**, *9*, 99-107.

139. Topol, I. A.; Tawa, G. J.; Caldwell, R. A., Eissenstat, M. A.; Burt, S. K. Acidity of Organic Molecules in the Gas Phase and in Aqueous Solvent. *J. Phys. Chem. A.* **2000,** *104,* 9619-9624.

140. Duarte,L.; Khriachtchev, L. An Aromatic Noble Gas Hydride C_6H_5CCXeH.**2017** doi:10.1038/s41598-017-02869-9